UNCLASSIFIED

AD 283 984

Reproduced
by the

ARMED SERVICES TECHNICAL INFORMATION AGENCY
ARLINGTON HALL STATION
ARLINGTON 12, VIRGINIA

UNCLASSIFIED

NOTICE: When government or other drawings, specifications or other data are used for any purpose other than in connection with a definitely related government procurement operation, the U. S. Government thereby incurs no responsibility, nor any obligation whatsoever; and the fact that the Government may have formulated, furnished, or in any way supplied the said drawings, specifications, or other data is not to be regarded by implication or otherwise as in any manner licensing the holder or any other person or corporation, or conveying any rights or permission to manufacture, use or sell any patented invention that may in any way be related thereto.

62-4-6

AFCRL-62-498
MAY 1962

283 984
28 3984
CATALOGED BY ASTIA
AS AD No. ____

Air Force Surveys in Geophysics
No. 145

Research Report

Summary Report—Project Ice Way

W. D. KINGERY, EDITOR

ASTIA
RECEIVED
SEP 18 1962
TISIA A

TERRESTRIAL SCIENCES LABORATORY PROJECT 7628

AIR FORCE CAMBRIDGE RESEARCH LABORATORIES, OFFICE OF AEROSPACE RESEARCH, UNITED STATES AIR FORCE

FOR ERRATA

AD 283 984

THE FOLLOWING PAGES ARE CHANGES

TO BASIC DOCUMENT

AFCRL-62-498

November 1962

AD-283984

ERRATA

The attached page 20 is hereby distributed as page 20 of AFCRL-62-498, Summary Report—Project Ice Way, dated May 1962.

AIR FORCE CAMBRIDGE RESEARCH LABORATORIES
OFFICE OF AEROSPACE RESEARCH
UNITED STATES AIR FORCE
Bedford, Massachusetts

ASTIA
MAR 2 0 1963
TISIA

500 ft with a center build-up of 4 ft. Floodings were to be made in 4-inch lifts on an every-other-day schedule to allow an approximate 48-hr curing period between floodings. The pump station was to be located in the center of the apron, and the snow cover on the area was to be left in place.

4.3.2 CONSTRUCTION SCHEDULE

The construction was scheduled for completion by the first week in March to allow a curing period prior to the start of the dynamic test phase.

Preflood preparation of the area consisted of: (1) leveling the natural snow cover, (2) installing deflection stakes across the east-west diameter, and (3) installing thermocouple instrumentation.

A large rubber-tired motor grader was used for initial leveling of the 4- to 8-inch snow cover. This was followed by finish leveling with a wood drag made from a crate cover. When the leveling was completed, the surface was fairly flat. The packed snow in the area was about 3 inches thick, and the natural ice was about 35 inches thick.

After the snow cover was leveled, deflection stakes were set at 100-ft intervals across the east-west diameter and extended, on each side, 400 ft beyond the anticipated 500-ft diameter. The stakes were all topped to an equal elevation above the ice surface. A preconstruction survey indicated that the ice sheet, for all practical purposes, was level and flat. A visual inspection disclosed no prominent cracks in the area; however, a detailed inspection was not possible because of the snow.

The first flooding was made on 1 February and the apron was completed with the eleventh lift on 1 March. The approximate freezing cycle maintained between the first four lifts was 46 hrs. The freezing cycle between the remaining lifts was approximately 42 hrs, except between the fourth and fifth and the sixth and seventh lifts. Between the fourth and fifth lifts there was a 193-hr cycle caused by a change of flooding pumps and other work interference. An 88-hr period between the sixth and seventh lifts was caused by equipment breakdown and bad weather.

The first lift covered a spread pattern approximately 100 ft in diameter. Each successive flooding increased the coverage, and by the sixth flooding the 500-ft diameter was reached. The diameter of the completed apron was about 650 ft.

Requests for additional copies by Agencies of the Department of Defense, their contractors, and other government agencies should be directed to the:

Armed Services Technical Information Agency
Arlington Hall Station
Arlington 12, Virginia

Department of Defense contractors must be established for ASTIA services, or have their 'need-to-know' certified by the cognizant military agency of their project or contract.

All other persons and organizations should apply to the:

U. S. DEPARTMENT OF COMMERCE
OFFICE OF TECHNICAL SERVICES,
WASHINGTON 25, D. C.

AFCRL-62-498
MAY 1962

Air Force Surveys in Geophysics
No. 145

Research Report

Summary Report—Project Ice Way

W. D. KINGERY, EDITOR

CONTRIBUTORS
D. L. Anderson, J. B. Brown, R. L. Coble,
J. E. Dykins, D. N. French, H. A. Hobbs, Jr.,
C. O. Horton, W. D. Kingery, D. W. Klick,
M. P. Langleben, and J. A. Pate

TERRESTRIAL SCIENCES LABORATORY PROJECT 7628

AIR FORCE CAMBRIDGE RESEARCH LABORATORIES, OFFICE OF AEROSPACE RESEARCH, UNITED STATES AIR FORCE, L. G. HANSCOM FIELD, MASS.

Abstract

Project ICE WAY was a joint field activity of the Terrestrial Sciences Laboratory, Air Force Cambridge Research Laboratories and the Naval Civil Engineering Laboratory. The project consisted of construction, operational evaluation, and scientific study of a sea-ice airfield on North Star Bay near Thule Air Base, Greenland, during January, February, March, April, and May 1961. This summary report of the engineering and scientific program includes a technical discussion of the site selection and engineering aspects of construction activities, together with technical evaluation of operational experience. A variety of scientific and engineering studies of sea-ice strength, mechanical properties, salinity, deformation, and deterioration characteristics were investigated along with the operational tests. Technical reports relating to (a) elastic and time-dependent deformation during aircraft operations, (b) influence of crack patterns on operational use, (c) temperature, salinity, density, and ring tensile strengths of natural and constructed sea ice, (d) stress-rupture data for sea ice, (e) in-place strength tests of sea ice, (f) long-time deformation of ice sheets, (g) elastic properties of sea ice from ultrasonic and dynamic measurements, and (h) ice deterioration are presented.

Successful operational tests of aircraft of different sizes up to and including a B-52 jet bomber indicated that sea-ice platforms can carry heavier loads than has previously been recognized. The major limitation, long-time bearing strength, has been investigated in more detail than previously and can provide a basis for fixing suitable operational requirements for heavy aircraft on sea ice. Parallel investigations of properties by different techniques on the same ice has provided a basis for correlating different types of measurements and deriving necessary operational criteria from them.

In general, this report presents results of individual studies but does not attempt a detailed comparison between them or an evaluation of their relative utility for defining operational criteria.

Contents

Contents (Continued)

Contents (Continued)

Contents (Continued)

Contents (Continued)

Illustrations

Illustrations (Continued)

Illustrations (Continued)

Illustrations (Continued)

Illustrations (Continued)

Tables

Foreword

This is a summary report of the engineering and scientific program of Project ICE WAY conducted from January to June 1961 on the ice of North Star Bay near Thule Air Base, Greenland. The project was a joint activity of the Terrestrial Sciences Laboratory (TSL), of the Air Force Cambridge Research Laboratories, and the Naval Civil Engineering Laboratory (NCEL), US Navy. For TSL, this activity was part of its Project 7628, Arctic Terrain Research Program (now Global Geoscience Studies), under Task 76296, Operational Applications. For NCEL, this work was conducted under Task Y-F015-11-014, North Star Bay Effort, which is a part of the Bureau of Yards and Docks research program on advanced base facilities in polar regions.

The various sections of this report were prepared by individuals who performed the field work. Their results are preliminary at this time, but it is anticipated that more comprehensive technical papers will be published later by the individual participants.

The extent of the work undertaken in Project ICE WAY is described under "Scope," and related work previously accomplished is summarized under "Introduction." A chart of the project organization is given in Appendix A and the names of participants are listed in Appendix B.

Special mention should be made of the contributions of various individuals and organizations assigned to Thule Air Base. The details of the logistics support received are too numerous to mention, but without the enthusiastic cooperation of these individuals and organizations the project could not have been successfully accomplished. The efforts of Col. H. B. Allen, Commander 4683rd Air Defense Wing, and Col. H. W. Jensen, Base Commander, of their staffs, and of the individual men assigned to them who aided the project are very much appreciated. Particular thanks are extended to Lt.Col.B. A. Zohn, Base Civil Engineer, who was the Thule AB Coordinating Officer, Capt. J. A. Pate, his assistant, and the men of the Roads and Grounds Branch of the 4683rd Civil Engineering Squadron who were especially helpful to many varied needs of the project.

Much of the research conducted for Project ICE WAY was sponsored by TSL through various contracts. By contractor and field investigator, they are: Arctic Institute of North America (W. D. Kingery) Contract No. AF19(604)3073, Arctic Institute of North America (D. L. Anderson) Contract No. AF19(604)7403, and McGill University (M. P. Langleben) Contract No. AF19(604)8378.

This report is also distributed as Naval Civil Engineering Laboratory Technical Report R-189.

All photographs in this report are official USAF photos taken by the Technical Photographic Branch, Air Force Cambridge Research Laboratories, except where otherwise noted. Photographers were M/Sgt Bruno Marchesini and Alc Ronald E. Hudson.

SUMMARY REPORT – PROJECT ICE WAY

1. INTRODUCTION (by W.D. Kingery)

1.1 Sea Ice Operations

Almost a third of the frontier of the North American continent faces on the Arctic Ocean. As a result there is a national requirement to be able to operate effectively in an Arctic environment for various operational purposes. To achieve this capability there have been numerous well-coordinated study and operational test programs carried out under the supervision of the Air Force, Army, and Navy. One special aspect of the Arctic environment with which the Air Force and the Navy have been particularly concerned is the sea ice that is always present on the surface of the Arctic Ocean. The Terrestrial Sciences Laboratory (TSL) of the Air Force Cambridge Research Laboratories and the Naval Civil Engineering Laboratory (NCEL) have supported programs related to construction on sea ice, development of superior ice properties, determining the force required to break through sea-ice sheets, understanding the mechanical properties of sea ice, predicting deterioration characteristics during the ablation season, and other aspects of sea-ice engineering and sea-ice properties.

Large-scale Air Force aircraft operations on sea ice first took place during construction of the DEW line during 1955[1] when 932 sorties of C-124 aircraft landings were conducted without difficulties due to ice failure. During 1957 TSL carried out a series of aircraft landing tests on sea ice at North Star Bay, Thule AB, Greenland. Five aircraft landings were made, including F-89, C-124, and KC-97

(Manuscript approved for publication, 19 January 1962)

aircraft. These test landings were considered to be completely successful. In association with this activity, scientific studies of sea-ice properties were also carried out.[2] Although these tests and calculations of probably-safe sea-ice bearing capacity[3] indicated the general usefulness of sea ice for operational purposes, test landings of heavy jet aircraft had not been made, and the load-bearing capacity calculations were inadequate with regard to thick ice and heavy loads. At the same time, investigations of sea-ice strength carried out under Air Force sponsorship indicated the possibility that additions to natural ice could significantly improve its properties such that heavier loads could be safely accommodated. Utilization of artificial flooding techniques and ablation control methods might effectively extend the period of operational usefulness of sea ice in the Arctic environment.

The Naval Civil Engineering Laboratory, Port Hueneme, California, has had a series of programs related to sea-ice construction that have been carried out mostly at Point Barrow, Alaska. Techniques were developed for construction of sea-ice platforms, but these techniques had been tested only on a small scale. Inasmuch as large-scale construction necessarily requires the development of modified techniques, construction of sizeable platforms utilizing sea ice and determining their properties (including load-bearing capacity) was considered desirable. The utility of stable sea-ice platforms in the Arctic Ocean and an understanding of the strength of sea-ice sheets is obviously of great interest for current and potential naval operations on and under the Arctic Ocean.

1.2 Present Status of Sea Ice Engineering (by J.E. Dykins, NCEL)

The first investigation by the Navy in the development of stable sea-ice platforms from which operations could be conducted was undertaken in 1951-52 at Point Barrow, Alaska.[4] To increase strength in an existing ice sheet, experimental techniques were used to thicken the ice sheet with surface layers of ice produced by flooding. A degree of success was achieved in this first effort. A plot of thickened ice approximately 400 feet square was produced. This led to a larger scale operation the following season. This second effort produced a 150-ft by 3000-ft sea-ice runway from which Navy aircraft made successful landings and take-offs. The total thickness of the ice under the runway was about 16 ft. Though this operation was termed successful, many problems were found to exist in the runway as well as the equipment used to produce it. Severe distortion of the ice sheet around the edge of the runway had resulted from the superimposed load of construction ice, causing cracking of the ice in this area and making ingress and egress

from the runway difficult. Large unfrozen areas, described as brine pockets, were found through the construction ice; these caused internal structural weakness.

In 1958-59, after several years of laboratory studies on the properties of sea-ice, a field operation was again conducted at Point Barrow[5] to investigate construction techniques, equipment improvement, construction shape (platform shape), and the effect of varying the depth of the flood layer. The operation resulted in the (1) development of a free-flooding technique, (2) determination that round shapes were best, and (3) conclusion that thin flood layers produced better ice with less construction problems. The following season a larger scale operation was undertaken at the same site to further develop the free-flooding technique and investigate the use of chipped-ice aggregate as a fill material. The culminant results of this operation were (1) chipped-ice aggregate fills have to be saturated with sea water to achieve strength; (2) the free-flooding technique produced the best results of any flooding technique experimented with to date; (3) pump stations could be sustained in the middle of a flooded area; and (4) a tube through which sea water could be drawn to the surface could be permanently set in an ice sheet and kept ice-free. This made it possible to use submersible pumps, which would eliminate many of the pumping problems associated with flooding in the arctic region.

This summary of the investigation and experimental work prior to the planning of Project ICE WAY briefly indicates the progress made in sea-ice engineering. Refinements and development in this field will no doubt be achieved with each new operation.

1.3 Project ICE WAY

Project ICE WAY, as mentioned in the Foreword, was conceived and carried out as a joint program of the Air Force Cambridge Research Laboratories and the Naval Civil Engineering Laboratory. The project was under the overall supervision of Colonel L. DeGoes (TSL) and Mr. Earl Moser (NCEL), with close coordination of the entire program. (The project organization is given in Appendix A.)

The program consisted of selecting a site for an aircraft landing strip and parking pads on North Star Bay near Thule Air Base, Greenland. The selection of the site was done jointly by TSL and NCEL personnel. After the site was selected, NCEL personnel directed and carried out the engineering and construction of parking pads suitable for testing with heavy aircraft. In addition they tested the characteristics of these parking pads during construction, use, and deterioration and participated actively in the operational testing program.

A sea-ice landing strip prepared by personnel of Thule Air Base was used for test landings by C-47, H-21, F-102, C-130, B-47, KC-135 and B-52 aircraft under

the direction of TSL personnel. During these operational tests extensively instrumented measurements were made of the reaction of the ice landing strip to the imposed loads. These instrumented landing tests provided valuable data for evaluating operational utility and at the same time were an essential safety requirement to insure against the remote possibility of ice failure during the tests. Prior to, during, and after these successful operational tests, a variety of scientific observations were made of ice structure, ice properties, and ice behavior under various imposed loads. The final phase of the project consisted of observing the ablation and breakup of the constructed sea-ice structures and immediately adjacent natural ice.

1.4 Engineering and Scientific Program

One of the major purposes of Project ICE WAY was to obtain sufficient engineering and scientific information during the construction, evaluation, operational testing, and deterioration of natural and constructed sea-ice platforms to provide more accurate criteria necessary for sea-ice operations and planning future Arctic test programs. The scientific program, with Dr. W. D. Kingery as Principal Investigator, included participants from TSL, NCEL, Arctic Institute of North America, Navy Electronics Laboratory, and associated contractor personnel. The engineering program, with J. E. Dykins as Chief Engineer, was undertaken by NCEL. Individual investigators carried out coordinated programs designed to (a) determine the relative value of different methods of evaluating ice characteristics, (b) determine the critical factors affecting the use of sea ice as a structural material, (c) evaluate the effectiveness of additions to increase strength, and (d) provide a sound basis for determining safe loads suitable for sea ice of various kinds. In the present report, individual investigators have summarized their main findings, some of which are preliminary. These investigators will prepare more detailed reports to be issued as separate scientific reports.

Subsequently, it is hoped that a comparison of the different detailed reports will allow general conclusions to be made as to sea-ice utilization.

2. SCOPE (by W.D. Kingery)

The scope of the engineering and scientific program associated with Project ICE WAY consisted of (a) preparing a suitable landing strip and parking pads for testing, (b) carrying out operational testing and evaluation, and (c) determining characteristics of sea ice independently of operational testing as a guide toward fixing ultimate capabilities and predicting requirements for future proposed operations.

2.1 Scope of the Engineering Program

The engineering program consisted of laying out and constructing four separate areas which could be utilized as parking pads by heavy aircraft or test areas for material evaluation. The construction techniques consisted of free-flooding methods using equipment developed from previous tests at Point Barrow, Alaska. In some cases Fiberglas-reinforced areas were built to test the effectiveness of Fiberglas reinforcement. Complete observations were made of the effectiveness of construction techniques, suitability of equipment, rate of ice build-up, and equipment and manhours required for the various techniques. In addition characteristics of the sea-ice product - including strength, density, salinity, and temperature - were continuously monitored during the construction in order to provide a sound basis for evaluating the characteristics of the product. After the operational tests were completed, the ablation and deterioration characteristics of the constructed ice were compared with natural ice in the same vicinity.

As a result of this program, it was anticipated that the entire engineering requirements for the layout, construction, and characteristics of operational sea-ice platforms under field conditions would be determined so that suitable techniques would be known and available for any future operational requirements.

2.2 Scope of the Operational Testing Program

The operational testing program consisted of instrumented landing, taxiing, and parking of a series of operational aircraft on the sea-ice landing strip, natural sea-ice parking areas, and specially constructed parking pads. The aircraft included high-landing-speed fighter aircraft as well as the largest aircraft in the Air Force inventory. During this testing program the ice was instrumented and pilot reaction to the sea-ice landing strip was obtained. As a result, a complete evaluation of

the operational capabilities of the sea-ice landing strip and parking areas with a wide variety of aircraft could be achieved. Definite conclusions as to the capability of sea ice for operational use by aircraft were a major aim of the project.

2.3 Scope of the Scientific Program

A substantial part of the difficulty of fixing requirements for operational use of sea ice has been inadequate information as to sea-ice properties. Thus, adequate recommendations could not be made as to its capability for load-bearing capacity in terms of ice thickness required, time of load bearing required, weight of aircraft landed, and so forth. Answering these questions required a better understanding of sea-ice property limitations and a better understanding of testing techniques. A major portion of the scientific program was concerned with evaluation of mechanical behavior of sea ice under conditions ranging from high-frequency elastic tests to long-time creep deformation studies. These measurements were carried out with special apparatus utilizing necessary loads including heavy aircraft during operational tests. In addition to and in parallel with these tests, a comparison between different methods of measuring strength was carried out utilizing ice formed and tested under similar conditions. This provided a direct comparison between results obtained by investigators using different test methods. Ice temperature and salinity and their variations with time are also evaluated to better understand the characteristics of sea ice and provide a reliable basis for determining sea-ice capabilities.

REFERENCES

1. "Summary Report on Project 572 for 1955." 3 vol., Hq, 18th Air Force, TAC (Aug 1955).
2. DeGoes, L., W. F. Weeks, D. L. Anderson, "Aircraft Landing Tests on Sea Ice in North Star Bay, Thule, Greenland, March 1957," GRD-TM-57-20, Geophysics Research Directorate, Air Force Cambridge Research Center (17 June 1957).
3. Assur, A., "Air Fields on Floating Ice," SIPRE Report 36, U.S. Army Corp of Engineers (1956).
4. "Sea-Ice Bases," TP-P1-16, U.S. Navy Bureau of Yards and Docks, Washington, D.C. (Jan 1955).
5. Dykins, J.E., and A.I. Funai, "Point Barrow Trials - FY1959, Investigations on Thickened Sea-Ice," NCEL TR-185, Naval Civil Engineering Laboratory, Port Hueneme, Calif. (to be published, 1962).

3. SITE SELECTION (by D.W. Klick)

3.1 Introduction

From a logistics standpoint and because it had been a satisfactory site for similar tests in 1957, North Star Bay at Thule, Greenland was considered the most suitable location for field operations of Project ICE WAY. Thule Air Base could then be used as a staging base.

The project site was chosen in late (22-26) January by Dr. Kingery, Mr. Hansen, and Capt. Klick. The site consisted of three elements: four parking and materials testing pads, a field camp, and an 11,000 ft by 300 ft runway shown in Figure 3.1. The darkness of the long winter limited extensive exploration, but the site as selected proved to be satisfactory in all respects.

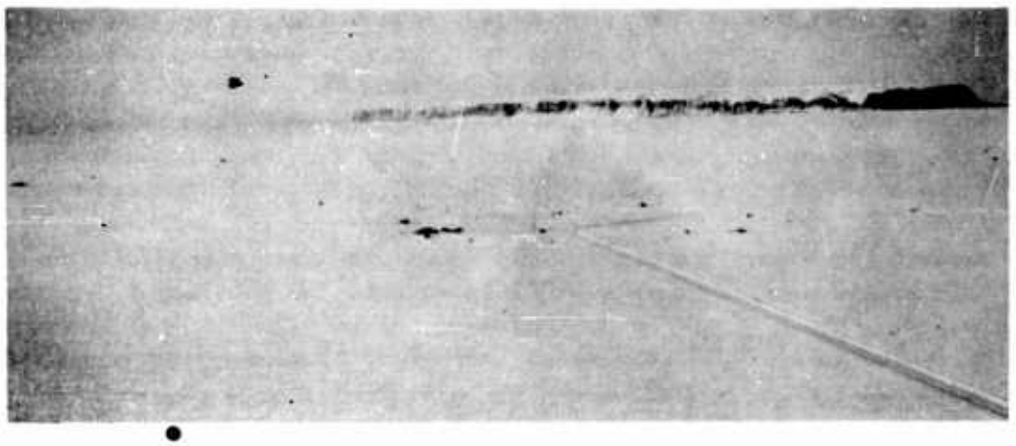

FIG. 3.1. Aerial view of project site looking west; camp and one parking pad to left of access road; two parking pads and test pit to right of access road; access road in lower right.

3.2 Criteria Used

The parking and materials testing pads and the field camp were to be sited in a group to facilitate construction and operational testing. They were to be located at the shoreward end of the runway to take advantage of the thicker ice.

The runway was to be located in a region of maximum ice thickness but no closer to the shore than 550 ft. This distance would place the site at least twice the influence

radius distance from the shore as recommended in Air Force Manual 86-5, Ice Airfields. In addition the runway was to be oriented to provide clear approaches for unobstructed landings and takeoffs.

Both the pads and the runway were to be located in areas requiring minimum surface preparation. It was hoped that little more than grading to remove snow would be required. Areas containing sastrugi and ice chunks frozen into the surface were to be avoided if possible, and the entire project site was to be free of wet cracks.

Because the project site for the aircraft landings in 1957 proved satisfactory, it was decided to investigate this area first. If this site met the criteria noted above, no further exploration would be conducted because the darkness limited extensive exploration of all likely areas.

3.3 Methods of Survey Employed

Surface exploration by weasel and on foot were the primary methods of survey employed in the selection of the project site. Two aerial flights by helicopter were also made. Although they were useful for preliminary low-altitude reconnaissance, the helicopters could not be utilized to a greater extent for two reasons. First, darkness prevented aerial visual reconnaissance at high enough altitudes to adequately reconnoiter large areas; and second, the pilots did not want to land on the ice for detailed surface reconnaissance because the surface was unfamiliar to them.

Three trips were made over the ice by weasel, one each on 22, 25, and 26 January. The first trip was an exploratory one along the coastline to examine the short and extensive tidal crack for an access road from Thule Air Base to the project site.

The second trip was a traverse over several specific areas, mainly in the vicinity of the 1957 site, which had looked fairly smooth and clear of icebergs during the helicopter flights on 23 and 24 January. Several hours were spent in examining the surface, looking for cracks, and taking ice thickness and snow depth measurements in each of the areas.

From data obtained during the flights and traverses, a rough map showing the location and characteristics of each area was drawn. The more promising areas were revisited on the third weasel trip and the project site was then selected.

3.4 Site Location and Layout

Figure 3.2 shows the Thule area and the general location of the project site, while Figure 3.3 presents in more detail the location of the site and the runway in North Star Bay. The location and centerline of the runway were determined accurately

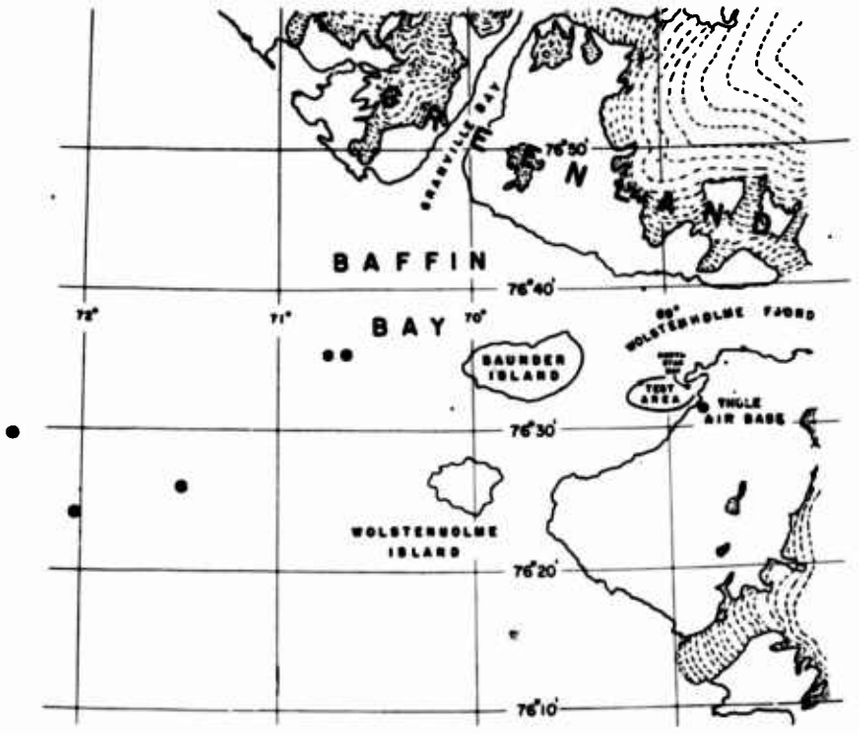

FIG. 3.2. Map of general Thule area

with an engineering transit, and the locations of the pads were set from the east end of the runway centerline.

The point on the centerline at the east end of the runway was determined by the intersection of bearing lines from two points on Thule Air Base — the north corner of the seaward end of DeLong Pier and the northwest corner of Hangar 1. The intersection was plotted on an AMS 1:25,000 scale map and the point was measured to be at 76° 31' 50" N latitude and 68° 56' 30" W longitude.

About 1500 ft of overrun extended to the east of this point. To the west of this point the runway extended for 11,000 ft along a centerline measured to bear 271°22' true. This bearing is 5° 52' more than the true bearing of the main runway at Thule Air Base. Beyond the west end of the runway there was an overrun area about 1500 ft long.

The pads and field camp were clustered around the east end of the runway. For locations of these elements see Section 4.

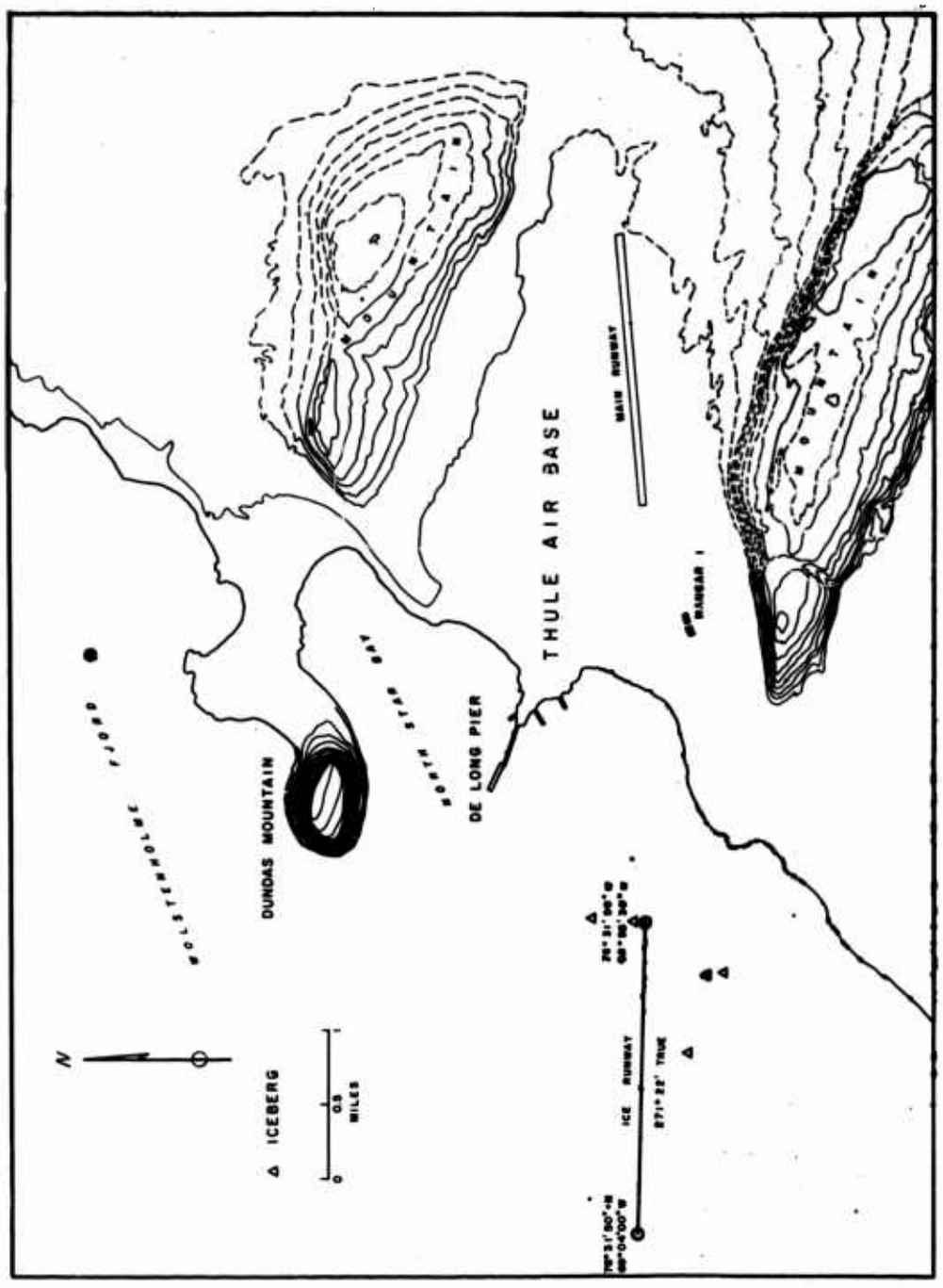

FIG. 3.3. Map showing location of site on North Star Bay

From the east end of the runway, the closest point of land was 3/4 mile to the southeast, the access road extended for 1-3/4 miles to the shore, and Delong Pier was 1-1/3 miles away.

3.5 Virgin Condition of Site

Figure 3.4 shows the entire site was characterized by a thin layer of snow over the fairly smooth ice sheet. The snow depth in the area of the east end of the runway at the pads and field camp varied from 3 to 5 inches, and it thinned out along the runway to 1 to 3 inches at the west end. The snow was quite firm and had a thin surface crust. An individual on foot would not break through this crust at many places, and when he did only a faint trace of a footprint would be made.

Around the east end of the runway and at several spots along the runway the generally smooth snow surface was marred by the protrusion of small bits of ice which had frozen in the surface (Figure 3.5). These areas were not sufficiently large to hinder the location of the pads and the camp in smooth areas, and they were graded down along the runway. It is assumed that such areas existed throughout the entire bay since they were undoubtedly caused by the freezing, breaking up, and refreezing of those areas during freeze-up the previous fall.

There were small scattered areas throughout the site where slight barchan drifts existed. They accounted for the variance in snow depth. This type of sastrugi was noted over a much wider area to the south of the runway closer to shore. The surface of the ice sheet was fairly smooth in general but was pitted from a sand-blasting action by the wind and snow. This condition was not detrimental; it was actually of some aid in providing greater traction for the aircraft and vehicles.

Only one crack was noted at the time the site was selected — a dry tidal crack about 3 inches wide running transverse to the runway several hundred feet west of the east end. There undoubtedly were more cracks but the snow cover hid them.

There were four icebergs in the general area of the site but only one was in the immediate vicinity (Figure 3.3). It was about 10 ft high and located between the two pads to the north of the centerline about 350 ft off the runway.

3.6 Other Suitable Sites in North Star Bay and Adjacent Areas

On 16 March Capt. Klick flew in an L-20 to survey North Star Bay and adjacent areas (Figure 3.6) for other sites that might be suitable for aircraft operations. Since no landings were made, ice thicknesses and detailed surface conditions were not determined, but apparent surface smoothness and extent of cracks and iceberg fields were observed. The flight was made at various altitudes up to 2000 ft.

All of North Star Bay and the ice west to a line between Saunder Island and Cape Athol were relatively free of icebergs and, except along the shores, seemed smooth.

FIG. 3.4. Natural surface condition on bay showing smooth snow cover over ice; view west

FIG. 3.5. Portion of rough area in vicinity of runway; ice chunks frozen into surface; small areas like this were scattered throughout bay; view northwest

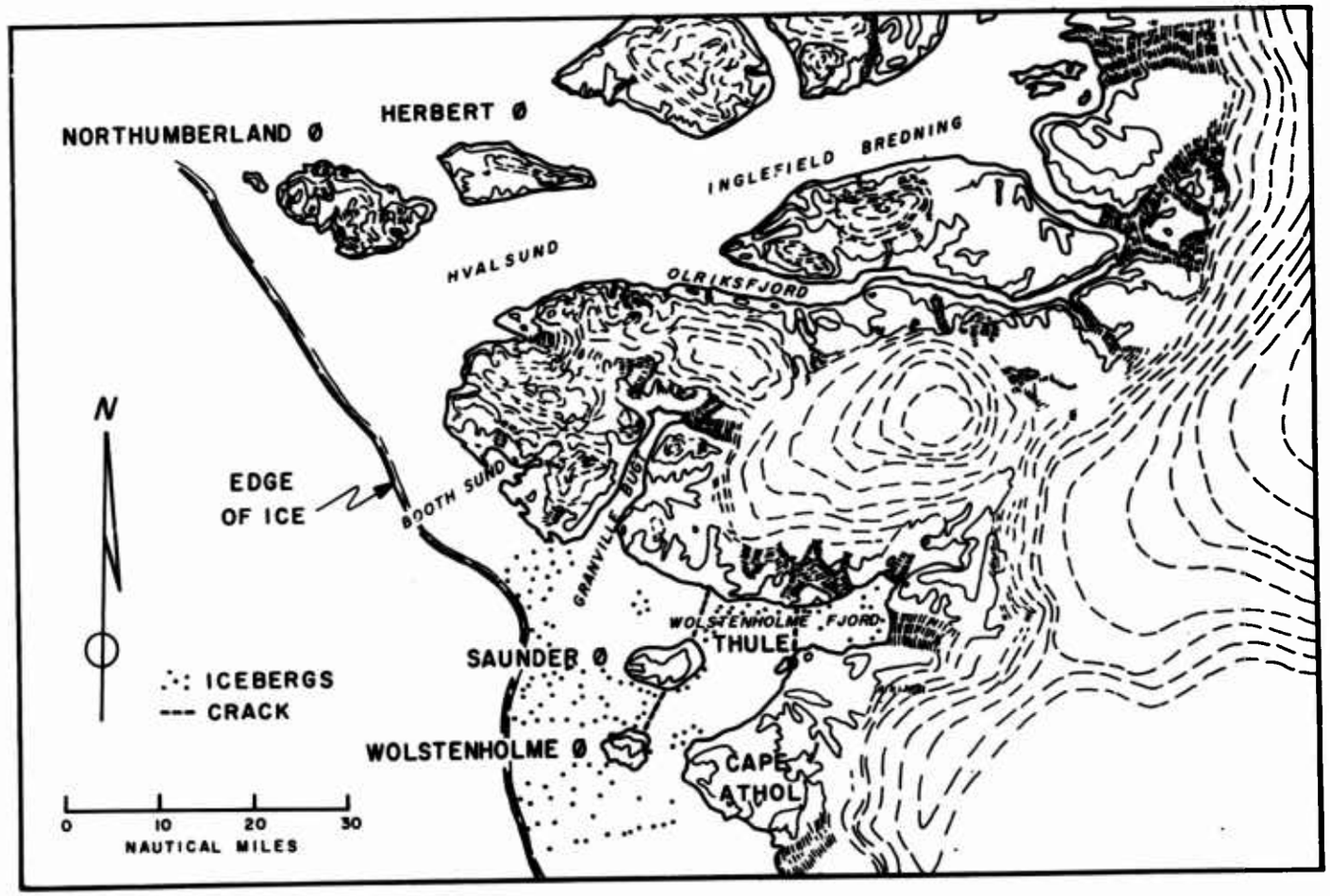

FIG. 3.6. Map of areas adjacent to Thule

West of this line, particularly south of Wolstenholme Island and west of Saunder Island, there were a great many icebergs. The flight did not extend south of the Coast Guard station at Cape Athol.

Almost all of Wolstenholme Fjord seemed suitable for operational sites. There were quite a few icebergs but they were at the head of the fjord and along the north shore. There were a few icebergs between shores but they were scattered and the surface appeared to be exceptionally smooth. There were indications of a tidal crack at the bottom of the bottom of the fjord.

This clear area ended at a line extending northeast from Saunder Island to Cape Abernathy or slightly east. There were many icebergs and a large crack in this region. Except for one small field, the area north of Saunder Island was relatively free of icebergs and quite smooth. However, an iceberg field appeared northwest of Saunder Island, extending out to sea.

Granville Bay was entirely free of icebergs and seemed to be smooth. The flight did not extend farther north than the mouth of the bay, so surface conditions could not be evaluated more accurately. The pilot reported, however, that he had flown over Hval Sound to the north and that this large area appeared to be more clear of icebergs than any other areas he had seen. He also reported that he had seen open water about 10 miles west of Wolstenholme Island and that the edge of the ice edge extended off in a north-northwesterly direction.

3.7 Conclusions

The site selected for the project had no serious drawbacks and was considered satisfactory in all respects. After daylight appeared, it was obvious that there might have been several areas just as suitable. The entire bay contained just a few scattered icebergs and much of the surface appeared to be smooth. However, ice thicknesses decreased away from shore and would limit loading weights on sites farther from the coast.

More intensive investigations of surface conditions and ice thicknesses would be required to evaluate North Star Bay and adjacent areas, but preliminary observations indicated that a number of sites would be available for aircraft operations. There were extensive areas free of icebergs and cracks, and the wind would have kept these areas free of excessive snow accumulation. Ice thicknesses would be the controlling factor in determining the use of these areas.

4. PARKING APRON CONSTRUCTION (by J.E. Dykins, NCEL)

4.1 Introduction

In Project ICE WAY, NCEL assumed as its main responsibilities the provision and operation of camp facilities and the construction of aircraft parking aprons. To accomplish these, a technically-trained arctic construction team was outfitted with equipment developed for such work.

Three parking aprons were built, each constructed by a different technique selected for its potential value as determined from previous experimental field work. The techniques selected were:

a. The NCEL wet-fill, free-flooding technique
b. A free-flooded fill reinforced with a Fiberglas technique developed under AFCRL sponsorship
c. A chipped-ice-aggregate fill reinforced with Fiberglas

The parking aprons were located adjacent to the proposed sea-ice runway for easy access by aircraft. As such, they could be load-tested by parked aircraft and also provide a safety zone should the heavier aircraft cause failure conditions in the thinner, unreinforced, natural ice runway.

In addition to the three parking aprons, two small test plots were built, duplicating the construction technique used in the two Fiberglas-reinforced aprons. They provided an area for conducting in-place beam tests since these could not be performed on the thicker ice of the aprons. All parking apron construction was completed by 1 March. The average air temperature for the construction month (February) was -29°F.

Because of the length of the project and an effort to utilize a minimum of manpower, the personnel were on an overlapping schedule of arrival and departure. In addition to the engineering personnel, there were four to six skilled tradesmen who were proficient in the techniques of ice construction.

Construction of all aprons was simultaneous; but, because of the somewhat adverse field conditions, precise records were not kept of manhours for each operation. The available records, however, support the construction time estimates for each construction area.

4.1.1 TERMINOLOGY

This section introduces to the unfamiliar reader the terminology, and briefly describes the procedures used to construct in sea ice.

Liquid or wet fill. This term is applied to the type of construction in which an ice sheet is built up or thickened by flooding the surface with a relatively thin layer of water and allowing it to freeze before adding the next layer. The water is pumped from beneath the existing ice sheet.

Free-flooding. This term is applied to a specific technique for placing liquid-fill layers. In this technique, the floodwater is allowed to flow freely in all directions from the discharge point. Dams or dikes are not used to control the shape of the flood area. The size and shape of the area to be thickened is accomplished by directional control over the pump discharge, and by taking advantage of the rapid freezing which occurs at the flood boundary. An area thickened by this technique is most easily produced as an oval or circular shape. The profile of this build-up can be described as a convexo-plane shape, the convex surface lying at the interface of the original natural ice-sheet surface. Though described as a plane, the upper surface of the free-flooded area has a slight crown; otherwise, its surface remains at nearly the same elevation as the surrounding unflooded ice sheet. Since the ice sheet is floating, this difference in elevation is a function of the thickness of the flooded ice area. For free-flooding, an optimum individual flood depth of 4 inches is most satisfactory. In Project ICE WAY each flooding was followed by a curing cycle of sufficient length to allow the layer to freeze. In air temperatures of -10°F or below, a curing cycle of 40 to 48 hr was generally sufficient.

Dry fill. This term is applied to sea-ice construction in which the build-up or thickening of the ice sheet is produced by adding lifts of chipped-ice-aggregate to the surface. To bond the aggregate and make it stronger, it is saturated with sea water. The most satisfactory individual fill depth for this technique is between 4 and 6 inches.

4.2 Camp and Ice Runway Layout

All personnel were berthed and messed at Thule Air Base. However, for the construction effort, a base camp was established on the ice sheet about 1-1/4 miles from shore adjacent to the test area. Most of the structures and materials for this camp and the construction effort were air-lifted from continental United States; fuel and other bulk material were furnished by the Thule Air Base.

Basically, the camp (Figure 4.1) consisted of a 16 ft by 32 ft Jamesway structure used as a headquarters building, two wanigans used as cold-room laboratories, and two instrumented mobile trailers used for test work. When the operation was completed, the camp was dismantled and removed from the ice.

The Jamesway, which was erected at the site, had been modified from the standard version by adding perimeter panels, 2 ft in height, between the floor panels and the arched ribs. This increase in ceiling height made the interior space more usable. The building was outfitted with two 30,000 Btu space heaters, a desk, work benches, and coffee mess. It served as a data recording and reduction center, a crew warmup and briefing area, a repair area for small equipment, and a briefing area for visitors.

One of the wanigans was the standard NCEL 10 ft by 20 ft type with a heavy-duty floor and skid system. Shipped dismantled, it was assembled inside a hangar at Thule AB and towed to the camp site. The other wanigan was an 8 ft by 20 ft sled-mounted structure loaned by Thule AB; it was also towed to the camp site.

The two instrument trailers were shipped assembled and outfitted with most of the instruments and test gear to fulfill their function. The smaller of the two trailers was a lightweight 5 ft by 8 ft plywood structure mounted on a light sled of 1-ton capacity. (See Figure 4.2) It provided the necessary laboratory for testing small ice samples extracted from the various test plots under the micro-sampling program. The other instrumented trailer was used in conjunction with the ice dynamic test phases including aircraft landings. It was a commercial house trailer 8 ft by 15 ft, mounted on the normal rubber-tired axle (Figure 4.3). The interior was tailored to receive the electronic instrumentation used for the dynamic testing. A 2.5-kw generator, on its own mount, accompanied this trailer to permit independence from the camp power supply. In use, the trailer was located some distance from the camp and along the edge of the cleared runway.

The road from the base to the camp was a well-maintained over-ice route, and rubber-tired and weasel-type vehicles were used for commuting. The road was well flagged for easy identification during bad weather. The only rough portion, and that requiring the most maintenance, was the short stretch of ice which was affected by tidal action adjacent to the shore line.

Figure 4.4 shows the final layout of the test areas and runway. Except for a slight alteration in the apron configuration (to allow a greater area for orienting the runway), the final layout was as originally planned. Inadequate daylight delayed determination of the best orientation for the runway until later in the season.

4.3 Free-Flooded Parking Apron

4.3.1 CONSTRUCTION TECHNIQUE

This parking apron, designated as No. 1, was constructed by the free-flood technique described in Section 4.1.1. It was planned to have a diameter of

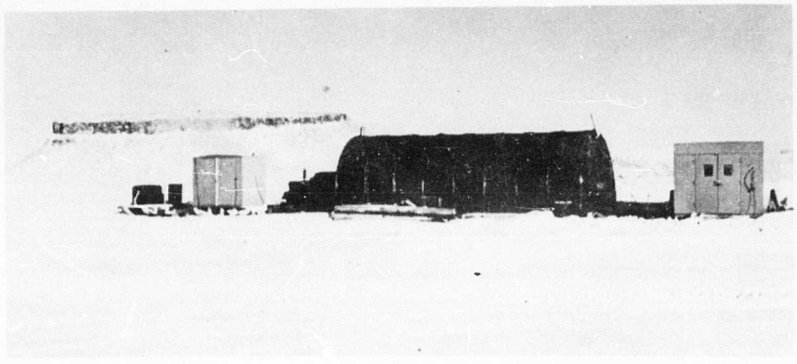

FIG. 4.1. Project ICE WAY camp on ice sheet about 1-1/4 miles from shore

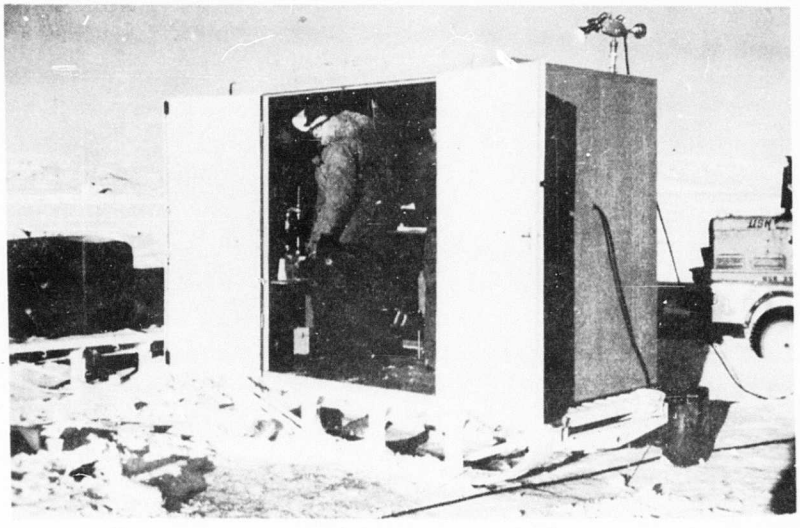

FIG. 4.2. Sled-mounted mobile laboratory used in micro-sampling (official photograph, U.S. Navy)

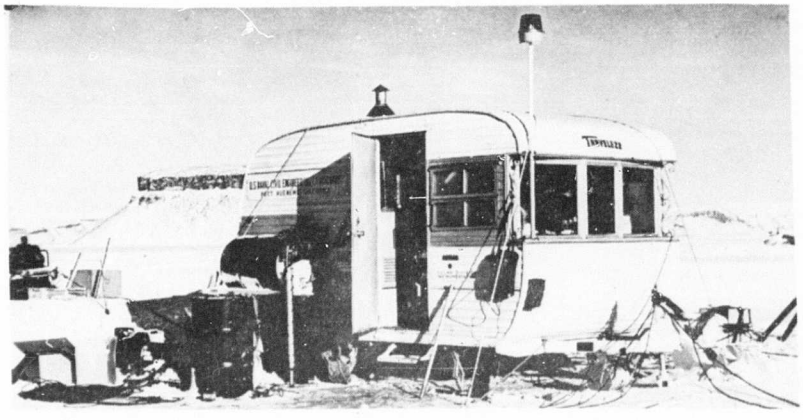

FIG. 4.3. Instrument trailer used in dynamic testing of the ice

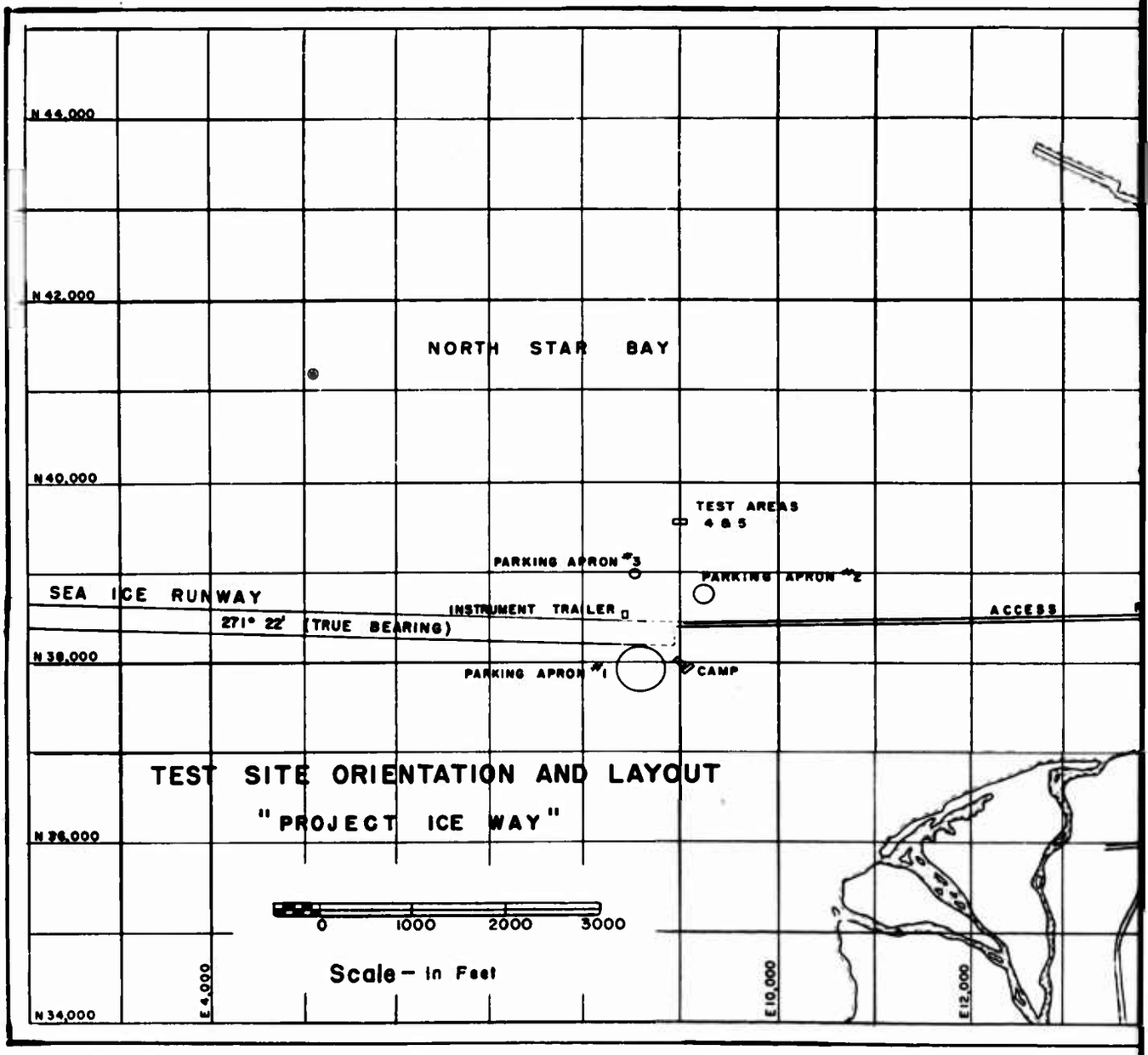
N 44,000
N 42,000
NORTH STAR BAY
N 40,000
TEST AREAS 4 & 5
PARKING APRON #3
PARKING APRON #2
SEA ICE RUNWAY
INSTRUMENT TRAILER
ACCESS
271° 22' (TRUE BEARING)
N 38,000
PARKING APRON #1
CAMP
TEST SITE ORIENTATION AND LAYOUT
"PROJECT ICE WAY"
N 36,000
0 1000 2000 3000
Scale – in Feet
N 34,000
E 4,000
E 10,000
E 12,000

1

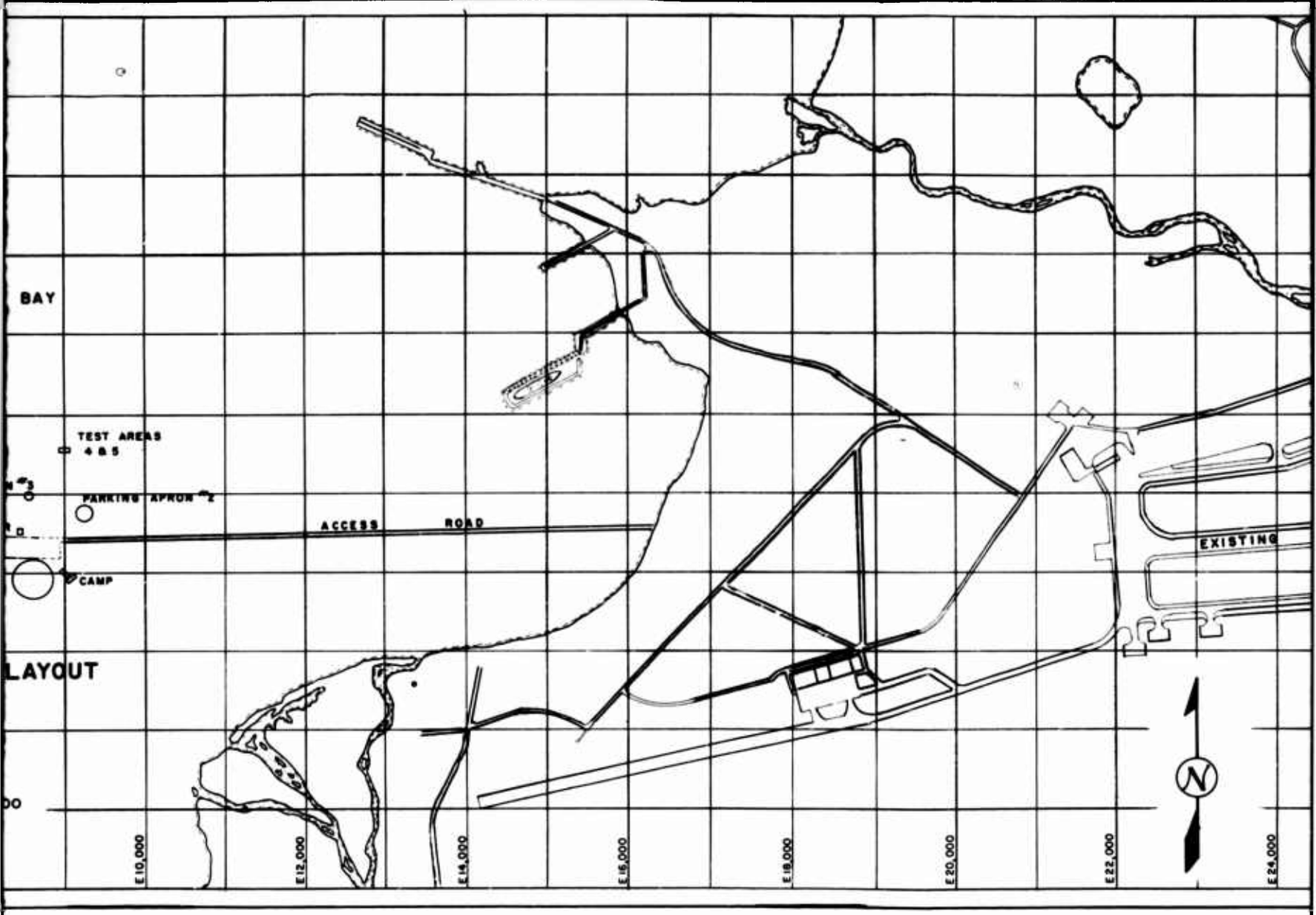
BAY
TEST AREAS
4 & 5
PARKING APRON
ACCESS ROAD
CAMP
EXISTING
LAYOUT
E10,000
E12,000
E14,000
E16,000
E18,000
E20,000
E22,000
E24,000
N

2

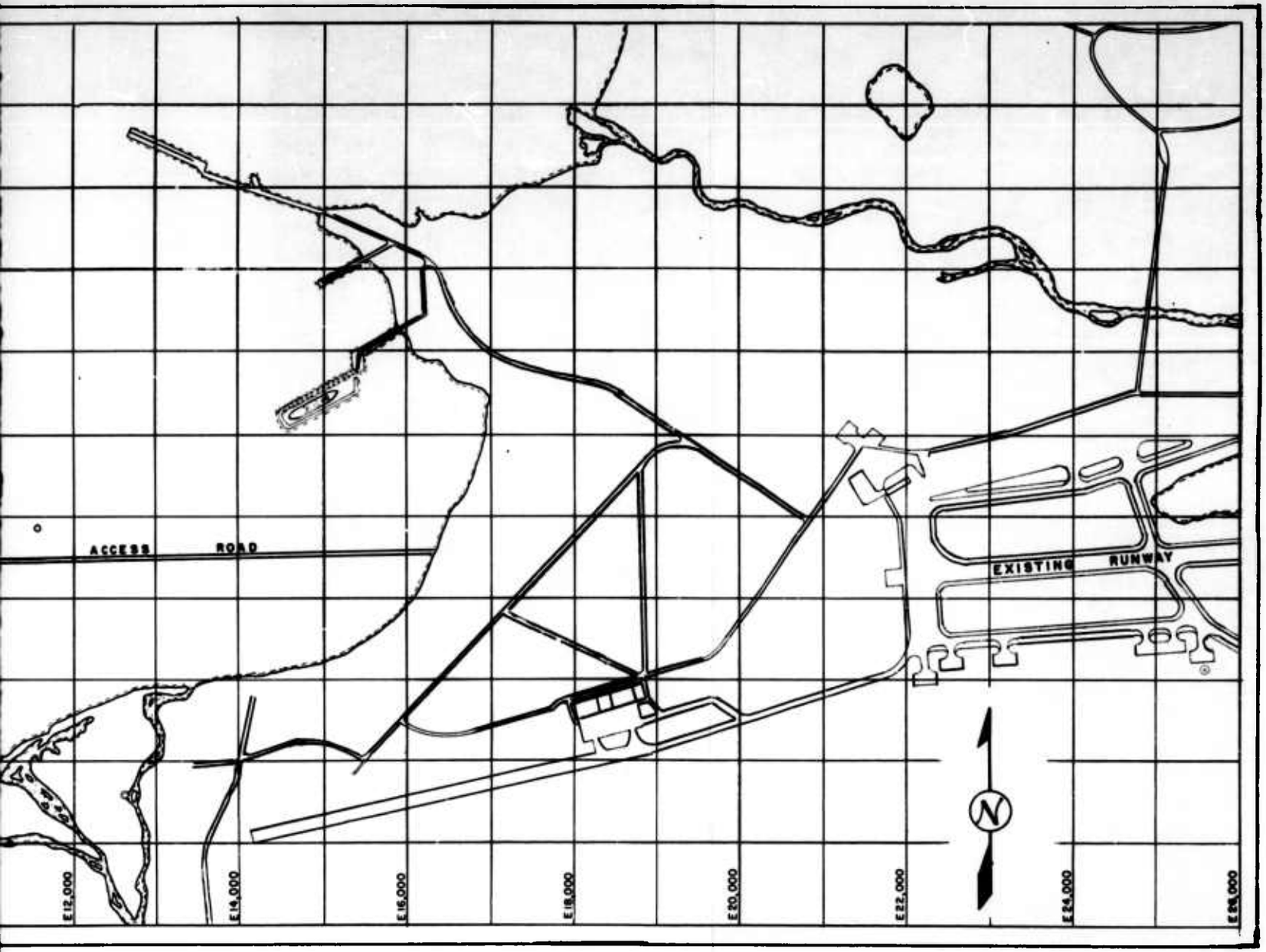
ACCESS ROAD
EXISTING RUNWAY
N
E12,000
E14,000
E16,000
E18,000
E20,000
E22,000
E24,000
E26,000

3

4.3.3 EQUIPMENT USED AND ITS SUITABILITY

An electric-motor-driven submersible pump was used for the flooding. However, because of a shipping delay, an alternate pump was used for the first four floodings. The alternate unit was a diesel-driven centrifugal pump with a rated delivery of 600 gpm. For this construction, the pump was located adjacent to the apron, and the water was discharged at the center of the area through a 4-inch aluminum irrigation pipe. The general operation of the pump was satisfactory except that the discharge pipe tended to gradually freeze shut; therefore, the pipe was placed in warm storage to thaw when not in use.

The submersible pump with a rated delivery of 1500 gpm was used for the fifth and subsequent floodings. It was a low head, electric-motor-driven, pusher-type pump with the motor close-coupled to the pump, and the complete unit was submerged in the water. The water was delivered to the surface through a 6-inch discharge tube which was shrouded by a 16-inch aluminum casing (Figures 4.5 and 4.6). The pump was frozen into the ice sheet at the center of the parking apron and left in place until the construction was completed.

Electrical energy to the pump was supplied by four multistrand, single-conductor insulated cables. The cables were laid directly on the ice surface from the pump station to the generator some 400 ft away, and were buried in the overflood. A 15-kw gasoline-engine-driven generator located in the camp was used to energize the pump.

From all aspects — handling, installation, operation and recovery — the 850-lb, electrical submersible pump was found to be exceptionally well adapted to the free-flood technique of construction. Its operation was trouble-free and its light weight, much less than previous pumps used for free flooding, reduced the time and effort required for installation and recovery. Also, many of the equipment problems associated with previous flooding efforts in the arctic were eliminated. These included: (1) engine cold-starting; (2) pump priming; (3) lay and recovery of discharge hose; and (4) daily maintenance of a well through the ice for the flood water.

4.3.4 ICE BUILD-UP ACHIEVED

Investigation after the parking apron was completed indicated it had assumed the typical configuration associated with free flooding. In plan, the apron had a circular shape, roughly 650 ft in diameter. From all appearances the apron

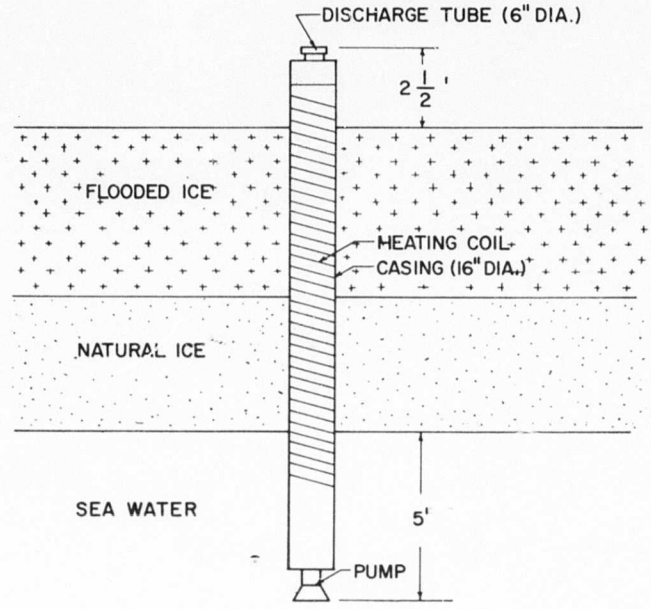

FIG. 4.5. Schematic of 15-1/2 ft long electrical submersible pumping unit

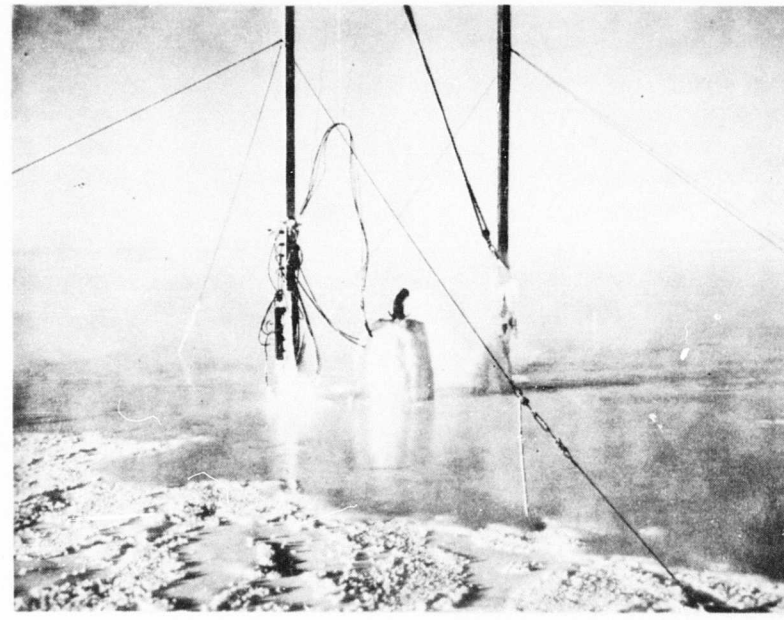

FIG. 4.6. Submersible pump in operation (official photograph, U.S. Navy)

looked perfectly flat and at equal elevation with the surrounding ice sheet; however, a survey showed it to be crowned 0.5 ft at the center.

The deflection stakes showed a 47-inch build-up of ice at the center. At the 250-ft radius points, 9 and 11-1/2 inches were the respective build-up of new ice. The total thickness of the apron at the center, including the natural ice sheet was 94 inches. Figure 4.7 shows the contours and profile of the apron, and Figure 4.8 shows the finished surface.

Using an average ice-sheet thickness of 35 inches before the start of construction, site personnel found that the natural ice growth at the center of the apron in the 40-day construction period was about 8 inches. There was a general increase in growth of the natural ice thickness toward the edges of the apron. Just outside of the apron the growth in natural ice thickness was about 14 inches during the construction period.

During construction two cracks appeared in the apron (Figure 4.9). As neither of these was wet, it was assumed that they were confined to the upper section of the ice. It was further assumed that they were sealed as new flood lifts were added to the apron. The last crack to develop in the apron (Figure 4.9) occurred on 8 March, or about a week after completion. It was about 1/2-inch wide at the surface and about 36 inches deep. This crack remained unchanged during the test phase. No apparent problems resulted from the cracks.

4.3.5 MANHOURS REQUIRED FOR CONSTRUCTION

About 160 manhours were spent in constructing Parking Apron No. 1. This included leveling the snow cover, installing, operating and removing the pumps, and service time for the electric generator.

The construction time would have been reduced by 25 manhours if the electric pump had been available for the entire construction period. The total pumping time for both pumps was 52 hrs.

4.3.6 RECOMMENDATIONS FOR FUTURE OPERATIONS

Though the free-flood technique of ice construction has been successful to date, a continued effort should be made to refine the technique and its associated equipment. Of particular interest would be a large-scale operation requiring the use of multiple pump stations.

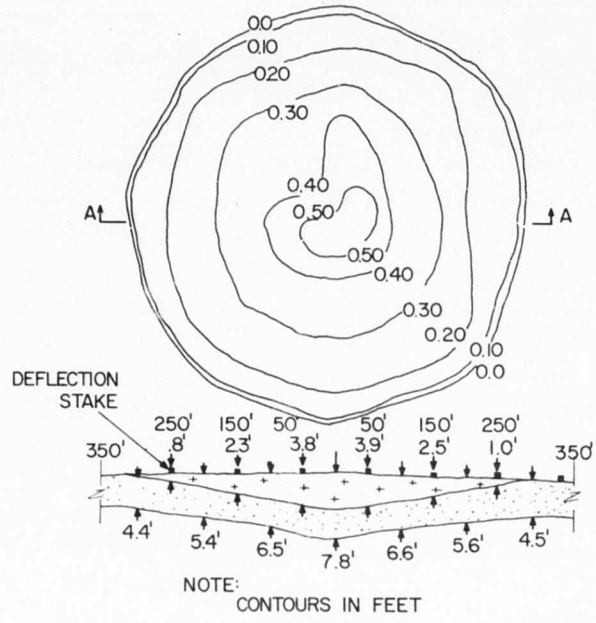

FIG. 4.7. Surface contours and vertical profile of Parking Apron No. 1

FIG. 4.8. Surface of Parking Apron No. 1 after completion (official photograph, U.S. Navy)

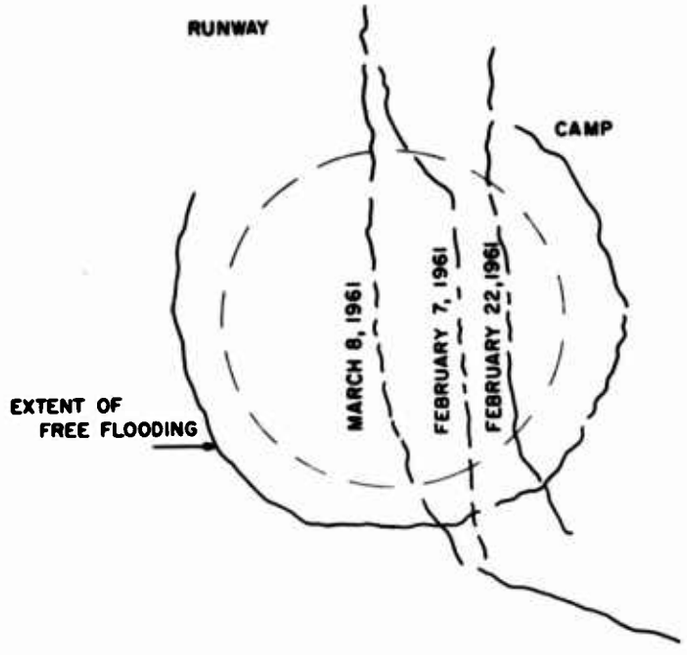

FIG. 4.9. Crack pattern developed during and after construction of Parking Apron No. 1

4.4 Reinforced, Free-Flooded Parking Apron

4.4.1 CONSTRUCTION TECHNIQUE

This parking apron, designated as No. 2, was constructed by the free-flooding technique, but differed from Apron No. 1 in that it was reinforced with a layer of Fiberglas at both the bottom and top of the flooded ice. It was planned to build up a 200-ft diameter area of flooded ice 2 ft thick at the center. Floodings were scheduled for 4-inch lifts with a 48-hr freezing cycle. The pump station was located outside of the apron area, and the water was piped to the center of the area for discharge.

The snow cover was removed from the construction area to lay the Fiberglas, and snowfall greater than 1/2-inch deep was removed during construction.

4.4.2 CONSTRUCTION SCHEDULE

The apron was to be completed by the first week in March to allow a minimum curing period of two weeks before the start of the dynamic tests.

Preparation of the area for flooding consisted of: (1) removal of the snow cover; (2) laying the Fiberglas reinforcement; (3) installing deflection stakes; and (4) instrumenting the ice with thermocouples.

The snow cover that was removed from an area about 250 ft in diameter was spread over a wide area to minimize drift accumulation. Measurements showed the ice to be reasonably flat and level. No prominent cracks were observed in the cleared surface.

The bottom layer of reinforcement (Figure 4.10) was placed on 3 February and consisted of three thicknesses of 1-1/2 oz/ft^2 Fiberglas matting. This material was 8 ft wide and about 3/16-inch thick. It was rolled out in place with a 2- to 3-inch overlap between individual runs. Each layer of matting was laid 90 degrees to the previous layer.

For the bottom layer of reinforcement, the area was flooded with 1-1/2 inches of water and the matting was laid directly in the water. (See Figure 4.11.) In addition, each layer was sprayed after placement for complete saturation. This method presented several problems. The floodwater turned to slush ice before all the matting was in place, thus nullifying it as a saturant. When the matting was wet it was easily torn and stretched out of shape, resulting in an uneven surface. To smooth out the matting an attempt was made to roll it flat with a small steel roller towed behind a weasel. This was soon abandoned because of the additional damage it was causing. The high spots were finally saturated with additional floodwater. Consequently the 2-inch layer of reinforcing became 4 inches thick.

A 116-hr freezing period was allowed for the reinforced layer. Following this, the first flooding was made on 8 February and the seventh and final flooding was made on 23 February. The average freezing cycle between floodings was 44 hrs.

The top single layer of Fiberglas mat was placed on the apron 130 hrs after the final flooding. A revised technique for laying the Fiberglas resulted in a smooth, wrinkle-free surface. Furthermore only 1 inch of water was required to saturate the mat. This was accomplished as follows: the Fiberglas was laid out on the dry ice surface, and then sprayed with water until it was saturated. Complete saturation was denoted by a color change in the Fiberglas. This method of laying the mat had one major drawback. Fairly calm weather was necessary because the unsaturated matting was easily whipped around by the wind.

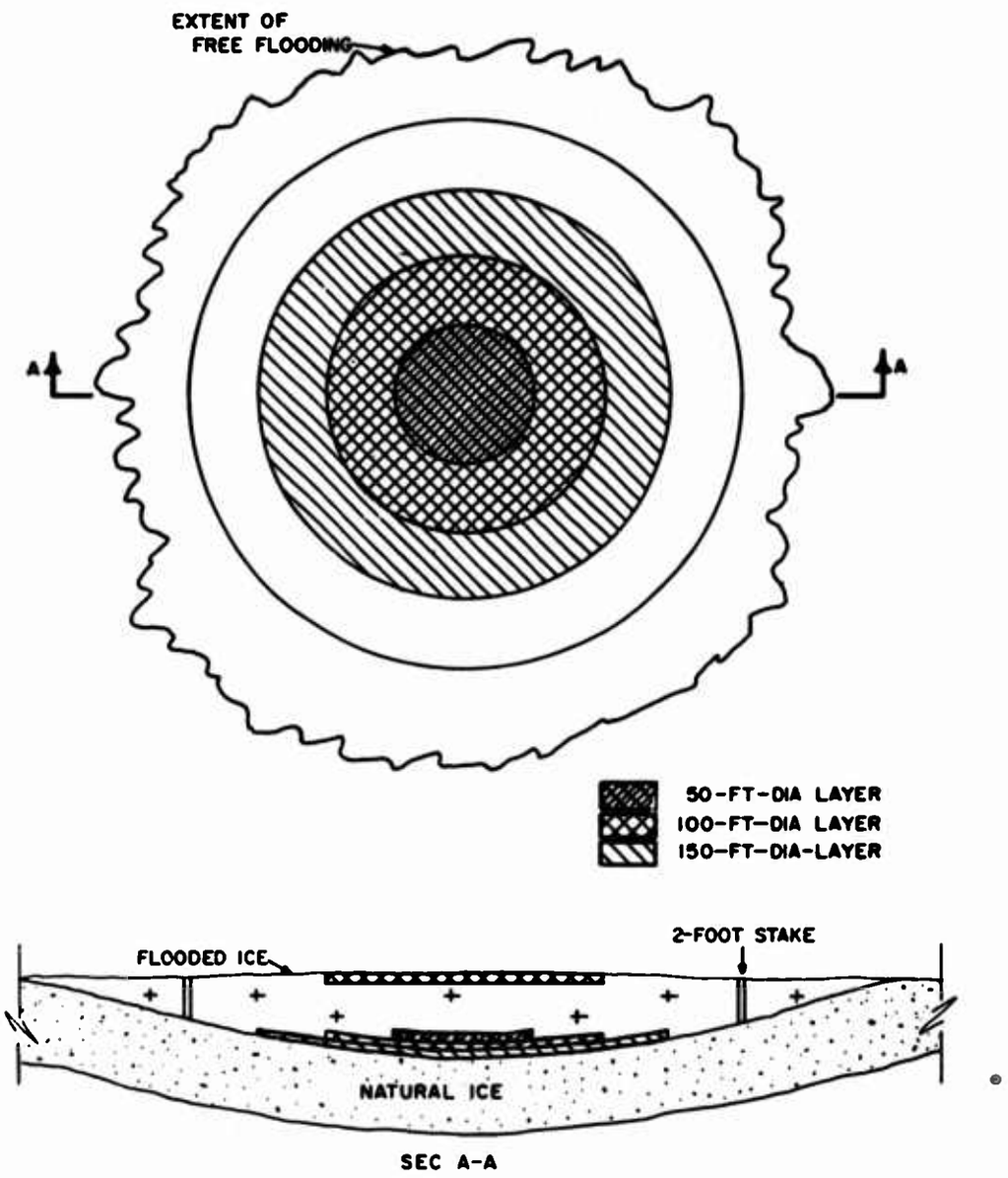

FIG. 4.10. Configuration of Fiberglas reinforcement for Parking Apron No. 2

FIG. 4.11. Laying Fiberglas reinforcement in flood water on Parking Apron No. 2 (official photograph, U.S. Navy)

4.4.3 EQUIPMENT USED AND ITS SUITABILITY

A 600-gpm pump, identical to that used for the early floodings of Apron No. 1, was used to construct Apron No. 2. It was positioned outside of the apron, and the water was piped to the center of the area for discharge. This pump and type of operation were discussed in Section 4.3.3.

Other pieces of equipment used on Apron No. 2 were a small, portable, 80-gpm pump, a steel roller, and a weasel. The portable pump was used for wetting the Fiberglas. The smooth-faced steel roller, which was 32 inches in diameter, 48 inches wide, and weighed approximately 1200 lbs, was used in an attempt to smooth out and press the Fiberglas reinforcing into place. This roller was towed by a lightweight, tracked vehicle.

4.4.4 ICE BUILD-UP ACHIEVED

Parking Apron No. 2 was completed in seven floodings plus the bottom and top reinforced layers. The diameter of the apron after the final flooding was about 350 ft. Figure 4.12 shows the surface contours and cross section of the apron.

The total thickness of the apron at the center was 85 inches. At 100 ft from the center the total thickness averaged 68 inches. As preplanned, the flooded ice was 24 inches thick at this point; therefore the natural ice sheet was 44 inches thick. Using 44 inches as the average thickness of the natural ice, the flooded ice at the center was 41 inches. Figure 4.13 shows the surface of the finished apron.

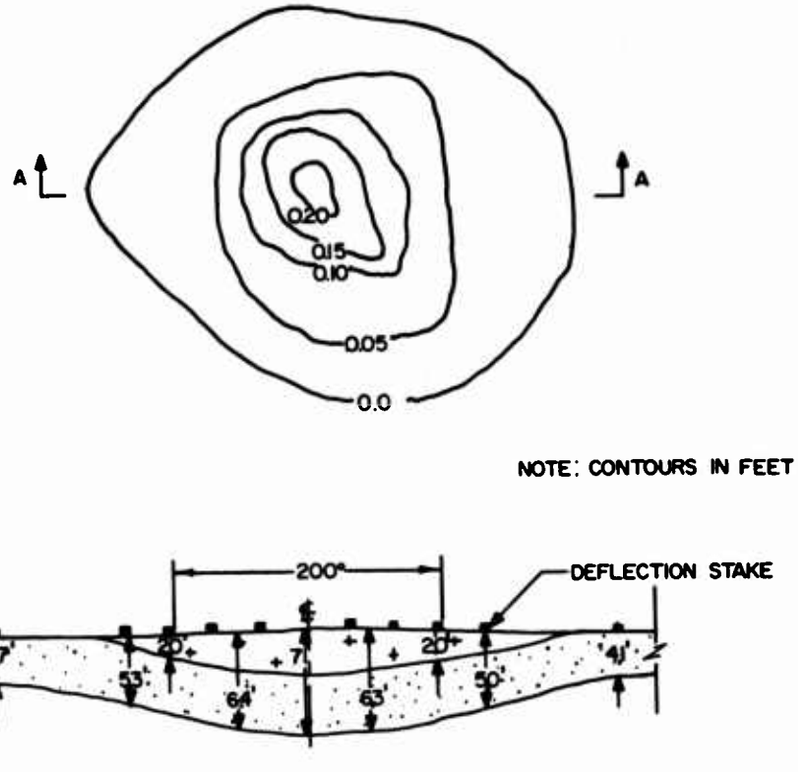

FIG. 4.12. Surface contours and vertical profile of Parking Apron No. 2

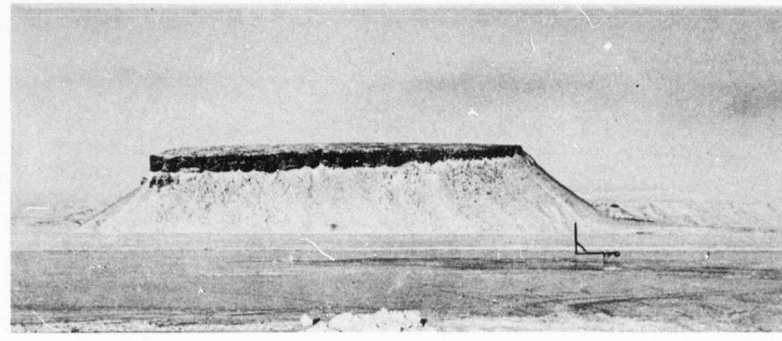

FIG. 4.13. Parking Apron No. 2 after completion
(official photograph, U.S. Navy)

On 7 and 8 February, general cracking of the entire bay ice occurred, and cracks completely encircled Apron No. 2 (Figure 4.14). These cracks varied from 1/16- to 1/4-inch in width. This is the only record of any cracking in this apron.

4.4.5 MANHOURS REQUIRED

Construction of Apron No. 2 took an estimated 148 manhours. About 26 percent of this time was required to place the reinforcement.

4.5 Reinforced, Ice-Aggregate Parking Apron

4.5.1 CONSTRUCTION TECHNIQUE

This parking apron, designated as No. 3, was constructed by the dry-fill technique described in Section 4.1. The plan was to build up a 100-ft diameter area 12 inches thick with chipped-ice-aggregate fill sandwiched between a top and bottom layer of Fiberglas-reinforced ice. The ice-aggregate was to be laid down in 4-inch lifts. Each lift was to be saturated with sea water and allowed to freeze before the next lift was placed. Water-filled, 6-inch diameter, polyethylene plastic tubing, with a 6-mil wall thickness was to be used as a dike around the construction area. The dike was to be built up concurrently with the ice-aggregate fill.

FIG. 4.14. Crack pattern around Parking Apron No. 2 after first flooding

Both the top and bottom Fiberglas layers were installed as follows: the ice surface immediately in front of the Fiberglas was wet down lightly as the matting was unrolled; then, the surface of the Fiberglas was sprinkled down to freeze it in place; finally, when all the matting was in place, it was given a light flooding for thorough saturation.

The ice-aggregate was stripped from the surface of the natural ice sheet with an experimental ice cutter currently under development by NCEL. The excavation area was located about 400 ft from the construction area. The average depth of excavation was about 6 inches and the aggregate size ranged from very fine material to chips 2 to 3 inches in diameter and 1 to 1-1/2 inches thick. As the material was produced it was windrowed with a motor grader. The aggregate was moved to the construction site with a 2.5-ton dump truck. It was loaded into the truck with a rubber-tired, front-end loader. After the material was dumped at the site (Figure 4.15) it was manually spread to a 4-inch depth over the area.

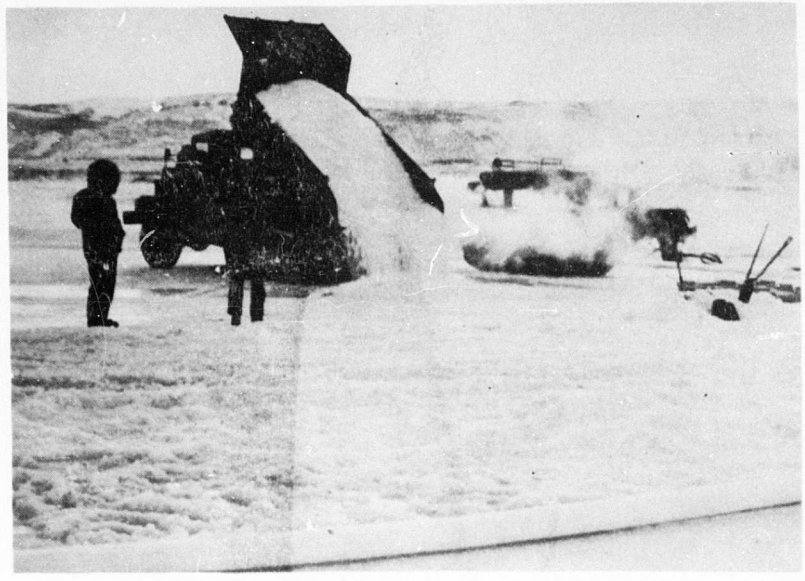

FIG. 4.15. Dumping ice-aggregate on Parking Apron No. 3
(official photograph, U.S. Navy)

For the first lift, the area was flooded with 2 to 3 inches of water, and then the aggregate was added. This method resulted in poor mixing, as the water turned to slush ice before all the aggregate was in place. As a result, for the second and third lifts the aggregate was placed and leveled, and then flooded until the fill was saturated. Better saturation was obtained if the fill was not compacted during the placement.

4.5.2 CONSTRUCTION SCHEDULE

Completion of this apron was also scheduled for the first week in March to allow a sufficient curing period before testing.

Before construction of the apron, the snow cover was removed and the site was inspected for cracks. None were found.

The bottom triple-thickness-Fiberglas reinforcement (Figure 4.16) was laid on 6 February. This reinforced layer, averaging 2 inches in thickness, was fairly uniform. The first lift of aggregate was placed on 9 February, the second on 16 February, and the third on 22 February. Both the first and second

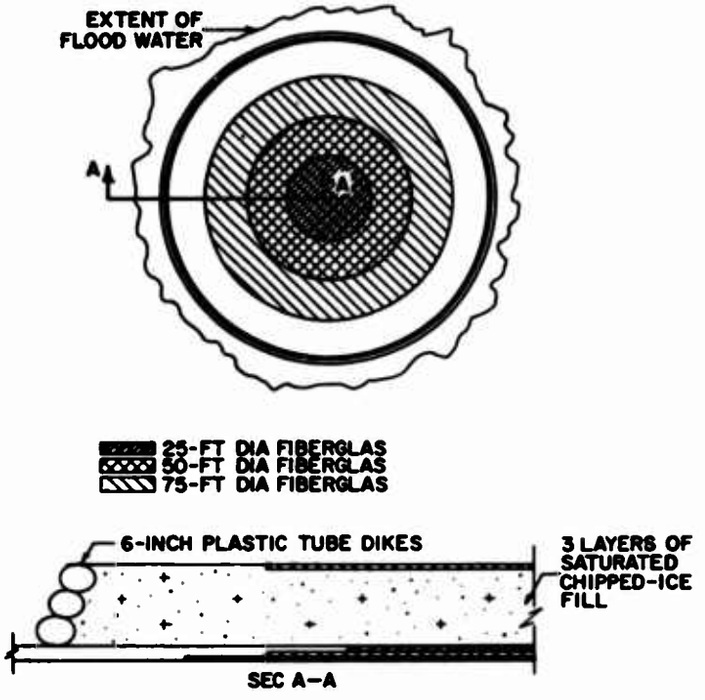

FIG. 4.16. Configuration of Fiberglas reinforcement for Parking Apron No. 3

lifts required two days to place, but the third lift was completed in one day. The aggregate for the first two lifts was mined the day before placement, while the aggregate for the third lift was mined three days before placement. The top reinforced layer, which consisted of a single thickness of Fiberglas mat, was placed on 25 February. It averaged slightly over an inch thick when completed.

The access ramp up onto the apron was constructed concurrently with the apron. This ramp was built by confined flooding using plastic dikes for the side boundaries. A slight depression in the natural ice sheet around the construction area, caused by the weight of the apron, obviated a need for dikes at the end of the ramp area.

4.5.3 EQUIPMENT USED AND ITS SUITABILITY

In general, suitable equipment was not available to construct this apron. As a result, its construction required a considerable amount of manual effort. Though smaller than Aprons 1 and 2, Apron No. 3 was too large for the handwork required to spread the aggregate inside the apron area.

At present, suitable equipment to undertake this type of construction has not been fully determined. From the effort to date, it appears that the amount of equipment required to construct built-up ice areas with this technique would be comparable to that required for a similarly-scaled earth-moving job. Such equipment should include: (1) lightweight, high-speed hauling equipment; (2) rapid-loading equipment; (3) controlled aggregate-spreading devices; and (4) simplicity of design for field servicing and maintenance.

The experimental ice cutter was very satisfactory for producing the ice aggregate. Its production capability far exceeded the yardage required for constructing the apron.

4.5.4 ICE BUILD-UP ACHIEVED

The thickness of the new ice on Apron No. 3, including the reinforced ice layers, averaged 11 inches around the outer edge and 20 inches at the center. Investigation showed that the surface of the apron was concave, with an average depression of 3 inches at the center (Figure 4.17). The natural ice sheet was depressed 17 inches at the center of the apron by the weight of the fill. The total weight of the apron was about 250 tons. The completed apron is shown in Figure 4.18.

4.5.5 MANHOURS REQUIRED

About 220 manhours were required to construct Apron No. 3 and about 8 manhours were required to construct the ramp. This estimate does not include maintenance time for the equipment used in the construction. The two reinforced layers were placed in 14 manhours, and the three aggregate fills were placed in 150 manhours. Fifty-six manhours were spent removing the snow cover, producing the aggregate, and installing the dikes. More suitable equipment, especially to handle the aggregate, would have resulted in a considerable reduction in manhours.

4.5.6 RECOMMENDATIONS FOR FUTURE OPERATIONS

The dry-fill technique of ice construction should be reviewed for its merits. If this review shows that it has advantages for specific applications, then proper equipment should be developed to handle and place the ice aggregate fill.

4.6 Test Areas

4.6.1 CONSTRUCTION TECHNIQUE

A test area, 15 ft by 90 ft, was divided in two approximately equal parts and designated as Plots 4 and 5. Plot 4 was constructed by the wet-fill technique and Plot 5 by the dry-fill technique.

After removal of the snow cover, a test site free of cracks was selected and excavated to a depth of 12 inches. The bottom surface of the excavation was irregular when completed, undulating as much as 3 or 4 inches. The cause of this irregularity was not determined; however, one possibility was plastic creep caused by hydrostatic pressures of the water on the thinned section.

The bottom of the excavated trench was reinforced with three layers of saturated Fiberglas mat (Figure 4.19). Then, a snow dike was used to divide the test area into two plots.

The wet-fill technique used to construct Plot 4 differed from the construction technique for Aprons Nos. 1 and 2 only in that the floodwater, applied in 4-inch lifts, was confined. The dry-fill technique used to construct Plot 5 differed somewhat from the technique used to construct Apron No. 3. In this plot the water and the ice aggregate, applied in 4-inch lifts, were added simultaneously and mixed to form a stiff "ice-crete" mixture, rather than first placing the ice aggregate and then the water.

4.6.2 CONSTRUCTION SCHEDULE

The plots were scheduled for completion before the parking aprons so that in-place beam tests could be completed before the start of dynamic and static load tests on the parking aprons. The last lift on each plot was placed on 25 February.

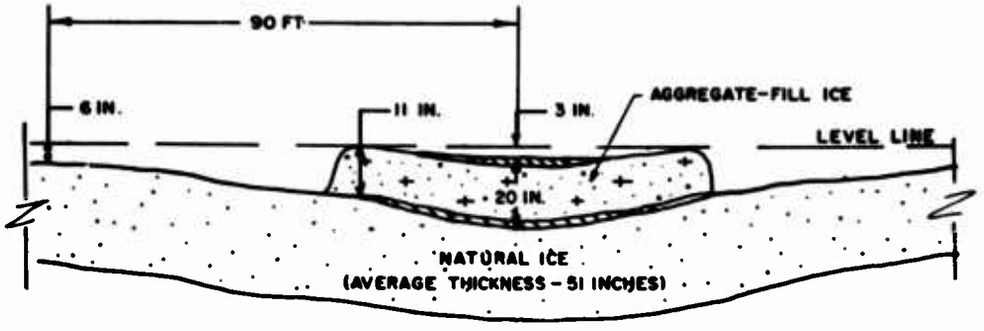

FIG. 4.17. Profile of Parking Apron No. 3 after completion

FIG. 4.18. Parking Apron No. 3 after completion; ramp section to left (official photograph, U.S. Navy)

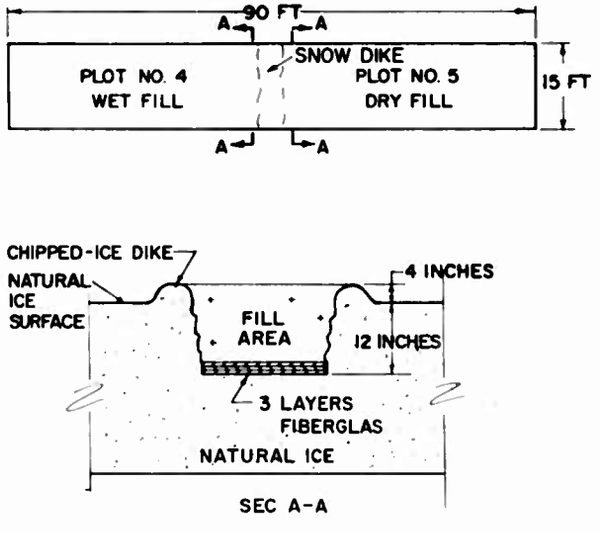

FIG. 4.19. Configuration for Test Plots Nos. 4 and 5

4.6.3 EQUIPMENT USED AND ITS SUITABILITY

The equipment used to construct the test plots was, in general, the same equipment used to construct the parking aprons. The primary pieces of equipment used to construct the test plots were the experimental ice cutter and a small, 80-gpm, flooding pump. A D4 tractor was used to tow the ice cutter. The ice aggregate was stockpiled alongside the test area and hand-shoveled into Test Plot 5.

4.6.4 TEST DATA

The micro-sample test data collected on the test plots are shown in Tables 4.1 and 4.2. In-place beam tests and other testing on this ice appear in other sections of this report.

TABLE 4.1

Average In Situ Temperatures* During March 1961 in Constructed and Underlying Natural Ice in Test Plots 4 and 5

PLOT	4 (Wet Fill)				5 (Dry Fill)			
ICE TYPE	Constructed	Natural			Constructed	Natural		
STRATA	0 to 12 inches	12 to 24 inches	24 to 36 inches	36 to 48 inches	0 to 12 inches	12 to 24 inches	24 to 36 inches	36 to 48 inches
DATE OF OBSERVATION								
5 March	-9	4	13	28	-9	4	12	28
9 March	-12	2	12	28	-12	0	9	24
11 March	-7	4	13	26	-6	5	13	27
13 March	-16	0	9	24	-19	-4	7	24
20 March	-3	5	11	21	-3	4	9	21

*All temperatures in Fahrenheit

TABLE 4.2

Average Salinity, Density, and Relative Tensile Strength During March 1961 in Constructed and Underlying Natural Ice in Test Plots 4 and 5

PLOT		4 (Wet Fill)					5 (Dry Fill)			
ICE TYPE		Constructed	Natural				Constructed	Natural		
STRATA		0 to 12 inches	12 to 24 inches	24 to 36 inches	36 to 48 inches		0 to 12 inches	12 to 24 inches	24 to 36 inches	36 to 48 inches
TEST	DATE					DATE				
SALINITY (ppt)	17 Mar	24.2	6.2	5.7	5.6	15 Mar	19.7	6.2	5.0	5.8
						22 Mar	16.0	8.3	5.6	5.6
DENSITY (gm/cc)	17 Mar	0.909	0.912	0.916	0.922	15 Mar	0.876	0.918	0.913	0.913
						22 Mar	0.861	0.916	0.915	0.918
RELATIVE TENSILE STRENGTH (psi)	17 Mar	175 (22°F)*	285 (25°F)	350 (26°F)	255 (27°F)	15 Mar	326 (4°F)	356 (9°F)	425 (8°F)	236 (10°F)
						22 Mar	232 (11°F)	334 (9°F)	332 (9°F)	287 (10°F)

*Ice temperature during tests

5. RUNWAY SURFACE PREPARATION (by Capt. James A. Pate)

5.1 Site Construction

The runway surface and parking pads were prepared and maintained by personnel of the Roads and Grounds Branch of the 4683rd Civil Engineering Squadron, 4683rd Air Base Group (ADC), USAF, with Captain James A. Pate as Officer in Charge.

The ice where the runway was constructed had approximately 4 inches of hard-packed snow cover. During removal of this snow cover, personnel found ridges 2 to 3 inches high in some areas of the ice. These ridges were "shaved" off with road graders to obtain a smooth surface.

The Snow Removal Section prepared the surface of the runway and four aircraft parking pads. The runway was approximately 3 miles from the end of the Thule Air Base runway. It was 14,000 ft long (including 3000 ft of overrun) and 300 ft wide; an estimated 60,000 cubic yards of snow was removed. One of the parking pads had a diameter of 500 feet.

The following is a tabulation of men and equipment required for initial runway preparation.

Equipment Type	Equipment Hours*	Manhours
Road Graders	224	224
Snow-Go Blowers	226	226
V-Plows	72	144
Water Truck (for dye marker)	11	22
Pickup Trucks	128	128
Military Supervision	---	150
TOTAL	661	894

*Total actual operational hours; this does not include mechanical breakdown of equipment or maintenance.

Very little maintenance was required. During the period the runway was used, only minor winds occurred, and almost no snow fell. An estimated total of 48 equipment hours and 48 equipment operator hours was used as snow-removal maintenance.

5.2 Runway Marking

Umbrella and panel markers were used to mark the sides of the runway. The runway was dye-marked by a 12-inch wide strip down the center and approximately an 8-inch strip down each side of the runway. Chevron-type markers were laid out on the approach end of the runway. According to pilot reports, the dye markings

showed up effectively to aircraft well above the runway but lost much of their effectiveness when making a low approach for landing.

5.3 Conclusions and Recommendations

All equipment proved capable of performing the job required. The V-plow seemed to be the most efficient, fastest, and most dependable piece of snow-removal equipment; the D-8 bulldozers with angle blade are useful in moving the heavier berms of snow; and the road graders are useful for final touches and "shaving" of rough ridges of ice.

For future operations care should be taken to avoid letting the snow pile up in high berms, the weight of which may cause cracks. These high berms can be avoided by use of snow blowers capable of blowing snow over an area 75 ft wide, thereby spreading the weight.

5.4 Comparison of Surface Preparation with the North Star Bay Runway Laid Out in 1957 (by D.L. Anderson and W.D. Kingery)

Two sea-ice runways were prepared in the winter of 1957 on North Star Bay as part of the Air Force Cambridge Sea Ice Bearing Strength Project.[1] The primary purpose of this phase of the project was to collect data on the static and dynamic deflection of the ice sheet and to determine the effect of high tire pressures and jet action on the operating surface. The actual construction of the runways was of secondary interest and time, equipment, and manpower was not available for a large construction effort. The major effort was expended in location of sites which could be used with little or no preparation. Many such areas could be found. After choosing an area free of icebergs and large snow drifts, it remained only to mark a strip and inspect carefully for protruding ice chunks which were remnants of the initial freezing process. These were removed by pickaxe and shovel.

The first runway was laid out approximately 5 miles from the Thule pier toward the center of Wolstenholme Fjord. The ice was relatively smooth and clear of ice ridges. A 2.5-ton truck run, repeated the length of the runway, served to level the slight undulations in the snow. Snow removal was neither necessary nor desirable, since snow ridges would cause snow drifting to occur in the runway area and a small amount of snow cover is desirable for good traction. Also, with cold-air temperatures snow removal causes the ice to contract, forming thermal cracks. The small amount of snow leveling was only necessary because of the small tires of the F-89. For larger aircraft no preparation at all would have been necessary. The F-89 tests were successfully run on the first strip.

To gain the advantage of thicker ice for the larger aircraft, a second strip was constructed closer to shore. In general, proximity to shore means thicker ice but also more severe snow undulations and more cracks.

The following is taken from the Technical Memorandum[1] describing the second runway.

"The sea-ice landing strip measured 11,000 feet x 300 feet with 5,000 foot overruns on each end, making it the longest in the Arctic. The airstrip centerline was purposely established roughly in line with the centerline of the permanent Thule runway so that GCA could be employed in landing aircraft onto the ice strip if necessary. The ice strip was situated roughly 2 miles from the Thule dock area and was covered by four inches of loose snow with isolated scattered snow drifts.

"The ice strip was prepared and marked in two days by four men (2 officers and 2 airmen) using a Grader, and a 1/4-ton jeep. Preparations entailed breaking the few hard-packed snow drifts, distributing the snow over the ice surface, compacting the thin layer of snow by passing vehicles over it, and marking the strip. This preparation was necessary largely because of the high-pressure tires and small nose-wheel of the F-89. No preparation but marking would have been necessary for landing C-124 and KC-97 aircraft.

"Shoulders of the landing strip were marked by large black inflated truck innertubes spaced at roughly 500-foot intervals. Ends of strips were marked by removing the snow and exposing the underlying darker ice in 6-foot wide bands transverse to the centerline. Touchdown was located 1,000 feet beyond the end of the ice strip and was marked by scientific equipment and vehicles placed at a safe distance away from the strip shoulders. Reports from pilots indicated that ice strip markings were very effective.

"Both strips were reported by the pilots to be smoother than the permanent Thule strip. The surface conditions of the 1957 strips and the 1961 strips were about the same except for the absence of thermal cracks and bare ice patches in 1957."

The surface preparation technique utilized in 1957 would certainly have been adequate for the present series of operation tests. Complete snow removal, on the other hand, is probably desirable for long-term use of a runway requiring maintenance of clear markings and no development of rutting. Which technique is preferable for any particular operation depends on the type of operation. The engineering studies regarding time and equipment necessary to prepare a completely cleared and marked runway carried out as part of Project ICE WAY allow a rational choice to be made.

REFERENCES

1. DeGoes, L., W. F. Weeks, and D. L. Anderson, "Aircraft Landing Tests on Sea Ice in North Star Bay, Thule, Greenland, March, 1957," GRD-TM-57-20, Geophysics Research Directorate, Air Force (17 June 1957).

6. OPERATIONAL EXPERIENCE (by D.W. Klick)

6.1 Introduction

The purpose of conducting aircraft operations was to provide realistic loads for static and dynamic testing of the natural ice along the runway and the processed ice at the parking pads. F-102, C-130, B-47, KC-135, and B-52 aircraft took part in the operations.

Static testing was provided by having the aircraft park on the ice for an extended period of time while deflection measurements were being taken with an engineering level and surveying rod. Dynamic testing was provided while the aircraft was traveling along the runway during a landing or takeoff roll or during taxiing. The runway was instrumented at various points to measure the dynamic deflections of the ice sheet caused by the moving load.

6.2 Description of the Runway

As previously mentioned, the ice runway measured 11,000 ft by 300 ft, with overrun areas 1500 ft long at each end. The orientation of the centerline was 271°22' true. The approaches to the ice runway were better than those to the main runway at Thule Air Base. From the west the approach was over the bay and entirely clear; from the east no obstacles were present above the standard 1:50 glide angle.

The ice varied in thickness along the runway from 54 inches at the east end to 38 inches at the west end. In general the thickness gradually decreased from east to west. The water depth varied irregularly from 50 ft at the east end to 80 ft around the midpoint.

The runway was marked in several different ways. Sea dye marker in a water solution was used to paint an orange stripe along both sidelines and the centerline and to mark each end with the standard three-chevron design. Fluorescent colored orange cloth markers were installed at distance points along the runway.

A pyramid type marker, 2 ft high, was installed every 1000 ft along each sideline, and a vertical panel 4 ft by 6 ft in area was erected at each corner to mark the ends of the runway; these panels were also placed at selected points along the south sideline to mark test zones. Fluorescent colored cloth was used for these markers also.

TABLE 6.1
Ice Thickness Along Runway

Station	Thickness
0	54-1/2"
1,000'	52-1/2"
2,000'	50-1/2"
3,000'	48"
4,000'	43"
5,000'	42-1/2"
6,000'	46"
7,000'	39"
8,000'	42"
9,000'	39"
10,000'	34"
11,000'	34"
12,000'	37-1/2"
13,000'	39-1/2"
14,000'	38"

Notes: 1. These thicknesses were measured on 21 March, the day before the aircraft test operations began.

2. Each measurement represents just one observation. Measurements were made with a SIPRE ice-thickness kit.

3. The 11,000 ft runway extended from Station 1500' at the east end to Station 12,500' at the west end. Stations before 1500' and after 12,500' were in the overrun areas.

Ten empty fuel-oil drums were placed every 250 ft along the centerline extended from the west end of the runway to guide the pilots during their approach (Figure 6.1). The crash truck and ambulance were stationed at one-quarter and one-half distance points from the west end to serve as reference points for the pilots during landing and takeoff.

It should be emphasized that the runway was not built-up or reinforced in any way. The natural sea ice was used without modification and the construction effort involved only the removal of snow.

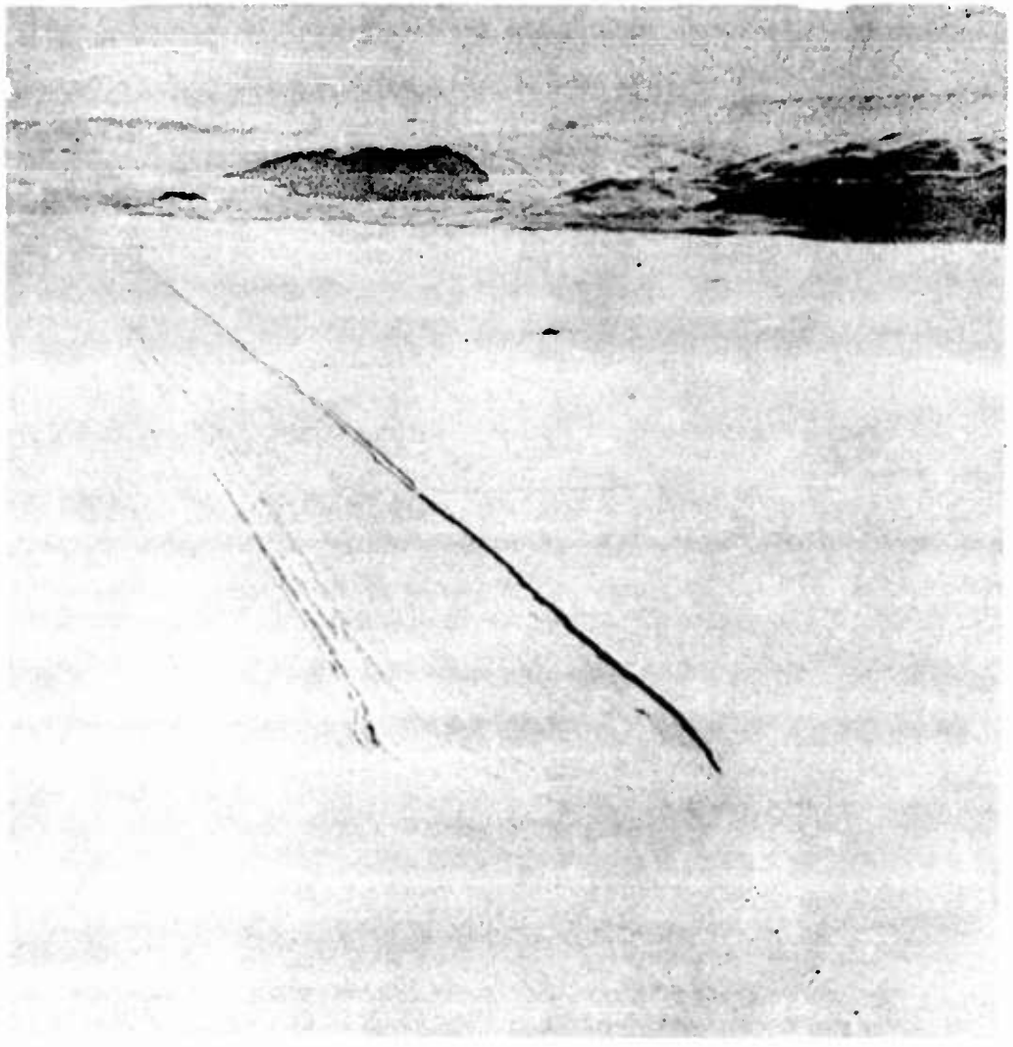

FIG. 6.1. Aerial view of project site looking east; pads and camp at far end of runway; line of dots in lower right are oil drums on extended centerline

6.3 Aircraft Operations

Five aircraft participated in the operational testing program F-102, C-130, B-47, KC-135, and B-52 . These are shown in Figures 6.2 through 6.6. Two other aircraft — a C-47 and an H-21 — made several landings and takeoffs but did not take part in the tests.

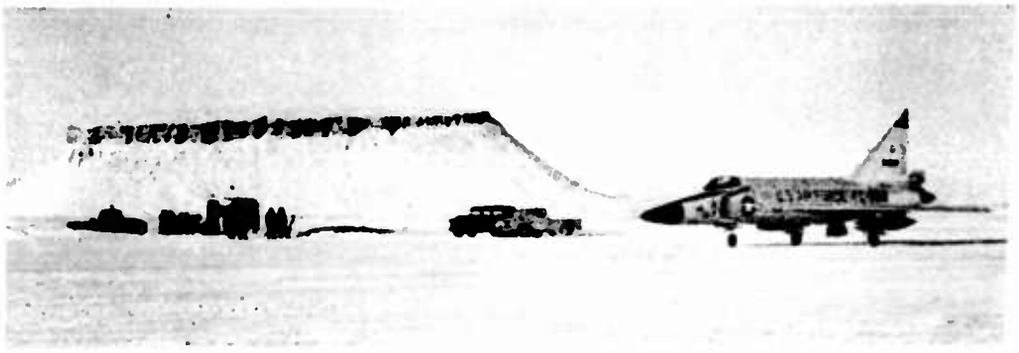

FIG. 6.2. F-102 parked in east overrun on natural ice; view north Mount Dundas in background

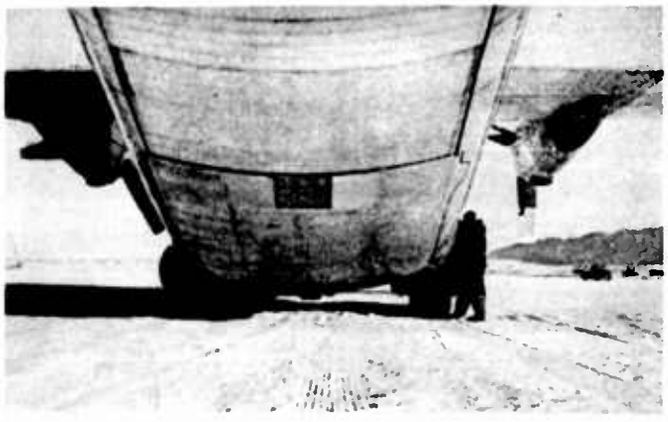

FIG. 6.3. Closeup rear view of C-130 parked on runway; note runway surface; view east

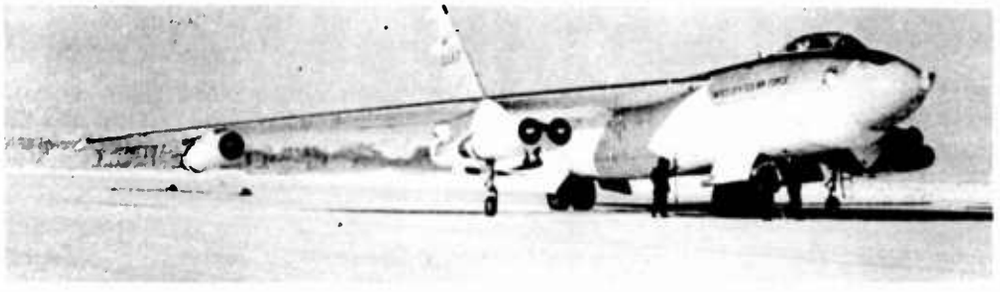

FIG. 6.4. B-47 parked on runway; static deflection measurements being taken; view northwest

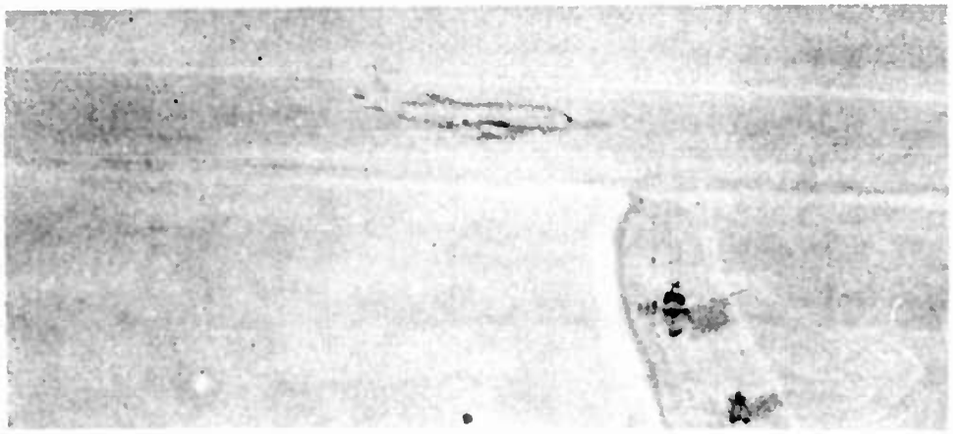

FIG. 6.5. Aerial view of KC-135 taxiing down runway to parking pads; vehicles are crash trucks at midpoint; view north

FIG. 6.6. Aerial view of B-52 parked on pad; note chevron markings at east end of runway; view east

Each aircraft made several landings and takeoffs along the natural ice runway and parked for periods of up to two hours on the runway and on the processed ice parking pads. Several aircraft also made taxi runs at various speeds along the runway. All landings were made at the west end of the runway heading toward shore and all takeoffs were made from the east end of the runway heading toward sea. Appendix G describes each test mission and presents aircraft weights.

Pilots were briefed immediately before each flight on the operations to be performed for the tests. Also, the aircraft crews visually inspected the runway and parking pads before making their first flight.

A crash truck and an ambulance were at the runway with full crews during all landings and takeoffs. An Air Police detail regulated vehicle and pedestrian traffic at the site. In addition arrangements were made for helicopter support if required and for ground-powered equipment and tow vehicles in case of an aircraft power shutdown or abort.

All missions were coordinated with Thule AB Operations and control tower. Thule would relinquish control of each aircraft immediately after takeoff to Captain Klick at the project site who would then relay all instructions to the pilots through the control tower from a radio-equipped vehicle.

6.4 Pilot Reaction

The pilots of each aircraft were asked to comment on the surface condition and markings of the ice runway. Their opinions are presented in Appendix C.

Every pilot considered the braking action to be good and the surface to be smooth. They expressed surprise at how well their aircraft maneuvered on the ice, and several pilots stated that the surface of the ice runway was better than that of the asphalt-concrete runway at Thule AB.

The pilots considered the markings to be satisfactory. They were particularly pleased with the positioning of the crash truck and ambulance at distance points along the runway and with the oil drums on the centerline extended to the west. They stated that the strips of sea dye marker showed up well at higher altitudes but could not be seen very easily during a low approach.

6.5 Deterioration of the Ice Surface

During aircraft operations the ice surface deteriorated in two ways: (1) cracking and subsequent spalling and (2) localized melting. This section deals only with the latter; the former is discussed in Section 8.

Localized melting occurred directly behind the engines of the B-47 while the aircraft was parked on the ice for extended periods of time (Figure 6.7). This melting was caused by heat from the exhausts of the engines which are slung low under the wing and tilted slightly downward from the horizontal.

During the 45-minute parking period on the runway, sizeable depressions were formed behind the outboard engines by the exhaust-blast blowing away the melt-water. These depressions measured 5 inches at the greatest depth and about 100 ft^2 in area. Only surface melting occurred behind the inboard engine groups. During the 20-minute parking periods on the two pads, no depressions were formed but surface melting took place behind all four engine groups. The largest areas were located behind the outboard engines and measured about 100 ft^2 in area (Figure 6.8).

Localized melting did not occur for any of the other aircraft. It is presumed that, although other aircraft had low-slung engines, the engines were located more along the horizontal.

6.6 Conclusions

All aircraft operations were conducted without incident. There were no reports of any aircraft skidding or sliding, and the surface of the ice runway could be considered to be as good as, if not better than, the main runway at Thule AB.

The importance of adequate communications cannot be overemphasized. Contact with the pilots from the radio-equipped vehicle was satisfactory but a greater degree of reliability should be attained. Blind spots occurred when the vehicle was parked in certain locations at the project site. Also, it would be highly desirable to have direct communication with the pilot instead of relaying instructions through the control tower. Such an arrangement was not possible because UHF radios were not available.

Sea dye marker stripes and pre-positioned vehicles along the runway were the most effective runway markings. The oil drums along the extended centerline were very useful, also, in aiding the pilots to line up their aircraft on final approach, and special attention should be paid to providing such a guidance line.

The degree of success of the aircraft operations is dictated, however, by the results of the tests which the aircraft performed. These results are presented in succeeding sections of this report.

Localized melting occurred directly behind the engines of the B-47 while the aircraft was parked on the ice for extended periods of time (Figure 6.7). This melting was caused by heat from the exhausts of the engines which are slung low under the wing and tilted slightly downward from the horizontal.

During the 45-minute parking period on the runway, sizeable depressions were formed behind the outboard engines by the exhaust-blast blowing away the melt-water. These depressions measured 5 inches at the greatest depth and about 100 ft^2 in area. Only surface melting occurred behind the inboard engine groups. During the 20-minute parking periods on the two pads, no depressions were formed but surface melting took place behind all four engine groups. The largest areas were located behind the outboard engines and measured about 100 ft^2 in area (Figure 6.8).

Localized melting did not occur for any of the other aircraft. It is presumed that, although other aircraft had low-slung engines, the engines were located more along the horizontal.

6.6 Conclusions

All aircraft operations were conducted without incident. There were no reports of any aircraft skidding or sliding, and the surface of the ice runway could be considered to be as good as, if not better than, the main runway at Thule AB.

The importance of adequate communications cannot be overemphasized. Contact with the pilots from the radio-equipped vehicle was satisfactory but a greater degree of reliability should be attained. Blind spots occurred when the vehicle was parked in certain locations at the project site. Also, it would be highly desirable to have direct communication with the pilot instead of relaying instructions through the control tower. Such an arrangement was not possible because UHF radios were not available.

Sea dye marker stripes and pre-positioned vehicles along the runway were the most effective runway markings. The oil drums along the extended centerline were very useful, also, in aiding the pilots to line up their aircraft on final approach, and special attention should be paid to providing such a guidance line.

The degree of success of the aircraft operations is dictated, however, by the results of the tests which the aircraft performed. These results are presented in succeeding sections of this report.

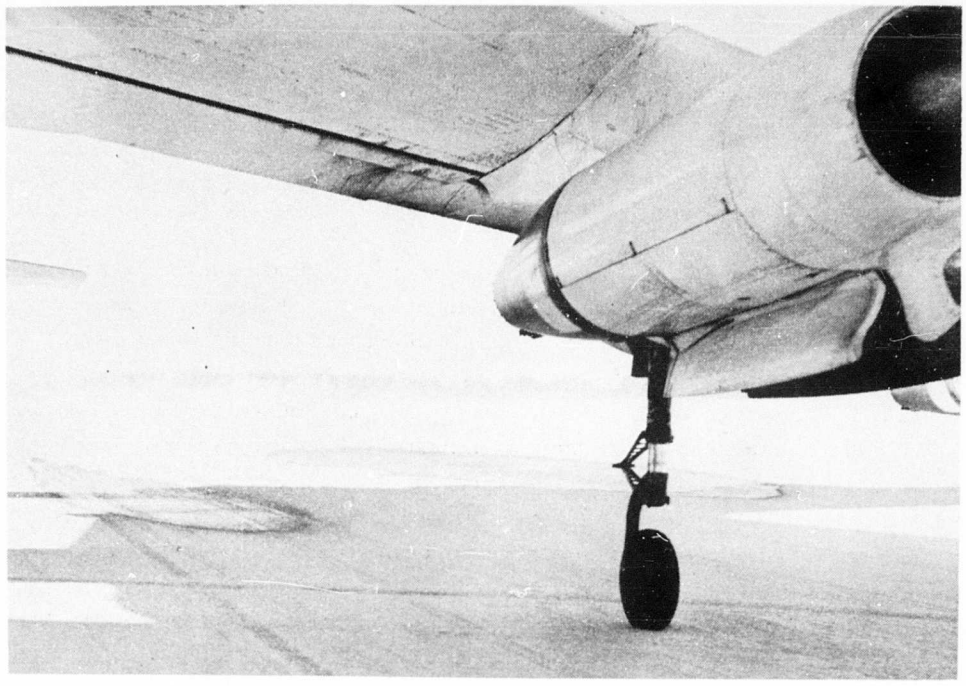

FIG. 6.7. Melt areas on ice surface from exhaust blast of B-47 engines; view West

FIG. 6.8. Extent and depth of melt area behind outboard engine of B-47; view west

7. ELASTIC AND TIME-DEPENDENT DEFORMATION OF ICE SHEETS DURING AIRCRAFT OPERATIONS (by W.D. Kingery)

7.1 Introduction

During aircraft operation two different types of deformation occur that may limit the utility of ice platforms. There is an immediate elastic deformation which is fully recovered when the aircraft or other applied load leaves the ice surface. If this elastic deformation is large, failure can occur by fracture equivalent to that measured in short-time strength tests such as discussed in Section 12. In addition to elastic deformation, however, there is a plastic deformation which is not recoverable and which is strongly dependent on the rate of load application. Thus, even if an aircraft did not fracture the ice immediately, delayed failure could occur. Few field studies of a quantitative nature have been reported on the elastic and plastic deformation resulting from heavy loads applied over a time period corresponding to operational use. Reporting data of this type is the purpose of this section. Longer time loads are generally required for evaluation of ice suitability for aircraft parking; these are discussed in Section 13.

7.2 Experimental Technique

The experimental method used available aircraft and other vehicles as a load applied to different ice locations having variable thickness and modes of deformation. A surveyor's level was used to obtain a zero reading prior to moving the load on the surface. Once the load was in place, a surveyor's tape or rod was placed on the vehicle or on the surface, and deflection measurements were made at various times during loading in order to obtain a deformation-time curve for each load test. The first measurement was taken at approximately one minute after the load was applied, and presumably corresponds to nearly elastic deformation. Time-dependent deformation was determined over time periods up to several hours. The precision of measurement depends on the amount of load and on the distance of the level from the measuring point. In general, reproducible deformation values were obtained within 0.01 ft. For measurements with the smaller loads (when the distance between the surveyor's level and the tape was smaller) reproducible readings within 0.005 ft were achieved. This means that small elastic deflections under light loads could not be determined with precision. However, deflections up to several inches could be measured without difficulty.

7.3 Ice Samples Tested

Details of the characteristics of the ice samples tested are described in other sections of this report. They consisted of:

a. Natural sea ice having a thickness which was determined for each test and having salinity and temperature profiles similar to those described in Section 9 and Section 11. In general the salinity was approximately 0.05 percent through most of the ice thickness with a somewhat higher salinity layer at the surface. The temperature of the ice varied almost linearly from the water temperature (approximately -2°C) at the bottom to the surface temperature, which for most of the tests was of the order of -20°C.

b. Parking Pad No. 1 (500 ft diameter free-flooded area described in Section 9).

c. Fiberglas reinforced, free-flooded and frozen Parking Pad No. 2 described in Section 9.

d. Fiberglas reinforced-aggregate Parking Pad No. 3 described in Section 9.

7.4 Vehicles and Aircraft Tested

Vehicles used to determine the deformation characteristics included D-8 tractors, a fire truck, and snow plows; the aircraft included a B-47, C-130, KC-135, and B-52's. The weights of these combinations are given in Table 7.1. Although the wheel configuration is necessary for a complete evaluation of the load-bearing characteristics, the center-point deflection is almost solely a function of the total load.

TABLE 7.1

Vehicles and Aircraft Used for Static Tests

Type Load	Gross Weight (lb)
D-8 Tractor plus Fire Truck	85,000
1 V-plow	46,000
2 V-plows	92,000
3 V-plows	138,000
4 V-plows	184,000
5 V-plows	230,000
C-130	96,400 - 94,500*
B-47	123,000 - 116,500*
KC-135	158,000 - 130,000*
B-52	201,000 - 194,000*

*Spreads indicate different landings, or difference between landing and takeoff weights.

In all cases, as a safety precaution, a larger gross weight of separate vehicles parked together (usually V-snow plows) was tested for static loading before carrying out aircraft operations. In no case were sufficiently large deflections observed to cause concern as to possible ice failure. Figure 7.1a and 1b are general views of ice deflection measurements under a load of five V-plows; and Figure 7.2 illustrates tests with aircraft.

7.5 Experimental Results

The precision of the experimental measurements improved during the test period from an initial scatter of 0.01 to 0.02 ft to a later precision of ± 0.055 ft. Figure 7.3 shows typical early measurements. An initial center deformation of approximately 0.2 ft increased in a period of 52 minutes to approximately 0.29 ft. When the load was released a residual deformation of about 0.05 ft, corresponding to the total permanent plastic flow was found. Duplicate measurements with two instruments and two measuring crews located at two different points gave values which are in good average agreement but show discrepancies between individual measurements. This is believed to result from the fact that deformation is not completely continuous radially or circumferentially; that is, the deformation is not a completely smooth viscous flow but also proceeds in discontinuous jumps. The precision of the measurements and the number of measurements taken was not sufficient to follow the discontinuities in detail. At some places, such as the 100-ft radius-reading in Figure 7.3, substantial discrepancies were observed that are believed to result from local crack formation and stress relief without general deformation of the sheet.

Figure 7.4 shows typical measurements illustrating the precision obtained later in the tests during aircraft landings. Here, also, discontinuous deformation is found which was not examined in detail.

In both Figures 7.3 and 7.4, the deformation is characterized by a rapid initial elastic deformation followed by an elastic or transient creep portion which is recoverable, and a subsequent steady-state deformation corresponding to permanent creep. The rate of creep for the heaviest load utilized (5 V-plows at 230,000 lb) corresponded to a deformation rate of approximately 0.4 ft/hr. For smaller loads the rate of deformation was less than this. After the load was removed, only a portion of the deformation was recovered; the recovered deformation usually reached a nearly stable value within 30 minutes after load removal within the precision of the experimental measurements.

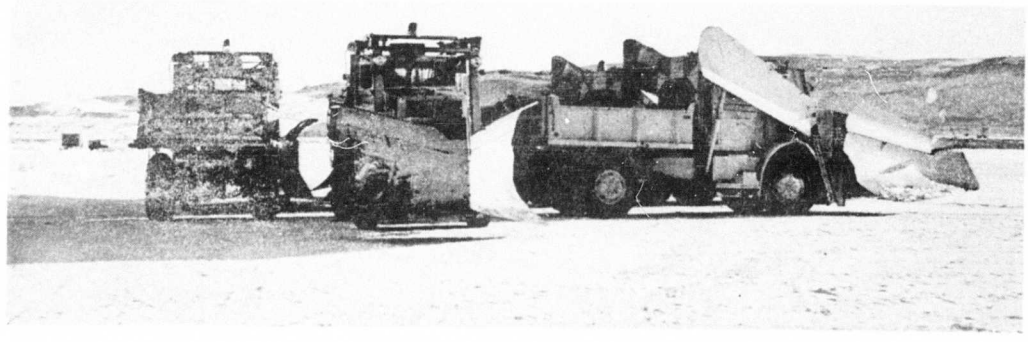

FIG. 7.1(a) General view and (b) close-ups of ice deflection measurement with a load of five V-plows

FIG. 7.2. Ice deflection measurements with C-130, B-47, KC-135, and B-52 aircraft

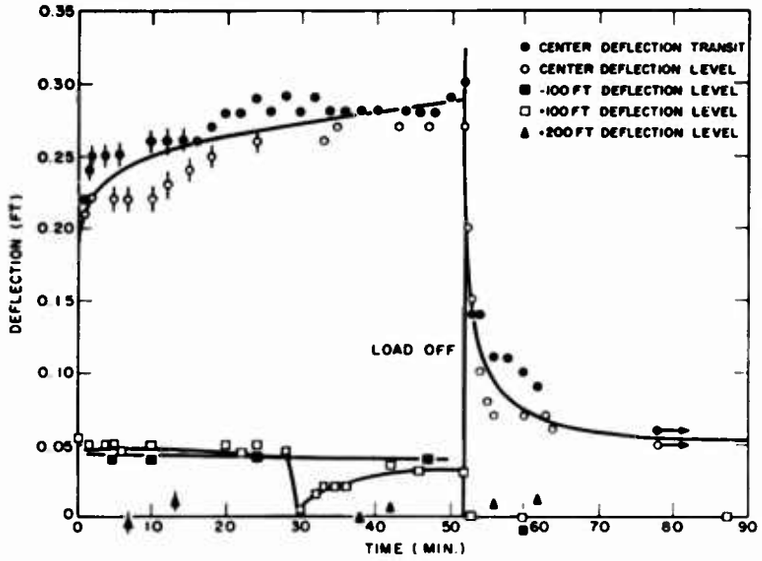

FIG. 7.3 Ice deflection at the center point, 100 ft radius and 200 ft radius for a load of 5 V-plows (230,000 lb) on 52 inches thick natural sea ice

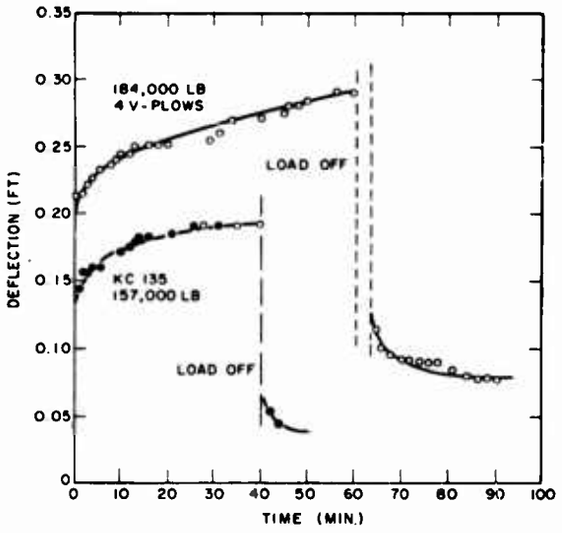

FIG. 7.4 Ice deflection at the center point for a load of 4 V-plows (184,000 lb) and for a KC-135 aircraft (157,000 lb) on 52 inches thick natural sea ice

The shape of the deflection dish was not examined in detail. For ice of a thickness h, the action radius L is given by,[1]

$$L^4 = \frac{Eh^3}{12(1-\mu^2)k} \qquad (7.1)$$

Assuming E = 150,000 psi, $\mu = 0.33$, and $k = 0.0366$ lb/in.^{3}, for h = 52 in., L = 46 ft. At a radius of 100 ft = 2.16L, the purely elastic deflection should be equal to 0.23 times the center deflection. At a radius of 200 ft = 4.32L, the elastic deflection should be less than 0.01 times the center deflection. The observed elastic deflection at 100 ft = 2.16L was 0.05/0.20 = 0.25, which is in good agreement with theory. The deflection at 200 ft = 4.32L is small, as expected.

Various methods of characterizing the deformation can be utilized for the load tests with vehicles and aircraft. The time of loading varied from a few minutes to a few hours. Sufficient data are available for periods or loads of greater than 30 minutes to make this a useful criterion for time-dependent deformation. Deformation data after periods of 1 minute, 30 minutes, and 60 minutes for a natural ice sheet having a thickness of 52 inches are collected in Table 7.2.

TABLE 7.2

Center Deflection of Load on 52-Inch Thick Natural Sea Ice

Load Type	Weight (lb)	Deflection (ft) after: 1 minute	30 minutes	60 minutes
D-8 tractor + fire truck	85,000	0.08	0.08	–
B-47	120,000	.13	.14	0.16
3 V-plows	138,000	.14	.18	–
5 V-plows	230,000	.215	.27	.285
1 V-plow	46,000	.05	–	–
4 V-plows	184,000	.21	.26	.29
C-130	95,000	.09	.11	.16
KC-135	156,000	.155	.19	–
4 V-plows on Parking Pad No. 3	184,000	0.115	0.165	0.190

The deflection of the thicker-constructed ice parking areas was less extensive than the natural ice, and the time dependence of deformation was not observed within the limits of precision and time (up to 1 hr) employed. Table 7.3 presents results for the different types of loads on each test area.

TABLE 7.3
Center Deflection of Parking Pads

Load Type	Weight (lb)	Pad No.	Deflection (ft)
C-130	95,000	1	0.025
		2	.045
3 V-plows	138,000	1	.07
		2	.05
		3	.11
B-47	123,000	1	.05
		2	.055
KC-135	147,500	1	.065
		2	.075
B-52	200,000	1	.070
		2	0.075

As shown in Table 7.3, within the precision of measurement, little difference was observed between the behavior of Parking Pad No. 1 and Pad No. 2. Measurements for identical loads on each area were usually within ± 0.01 ft. Pad No. 2 usually showed slightly greater deformation, but in some cases the deformation of Pad No. 1 was found to be larger. The deformation of the parking areas was always about half that observed for the natural ice. However, the rate of deformation after loading was very small.

In no case during the tests were cracks observed to have formed on the ice surface while the load was in place. In several cases, however, it was observed that cracks were found to have formed at the site of the test several hours after the load was removed.

When the C-130 was parked for a period of more than one hour, giving a deformation of about 0.16 ft, a hairline crack was observed to grow to approximately 3/16 inches in width several hours after the load was removed. Similarly, on the parking tests employing four V-plows and and also in the parking tests utilizing the KC-135 aircraft, one or more radial cracks were observed to form or enlarge in a period of about an hour after the load removal. These occurred after test deflections of approximately 0.3 ft, corresponding to a substantial portion of permanent plastic deformation in the ice sheet.

7.6 Discussion of Results

From the shape of the time-deformation curves and from the amount of deformation observed, it is clear that heavy loads on thick cold ice sheets cannot

satisfactorily be treated solely as a problem in elasticity. The deformation consists of an elastic part, an anelastic portion which is substantial, and a creep deformation part which occurs extensively prior to any cracking of the surface layer. As a result the stress distribution will be substantially changed from the initial elastic condition at the time of subsequent fracture.

The application of a load of 230,000 lbs on a 52-inch thick natural sea-ice sheet without the appearance of any cracking, although a total deflection of about 3 inches was observed, indicates that this load is satisfactory for short-time applications. At the same time, however, continuous deformation is taking place which indicates that such a load may not be withstood by the ice indefinitely. Long-time loading is considered in somewhat more detail in Section 13. In contrast the behavior of solidified free-flooded ice sheets showing no time-dependent deformation indicate that substantially greater loads than 230,000 psi can be carried satisfactorily and that these constructions would be entirely sutiable for the heaviest operational aircraft; that is, loads of the order of 400,000 to 500,000 lbs.

For the deflections after a 1-minute loading time, the strain is proportional to the applied load. See Figure 7.5 . As a result, the amount of deflection occurring at this time can be treated as an anelastic deformation in which the effective elasticity is proportional to the time of loading. This is in agreement with previous investigators and with general concepts of time-dependent anelastic behavior. However, when loads are applied for times as short as 30 or 60 minutes, the total deflection is no longer proportional to the load but includes plastic flow or creep which is not truly viscous (that is, it is non-Newtonian; the strain rate is not proportional to the load). This can be illustrated, as shown in Figure 7.6, by plotting the deformation occurring between 1 and 30 minutes of loading against the applied load. This indicates yield load of approximately 75,000 lb for a natural sea-ice plate 52 inches thick. The precision of our measurements here is insufficient to obtain reliable data for the strain rate as a function of load. In fact some of the smaller loads have an apparently larger rate of deformation than heavier loads. This is believed to result from local variations of ice characteristics on a day-to-day or position basis, perhaps because of the jerky nature of the deformation. These aspects are not satisfactorily defined in the present series of measurements.

An evaluation of the effective elasticity of the sea-ice sheet can be obtained from the center deflection δ_o and the relation,[1]

$$\delta_o = \frac{P}{8kL^2}; \qquad L^2 = \frac{P/\delta_o}{8k} \tag{7.2}$$

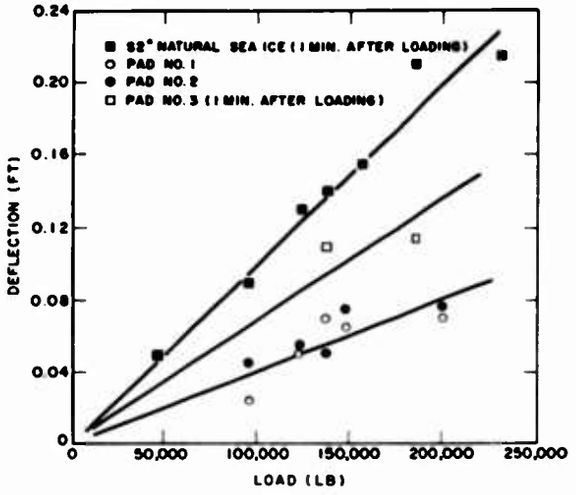

FIG. 7.5 Deflection of ice sheet after one minute loading time

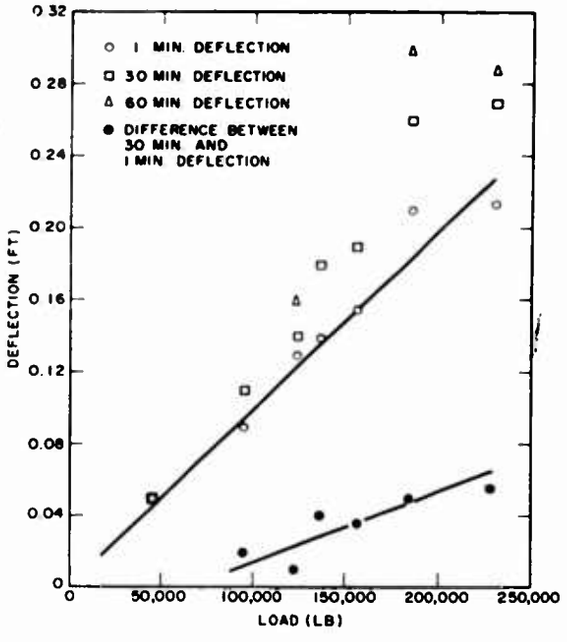

FIG. 7.6 Deflection of ice sheet after 1-, 30-, and 60-minute loading times

where δ_o/P is the slope of Figure 7.6. Combined with Equation (7.1) we obtain,

$$E = \frac{(1-\mu^2)(P/\delta_o)^2}{6kh^3} \qquad (7.3)$$

Taking $\mu = 0.33$, $k = 0.0366$ lb/in.^{3}, $h = 52$ in., and $(P/\delta_o) = \frac{100,000}{1.2} = 83,300$ lb/in., we calculate that $E_{eff} = 200,000$ psi. This elastic modulus is an average for tensile and compressive stresses and over the temperature range from about -2°C to about -25°C. It is of the right order of magnitude.

From the Westergaard elastic analysis,[1] the maximum stress is given by

$$\sigma = \frac{3(1+\mu)P}{2\pi h^2}\left(\ln\frac{L}{a} + 0.6159\right)$$

when the loaded surface radius a is much greater than the ice thickness, always true here. For a typical aircraft or vehicle, with $a \approx 15$ ft and $L = 58$ ft, $\mu = 0.33$ and $h = 52$ in., we calculate,

$$\sigma = 4.7 \times 10^{-4} P$$

For the heaviest load used, 5 V-plows at 230,000 lb, the calculated bottom stress is 108 psi. This is somewhat larger than the in-place beam strength tests described in Section 14 (average about 80 psi). This fact that ice sheets support loads heavier than those calculated from elastic theory is well known.[2-6] Theoretical analyses commonly account for this by invoking "plastic flow" with a yield point as a new failure criterion. In our opinion time-dependent processes which allow for the healing of incipient cracks and for stress relief, particularly in the warm bottom layers of the ice sheet, are more probable. These phenomena are known to occur, although yield strengths under rapidly applied loads are not found in any experimental studies. The linear stress-strain relationship on initial loading shown in Figure 7.5 clearly indicates elastic behavior; it is only when time, or the rate of loading is brought in as an additional variable that plastic flow is observed (Figure 7.6).

Evaluation of the time-dependent deformation characteristics in meaningful terms requires a stress analysis in terms of an ice sheet having a temperature gradient with temperature dependent properties. The general characteristics of the deformation and residual stress behavior are in accord with a model in which the bottom layer of the ice (at the melting point) is easily deformed while the top surface (at a much lower temperature) is rigid. As a result of deformation the neutral axis will not remain fixed but will tend to move up through the ice, giving high compressive stresses on the surface and lower tensile stresses at the ice-water contact layer. As a result, even though the ice deforms substantially, stresses do not reach a point where fracture occurs. Evaluation of such a model is now in progress. To utilize the present data for determining better load-bearing criteria for thick ice sheets, this stress analysis will have to be completed.

7.7 Conclusions

Observations of the elastic and time dependent deformation of ice sheets when loaded for periods up to one hour with wheeled vehicles or aircraft indicate that both elastic and time-dependent plastic deformation processes take place. Substantially larger loads can be carried than are predicted from purely elastic theory. This is attributed to the strong temperature dependence of ice properties and the variation of properties through the ice sheet. An additional stress analysis is necessary before the data reported here can be interpreted in terms of that model.

REFERENCES

1. Westergaard, H. M., "Stresses in Concrete Pavements Computed by Theoretical Analysis," Public Roads, Vol. 7, No. 2, (Apr 1926).
2. Persson B. O. E., "Durability and Bearing Capacity of an Ice Layer," Svenska Vag fereningens, Vol. 35, (Dec 1948). (Arctic Construction and Frost Effects Lab, U. S. Army Crops of Engineers, Translation by W. C. Dias, Apr 1954) Boston, Mass.
3. Linell K. A., "Use of Ice as a Load-Supporting Surface," Misc. Paper 19, Amer. Soc. Civil Engrs. Annual Convention, New York, (1951). (Arctic Construction and Frost Effects Lab, U. S. Army Crops of Engineers, Aug 1958) Boston, Mass.
4. Volkov, G., "Airfields on Ice," Morskoi Sbornik, No. 3, p. 77-88. (1940).
5. Assur, A., "Airfields on Floating Ice Sheets," S.I.P.R.E. Report No. 36, (1956).
6. Meyerhof, G. G., "Bearing Capacity of Floating Ice Sheets," Proc. A.S.C.E., 86, No. EM5, p. 113-145, (Oct 1960).

8. CRACKS IN SEA ICE AND THEIR EFFECT ON OPERATIONS
(by W.D. Kingery and R.L. Coble)

8.1 Introduction

In field operations, one must frequently make decisions as to the extent that cracks limit the possibility of operating on sea ice. A few rules concerning effects of cracks are given by Assur in recommendations for aircraft operations on ice sheets.[1] Only cracks greater than 1/2-inch in width must be included in a survey of an area proposed for aircraft use; those over 1-1/2 inches wide are to be healed with slush. Assur also recommends that 10 percent greater ice thickness is required when cracks 1-1/2 inches wide are present and 30 percent thickness when there are wet open cracks. Heavy loads should not be parked on a crack, or allowed to pass over intersections of several cracks; parking is permitted at distances equal to the load influence radius from a crack or free edge.

Cracks are formed in ice in various ways and sizes. In discussions of their effect on sea-ice strength, no quantitative analyses have been made. In this section we do not carry out a complete quantitative analysis, but we develop a rational basis for estimating effects of cracks.

8.2 Types of Ice Cracks and Their Sources

8.2.1 OPEN WET CRACKS

Cracks passing completely through the ice sheet have the most deleterious effect on load-bearing capacity. Open wet cracks can result from wind, tidal, or wave action. Tidal cracks are frequently observed in shore-bound ice, occurring when tidal action lifts the ice sheet above or below the level at which it is shore bound. Cracks tend to form parallel to the shore at a distance from the shore related to an "action radius" which depends on the ice thickness. These cracks tend to continuously open, refreeze, and open again. They are frequently wet and of variable width.

Cracks from wind and wave action appear in free-floating ice, such as the Arctic ice floe. Wind and wave forces produce stresses in the ice sheet that frequently cause cracking and fracture. The magnitude of stress depends on the ice thickness, its configuration with regard to adjacent ice structures, and a variety of other factors which are beyond the present discussion. They do not occur in protected areas such as North Star Bay.

8.2.2 SUPERFICIAL CRACKS

In addition to the cracks which penetrate the ice sheet, both top and bottom surface cracks can result from several causes.

Thermal stress cracks are common and result from two sources. Some result from sudden air-temperature changes that chill the upper surface of the ice sheet; others can result from removal of surface insulation (usually snow) which lowers the ice surface temperature. Lowering the surface temperatures leads to tensile stresses in the surface; these may exceed the tensile strength and cause cracks which vary from "hairline" to 1 inch in width, depending on the temperature cycle and ice thickness. Thermal stress cracks are common in lake ice on cold cloudless nights when radiation from the surface causes low surface temperatures and high surface tensile stresses. Audible cracking is frequent under these circumstances.

Cracks result from applied loads. When a load is applied to an ice sheet that is greater than the breaking strength, cracks form preliminary to ultimate failure. These cracks are radial, starting from the lower surface of the ice, with a circumferential crack forming from the upper surface. These crack patterns have been observed while forming and are in accordance with calculated stress distributions. They have been most studied for lake ice which is relatively thin and for loads which are rapidly brought up to a value sufficient to cause failure. They are adequately described in the literature.

Cracks can form on load removal. As discussed in Section 7, cracks were observed to form after the load had been removed during the North Star Bay tests. These cracks are believed caused by residual stresses in the ice resulting from plastic deformation that gives a permanently bent sheet when the load is removed. As the ice tends to spring back into position, the permanent deformation present resists the buoyant force and results in a tensile stress at the surface that produces radial cracks extending from the point where the load was situated. These cracks occurring in sea ice are strong evidence that permanent deformation has occurred.

8.3 Crack Observations at North Star Bay

During the North Star Bay exercise, cracks were observed to form from several probable sources. One source of cracks, which has already been mentioned, is new small cracks or enlargement of old cracks upon load removal. These are presumed to result from an apparent reverse loading from the buoyant force of the

water and release of residual stresses. On subsequent loading and unloading, these stresses will be renewed such that new cracks will tend to form on each load cycle. As a result, a factor that must be considered for extensive use of one area for aircraft operations is the extent to which cracks of this kind form and grow, possibly leading to ultimate "fatigue" failure.

In addition to the cracks that formed on load removal, numerous hairline cracks were observed in the ice surface. These were believed to be thermal stress cracks although their origin was not investigated in detail.

The largest crack observed was one along the centerline of the runway; cracks also formed along each edge of the runway. Figures 8.1 and 8.2 illustrate the approximate structure of the cracks. The center crack was parallel to the centerline (Figures 8.2 and 8.3). It was nearly 1 inch wide at the surface in several places (Figure 8.4), and ran about 5000 ft from the offshore end of the runway to near the runway midpoint. During aircraft landings the crack width was measured at five points immediately before and after each landing. In no case did the width change within the precision of the measurements, nor did the crack dimension change over this 10-day period of observation (± 0.0312 inch).

On two occasions blocks of ice at crack junctions were lifted up from the surrounding surface overnight, twisted in position, and cracked (such as shown in Figure 8.5). Some changes in crack configuration were also observed during overnight periods. These minor changes are believed to result from temperature or tidal fluctuations.

8.4 Source of the Runway Cracks at North Star Bay

The cracks that formed on the North Star Bay runway occurred after snow removal, presumably because the upper surface of the ice was cooled following the removal of the insulating snow blanket. Assuming that the upper-surface temperature is equal to the average ambient temperature, the snow:ice interface temperatures are calculated by noting that the heat flow through the two layers in series must be equal.

$$Q_{snow} = Q_{ice} = \frac{kA \Delta T}{\Delta X} \qquad (8.1)$$

FIG. 8.1 Runway crack at North Star Bay runway

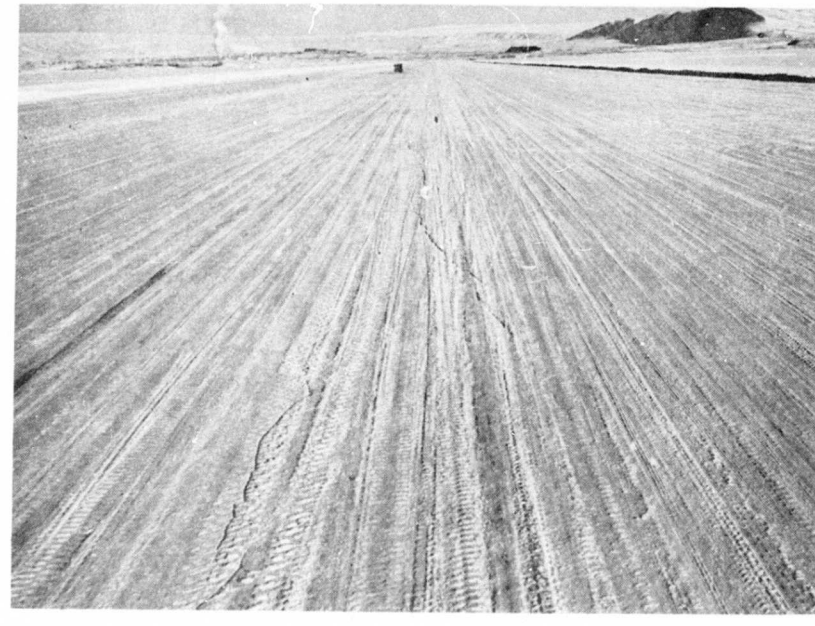

FIG. 8.2 Runway crack at North Star Bay runway

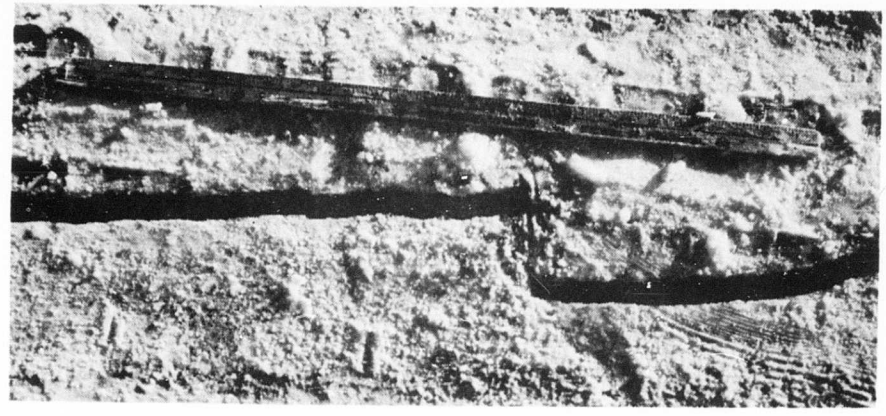

FIG. 8.3 Runway crack at North Star Bay runway; ruler is parallel to runway centerline

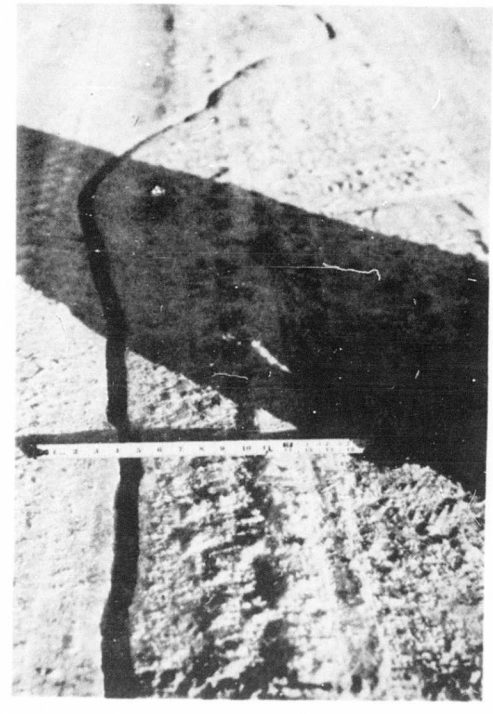

FIG. 8.4 Runway crack at North Star Bay runway

FIG. 8.5 Block of ice lifted from crack and broken by overnight "working" of ice

The thermal conductivity of ice is about five times as great as that for snow, $k_{ice} = 5k_{snow}$. For the 40 inches of ice and 4 inches of snow originally present,

$$\frac{k_s A \Delta T_s}{4''} = \frac{5k_s A \Delta T_i}{40''} \qquad (8.2)$$

and, $\Delta T_{ice} = 2\Delta T_{snow}$.

The average air temperature in March 1961 was -23° F; the water temperature was 28 °F. The total temperature difference equals 51 °F, and the snow:ice interface temperature would have been -6 °F. After the snow layer is removed, the ice surface is assumed to have dropped to the -23 °F ambient. The 17° temperature

change in the upper surface of the ice would produce a strain in half the runway width (150 ft) given by,

$$L\alpha\Delta T = (150') (12') (28 \times 10^{-6}/°F) (17°F) = 0.85'' \qquad (8.3)$$

If the total strain was relieved by cracking, the crack would be 0.85 inch wide at the top surface. This is in good agreement with the directly-measured crack widths (maximum observed width was 1 inch) providing quantitative support for the view that the crack was of thermal origin. The fact that the region where the ice was thicker (50 inches, average) did not crack may be simply due to the lower stresses that would be induced because of smaller temperature change (15° instead of 17° for 4 inch snow). The stress introduced in either case is very nearly equal to the strength; and whether or not cracking occurred would depend on how rapidly the snow layer was removed, that is, how much time was available for compressive creep to occur at the base of the sheet to reduce the thermal stress.

The good agreement observed here suggests that temperature data should be collected and analyzed at the site to anticipate whether cracking is likely. Overnight cold snaps have been observed to cause otherwise unexpected failures during loading of ice landings.[2] Apparently, upper-surface cracks form because of the temperature transient, and (if the temperature is very low) do not heal by surface diffusion or sublimation. To avoid low temperature brittleness, Assur[1] recommends that the necessary ice thickness for regular operation at very low temperature be increased to that for emergency operation at temperatures near the melting point.

8.5 Crack Frequency

Knowledge of the distribution and frequency of different crack lengths and depths would be necessary to make any general assessment of the load-bearing capacity of floating ice sheets. However, because there are many different sources of cracks, no simple statistical description of crack occurrence seems possible. For instance, the frequency of wet open cracks from tidal action would depend on the latitude, coastline shape, general topography of the ocean floor, and current patterns in a local area. Shore spacing in a bay or lake is as important as any property of the ice. Similarly, the occurrence of cracks from temperature transients depends on the ice thickness, snow cover, and average temperature fluctuations in a given locality. Because of the sensitivity of ice cracking on environment, the following specific observations on crack spacing are not to be considered as general.

Linell[3] mapped a test area in which the thermal crack spacing was approximately 10 ft. The cracks were essentially continuous, separating the total area into crack-free areas averaging approximately 100 ft^2. He noted that the depth of thermal cracks is generally less than half the thickness of the ice sheet. In a different location, Barnes[4] recorded an average spacing of about 40 ft for all cracks that had formed up to the date of observation, most of which had rehealed. In the North Star Bay tests, the spacing between cracks resulting from snow removal from the runway was about 150 ft at one end of the runway; no cracks of this kind formed at the other end. Thus, typical spacings range upward from a few feet to hundreds of feet for cracks resulting from temperature transients. The length of these cracks will have a minimum approximately equal to their spacing, with maximum lengths many times their spacing. Open cracks are of much less frequent occurrence; areas free from open cracks are specified for use as runways.[1]

8.6 Open Cracks

Of the several types of cracks, open wet cracks have the greatest effect on ice operations. Load-bearing capacity in the vicinity of the crack is reduced; and, for ice islands or cracks in the center of an ice sheet on a lake, the crack width may be variable and erratic.[5] In general, areas where the cracks may open to an extent that they cannot safely be crossed can and should be avoided. We can therefore restrict our attention to the effect of open cracks on the load-bearing capacity. Gold, et al[6] have experimentally measured the elastic deflection of edge-loaded plates, and shown that the load-carrying capacity is about 43 percent of that of a centrally-loaded place. Thus for a distributed load placed on top of a crack in such a way that the load bears on both sheets, the load-carrying capacity is 85 percent of that for the uncracked or centrally-loaded sheet. Black[7] has experimentally confirmed that with edge loading the load-bearing capacity of a glass sheet is about 40 percent of the central-load capacity.

This relative load-bearing resistance supports the technique recommended for ice landings,[2] where it is suggested that vehicles traveling over cracked ice should straddle the cracks. On the other hand the procedure suggested by Assur[1] is that active cracks be crossed at right angles. This is at variance with the optimum load-bearing capacity and may have been recommended to minimize the possibility of having a wheel jam in the crack or to minimize the dangers involved if a crack opened unexpectedly.

8.7 Bottom Cracks

Bottom cracks in floating ice sheets are not a great hindrance since they easily heal because of the access of water and because the ice sheet is usually below the freezing point. However, occurrence of bottom cracks after loading is the first step toward failure; the collapse load for ice sheets is twice that at which bottom cracking first occurs for short-time loading. For longer loading times, the ratio of time to initial cracking to the times to final failure has not been studied, but should provide a useful relation for governing parking duration.

8.8 Top Surface Cracks

Top-surface cracks do not have the access to water that allows healing or filling in without maintenance. However, passage of time lessens their severity because of shape change at the crack tip by surface diffusion and sublimation. The load-bearing capacity of an ice sheet, and the formation of radial and circumferential cracks prior to failure, has been shown by Linell[3] to be independent of a few open and healed cracks in the vicinity. This insensitivity results first from the fact that the stress in the upper surface is compressive out to a distance from the center of load known as the radius of relative stiffness,

$$r_s = \sqrt[4]{\frac{Eh^3}{12\,(1-\mu^2)\rho}} \,.$$

Linell also noted that thermal cracks rarely penetrate one-half the thickness of the ice sheet; therefore, within the circle of radius r_s upper-surface cracks cannot propagate because the region of the ice sheet that they occupy is in compression. The curvature of the ice sheet changes at $r = r_s$ and at greater radii the upper surface is in tension. However, the peak surface tensile stress is approximately ten times smaller than that occurring on the bottom surface of the sheet immediately below the load.

The weakening influence of cracks can be estimated from a calculation of the average apparent "flaw" size required to explain observed ice strengths. From Griffith's theory of strength, the theoretical strength (σ_t) is approximately 1/10.

the elastic modulus, or σ_t = 30,000 psi for ice. The ratio of crack or flaw length (b) to tip width (a) is given by,[8]

$$\frac{\sigma_t}{\sigma_a} = 2\ b/a \qquad (8.4)$$

For a strength σ_a of 300 psi, b/a = 2500. If we assume that the base of a crack is rounded by surface diffusion to 4μ, then the crack length b required to satisfy the above equations is about 1 cm. If the observed strength we wish to rationalize is 100 psi, the required crack length is 10 cm.

Ten centimeter cracks or flaws are exceedingly large compared with the crack length of about 1 micron estimated for glass of usual strength. This difference results from the fact that the surface mobility in the ice prevents the maintenance of small radius crack tips, and the length must be much longer. The crack lengths calculated above are obviously large enough to be readily visible. Tensile strengths of ice measured in crack-free samples range from 100 to 400 psi; this suggests that either grain boundary fracture or cleavage in certain directions occurs at significantly lower stresses than those calculated from theory. Because of this apparent intrinsic weakness, the effect of macroscopic cracks with rounded tips must be much smaller than otherwise would be the case. Barnes[4] observed that the strength of melting lake ice was almost unaffected by the introduction of saw-cut notches up to 20 inches in depth (he attributed this effect to the presence of an ice layer 20 inches thick at the top surface of zero strength); Linell[3] observed that previous cracks had almost no effect on subsequent crack development. These observations may simply result from the fact that large cracks with rounded ends yield strengths equivalent to those observed in crack-free specimens.

We may conclude then that superficial cracks in the upper surface of the sheet at distances greater than the radius of relative stiffness will have little effect on the strength.

8.9 Load Bearing Capacity Based on Buoyancy

Even if we adopt the view that cracks beyond r_s do propagate through the sheet, there will be a finite load-bearing capacity of the remaining slab. Let us assume that the crack propagates forming a circle surrounding the point of load application. The load-bearing capacity based on buoyancy alone is presented in Table 8.1 for peripheral

cracks at $r/r_s = 1$ and $r/r_s = 2$. This shows that the buoyancy is greater for cracking at $r = r_s$ than the recommended loading for normal operation in 10°F air[1] and that peripheral cracking at $r = 2r_s$ still provides a buoyant force sufficient to carry the loads recommended for emergency operation. The significance of these results is that the minimum allowable spacing between cracks is small and the area which must be surveyed for cracks is also small.

8.10 Ice Sheet Fracture

All of the above comments are based on elastic deformation of the ice sheet, for which the relation between load and deflection has been given by Westergaard.[9] With a critical tensile stress as the fracture criterion, the load required to initiate fracture is simply related to the thickness,

$$P = (\text{const})\ h^2 \tag{8.5}$$

Because the tangential moments are greater than the radial moments, the fracture (which initiates immediately beneath the load on the bottom surface) must propagate radially. This reduces the tangential moments to nearly zero in the isolated wedges, and causes the radial moments to change sign, transferring the tensile stress to the top surface at some distance out from the load, related to the length of the radial cracks. If a point load had been applied, the moment would be constant with increasing radius. With a distributed load, the moment and maximum radial tensile stress increases with increasing radius (neglecting buoyant forces). The second crack which occurs during failure of an ice sheet propagates circumferentially, at some distance from the load. The most probable radius where circumferential cracking will occur is given in Table 8.1. This behavior suggests that a critical tensile stress is the most suitable fracture criterion, because the maximum shear stress occurs at the periphery of the loaded area and decreases with increasing radius.

It is to be noted that the most probable radius of circumferential cracking is smaller than the radius of relative stiffness r_s (also given in Table 8.1); r_s is a radius within which the upper surface is in compression prior to bottom cracking. The presence of pre-existing upper-surface cracks within the radius of circumferential cracking would probably reduce the margin of safety between the load for first cracking and the load for final break-through. Final break-through does not occur until sometime after a circumferential crack has completely formed. This

TABLE 8.1

Recommended Operational Loadings, Buoyant Forces, Radii of Relative Stiffness, and Probable Circumferential Crack Radii Related to Sea-Ice Thickness.

Ice Thickness	r_s (ft)	Buoyant Force ($r = r_s$)	Buoyant Force ($r = 2r_s$)	Emergency Op'n 10°F Air	Regular Op'n 10°F Air	R (ft)	$L = 4.94\ r_s$ (ft)
15"	22	9,800 lb	39,200 lb	16,000 lb	8,000 lb	13	110
20"	28.5	21,300	105,000	30,000	15,000	17	140
30"	36.5	54,400	218,000	85,000	40,000	25	180
40"	46.5	117,000	468,000	160,000	80,000	32	230

$$r_s = \sqrt[4]{\frac{Eh^3}{12(1-\mu^2)k}}$$

L = 4.94 r_s = Basic load influence radius (Assur)

R = expected distance to circumferential crack (SIPRE Report No. 36)

failure may result from shear deformation from the bottom of the circumferential crack. If pre-existing cracks were within this most probable radius, the shear stresses would be higher and the load-bearing capacity would be reduced (if final fracture is by shear). This suggests that in surveying cracks to locate suitable parking areas, loads should not be located nearer to cracks than the radius of relative stiffness. This provides sufficient flotation for supporting the loads under normal operation, as specified by Assur.[1]

Meyerhof[10] has extended the elastic analysis of load-bearing resistance of ice sheets by introducing Tresca's shear-stress criterion as that which governs deformation. His model leads to the same pattern of failure as is observed, but the radius at which circumferential cracking actually occurs is significantly less than that predicted. Whether this means that the actual yield strength in shear is greater than half the tensile strength, or that the shear criterion is less important, is not known to the authors.

Both the elastic and plastic analyses of the ice sheet only approximate true behavior for long-time loading because a temperature gradient generally exists through the sheet, and the creep properties of ice are strongly temperature dependent. Rigorous analysis of deformation to failure and of effects of cracks on load-bearing resistance must await solution of the more general case.

8.11 Conclusions

Unless there are open wet cracks in the immediate area of loading, ice is remarkably insensitive to the presence of cracks. This insensitivity of the load-bearing resistance of ice is attributed to several factors:

a. Cracks penetrating completely through the ice sheet are of sufficiently infrequent occurrence that suitable areas can be found in which few or none are present.

b. Top surface cracks have relatively little effect on initial cracking because (1) in the region near the load where the bending moment and stress are highest, the upper-surface stress is compressive and cracks do not propagate, and (2) at relatively large distances from the load where the upper-surface stress is tensile, the moments are much smaller than the maximum moment under the point of loading.

c. Because of apparent easy cleavage or grain boundary fracture in crack-free ice, large cracks which have had an opportunity to undergo rounding at the tip do not cause excessive strength reduction.

d. Load-bearing capacity based on buoyancy shows that cracks in the region beyond the radius of relative stiffness, r_s, are not as serious as supposed when it is assumed that the ice sheet derives little load-bearing capacity from bouyancy. Therefore, recommended precautions about parking at distances of about $5r_s$ from the edge of a sheet or an open crack appear to be overly conservative.

e. A change in sign of the bending moment <u>after</u> initial bottom-surface cracking occurs within r_s. Therefore within this distance the presence of top-surface cracks should be critically surveyed in deciding on the suitability of a given area for parking.

REFERENCES

1. Assur, A., "Airfields on Floating Ice Sheets for Regular and Emergency Operation," SIPRE, Report 36, (Jan 1956). SIPRE, Corps of Engineers, U. S. Army, Wilmette, Illinois, Suppl. 2, SIPRE, Report 36, (Oct 1956). Suppl. 3, SIPRE, Report 36, (Oct 1956).
2. Duff, C. H., "Ice Landings," Trans. EIC, 2(3) p. 99 (Sep 1958).
3. Linell, K. A., "Use of Ice as a Load-Supporting Surface," presented Amer. Soc. Civil Engrs. Conv., New York (23 Oct 1951). (Arctic Construction and Frost Effects Lab, New England Div. Army Corps of Engineers, Boston, Mass. (Aug 1958).
4. Barnes, D. F., "Preliminary Measurements of the Strength of Melting Lake Ice," Trans. EIC, 2 (3) p. 108 (Sep 1958).
5. Persson, Burgt O.E., Svenska Vagforenngens, Vol. 35 (Dec 1948). Translated W. Dias, Arctic Construction and Frost Effects Lab, New England Div. Army Corps of Engineers, Boston, Mass. (1954).
6. Gold, L. W., L. D. Black, F. Trofimenkof, and D. Matz, "Deflections of Plates on Elastic Foundation," Trans. EIC, 2 (3) p. 123 (Sep 1958).
7. Black, L. D., "Relative Strength of Plates on Elastic Foundation," Trans. EIC, 2 (3) p. 129 (Sep 1958).
8. Kingery, W. D., Introduction To Ceramics, p. 604-605, John Wiley and Sons, New York (1960).
9. Westergaard, H. M., "Stresses in Concrete Pavements Computed by Theoretical Analysis," Public Roads, Vol. 7, No. 2 (April 1926).
10. Stearns, S. Russell, "Aircraft Operations on Floating Ice Sheets," J. Air Transport Div., 83 (ATI) (Jul 1957).
11. Meyerhof, G. G., "Bearing Capacity of Floating Ice Sheets," Proc. Amer. Soc. Civil Engrs., J. Engineering Mech. Div., 86 (EM5) 10, 113 (1960).

9. TEMPERATURE, SALINITY, DENSITY, AND RING TENSILE STRENGTH DATA FOR NATURAL AND CONSTRUCTED SEA ICE (by J.E. Dykins, NCEL)

9.1 Introduction

One study on the properties of the natural and constructed ice in North Star Bay was a determination of temperature, salinity, density, and relative tensile strength of the ice types during and after construction. The objective of this study was to determine the relationships of these properties as a function of depth and time. Temperature measurements were made with thermocouples frozen into the ice; salinity, density, and relative tensile strength determinations were made from samples cored from the ice. The data has been analyzed to indicate trends rather than individual values of specific properties.

The study began in early February 1961 and ended on 31 May. The individual tests, while not as extensive as originally planned because of a manpower shortage, were conducted systematically on all constructed ice and on the natural ice in the test area.

9.2 Experimental Techniques

Correlation of salinity, density, and relative tensile strength as a function of depth and time necessitated a revision of test procedures used in the past by NCEL. Primarily, this change was to process the test specimens as soon as possible after extraction rather than to store them for indefinite periods before testing.

Immediate processing demanded that all specimens be tested as extracted. As a result a mobile, sled-mounted, test trailer (Figure 4.2) was designed and equipped to take salinity, density, and strength measurements at the core sites. All test specimens were extracted from the ice sheet with a 3-inch diameter SIPRE coring auger.

9.2.1 TEMPERATURE

Thermocouples were used to measure the in situ temperature of the ice at selected points in each constructed ice area and in one natural ice area away from the construction areas. Before construction, a harness of thermocouples consisting of a series of copper constantan, field-made couples was installed through a 4-inch hole in the natural ice. The individual thermocouples were 1/2-inch long and

projected 90° to the h' .ness. A weighted fishline was used to hold the harness in position during freez -in. This method was selected in preference to the use of a wooden pole support in order to reduce the thermo-conducting capacity of the support.

The two bottom thermocouples on the harness projected into the sea water below the ice sheet. Generally, the bottom couple projected 14 inches below the ice. In the natural ice the thermocouples were spaced 12 inches apart. Spacing in the built-up ice was either 4 or 6 inches, depending on the method of construction. In Parking Aprons Nos. 1 and 3 and Test Plots 4 and 5 the spacing in the built-up ice was 4 inches; in Apron No. 2 the spacing was 6 inches. At all sites a thermocouple to measure air temperature was kept at a constant height of 54 inches above the ice surface.

The thermocouples were read with a portable potentiometer equipped with an automatic reference junction temperature compensator. The instrument scale, covering the range from -100° F to +100° F, was calibrated to read in direct temperatures. To prevent freezing, the standard cell used in the potentiometer was carried next to the observer's body.

Temperatures were read to the nearest one-half degree Fahrenheit. The accuracy of the recorder was checked periodically by comparing air-temperature readings with simultaneous readings from an accurate alcohol thermometer.

Special temperature observations were scheduled for Apron No. 1 in an attempt to obtain a detailed record of the freeze-up in selected flood layers and the thermal shock in the underlying natural ice. Thermocouples were spaced 1 inch apart at certain locations, and an electrically-driven automatic recorder was installed to make hourly recordings. No satisfactory record of these temperatures was obtained because of electrical trouble in the instrument.

9.2.2 SAMPLE COLLECTION

Each specimen was used to measure one or more ice properties. All specimens regardless of condition were tested for salinity but only the whole specimens were used for density measurements and ring tensile strength tests.

During the construction period, measurements were made only for salinity and density. Specimens for these tests were taken just prior to the addition of each new layer. In the constructed ice the length of specimen for salinity was determined by the thickness of the constructed layer. These specimens were usually between 4 and 5 inches long. For density, a 3-inch segment was cut from these specimens. In the natural ice below, a 3-inch specimen out of every 6 inches of core was sampled for both salinity and density.

Apron No. 1, which was not reinforced with Fiberglas, was the only one in which the underlying natural ice was sampled during the construction period. This was to prevent damage to the reinforcement in Aprons Nos. 2 and 3 prior to the aircraft tests. When sampling, two cores were taken from each constructed ice area, but only one of these cores was taken completely through the underlying natural ice.

During the post-construction period, specimens were tested for relative tensile strength, as well as for salinity and density. Further, the sampling procedure was altered for this period. Each core was cut into 3-inch lengths regardless of the occurrence of layer interfaces, and Aprons Nos. 2 and 3 were sampled all the way through the natural ice after completion of the aircraft tests.

To observe and retain any brine drainage each core was cut immediately after extraction and the specimens were placed in covered plastic canisters. Those selected for measurement of density and strength were processed as rapidly as possible and returned to the canisters. Then, all specimens were melted at room temperature for salinity tests.

In the first half of the test season, when the air was cold, wet core surfaces would almost immediately glaze, and no brine drainage was observed in the containers. However, in the latter half of the test season, when the air temperature was warmer, a small amount of drainage was observed in canisters containing some of the wetter specimens.

9.2.3 SALINITY

The salinity was determined with a hydrometer graduated to read direct salinity in two-tenths of a part per thousand. The temperature of the meltwater from the specimen was measured with a mercury thermometer to the nearest degree Centigrade. Then, the observed values were converted to salinity at 15°C.

9.2.4 DENSITY

For density, the specimens were cut in a miter box modified to hold the specimen securely and automatically gage the cutting length. Square-end specimens with little or no edge-chipping could be produced by using the proper sawing technique. Specimens with excessively chipped edges or other nonuniform dimension characteristics were rejected.

The volume of the specimen was obtained using an average of three length measurements and three diameter measurements. A modified dial-face caliper graduated in millimeters was used to measure the specimen. The caliper was modified by increasing the length and width of the measuring blades; the longer blade permitted a more positive diameter reading, and the wider blade prevented penetration of the specimen. The specimens were weighed in air on a triple-beam balance graduated to read to the nearest one-tenth gram.

Density calculations were computed to three significant figures using the volume and weight measurements.

9.2.5 RING TENSILE STRENGTH

Strength of the 3-inch-diameter by 3-inch-long density specimens was determined by the SIPRE ring tensile test.[1] This test consists of applying a compressive load normal to the axis of the cylindrical specimen to cause failure in tension. The failure plane occurs directly under the load and is parallel to the direction of the applied load. In most test work using the ring tensile test, a small hole is drilled in the specimen concentric with the diameter and parallel with the cylinder axis. However, in Project ICE WAY the specimens were tested as solid cylinders. Elimination of the center hole in the specimen expedited sample preparation and testing. In the analysis of the test results, the assumption was made that an infinitesimal passage parallel to the cylinder axis of the specimen exists, causing the initial stress concentration and the resulting tension failure. This assumption was based on parallel orientation existing between the cylinder axis of the test specimen and the normal growth direction of the ice crystal. The ice cores were taken normal to the surface of the ice sheet. Available literature indicates that the ice crystal is a lamination of ice plates, each separated by a brine layer either of a continuous or discontinuous nature depending on the ice temperature. Since the samples were all tested well above the eutectic point of sodium chloride (about -23°C) it appears reasonable to assume that liquid and/or air-filled passages exist.

The theoretical formula used for calculating the ring tensile strength was:

$$\sigma = \frac{KP}{\pi r \ell}$$

where:

σ = ring tensile strength
K = stress concentration factor
P = total applied load at failure
r = radius of test specimen
ℓ = length of test specimen

For this set of data, a value of 6 was assigned as the stress concentration factor. The value 6 assigned to K is the theoretical constant for a test specimen with an infinitesimal hole through its center. In theory, K has a value of 1 for a solid specimen and passes discontinuously from 1 to 6. For specimens that have had a definite hole drilled through their center, a K value of 7.1 is generally used. Limited experimentation by NCEL has indicated that different strength values can be obtained by varying the size of the hole that is drilled in the specimen. Higher strength values were obtained as the size of the hole was decreased. Likewise the ice strength values for the work contained in this report are higher than those found in other NCEL test work on sea ice in which the specimens were tested with a 1/2-inch hole. With this apparent discrepancy in the application of this theoretical formula, all tensile strengths shown in this report are considered to represent only relative strength and not a value for true tensile strength.

Possible causes for the scatter found in the strength data would be (1) the effect of random structural defects in the specimens, and (2) the varied orientation of the plane of the crystal plates in respect to the direction of load application.

All specimens were tested in a hand-operated mechanical loading press employing a small, screw-jack, soil-test press. A 2000-lb load cell connected to a brush recorder and analyzer was used to measure and record the breaking load, as well as to indicate the loading rate. The pen writing mechanism of this instrumentation, however, was a constant source of trouble and it was early abandoned in favor of the simpler proving-ring method.

The proving ring had a load capacity of 1500-lb. Total load-application time for checking the rate of loading was measured with a stop watch. This method resulted in some specimens being tested at a lower rate of loading than the recommended minimum of 7.1 psi/sec. To retain as much of the data as possible, 6 psi/sec was arbitrarily set as the minimum load rate from which data would be used. Upon examining all of the data, no discernible difference in strength appeared to have resulted from the various load rates beyond the normal scatter. The proving ring was checked for accuracy after the field tests were completed.

9.3 Experimental Results

For analysis of each ice type, the test data was reduced to mean values for each 1-ft stratum and for the total ice thickness. These were developed into general behavior trends in depth and time for each ice type rather than individual values for specific properties. Curves depicting these trends were compiled by the statistical method of moving averages using three sampling periods in order to smooth out most irregularities which occurred in the day-to-day measurements. The basic data used to develop these curves is summarized in Appendix D.

9.3.1 UNDISTURBED NATURAL SEA ICE

The sampling area for undisturbed natural sea-ice was 48 inches thick at the start and 54 inches thick at the end of testing. General behavior trends for this ice are shown in Figures 9.1, 9.2, and 9.3.

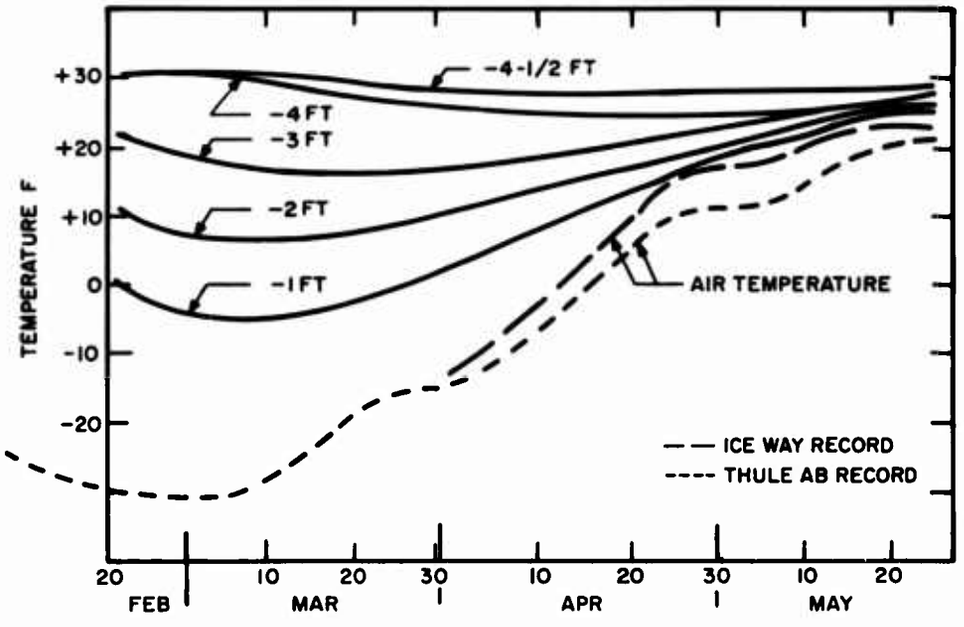

FIG. 9.1 Ice temperature profiles by stratum in the undisturbed natural sea ice

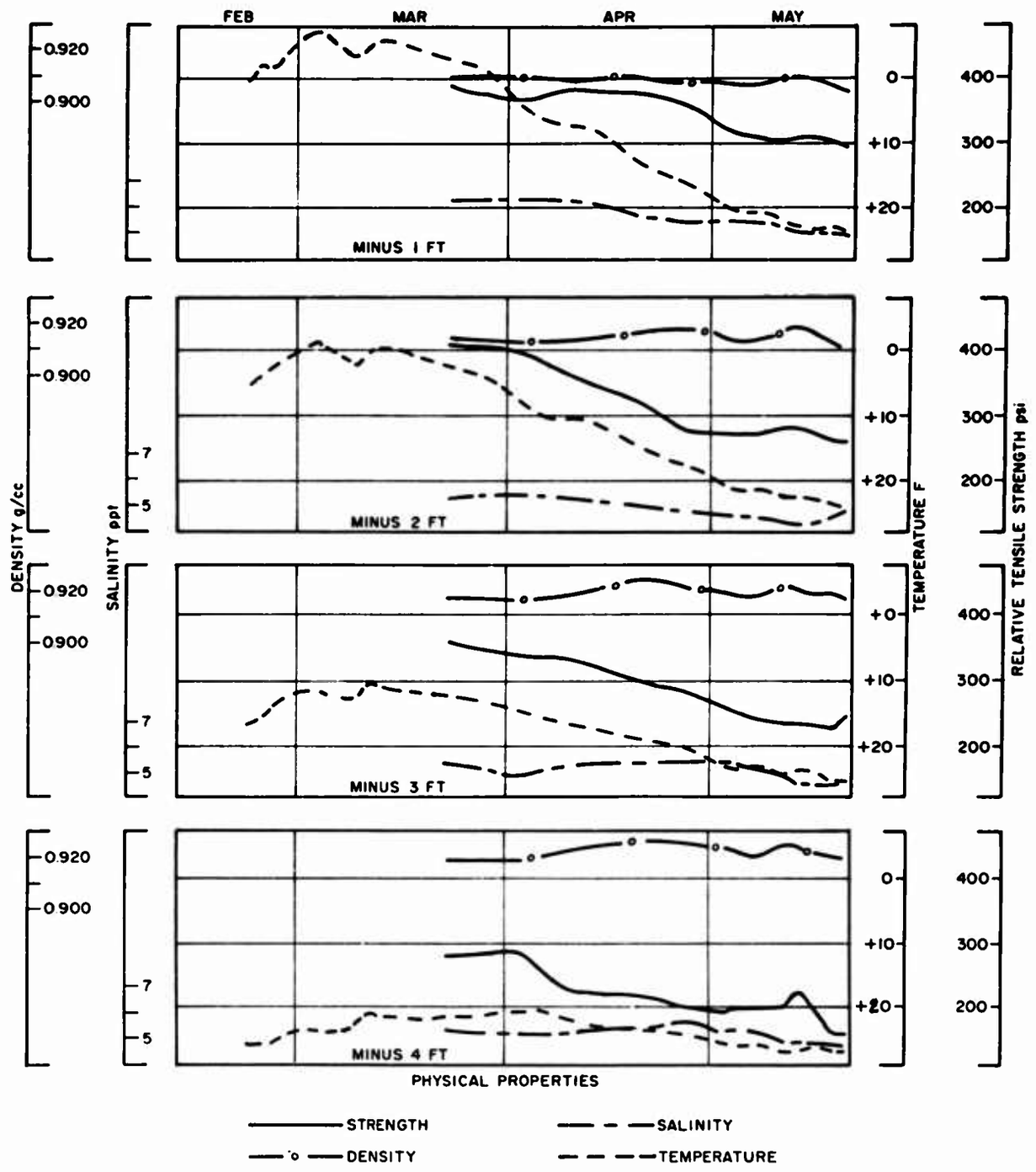

FIG. 9.2 Trend curves of physical properties by stratum for the undisturbed natural sea ice

The continuous temperature profiles for each stratum of natural ice are compared with the mean weekly air temperature in Figure 9.1. Except for the top foot, the profile of each stratum is the mean of the upper and lower in situ boundary temperatures. Only the lower boundary temperature was available for the profile of the top stratum. The 4-1/2 ft, or bottom, profile represents sea-water temperatures in February and the temperature of sea-ice in May. The profiles show that the temperatures in the top strata of ice generally followed the warming trend of the air temperature, and that the average temperature for the total ice thickness was increasing. The temperature gradient through the ice, which was nearly 30 F in early March, narrowed to about 5 F in late May. During this same period the average total ice temperature increased from about 10° F to 25° F (Figure 9.3). Examination of the data showed that the temperature gradient through the ice at any given time was almost a straight line pivoting about the water-ice interface, or skeletal layer.

Trend curves for temperature, salinity, density, and strength of each stratum are compared in Figure 9.2. Examination of the salinity curves shows that the top stratum is more saline than the lower strata. Also, a decrease in salinity in the top two strata during March and April shows up as an increase in the bottom two strata during April. This indicated the retention of some brine in the lower strata, even though there was a decrease in salinity for the total ice thickness (Figure 9.3).

There was a general increase in density in all except the top strata during April (Figure 9.2) with the most pronounced increase occurring in the bottom two strata. During May there was a decrease in density for the total ice thickness, although the bottom two strata still had a slightly higher density than in March. As shown in Figure 9.3 the decrease in total density follows the decrease in total salinity. This indicated that the inclusions within the crystal matrix, from which brine was draining, were not being refilled by sea water under hydrostatic head or by infiltration of surface melt. The increase in density of the lower strata probably resulted from retention of at least part of the brine migrating from the upper strata.

The variation in individual density values for each stratum increased as the ice became warmer. This trend also was observed in the salinity values, indicating that the ice became more heterogeneous as it warmed. This increasing dissimilarity between specimens was probably caused by random interconnection of the brine inclusions during migration.

The relative tensile strength decreased with depth and with the increase in temperature of the total ice thickness during the test period. This is shown for the individual strata in Figure 9.2 and for the total thickness in Figure 9.3.

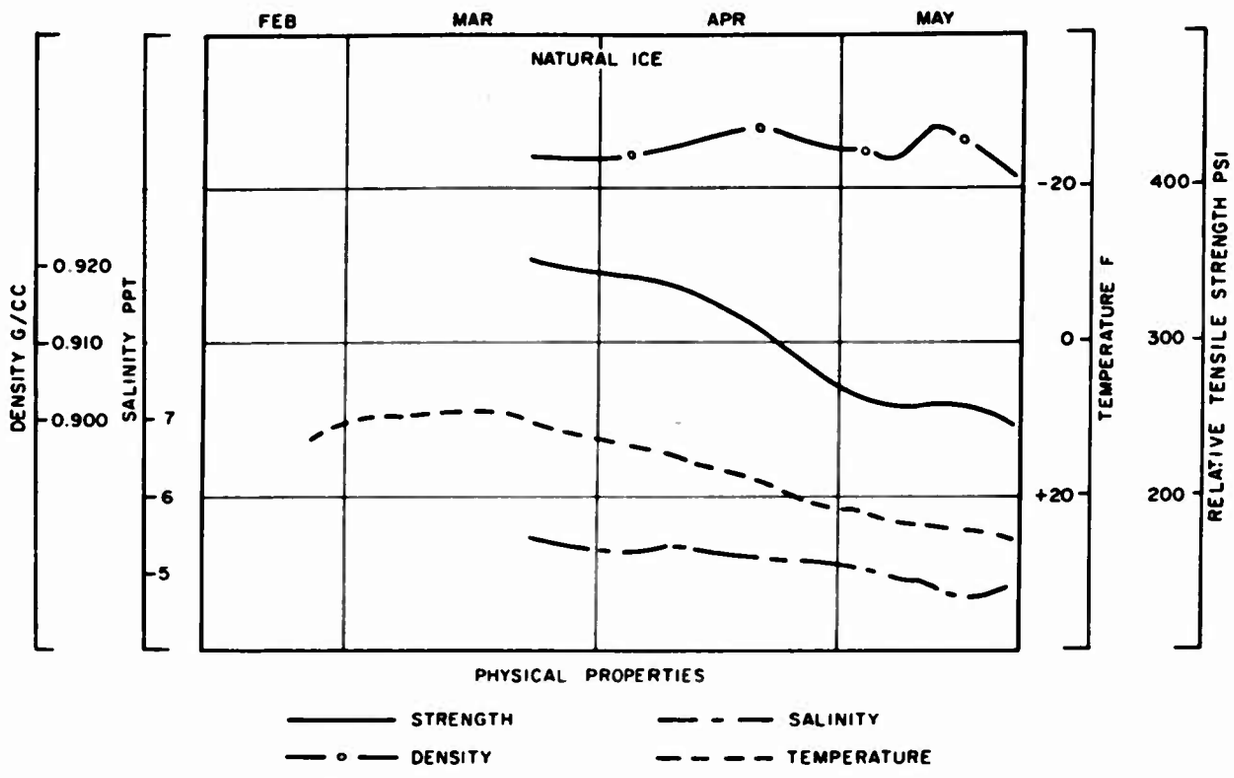

FIG. 9.3 Trend curves of physical properties for the total ice thickness in the undisturbed natural sea ice

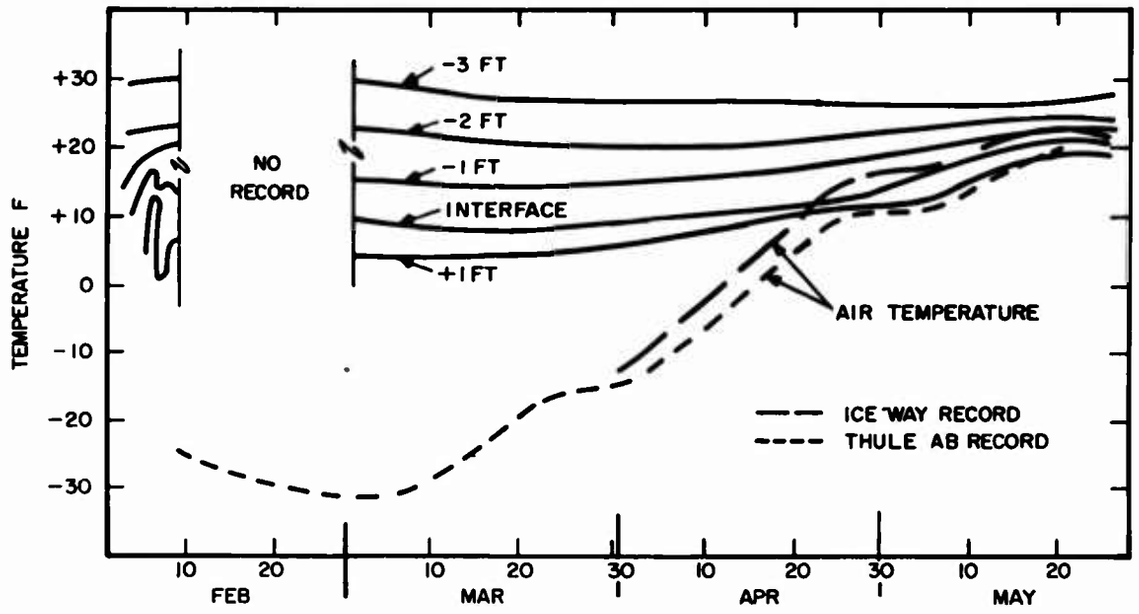

FIG. 9.4 Ice temperature profiles by stratum in the free-flooded parking apron (Parking Apron No. 1)

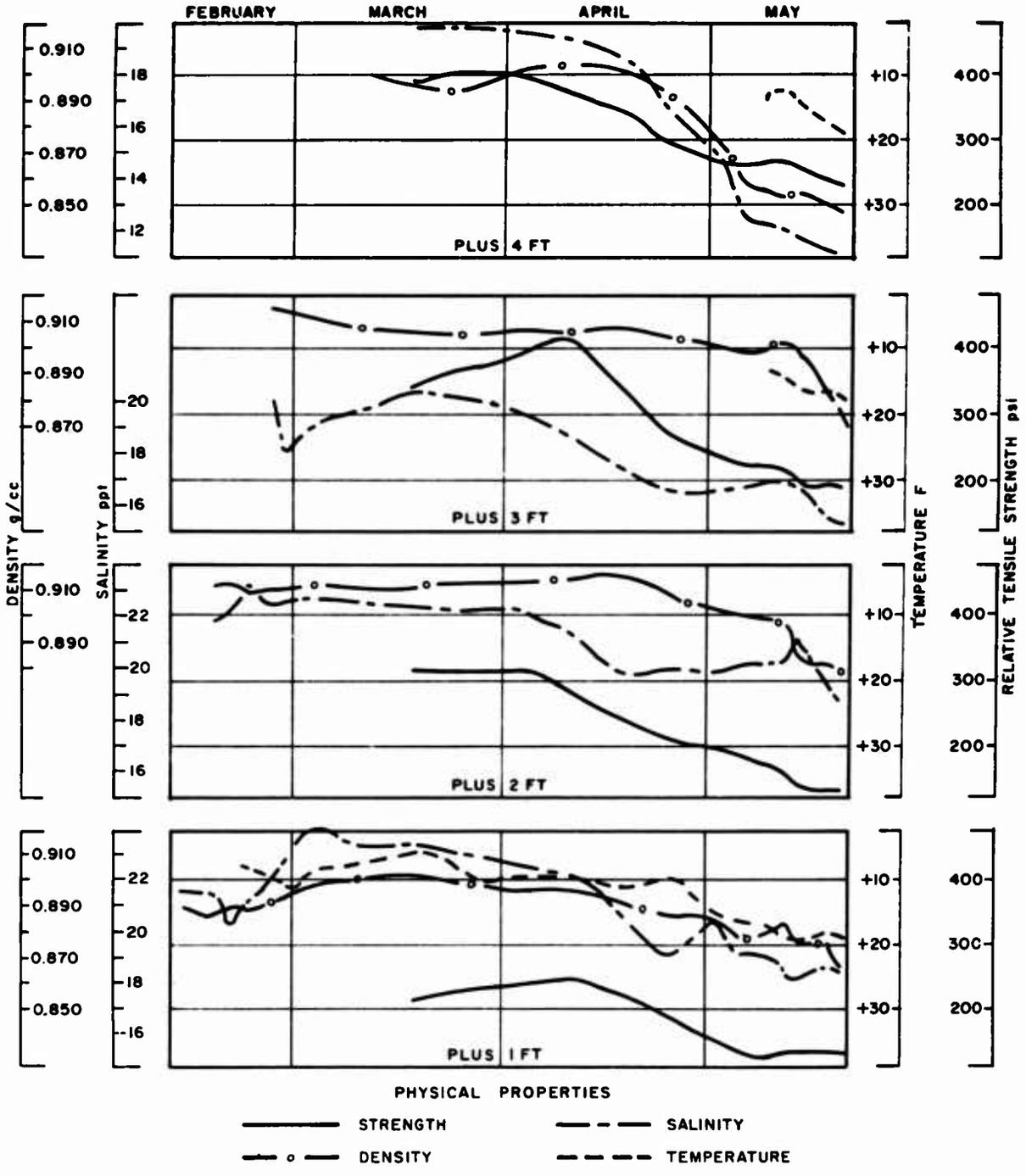

FIG. 9.5 Trend curves of physical properties by stratum for the constructed ice in the free-flooded parking apron (Parking Apron No. 1)

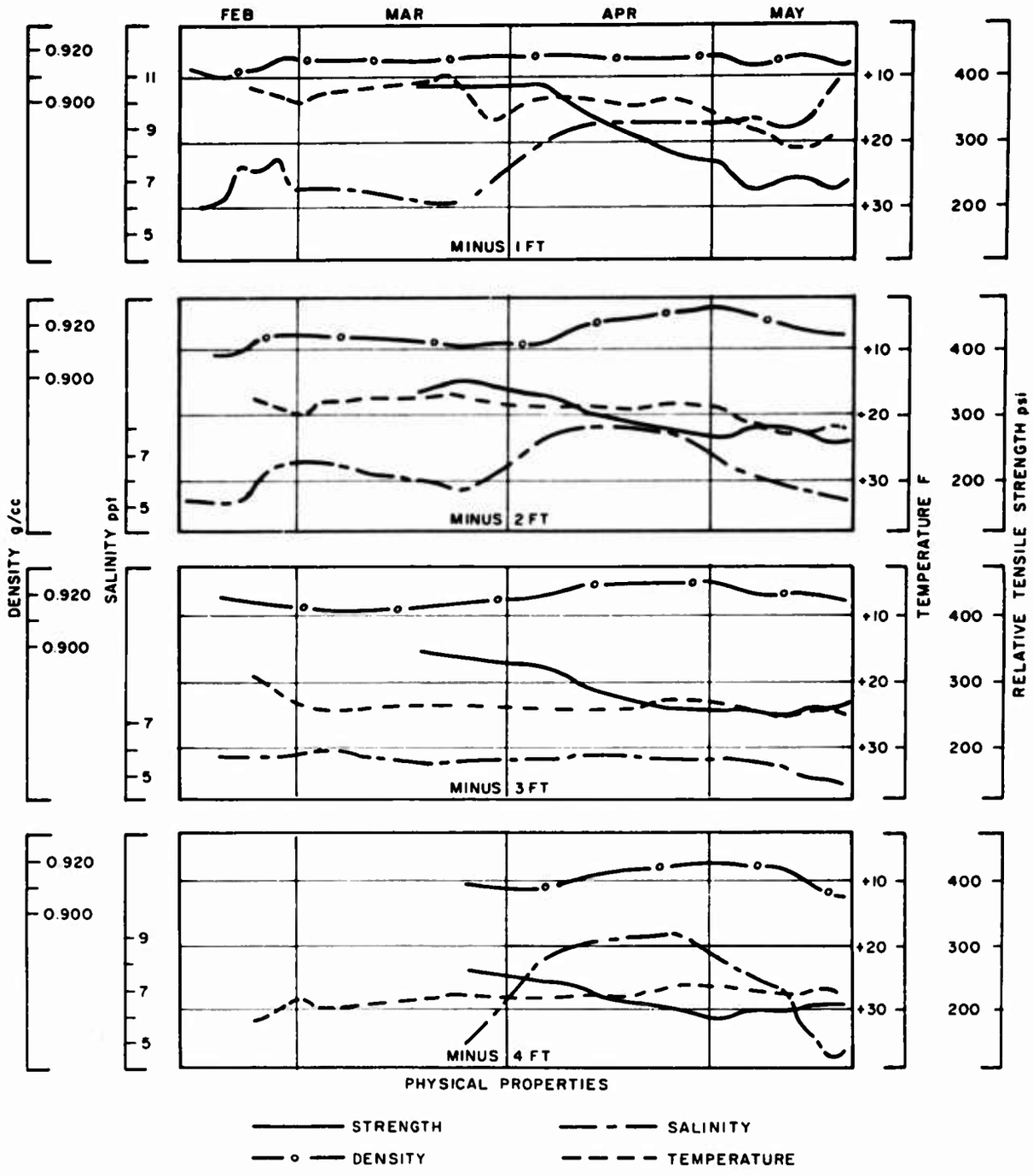

FIG. 9.6. Trend curves of physical properties by stratum for the underlying natural ice in the free-flooded parking apron (Parking Apron No. 1)

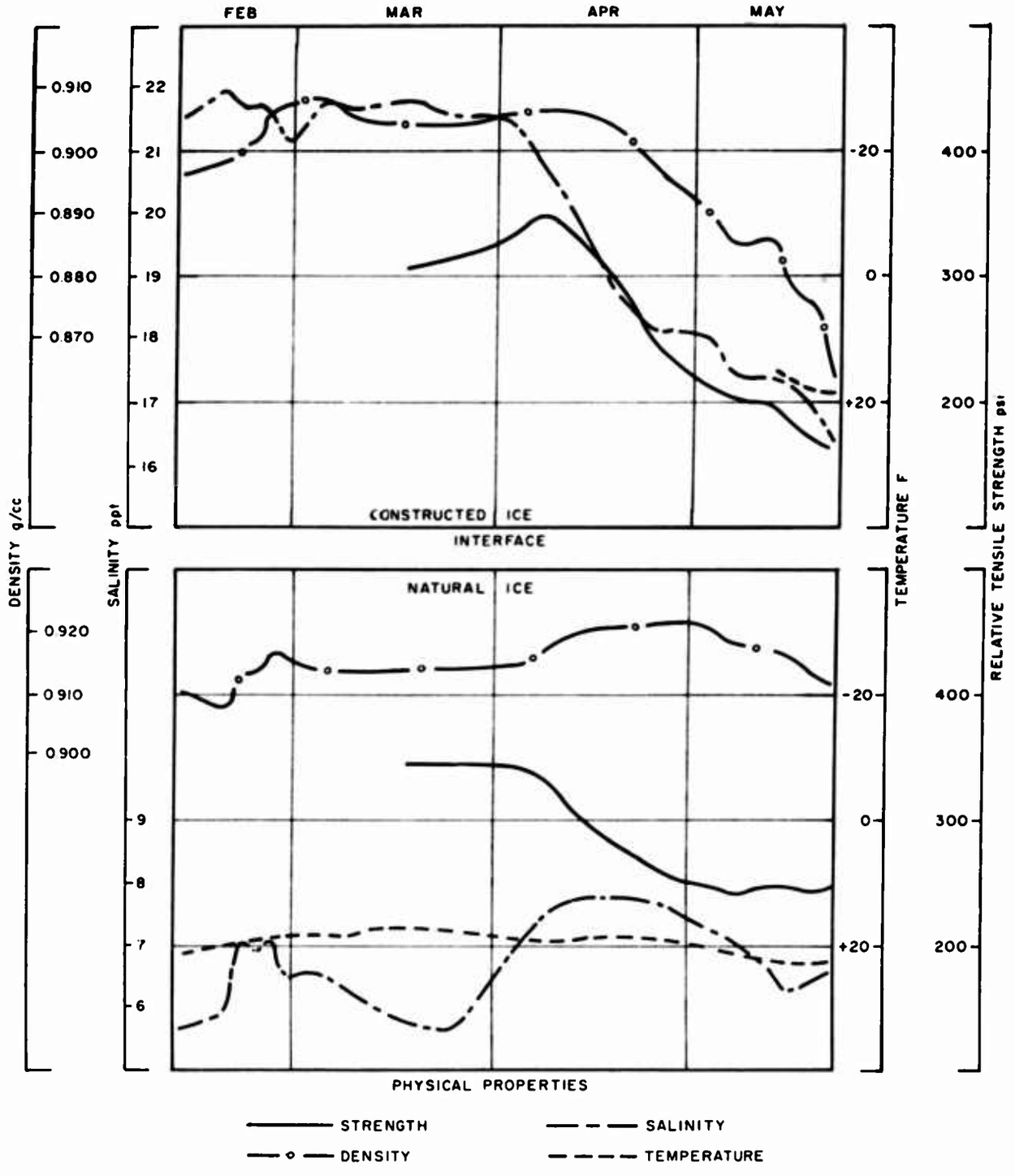

FIG. 9.7. Trend curves of physical properties for the total ice thickness in the free-flooded parking apron (Parking Apron No. 1)

9.3.2 FREE-FLOODED PARKING APRON

This analysis of Parking Apron No. 1 covers the entire cross-section of constructed and underlying natural ice. The total ice-thickness in the sampling area, which ranged from 7 to 8 ft, was equally divided between constructed and natural ice. For analysis the original natural ice surface was used as a reference point from which the constructed ice was designated as plus stratum as opposed to minus stratum for the natural ice. General behavior trends for this ice are shown in Figures 9.4 through 9.7. In examining the data the most apparent feature was the fact that the two ice types displayed similar but individual profiles for each property.

Temperatures data for the parking apron was meager due to malfunction of the automatic recorder. The temperature profiles for the natural ice stratum in Figure 9.4 are the mean of the boundary temperatures for the stratum indicated. The profile for the interface temperature and the plus 1-ft stratum (constructed ice) are individual temperatures. No other temperatures were obtained for the constructed ice except for the month of May; but, because of its brevity, this data was not included in Figure 9.4. The warming of the natural ice in early February was the result of flooding the ice during construction of the parking apron. Following completion of construction on 1 March the profiles flatten, indicating a slight cooling. The sharp rise in air temperature, beginning about 1 April, caused a gradual climb in the ice temperature. By the end of May there was about a 10° F temperature gradient through this ice thickness as compared with the 25° F gradient in early March.

A well-defined decrease in salinity in each strata was observed for the constructed ice (Figure 9.5) during the post-construction period with the greatest decrease occurring in April. For the underlying natural ice (Figure 9.6) the salinity increased in each strata during April, followed by a decrease in salinity during May except for the top stratum. Comparing the total salinity change in the two ice masses (Figure 9.7) indicates that some brine draining from the constructed ice was retained in the natural ice during April. However, during May sufficient channeling apparently had developed in the natural ice, not only to discharge the current brine draining from the construction ice but also to drain most of the brine accumulation of April.

The densities for each stratum in the constructed ice (Figure 9.5) changed very little from early March to mid-April. A large decrease, however, occurred between mid-April and late May with the most pronounced decrease occurring in the top stratum. In the underlying natural ice a small increase in the density occurred in April and a slight decrease in May.

The relative strength curves for corresponding strata in the constructed and underlying natural ice were nearly the same in late March and early April (Figures 9.5 and 9.6). In April there was a decline in strength in both types of ice; for constructed ice this decline continued into May. This decrease probably was the result of warmer weather duruing this period (Figure 9.4).

The reduction in strength was about 50 percent for the constructed ice and about 26 percent for the natural ice. This is somewhat misleading, however, because the test temperatures of the specimens were different from their in situ temperatures (Appendix D). The strength of the natural ice under the parking apron (Figure 9.7) differed little from the undisturbed natural ice shown in Figure 9.2.

The trend curves for the total thicknesses of each ice type (Figure 9.7) show very clearly the effect and interrelationship of the events that resulted from thickening an ice sheet by surface flooding. Within 15 days after construction started, the salinity of the underlying natural ice had increased nearly 25 percent. An increase in density accompanied this salinity shift. During this same period there was also a general increase in density of the constructed ice. During March little or no change occurred in the salinity and density of the constructed ice. In contrast the underlying natural ice experienced a decline in salinity with the density remaining stable. A fairly sharp upswing appeared in the strength of the constructed ice, while the strength of the underlying natural ice remained stable.

From early April through May there was a general deterioration in the strength of both ice types. This was accompanied by a steady decline in the salinity and density of the constructed ice and a fluctuation in the salinity and density in the underlying natural ice. This implied that brine was migrating from the construction ice into the underlying natural ice.

9.3.3 REINFORCED FREE-FLOODED PARKING APRON

Parking Apron No. 2 was constructed with the same flooding technique used on Apron No. 1. The principal difference was the addition of a reinforcing layer of Fiberglas under the constructed ice at the original natural ice surface and at the top of the constructed ice. The total thickness of the cross-section of constructed and underlying natural ice in the sampling area was about 7 ft; approximately 3 ft was constructed ice. Like Apron No. 1, the original natural ice surface was used as a reference point; and, for analysis, the constructed ice was designated as plus strata and the natural ice as minus strata. General behavior trends for this ice are shown in Figures 9.8 through 9.11.

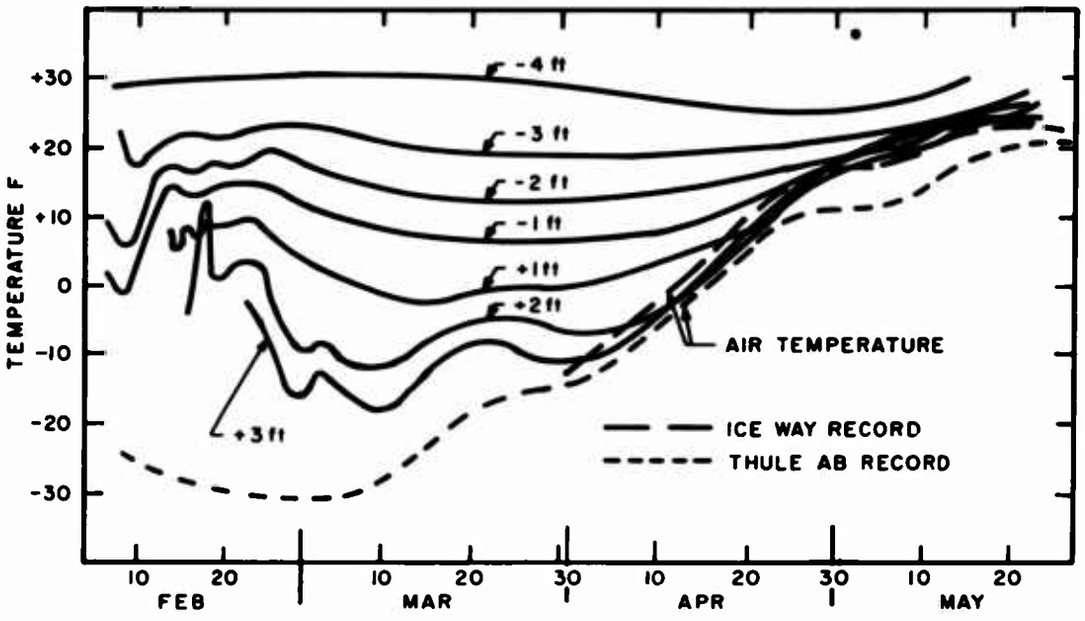

FIG. 9.8. Ice temperature profiles by stratum in the reinforced free-flooded parking apron (Apron No. 2)

Warming of the natural ice in early February and fluctuations in the ice temperatures into early March (Figure 9.8) were the result of flooding the ice during construction. Following the completion of construction on 1 March the profiles indicate some cooling of the ice until the sharp rise in air temperature starting in early April. As the ice temperature profiles closely followed this rise in the air temperature, by the end of May there was about an 8°F temperature gradient through the total ice thickness as compared with 48°F gradient in early March.

Because of similarity in construction technique between Aprons No. 1 and 2 the test data for salinity, density, and relative tensile strength in Apron No. 2 was examined chiefly for the influence of the Fiberglas layer at the interface between the two ice types. This was done by comparing the top three feet of constructed ice in the two aprons.

Table 9.1 shows the monthly average for salinity, density, and strength in the top three feet of constructed ice in each apron. The salinity range for Apron No. 2 was about 10 to 15 percent higher than that for Apron No. 1 for the entire period. The ice density of the two aprons was not appreciably different,

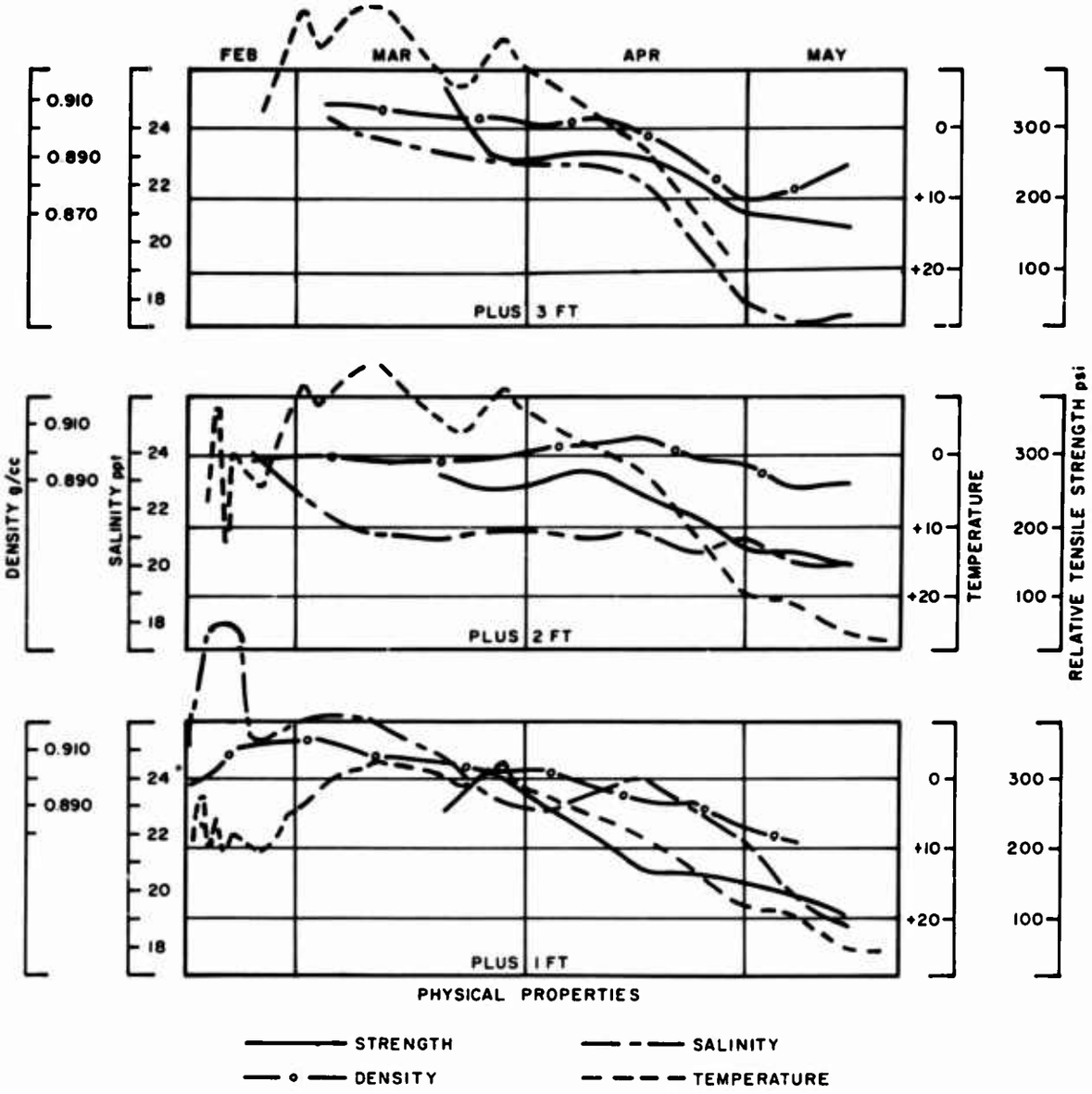

FIG. 9.9 Trend curves of physical properties by stratum for the constructed ice in the reinforced free-flooded parking apron (Apron No. 2)

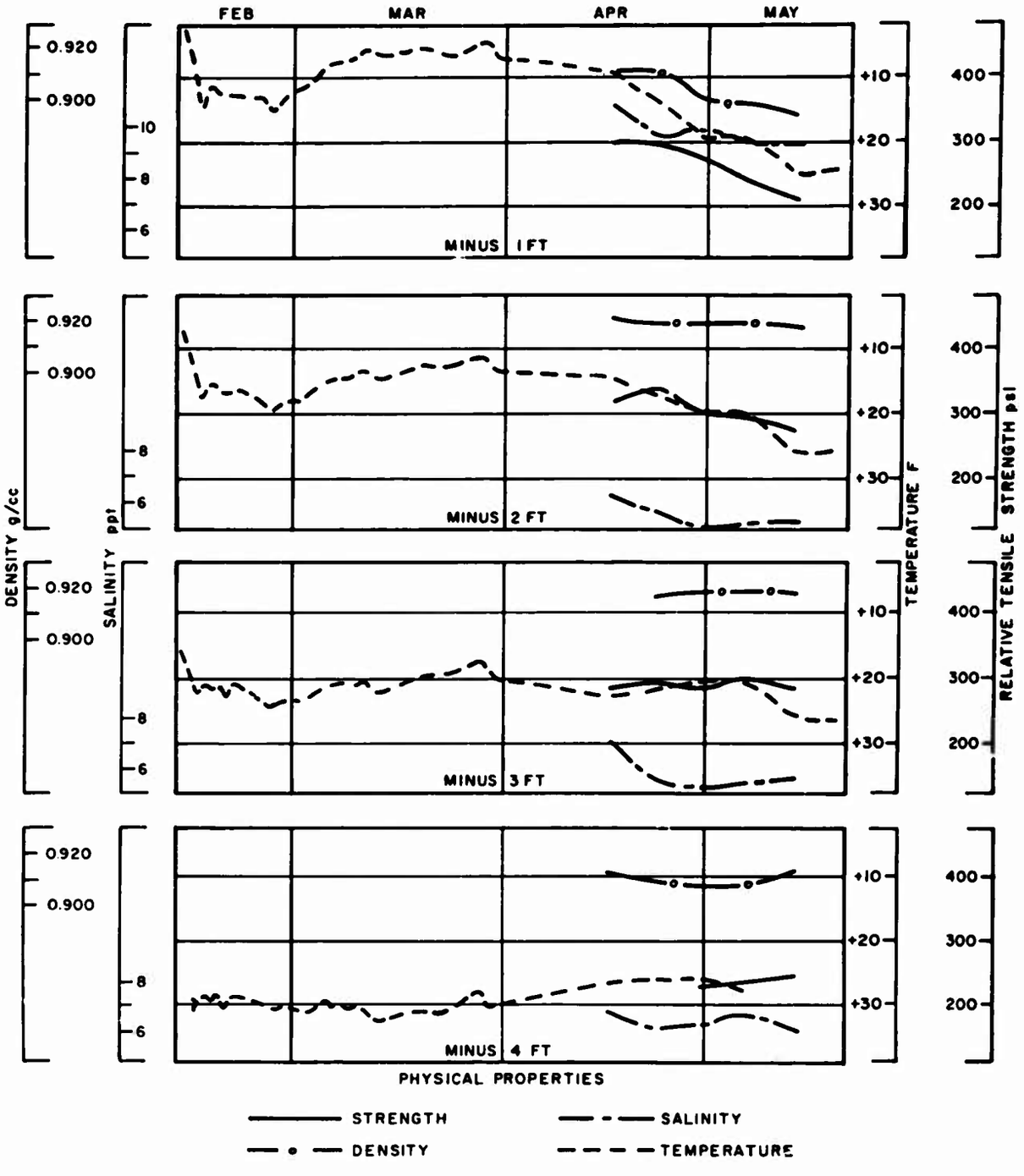

FIG. 9.10 Trend curves of physical properties by stratum for the underlying natural ice in the reinforced free-flooded parking apron (No. 2)

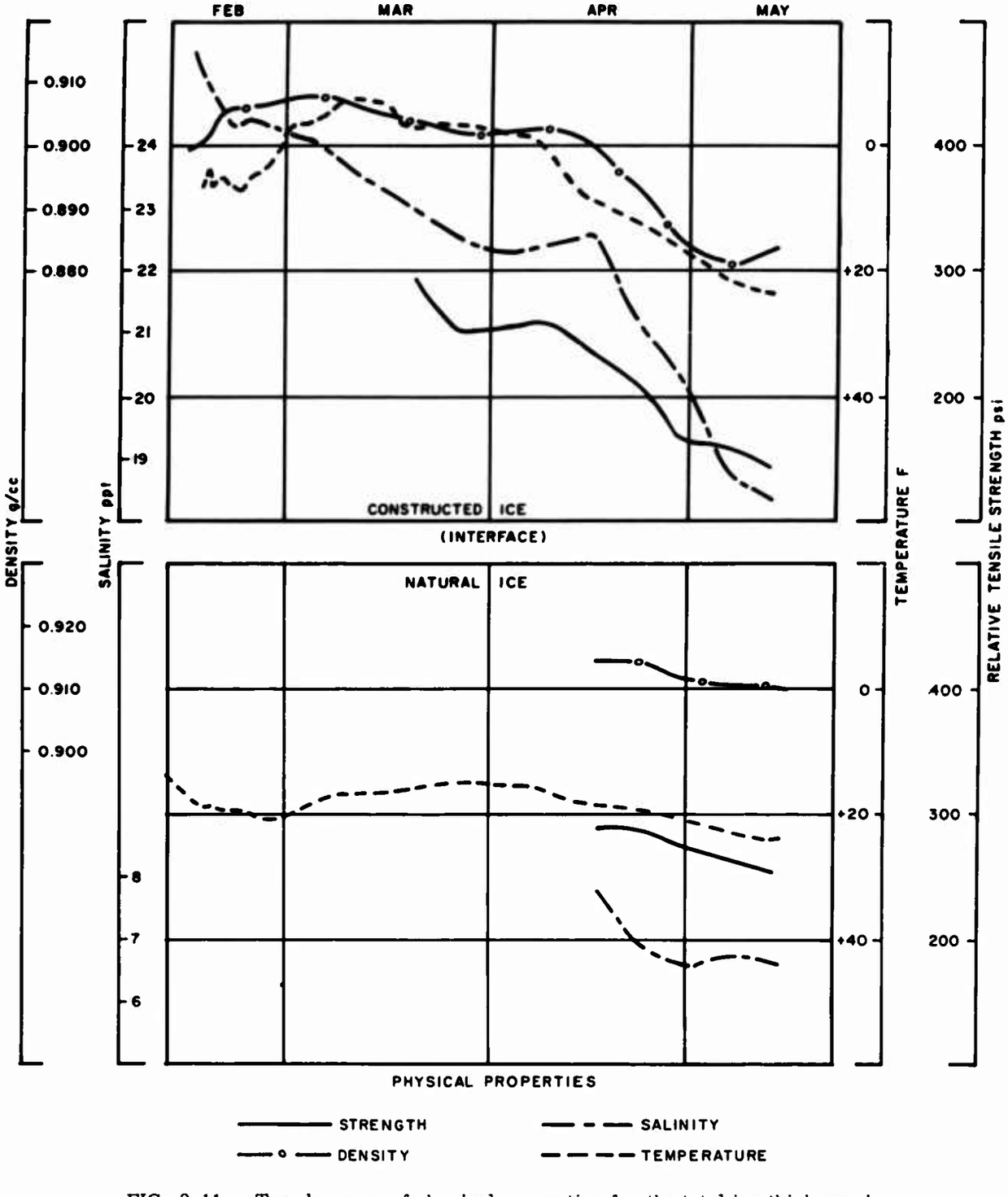

FIG. 9.11 Trend curves of physical properties for the total ice thickness in the reinforced free-flooded parking apron (Apron No. 2)

but the strength of Apron No. 2 ice was less. This strength difference may be due, in part, to the difference in test temperatures. In late April and May the natural ice underlying the two aprons had similar values for salinity, density, and strength, (as shown in Figures 9.6 and 9.10).

From the data, it appears that the Fiberglas layer in Apron No. 2 acted as a barrier to the natural brine migration process, but did not completely inhibit it, as illustrated by the decline in salinity of the constructed ice through the test period (Figure 9.11).

TABLE 9.1

Monthly Average of Salinity, Density, and Strength for Top 3 Feet of Constructed Ice in Aprons Nos. 1 and 2

	Salinity (ppt)		Density (g/cc)		Strength (psi)	
Apron	1	2	1	2	1	2
March	20.9	23.0	0.906	0.903	300(5°F)	295(4°F)
April	19.5	22.4	0.908	0.901	310(8°F)	250(15°F)
May	15.8	18.9	0.876	0.883	185(21°F)	150(21°F)

9.3.4 REINFORCED, ICE-AGGREGATE PARKING APRON

Apron No. 3 was constructed within a dike using chipped-ice-aggregate fill sandwiched between Fiberglas mats. As a result the edges of the apron were nearly vertical and the surface was above the surrounding natural ice. The total thickness of the entire cross-section of constructed and underlying natural ice in the sampling area was about 5-1/2 ft; approximately 1-1/4 ft was constructed ice. Like Apron No. 1, the natural ice surface was used as a reference; and, for analysis, the data was designated plus and minus stratum for constructed and underlying natural ice, respectively. Trends of physical properties for this ice are shown in Figures 9.12 throug 9.15.

The temperature of the ice (Figure 9.12) fluctuated several times during February because of construction. The three construction fills required to build this apron are clearly reflected in these fluctuations.

The plus 2-ft stratum of constructed ice in Figure 9.13 represents a maximum of 6 inches of ice. A sizeable decline in salinity in this stratum occurred

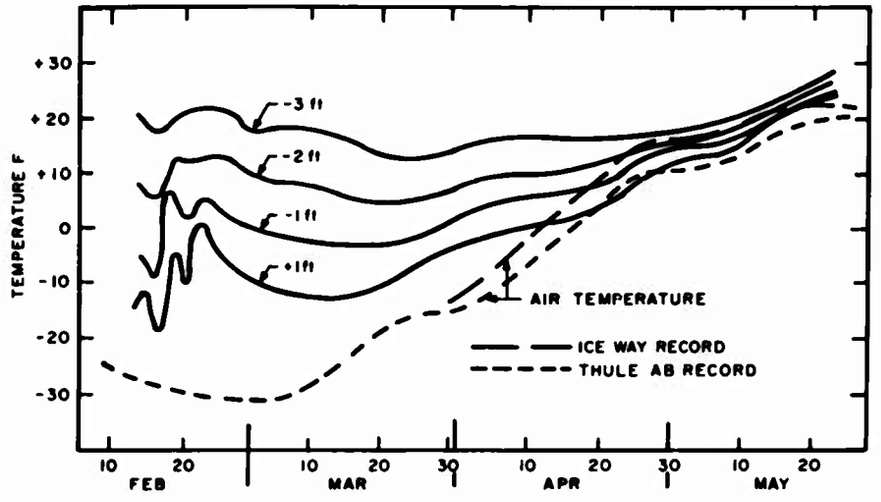

FIG. 9.12 Ice temperature profiles by stratum in the reinforced ice-aggregate parking apron (Apron No. 3)

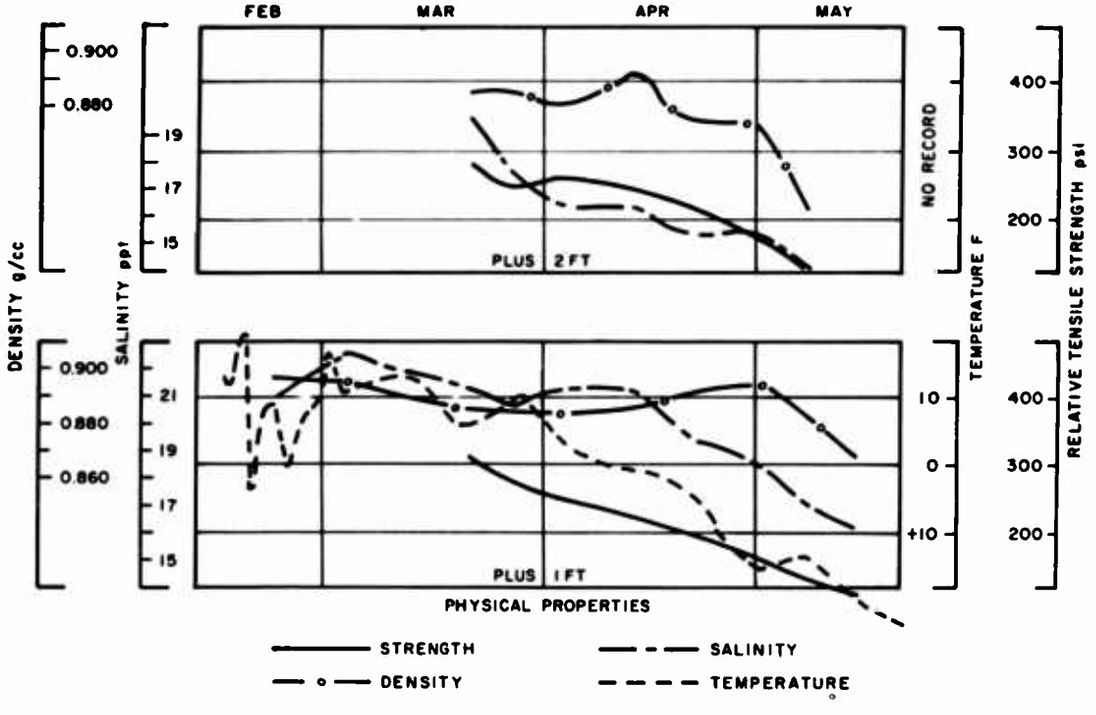

FIG. 9.13 Trend curves of physical properties by stratum for the constructed ice in the reinforced ice-aggregate parking apron (Apron No. 3)

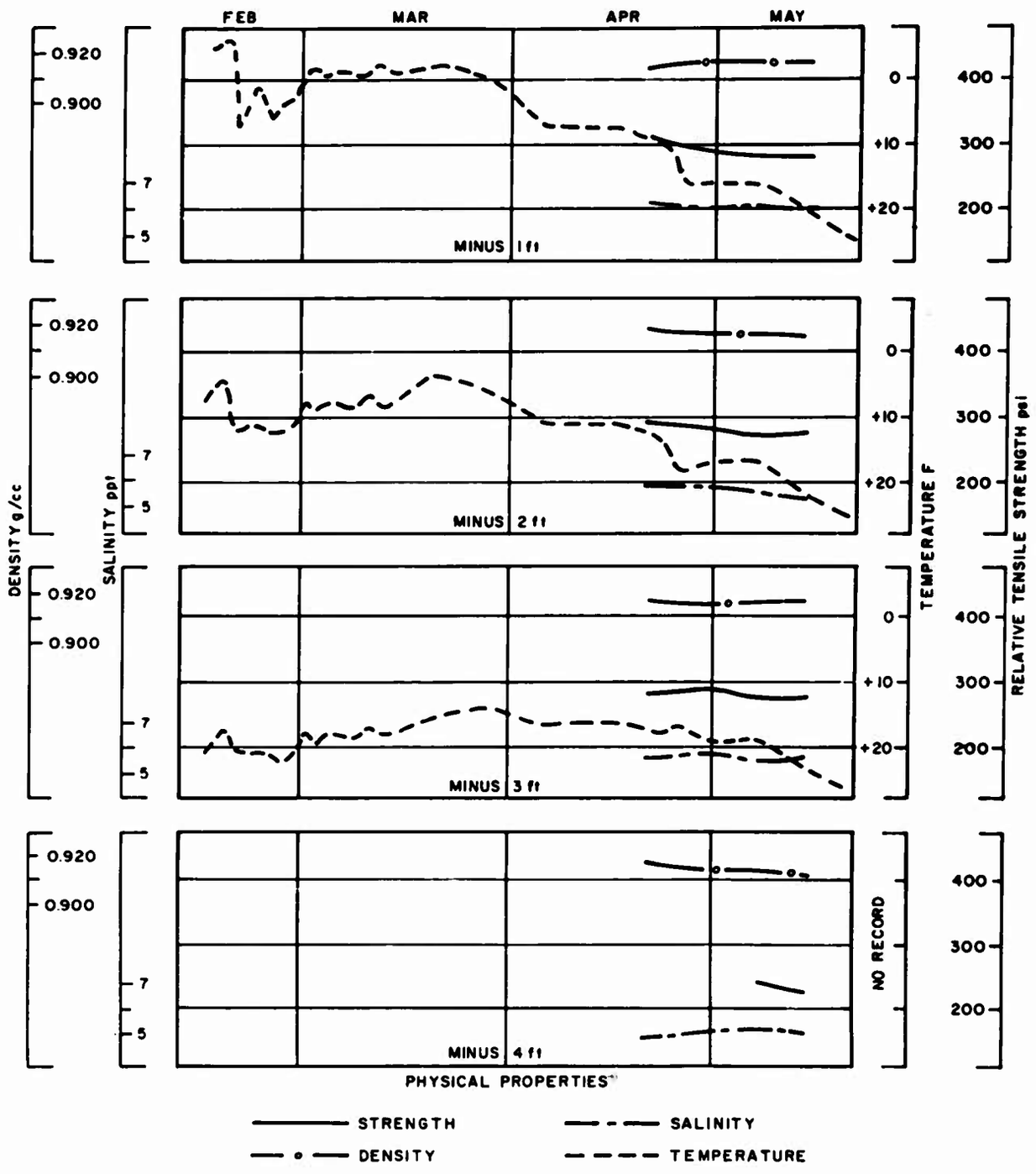

FIG. 9.14 Trend curves physical properties by stratum for the underlying natural ice in the reinforced ice-aggregate parking apron (Apron No. 3)

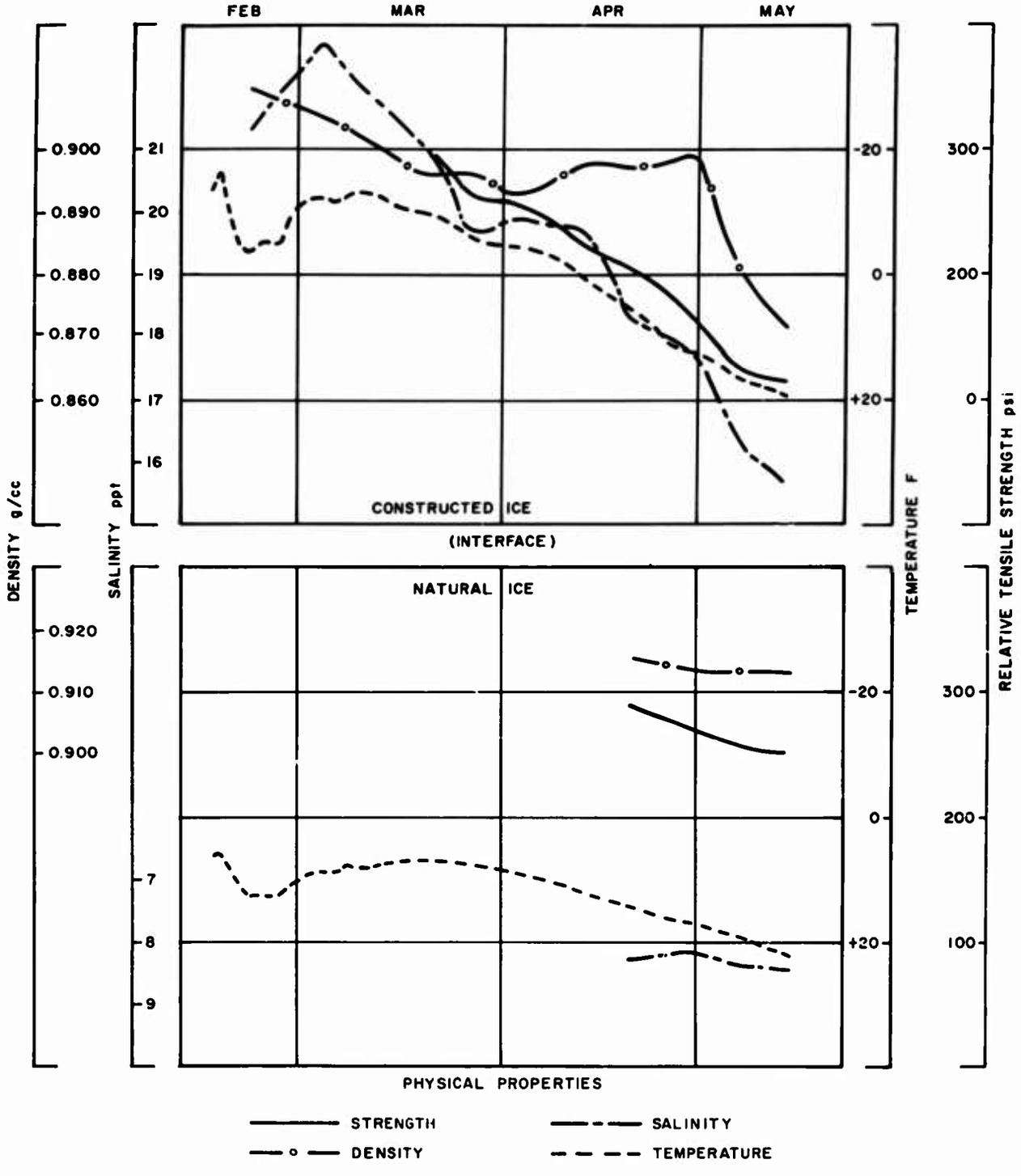

FIG. 9.15 Trend curves of physical properties for the total ice thickness in the reinforced ice-aggregate parking apron (Apron No. 3)

in late March and early April, but little shift in salinity was observed during this same period in the plus 1-ft stratum.

Examination of the original field data shows a wide range of values for salinity at the lower boundary of the plus 1-ft stratum, which rested directly on top of the Fiberglas reinforcing mat. This variation and the limited salinity decline in the plus 1-ft stratum until mid-April (Figure 9.13) strongly indicated that the Fiberglas mat was retarding the migration of the brine. In turn, the rapid decline in salinity after mid-April would indicate that the mat became less resistive to migration as the ice temperature increased. However this is not supported by a salinity increase in the underlying natural ice (Figure 9.14). It is possible that lateral brine drainage occurred as the ice became warmer and that the brine collected or drained away in the depressed center of the apron (Figure 4.17). No samples were collected within 20 ft of the mat center.

Density of the constructed ice (Figure 9.13) decreased progressively during the observation period. A particularly notable decrease was observed for the top stratum in May. The slight increase in density for this stratum in mid-April was very likely due to heterogeneity of the ice within the sampling area. Very little change in density occurred in the underlying natural ice during the 2-month period (Figure 9.14).

The constructed ice progressively lost strength throughout the period of observation (Figure 9.13). Strength profiles for the underlying natural ice in April and May (Figure 9.14) are comparable with those of the underlying natural ice in Aprons 1 and 2 during the same period (Figures 9.6 and 9.10).

9.4 Comparative Analysis

For comparative analysis of all ice types, all salinity, density and ring tensile strength measurements for April and May were reduced to average monthly values. These averages are tabulated in Table 9.2 and are for the total thickness of each ice type. The comparison was limited to April and May as this was the only period when comparable data was available for all test areas. Because the data represents average values and since the sampling was under field conditions rather than controlled conditions, the comparisons are in general terms rather than specific value differences.

The salinity of the undisturbed natural ice decreased about 7 percent during April and May. The constructed ice in Apron No. 1 (unreinforced) during this same period was almost four times more saline than the natural ice (Table 9.2). At the same time the constructed ice in Apron No. 2 (over reinforcing) was about 10 percent more saline than the constructed ice in Apron No. 1. While this 10 percent

difference in salinity suggested retardation of brine drainage through the Fiberglas matting, the salinity decline in the constructed ice of both aprons during April and May was about the same, 3 ppt, or about 15 percent of the initial volume. This indicated that the excess brine in the constructed ice of Apron No. 2 accumulated at the colder ice temperatures occurring prior to the comparative period and that drainage through the Fiberglas matting was temperature-dependent. Examination revealed that average ice temperature for March adjacent to the matting in Apron No. 2 was only 5°F, but in April it was 9°F and in May it was 22°F.

The salinity of the constructed ice in Apron No. 3 (dry fill saturated with sea water over a Fiberglas mat) was only about 5 percent less than the average salinity of Apron No. 1. This is notable because Apron No. 1 was produced entirely with sea water, which was initially far more saline than the dry fill. A comparison of the salinity values in Table 9.2 indicates that the rate of brine migration from the constructed ice in Apron No. 3 was slightly higher than in Aprons No. 1 and 2. The restrictive effect of the Fiberglas mat on brine migration in Apron No. 3 cannot be determined from Table 9.2. However, review of the salinity profiles for Aprons No. 2 and 3 (Figures 9.9 and 9.13) indicates that the Fiberglas tended to restrict brine migration prior to mid-April.

The salinity of the natural ice under Aprons No. 1 and 2 was found to be more than 35 percent greater than that of the undisturbed natural ice. This is a direct indication of brine migration from the constructed layer in these two aprons. On the other hand, the salinity of the natural ice under Apron No. 3 was only slightly greater than that in the undisturbed natural ice. This would indicate that the Fiberglas mat in this apron was restricting brine migration. Therefore, in order to account for the salinity decrease in the constructed ice of this apron, lateral migration must have been taking place.

The density values in Table 9.2 show that all ice types lost density during April and May. The decline was small (about 1/2 percent) for all natural ice areas, both undisturbed and that underlying the constructed ice. At the same time all constructed ice (wet and dry fill) lost about 3 percent in density.

The ice constructed by the dry fill technique was the least dense of all the ice types. It averaged 2-1/2 percent less dense than the undisturbed natural ice, while the ice constructed by the wet fill technique averaged only 1-1/2 percent less dense.

A direct comparison of the average strength values shown in Table 9.2 could lead to erroneous conclusions because strength is highly dependent upon temperature. In the table each strength value is accompanied by an average test temperature for that particular group of specimens. A direct comparison of the strength values can be made only where the test temperatures are the same. Also, as noted

TABLE 9.2

Average Monthly Physical Property Value for Total Thickness of Each Ice Type for April and May

	Natural Ice				Constructed Ice			
	Undisturbed		Underlying		Wet Fill		Dry Fill/3	
	April	May	April	May	April	May	April	May
Salinity	5.3	4.9	7.8/1 8.4/2 5.7/3	6.6/1 6.7/2 5.5/3	20.1/1 22.4/2	17.0/1 18.9/2	19.7	15.7
Density	0.919	0.914	0.920/1 0.915/2 0.917/3	0.915/1 0.912/2 0 916/3	0.905/1 0.902/2	0.877/1 0.883/2	0.888	0.868
Relative Tensile Strength	310(20°F)*	260(26°F)	300(15°F)/1 290(18°F)/2 310(16°F)/3	260(25°F)/1 265(24°F)/2 270(25°F)/3	325(8°F)/1 250(15°F)/2	135(22°F)/1 145(21°F)/2	225(16°F)	120(24°F)

/1 - Apron No. 1 (unreinforced)

/2 - Apron No. 2 (reinforced)

/3 - Apron No. 3 (reinforced)

* - Ice temperature at testing

earlier, the strength values shown, which were obtained by the ring tensile test method, are considered relative values and not true tensile strengths.

In general, however, the strength behavior of the different ice types in the table indicates that:

a. The constructed ice had little effect on the strength of the underlying natural ice. Both the undisturbed natural ice and that underlying constructed ice had about the same initial strength in April and deteriorated at about equal rates through May.

b. The more highly saline constructed ice had a high strength at low temperatures, but deteriorated more rapidly than the natural ice when the ice temperatures rose.

c. The ice constructed by the dry fill technique appears to have less initial strength and a faster rate of strength deterioration than that produced by the wet fill technique.

9.5 Strength as a Function of Brine Content

The relationship between strength and brine content of sea-ice has been given considerable discussion in current sea-ice literature. Research by Assur[2] and Weeks[3] indicates that ice strength decreases as brine volume increases. Assur suggests a theoretical correlation by which strength can be expressed as a function of the square root of the brine volume present. Weeks analyzed data collected from a controlled experiment, using Assur's correlation. Both indicate that additional research is necessary in order to better establish this correlation. Knowledge of the theoretical correlation between strength and brine volume or a temperature-salinity relationship would be of great benefit, particularly if continuous strength monitoring of an ice sheet were undertaken. With this knowledge, it would be only necessary to measure in situ temperatures and salinities since strength could be determined by table or graph. Thus far, however, the approach to establish a strength prediction equation has neglected the effect of density. In the final form a density coefficient will no doubt have to be included in the equation.

In an effort to correlate the Project ICE WAY data with the works of Assur and Weeks the data was examined for the correlation of strength as a function of the square root of the brine volume present in the ice. Assur's table, "Volume of Brine (ppt)," was used to determine the volume of brine present in the specimens. In this table, values for the volume of brine in ppt are given for standard sea ice at 1 ppt salinity, depending upon temperature. By using this table, the temperatures and salinities of the test specimens were converted to brine volume present at the time strength measurements were made. Then, strength versus the square root of the brine volume for all strata of each ice type was plotted as

shown in Figure 9.16. Each of the plotted points represents the average for a 1-ft stratum of specific ice. The type of ice and sampling periods are identified in the Figure 9.16 legend.

To determine the equation for the best fit line to the data a statistical method reported by Bartlett[4] was selected which did not require prior knowledge of the variances for the two equation variables, measured strength of the ice, and calculated brine volume. This led to the equation for the linear relation shown in Figure 9.16. The 95-percent confidence limits for the coefficient for the square root of brine volume are -2.57 and -5.34. The correlation coefficient (r) for the strength, and the square root of the brine volume in the ice, was found to be -0.674. The minus sign indicates a negative slope to the line. By the t-test, the correlation coefficient was found to be statistically significant. However, despite the statistical significance of the correlation coefficient, the total variation in the strength values explained by the correlation is only 45.4 percent, leaving 54.6 percent of the variation unexplained. From this it can be seen that although a statistically significant correlation between the strength of the ice and the square root of the brine volume was found in the analysis, there is still a considerable amount of variation in the observed values about the line relating the two quantities. In comparing the strength versus the square root brine volume equation shown in Figure 9.16 with Weeks' equations, very close agreement was found in the value of the coefficient of the square root of the brine volume. However the best fit line as determined by the equation in Figure 9.16 has a higher strength intercept than Weeks' curves. This is explained by the higher strength values obtained for this set of data.

Many factors could contribute to the wide scatter of points about the best-fit line. Such factors as the natural heterogeneity of the ice, varying crystal orientation with respect to load application, test equipment limitations, and human error are probably the major causes for the scatter.

9.6 Findings

a. All of the natural and constructed ice types studied displayed an ever-changing gradient with depth and time for temperature, salinity, density, and strength, with the behavior of the flooded ice slightly more erratic than that of natural ice.

b. The average salinity of young flooded ice was three to four times greater than the salinity for the 6- to 8-month-old natural ice.

c. The salinity of ice constructed with chipped-ice aggregate (dry fill) was not appreciably different from the salinity of ice constructed by flooding (wet fill).

d. The density of ice produced by flooding was less than that of undisturbed natural ice, although the percentage of difference was small.

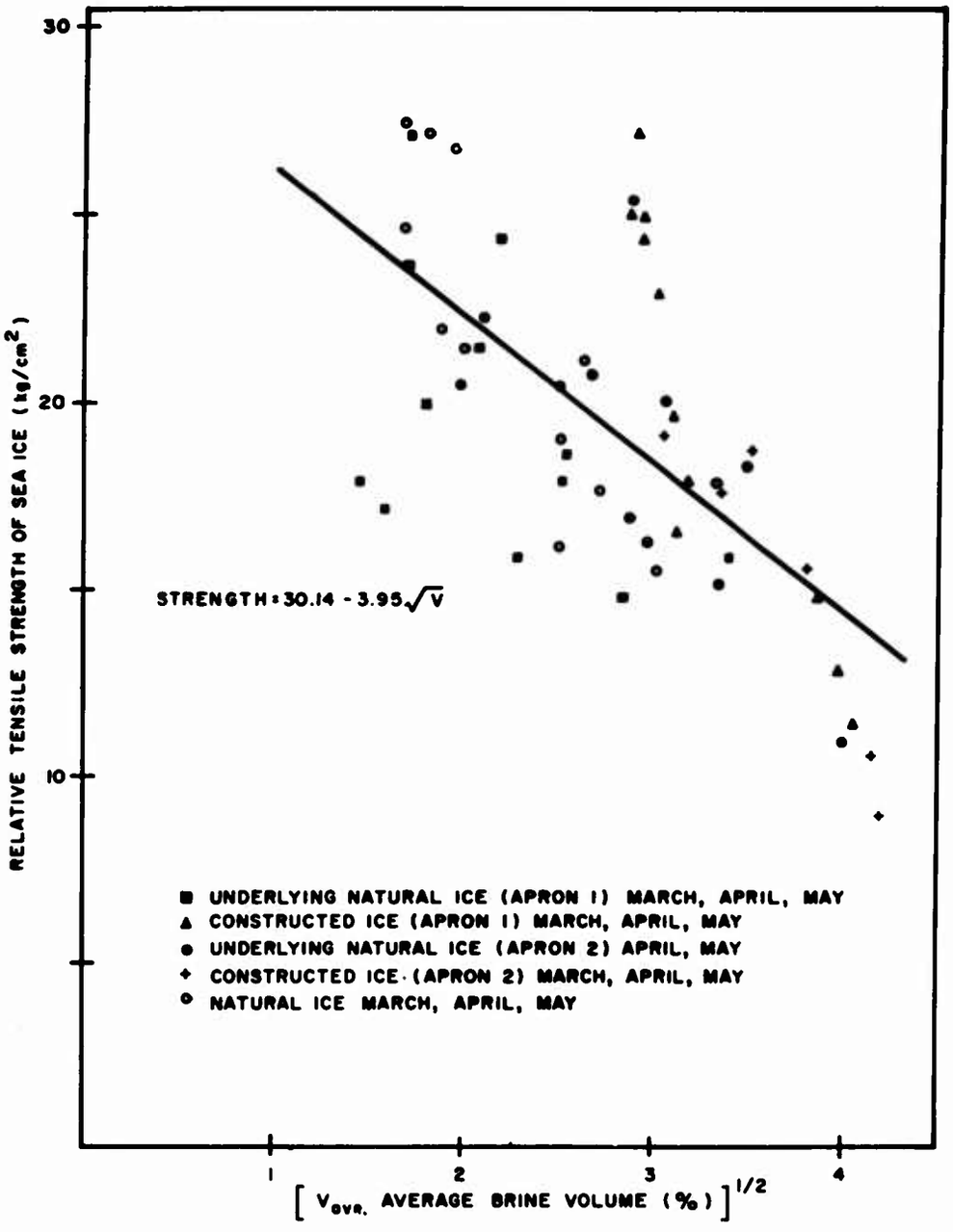

FIG. 9.16. Average relative tensile strength versus the square root of average brine volume by 1-foot stratum for all ice types. Tensile strength by ring tensile test using K value of 6. Data range: temperature -3° to -19°C; salinity 4.6 to 24.8 ppt.

e. The overburden of constructed ice did not appreciably affect the strength or the rate of strength decay in the underlying natural ice.

f. The strength of the young, flooded ice approached that of slightly older natural ice when the ice temperature was low; however, its strength decline was more rapid as the ice temperature rose.

g. The strength of young, flooded ice was greater than that produced by chipped-ice aggregate.

h. The Fiberglas matting placed at the lower boundary of constructed ice retarded the migration of brine sufficiently to cause a higher salinity than that produced without this matting.

i. The ice strength equation in its present form includes only two of the three variables affecting the strength. It considers strength solely as a function of brine volume (which is derived from temperature and salinity) and neglects the effect of density.

j. The ring tensile test method produces a wide variation in strength values, depending upon the theoretical stress concentration factor selected for the equation used to calculate strength.

9.7 Conclusions

a. The continual state of change in depth and time for temperature, salinity, density, and strength necessitates the need to use average rather than specific values for these properties in the analysis of ice masses.

b. Any mat-type material used to reinforce the constructed ice should be highly permeable to allow drainage of the brine.

c. To develop a strength prediction equation for both constructed and natural sea-ice it is necessary to establish the relationship of strength as a function of density as well as temperature and salinity.

d. A test procedure other than the ring tensile test method is needed for true tensile strength measurements on test specimens.

REFERENCES

1. Butkovitch, T. R., "Recommended Standards for Small Scale Strength Tests," Tech. Report 57, SIPRE Corps of Engineers (Nov 1958).

2. Assur, A., "Composition of Sea-Ice and its Tensile Strength," Publication 598, Arctic Sea-Ice, pp 106-138, National Academy of Science, National Research Council (1958).

3. Weeks, W. F., "Tensile Strength of NaCl Ice: A Summary" in "Proceedings of Third Annual Arctic Planning Session," GRD Research Notes No. 55, Geophysics Research Directorate, Air Force Cambridge Research Laboratories, Bedford, Mass. (Apr 1961).

4. Bartlett, M. S., "Fitting a Straight Line when both Variables are Subject to Error," Biometrics, Vol. 5, No. 3, pp 207-212 (Sep 1949).

10. STRESS-RUPTURE BEHAVIOR OF SEA ICE
(by W.D. Kingery and D.N. French)

10.1 Introduction

At temperatures near the melting point, many materials exhibit stress-rupture failure in which a stress well below the short-time fracture stress ultimately causes failure if applied for a long time. This behavior usually results from time-dependent processes that are effective in developing or propogating cracks. Once formed, small cracks act as stress concentrators and lead to accelerated deformation and ultimate failure. Plots of stress-log rupture time or log stress-log rupture time are found to show linear behavior, with lower stresses corresponding to a longer time-to-rupture. Since the rate of the controlling processes is strongly temperature-dependent, it is usually found that the stress-rupture behavior is also strongly temperature-dependent.[1, 2]

Pure ice has been found to demonstrate typical stress-rupture failure when tested in transverse tests[3] and in tensile tests[4] at -20 °C. If this behavior is also found for sea ice, it implies that care must be exercised in defining failure conditions in terms of the load duration as well as the stress level. As a result the stress-rupture behavior of sea ice was investigated as part of Project ICE WAY.

10.2 Experimental Techniques

All experiments were performed on simply-supported beams with a 1-inch by 1-inch cross section and 6-inch length between 1/2-inch diameter aluminum rod supports. The load was applied to a 1/2-inch diameter rod at the center of the span by means of a yoke connected to weights hanging below the sample and frame. On fracture, the weight fell on a microswitch, stopping an electric timing clock. In order to improve precision, a hand stop-watch was used for rupture times less than two minutes. Between five and nine tests were run at each stress level. After time periods of 4 to 7 days, unbroken samples were removed and new tests begun.

The average temperature during the measurements was -20°C with a total range of -10° to -28°C.

The maximum tensile stress, σ_t, was calculated from the standard relation for a short beam,[5, 6]

$$\sigma_t = \frac{3P}{2bd}\left(\frac{\ell}{d} - \frac{4}{3\pi}\right) \qquad (10.1)$$

where P is the load, b the sample width, d the sample depth, and ℓ the distance between supports.

10.3 Samples Tested

Samples of natural sea ice were taken from a layer of natural sea ice one to three inches from the surface in a single 10 ft by 10 ft area about 1-1/2 miles from shore. Samples were collected on 6 and 20 March; each specimen was cut to size on a power band saw, with no further treatment prior to testing. All samples were tested with the top of the specimen (compression side) corresponding to the top of the natural sea-ice sheet. Table 10.1 shows density, salinity, and grain size data.

TABLE 10.1

Density:	0.809 gm/cm^3
Salinity:	0.80%
Grain Size:	~ 0.14" wide x 0.4" long

10.4 Experimental Results

Experimental values for the applied stress and resulting rupture time are given in Table 10.2, and plotted in Figure 10.1. Three specimens removed unbroken after long times evidenced considerable plastic deformation, as shown in Table 10.3. For these three samples higher stresses caused greater deformation.

The data are adequately represented by the least-mean-squares equation:

$$\sigma_f = 245 - 12.5 \log_{10} t \qquad (10.2)$$

with a standard deviation of $\log_{10} t = 1.75$.

TABLE 10.2

Applied Stress and Measured Rupture Time

Stress (psi)	Time to Failure (sec)
129	> 144,000 (bar removed unbroken)
158	337,000; > 86,000 <130,000; >3,600 < 57,600; >193,000 < 259,000
160	> 130,000
176	> 130,000
181	> 130,000
186	60; 9,300; 120
188	192; 16,200; 8; 823; 4; 190; 3,650; 22,700; >605,000
199	> 420 <3,300; >346,000; >23,400 <82,800; >259,000
200	>115,000 <169,000
214	300; 300; 120; 120; 12,600
216	120; 120; <1; 112; 1.5; 588; 3,240
217	12; 2090; 1; >194,000 < 252,000
234	2.5; 227, 0.1; 0.5; 1.0; 18; 34; 53; 41
245	0.1
253	12; 4; 0.1; 0.1; 38; 43; 0.1; 17; 87
266	0.1
270	0.1; 0.1; 14; 0.1; 17; 2; 0.1; 8

TABLE 10.3

Stress (psi)	Center Deformation (inches)	Time (hours)
189	1/8	164
199	3/32	96.5
199	3/32	71.7

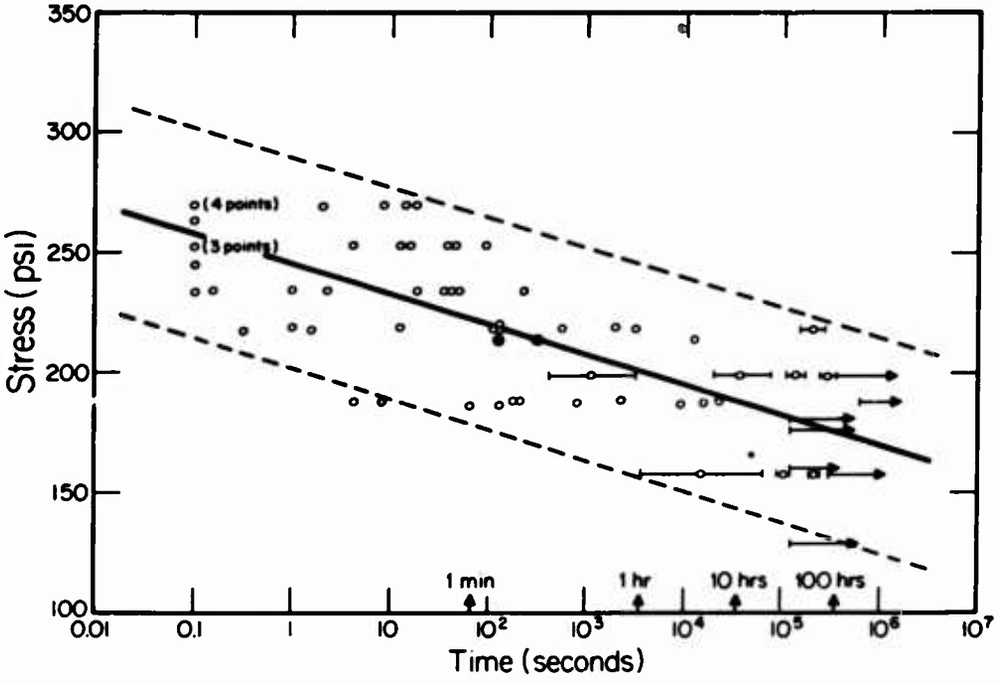

FIG. 10.1 Stress-rupture behavior of natural sea ice at -20°C (range -28°C to -10°C). Dashed lines indicate 95% confidence limits.

10.5 Discussion of Results

A large amount of scatter was observed for the stress-rupture data. This is typical of sea-ice strength measurements[8] and results from the fact that sea ice is a heterogeneous mixture of pure ice crystals, brine, and salt hydrate crystals (at temperature <-8°C). Fracture is initiated on the tension side of the test bar and the detailed configuration of the specimen in the immediate area of maximum stress is all-important. If there is an imperfection, brine bubble, salt crystal, or grain boundary, failure may occur quickly. If, on the other hand, no imperfection exists at or near the surface in the immediate area of maximum stress application, considerable plastic deformation and a long rupture time result.

Some scatter can also be assigned to deviations in specimen dimensions and load concentrations. Precision of sample size measurements (±0.02") leads to a maximum fiber stress error of ±9 psi at 150 psi load and ±17 psi at 290 psi load, that is, about ±6 percent.

Another source of scatter lies in the fact that the specimens were stored for up to 17 days prior to use at a temperature of -26° to -10°C. Some brine drainage and crystal growth may have occurred over these periods. To keep this variable to a minimum, experiments at a particular stress were done within a two or three-day time period. Thus, any storage effects appear between stress levels rather than within a single stress level.

At any particular time-to-rupture, the range of fracture stresses found is similar to those found by Butkovich[7] in short-time tests of sea-ice strength. For one series of tests with 10 samples, Butkovich observed fracture stresses between 73-155 psi at fracture times of 2 to 3 seconds for transverse test samples 90 cm long. From Figure 10.1 a similar range (about 200 to 280 psi) is observed for these conditions. This range is not unexpected in view of the large number of variables that can affect sea ice strength.[8, 9, 10]

10.6 Conclusions

As is the case for other materials tested at temperatures near their melting point, sea-ice exhibits typical stress-rupture failure in which the average rupture stress decreases from 258 psi for 0.1-sec loading to about 175 psi at 100-hr loading. As a result, it is essential to define the time of loading as one of the parameters fixing the load-bearing capacity of sea ice.

REFERENCES

1. Kingery, W. D., Property Measurements At High Temperatures, pp 154-160, John Wiley & Sons, Inc., New York (1959).
2. Grant, N. J., and A. G. Bucklin, "On the Extrapolation of Short-Time Stress-Rupture Data," Trans. A.S.M., 42, 720 (1950).
3. Kingery, W. D., and E. Montrone, unpublished data.
4. Kingery, W. D. and R. S. Voog, unpublished data.
5. Timoshenko, S., Strength of Materials: Part II, Advanced Theory and Problems, pp 352-355, Second Edition, D. van Nostrand Co., New York (1941).
6. Duckworth, W. H., "Precise Tensile Properties of Ceramic Bodies," Jour. Am. Ceram. Soc., 34, 1-9 (1951).
7. Butkovich, T.R., "Strength Studies of Sea Ice," Research Report 20, SIPRE, Corps of Engineers, U. S. Army, Wilmette, Illinois (Oct 1956).
8. Weeks, W. F., "The Structure of Sea Ice: A Progress Report," p. 96, Arctic Sea Ice, Pub. 598, National Academy of Science, National Research Council, Washington, D. C. (1958).
9. Anderson, D. L., "A Model for Determining Sea Ice Properties," p. 148, Arctic Sea Ice, Pub. 598, National Academy of Science, National Research Council, Washington, D. C. (1958).
10. Assur, A., "Composition of Sea Ice and its Tensile Strength," p. 106, Arctic Sea Ice, Pub. 598, National Academy of Science, National Research Council, Washington, D. C. (1958).

11. MEASUREMENTS BY NEL FOR PROJECT ICE WAY
(by James H. Brown and Coy. O. Horton)

The U. S. Navy Electronics Laboratory's part in Project ICE WAY consisted of the following measurements: seismic wave velocities and frequencies, flexural strength, ice temperature profiles, and salinity profiles.

11.1 Seismic Measurements

The plate wave velocity, transverse wave velocity, and the air-coupled flexural wave frequency were measured. The waves were generated by C-3 electric caps and blown from a hammer. Figure 11.1 shows the area in which measurements were made. The recording equipment was an S.I.E. P-33 seismograph system, using S.I.E. S-19 5-cycle geophones, and a RCA Model M-10 dynamic microphone. There were four plants of geophones spaced 50 meters apart in a line. At each plant, three geophones were orientated in the three vector directions in the ice, and one geophone was placed on top of the snow normal to the plane of the ice sheet. Only one microphone was used to measure the time of arrival of the air wave.

The velocities of the waves were taken from the slope of a travel-time graph. In determining velocities only those waves with sharp breaks were used. No difficulty was encountered in obtaining well-defined air-coupled flexural waves from surface and air shots. The results are shown in Figures 11.2 and 11.3 and in Table 11.1.

TABLE 11.1

Summary of Seismic Measurements

Plate Wave Velocity	: 3125 m/sec
Transverse Wave Velocity	: 1744 m/sec
Young's Modulus	: 7.71×10^{10} dynes/cm^2
Shear Modulus	: 2.80×10^{10} dynes/cm^2
Poisson's Ratio	: 0.377
Frequency of Air-Coupled Flexural Wave	: 27.1 cps
Ice Thickness Calculated from Air-Coupled Flexural Wave	: 1.03 m
Average of Eight Measured Ice Thicknesses (with S.D.)	: 1.35 ± .08 m
Ratio of Calculated to Measured Ice Thickness	: 0.763

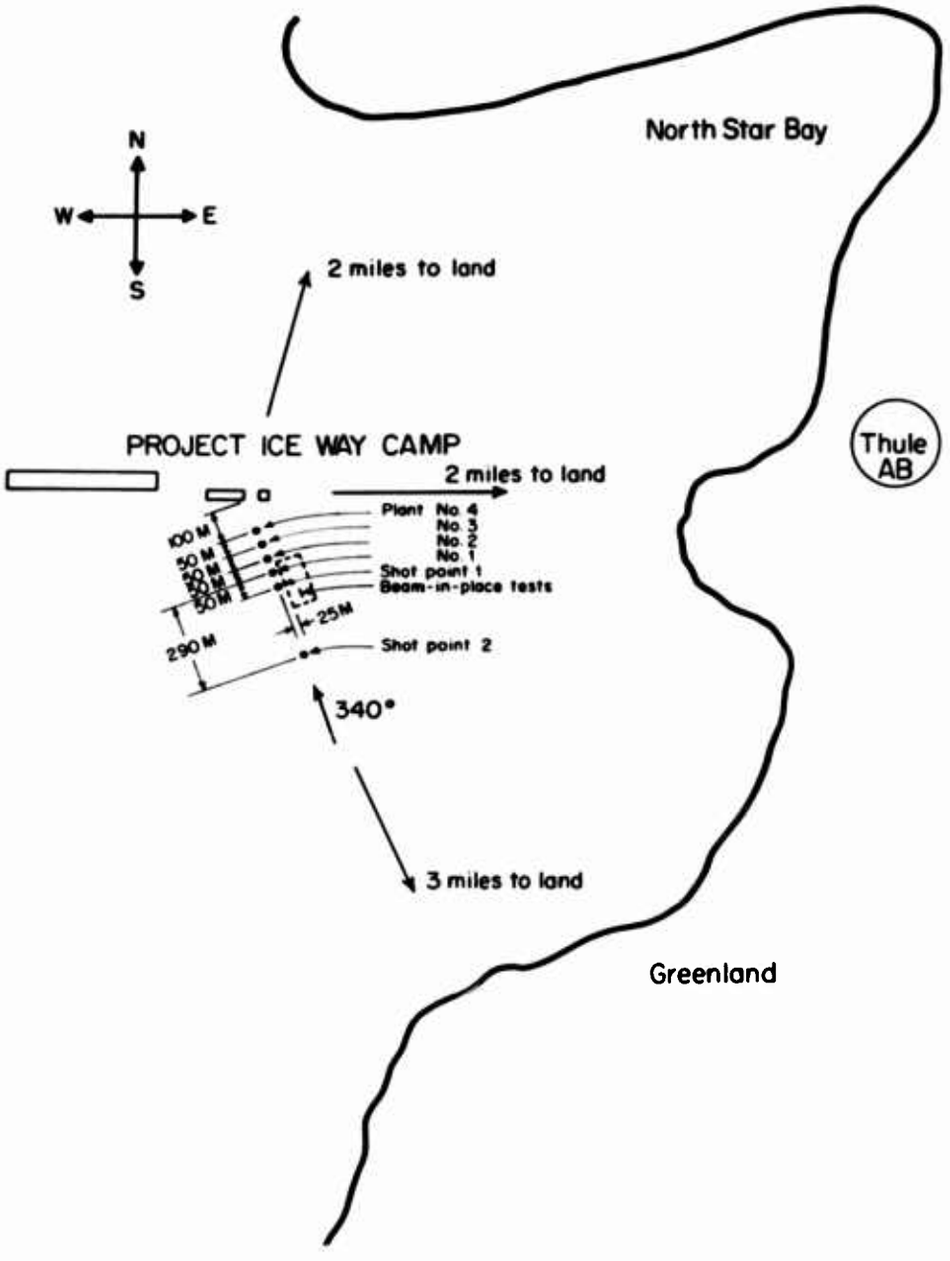

FIG. 11.1 Area in which seismic measurements were made

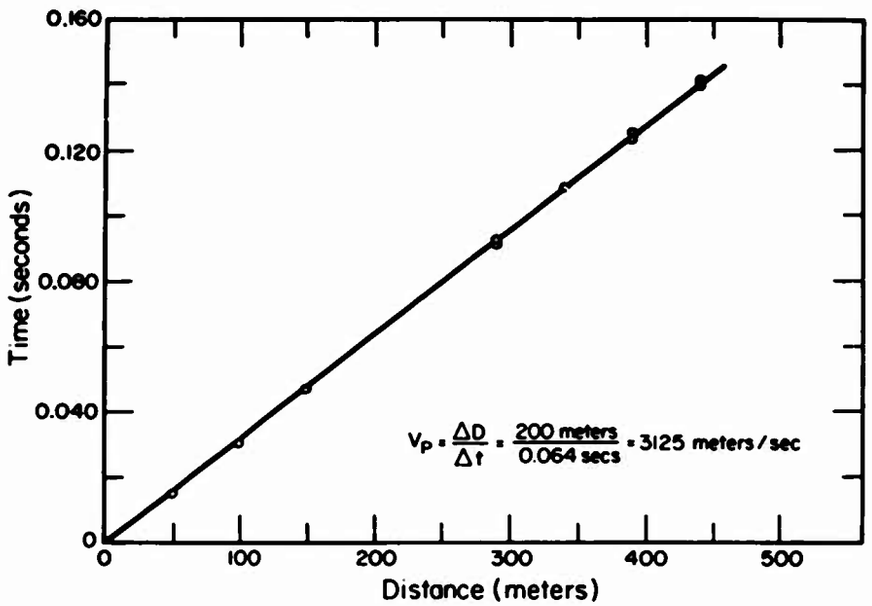

FIG. 11.2 Seismic measurements

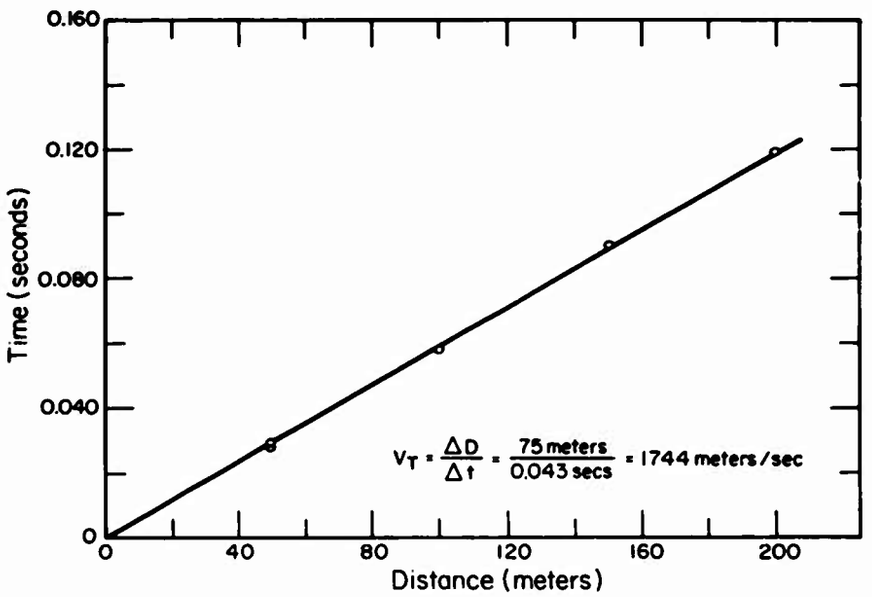

FIG. 11.3 Seismic measurements

The following formulas [1, 2] were used in determining Young's modulus (E), shear modulus (μ), Poisson's ratio (σ), and ice thickness (h) from air-coupled flexural waves:

$$E = \rho_i V_P^2 (1 - \sigma^2)$$

$$\mu = \rho_i V_T^2 = \frac{E}{2(1 + \sigma)}$$

$$\sigma = 1 - 2 \left(\frac{V_T}{V_P}\right)^2 .$$

$$h = \frac{\gamma_a V_a}{f_a} : \text{ where } V_a^2 = \frac{1/3 \, \pi^2 \gamma_a^2 V_P^2}{1 + (\rho_w/\rho_i)/2 \, \pi \gamma_a [1 - (V_a/V_w)^2]^{1/2}}$$

Density profiles were furnished by U. S. Naval Civil Engineering Laboratory scientists, and the value $\rho_i = 0.920$ was used for this report. The uncorrected velocity of sound in air, $V_a = 304$ m/sec, was taken from the seismic records. The velocity of sound in sea water, $V_w = 1452$ m/sec, was determined from the formula found on page 52 in "Acoustic Measurements," by Leo L. Beranek.

11.2 Flexural Strength

The in situ measurements of ice strength were made by cutting an attached beam in the ice sheet (Figure 11.4) and loading the beam at the rate of 4-8 kg/cm^2/sec. A Dillon dynamometer with a maximum load indicator was used to measure the force. These dynamometers were calibrated to better than 1 percent of value prior to measurements. Table 11.2 presents the measurements and values of flexural strength of the different types of ice. It is recognized that the cantilever test gives a lower value for the flexural strength than the simple beam test because of stress concentration. Calculations show buoyancy effects are insignificant for the flexural strength measurements presented in this report. The bottom of the beams had approximately a 5-cm layer of slush ice, which was included in all calculations.

TABLE 11.2

Flexural Strength by the Cantilever Beam Method

NATURAL SEA ICE (FIG. 11.1)

Date	Beam Thickness (h)	Beam Width (w)	Beam Length (l)	Force (p)	Flexural Strength (σ)
17 Mar 61	119.5 cm	24.6 cm	432.1 cm	450.0 kg	3.32 kg/cm^2
10 Mar 61	123.9	29.8	497.8	943.2	6.16
10 Mar 61	125.2	57.8	512.8	1454.5	4.94
10 Mar 61	125.2	20.3	529.0	677.3	6.76
Average Flexural Strength (with S.D.), σ = 5.30 ± 1.32 kg/cm^2					

Plot No. 4

NATURAL SEA ICE-FIBERGLAS-FLOODED SEA WATER ICE

Date	Beam Thickness (h)	Beam Width (w)	Beam Length (l)	Force (p)	Flexural Strength (σ)
19 Mar 61	136.6 cm	24.2 cm	447.0 cm	920.5 kg	5.47 kg/cm^2
19 Mar 61	132.1	30.1	499.1	1034.1	5.90

Plot No. 5

NATURAL SEA ICE-FIBERGLAS-CRUSHED SEA WATER ICE

Date	Beam Thickness (h)	Beam Width (w)	Beam Length (l)	Force (p)	Flexural Strength (σ)
17 Mar 61	126.4 cm	21.9 cm	455.9 cm	838.6 kg	6.56 kg/cm^2

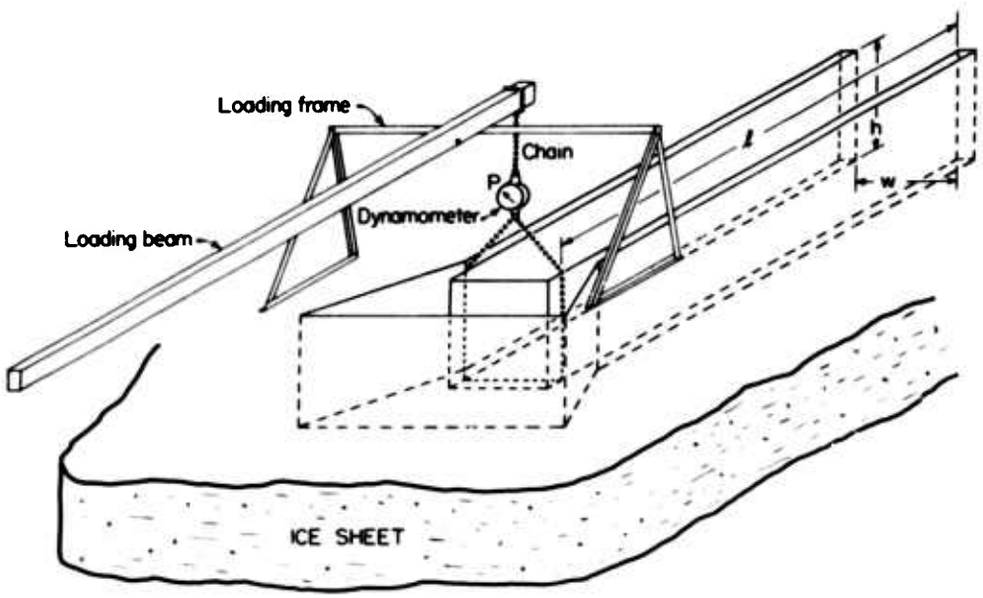

FIG. 11.4 In situ measurements of ice strength

The relaxation for determining flexural strength is:

$$\sigma = \frac{6Pl}{wh^2}$$

11.3 Ice Temperature

Ice temperature measurements were made by cutting blocks of ice approximately 40 cm square from the ice and immediately removing the block from the ice sheet. At each depth, level holes were drilled 15 cm into the ice; and the stem of the dial-indicating thermometers were snugly inserted into the hole. The temperature was then read after equilibrium was reached. The data are presented in Table 11.3. The thermometers were made by Germanow-Simon Co., and the dial had 1°C divisions. The calibrated accuracy of the thermometers was =0.5°C.

TABLE 11.3
Ice Temperature Profiles

Location of Measurements	Beam Test No. 2	Geophone Plant No. 2	Geophone Plant No. 3
Date	10 Mar 1961	15 Mar 1961	15 Mar 1961
Ice Thickness	124 cm	127 cm	131 cm
Air Temperature	-34.5°C	-33.0°C	-33.0°C
Ice Temperatures Top of Ice Sheet Down:			
- 5 cm	-15.2°C	-19.2°C	-25.5°C
- 15	-20.6	-20.0	-21.6
- 25	-18.5	-16.8	-18.9
- 35	-16.6	-15.2	-17.4
- 45	-14.4	-13.9	-16.1
- 55	-12.3	-12.1	-14.3
- 65	-10.4	-11.9	-13.0
- 75	- 9.8	-11.7	-12.5
- 85	- 8.1	- 8.1	- 9.9
- 95	- 6.8	- 6.8	- 8.4
-105	- 4.9	- 5.4	- 6.5
-115	- 3.2	- 4.0	- 4.6
-125		- 2.1	- 2.1
Water	- 1.9	- 1.9	- 1.9

In cutting the ice with a chain saw, warm water was drawn to the top of the ice sheet where it formed a puddle. This procedure causes a noticeable rise in ice temperature at the top 5-cm level. In comparing our temperature readings with the frozen-in thermocouple readings of NCEL, we found that the increase in ice temperature did not extend much below the 5-cm level.

11.4 Salinity

Salinity measurements were made by cutting blocks of ice approximately 40 cm square from the ice sheet. Then after immediate removal of the block from the sheet, the center 12 cm square section of the block was removed. The salinity profile was made by analyzing 10-cm vertical sections of the block. The data are presented in Table 11.4. The measurements were made by using a G.M. Manufacturing Co. hydrometer-salinity kit. The observed readings were

TABLE 11.4

Salinity Profiles of Ice Sheet

Core taken at Geophone Plant No. 2

Core Taken	15 Mar 1961
Core Bottled	15 Mar 1961
Samples Run	20 Mar 1961

Depth Below Surface of Ice	Meltwater Temperature	Observed Salinity	Corrected Salinity To 15°C
0 to 10 cm	+ 27.1°C	8.0 o/oo	11.7 o/oo
10 to 20 cm	26.4	1.8	4.9
20 to 30 cm	26.2	1.6	4.6
30 to 40 cm	26.2	2.8	5.9
40 to 50 cm	26.0	2.6	5.6
50 to 60 cm	26.2	1.7	4.7
60 to 70 cm	26.2	1.2	4.2
70 to 80 cm	26.0	1.8	4.7
80 to 90 cm	26.2	1.6	4.6
90 to 100 cm	26.7	1.1	4.3
100 to 110 cm	26.2	1.8	4.8
110 to 120 cm	26.7	2.2	5.4
120 to 127 cm	27.1	2.2	5.6

Core taken at Geophone Plant No. 3

Core Taken	15 Mar 1961
Core Bottled	15 Mar 1961
Samples Run	20 Mar 1961

Depth Below Surface of Ice	Meltwater Temperature	Observed Salinity	Corrected Salinity To 15°C
0 to 10 cm	+ 26.1°C	5.5 o/oo	8.8 o/oo
10 to 20 cm	26.0	1.2	4.1
20 to 30 cm	24.9	2.2	4.8
30 to 40 cm	24.8	3.2	5.8
40 to 50 cm	24.9	2.6	5.2
50 to 60 cm	25.1	2.8	5.4
60 to 70 cm	25.2	3.2	6.0
70 to 80 cm	25.3	2.8	5.5
80 to 90 cm	24.9	1.7	4.2
90 to 100 cm	25.3	1.4	4.1
100 to 110 cm	25.6	1.3	4.1
110 to 120 cm	25.5	2.1	4.9
120 to 129.5 cm	25.5	6.0	9.0

TABLE 11.5

Salinity Profiles of Ice Sheet

Core taken from Beam Test No. 2

Core Taken	10 Mar 1961
Core bottled	20 Mar 1961
Samples Run	21 Mar 1961

Depth Below Surface of Ice	Meltwater Temperature	Observed Salinity	Corrected Salinity To 15°C
0 to 10 cm	+ 23.9°C	3.4 o/oo	5.8 o/oo
10 to 20 cm	24.3	1.2	3.5
20 to 30 cm	23.6	3.2	5.4
30 to 40 cm	22.9	3.5	5.5
40 to 50 cm	20.3	3.9	5.2
50 to 60 cm	18.5	3.8	4.6
60 to 70 cm	17.2	4.0	4.5
70 to 80 cm	13.6	4.5	4.3
80 to 90 cm	18.2	4.0	4.8
90 to 100 cm	16.1	4.2	4.4
100 to 110 cm	17.9	3.9	4.6
110 to 124 cm	19.6	4.0	5.1

corrected to 15°C by use of the manufacturer's tables. The water temperature was measured with a mercury thermometer made by the Brooklyn Thermometer Co. and calibrated to ±0.3°C.

Note the salinity profile in Table 11.5. This profile was run on a 50-cm square block which had laid on top of the ice sheet from 10 March to 20 March. The samples were taken from the center 10-cm square section of the block as above. The salinity profile appears to be about the same as the other two profiles except for the top 20 cm. Temperatures during this period were generally below -30°C; however, temperatures as high as -19.5°C were recorded.

REFERENCES

1. Ewing, M., A.P. Crary, and A.M. Thorne, Jr., Physics, 5, 165 (1934).
2. Press, F., M. Ewing, A.P. Crary, S. Katz, and J. Oliver, "Air-Coupled Flexural Waves in Floating Ice," Geophysical Research Papers No. 6, Air Force Cambridge Research Laboratories (Nov 1950).

12. COMPARISON OF DIFFERENT METHODS FOR MEASURING SEA ICE STRENGTH (by W.D. Kingery and D.N. French)

12.1 Introduction

Many variables, including test temperature, salinity, grain size, grain orientation, thermal history, and prior treatment are known to affect sea-ice strength. In addition, the size and shape of test specimens and mode of testing is reported to have important effects on measured values.[1] During Project ICE WAY four different techniques for strength measurement were used: ring tensile tests, two sizes of small-scale transverse tests, and in-place beam tests. The ring tensile tests and associated salinity, density, and temperature determinations were done by NCEL personnel (Section 9); in-place beam tests were done by NEL personnel (Section 11); small-scale transverse tests were mostly done by D. N. French.

12.2 Experimental Techniques

To keep as many variables related to the condition and temperature of the ice as constant as possible for all strength tests, these measurements were conducted in the 7 day period, 13 to 20 March. One set of salinity, density, and temperature measurements were made in the middle of this period and are assumed to be representative of the ice conditions at test time.

12.2.1 RING TENSILE TESTS

Cores were taken with the standard 3-inch ID, SIPRE coring auger and processes as soon after removal as possible. Each core was cut into 3-inch long pieces. The 3-inch long cylinders were then weighed to 0.1 gram on a triple beam balance, and diameter and length were measured with calipers to 0.1 mm for density calculations. Following these operations, the cylinders were broken as ring tensile specimens without any axial hole being drilled. The broken pieces were next crushed and temperature recorded; salinity was measured by means of a hydrometer technique after the sample had melted in a closed container. Sample temperatures were those of a warm wannigan, that is, +10° to 28°F. From one core, the strength, salinity, and density profiles through the ice were determined (for further details see Section 9).

12.2.2 SMALL-SCALE TRANSVERSE TESTS

Two sizes of beams, 1" x 2" x 6" and 3" x 3" x 18", were used to measure tensile strengths. The smaller beams were collected at 3-inch intervals in the natural ice and the flooded sea water. The larger beams were taken at 16-inch intervals from the three types of ice tested. In the cases of the ice cast on the surface of natural sea ice, samples were taken at the new ice-old ice interface to include the Fiberglas layer. Each sample was cut to size on a power band saw and stored for periods up to two days; each specimen is assumed to be at the atmospheric temperature at the time of testing, that is, -25°C.

The beams were broken in tension as simply-supported beams loaded at the center of the 6-inch span. All ring tensile and small-beam tests were made on a "Soiltest" compression-testing device with the load measured on a 1000-lb Baldwin load cell and recorded on a Brush recorder. Ice is assumed to behave elastically up to failure, and the rupture stress is given by:

$$\sigma_B = \frac{3}{2} \frac{P}{bh} \left(\frac{\ell}{h} - \frac{4}{3\pi} \right)$$

12.2.3 IN-PLACE BEAM TESTS

In-place beam tests were cantilever beams broken without removing the specimen from the ice sheet, as described in detail in Section 11. Two parallel cuts were made through the ice extending about four times the ice thickness (16 ft for 4 ft thick ice), one end was cut free and a chain was looped around the beam end and connected to a long lever through a dynamometer. The fracture stress is given as;

$$\sigma = \frac{6P\ell}{bh^2}$$

12.3 Samples Tested

Ring tensile tests were performed on natural sea ice, flooded, and frozen sea water, and the chipped ice-sea water mixture. Preparation of these samples is discussed in Section 4. Small-scale transverse beam tests were done on natural ice,

flooded, and frozen sea water (both beam sizes), and on the chipped ice-sea water aggregate (3" x 3" x 18" beam size only). Since many of the ice chips used were greater than 1 inch thick, the 1" x 2" x 6" beam could not be representative of the chipped ice aggregate. In-place beam tests were done on all three types of ice.

12.4 Experimental Results

Strength data for all samples tested are listed in Tables 12.1 through 12.4. Figure 12.1 shows the temperature profiles at the time the ice samples were collected.

12.5 Discussion of Results

Insufficient measurements were made during Project ICE WAY to provide a satisfactory quantitative comparison of the ring tensile test and the transverse test. Within the wide range of scatter found for each test method, nearly equivalent results were found, with somewhat higher values resulting from the ring tensile tests.

Both the ring tensile tests and the transverse bend tests indicated that the denser lower-salinity natural sea ice was stronger than the flooded and frozen sea water or the chipped ice plus sea water. From the present data, differences between the two processes materials are not clearly significant.

Either the ring tensile test or small beam test seems suitable for comparison between different ice populations. The ring tensile test is more rapid, easier, and thus generally preferable.

Of greater importance than the comparison between small-scale tests is the lack of correlation between these measurements and the in-place beam tests, as was found by Butkovich.[1] The similarity between results on natural and constructed ice for the in-place beam tests suggests that the nature of the bottom surface, equivalent in all samples, determines the in-place beam test strength. If so, strength profiles through an ice sheet are of little use in defining sheet failure criteria. These results also indicate that application of any ice strength data to fixing safe load limits must consider the load distribution in detail.

REFERENCES

1. T. R. Butkovich, "Strength Studies of Sea Ice," Research Report 20, Snow, Ice, and Permafrost Research Establishment, Corps of Engineers, U. S. Army, Wilmette, Illinois (October, 1956).

TABLE 12.1

Strength Measurements of Natural Sea Ice

Position Below Surface	Salinity, %	Density	Ring Tensile Strength*(psi)	Transverse Strength**(psi) 6" Beams	18" Beams
0 - 3				259	345, 259
3 - 6	0.83	0.910	322, 431		
6 - 9				201, 210	
				335, 243	
9 - 12	0.59	0.908	459, 425		
15 - 18	0.45	0.914	382, 431	260, 176	279, 316
21 - 24	0.64	0.924	408, 365		
24 - 27				234, 210	
27 - 30	0.58	0.920	400, 348		
33 - 36	0.55	0.918	314, 425		
39 - 42	0.55	0.918	374, 306		
45 - 48	0.53	0.917	289, 200		

* Sample temperature at testing ranged from +3 to +28°F.
** Sample temperature at testing was -25°C.

TABLE 12.2

Strength Measurements of Flooded and Frozen Sea Water
(Fiberglas at Natural Ice Surface)

Position Below Surface	Salinity, %	Density	Ring Tensile Strength*(psi)	Transverse Strength**(psi) 6" Beams	18" Beams
0 - 3	2.42	0.920	162, 187	134, 134	65, 102
3 - 6	1.95	0.903	174, 246		
6 - 9	3.25	0.877		168, 234	
				234	
9 - 12	2.10	0.908	144, 149		
12 - 15				(includes Fiberglas layer)	
				1680, 708	149, 149 φ
15 - 18	0.70	0.915	221, 314		
21 - 24	0.55	0.912	340, 264	224	
27 - 30	0.58	0.912	255, 425		
30 - 33				293, 478	186, 168
33 - 36	0.57	0.916	366, 352		
39 - 42	0.65	0.922	289, 323	231, 218	
45 - 48	0.55	0.920	213, 188		

* Sample temperature at testing ranged from +3 to +28°F.
** Sample temperature at testing was -25°C
φ Natural ice interface.

TABLE 12.3

Strength Measurements of Chipped Ice and Sea Water Aggregate
(Fiberglas at Natural Ice Surface)

Position Below Surface	Salinity, %	Density	Ring Tensile Strength*(psi)	Transverse Strength**(psi) 18" Beams	
0 - 3	1.42	0.876	298	75, 195	
3 - 6	1.74	0.868	229, 153		
6 - 9	1.66	0.899	144		
9 - 12	1.65	0.825	204		
12 - 15	1.38	0.896	298, 293	280, 225 (includes Fiberglas)	
18 - 21	0.61	0.918	314, 331		ϕ
24 - 27	0.55	0.915	361, 365		
30 - 33	0.53	0.914	306, 450		
36 - 39	0.57	0.922	280, 289		
42 - 45	0.62	0.923	364, 331		
48 - 51	0.56	0.916	364, 289		

* Sample temperature at testing ranged from +3 to +28°F.
** Sample temperature at testing was -25°C.
ϕ Natural ice interface.

TABLE 12.4

In-Place Beam Strengths

Type of Ice	σ_B(psi)
Natural Sea Ice	47.4
	87.5
	70.2
	95.9
Chipped Ice + Flooded Sea Water + Fiberglas	93.1
Flooded Sea Water + Fiberglas	77.2
	83.2

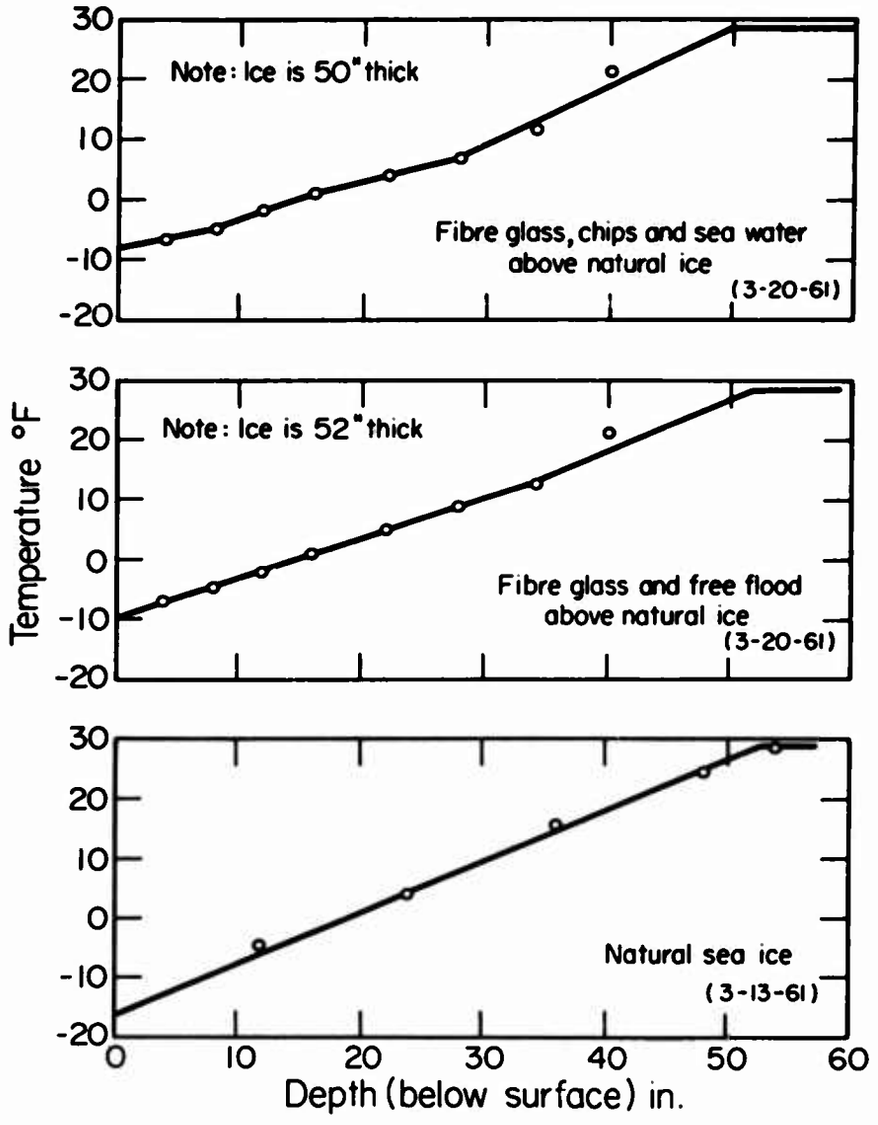

FIG. 12.1. In-Place temperature profiles for ice samples tested

13. LONG-TIME TESTS OF SEA ICE SHEET DEFORMATION
(by H.A. Hobbs and W.D. Kingery)

13.1 Introduction

Long-time load tests were carried out on four different test areas during Project ICE WAY. In general the deformation curves were similar to high-temperature creep curves found in metallic or ceramic systems. Data have not, as yet, been subjected to a detailed stress analysis. Such an analysis is now in progress.

13.2 Experimental Technique

To obtain concentrated heavy loads, plastic-lined tanks (commercial swimming pools) were used. These pools consisted of an outer metal frame (24 ft in diameter) an inner sheetmetal liner, and a 23 ft diameter by 4 ft high plastic bag. The inner metal linear was 3 1/2 ft high, and this was the maximum height to which the pools were filled. When filled with 3 1/2 ft of water, each pool of this size weighed approximately 95,000 lb.

On three of the four test areas, the swimming pools were stacked on top of one another so that heavier concentrated loads could be obtained. This required a decrease in diameter of the top swimming pool in a stack of three such that on the 52 inch thick natural ice test area the top pool was 19 ft in diameter; on the 44 inch thick natural ice test area the top pool was 21 ft in diameter, and on Test Pad No. 2, the third pool was 22 ft in diameter. Figure 13.1 shows the pools being set-up and filled.

A surveyor's level was used to measure deflection of the ice surrounding the swimming pools. Stakes with attached surveyor's tapes were frozen into the ice at the side of the pool (12 ft from the center) at 25, 50, 100, and 200 ft from the center of the pool, and a reference stake 350 ft from the pool. The tripod on which the level was mounted was frozen into the ice at a distance of 350 ft from the pool.

When sighting through the level, it was possible to read the tapes on the stakes to within one-half of one division, ± 0.005 ft. On all tests, this precision was reproducible.

13.3 Ice Samples Tested

Four ice areas were selected for the long-time studies of deformation and creep.

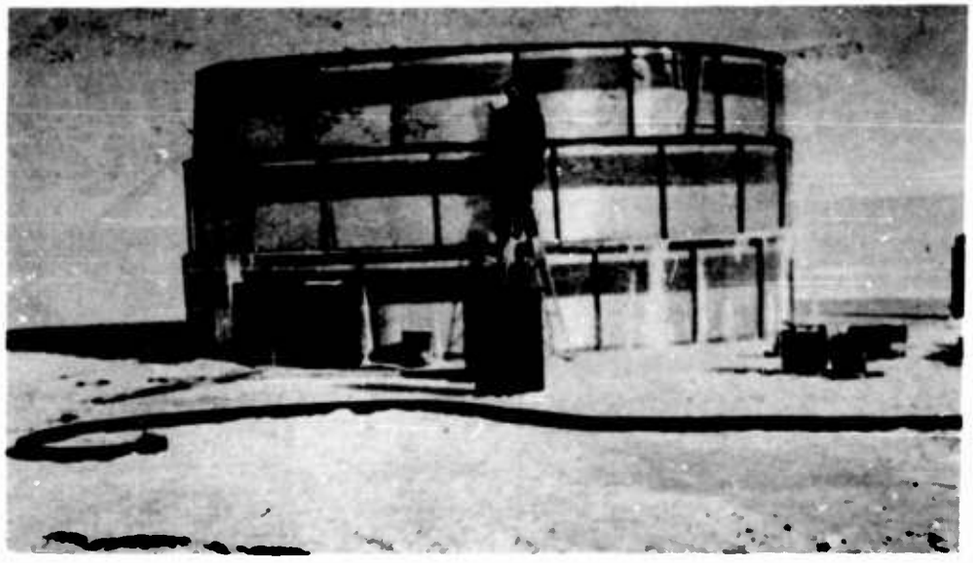

FIG. 13.1. Photograph of plastic pools being set up and filled

Two of these test areas were on natural sea ice; one area had an average thickness of 52 inches and the other area a thickness of 44 inches. The other two areas were Parking Pads No. 2 and No. 3. Pad No. 2 consisted of a 400-ft diameter area upon which Fiberglas was laid and sea water free-flooded for 2 1/2 ft above it. Pad No. 3 was a 100-ft diameter area of chipped ice free-flooded with sea water, and contained Fiberglas at the top and bottom of the chipped-ice region. Figure 13.2 shows thickness profiles of the test areas.

13.4 Experimental Results

Tables 13.1 through 13.4 presents experimentally measured values of load and deflection of the test areas.

The deflection data is plotted as (a) deflection versus time at constant radius, (b) deflection versus distance from center of pool and (c) change in deflection versus distance. Twelve graphs plotting these data are shown in Figures 13.3-13.14.

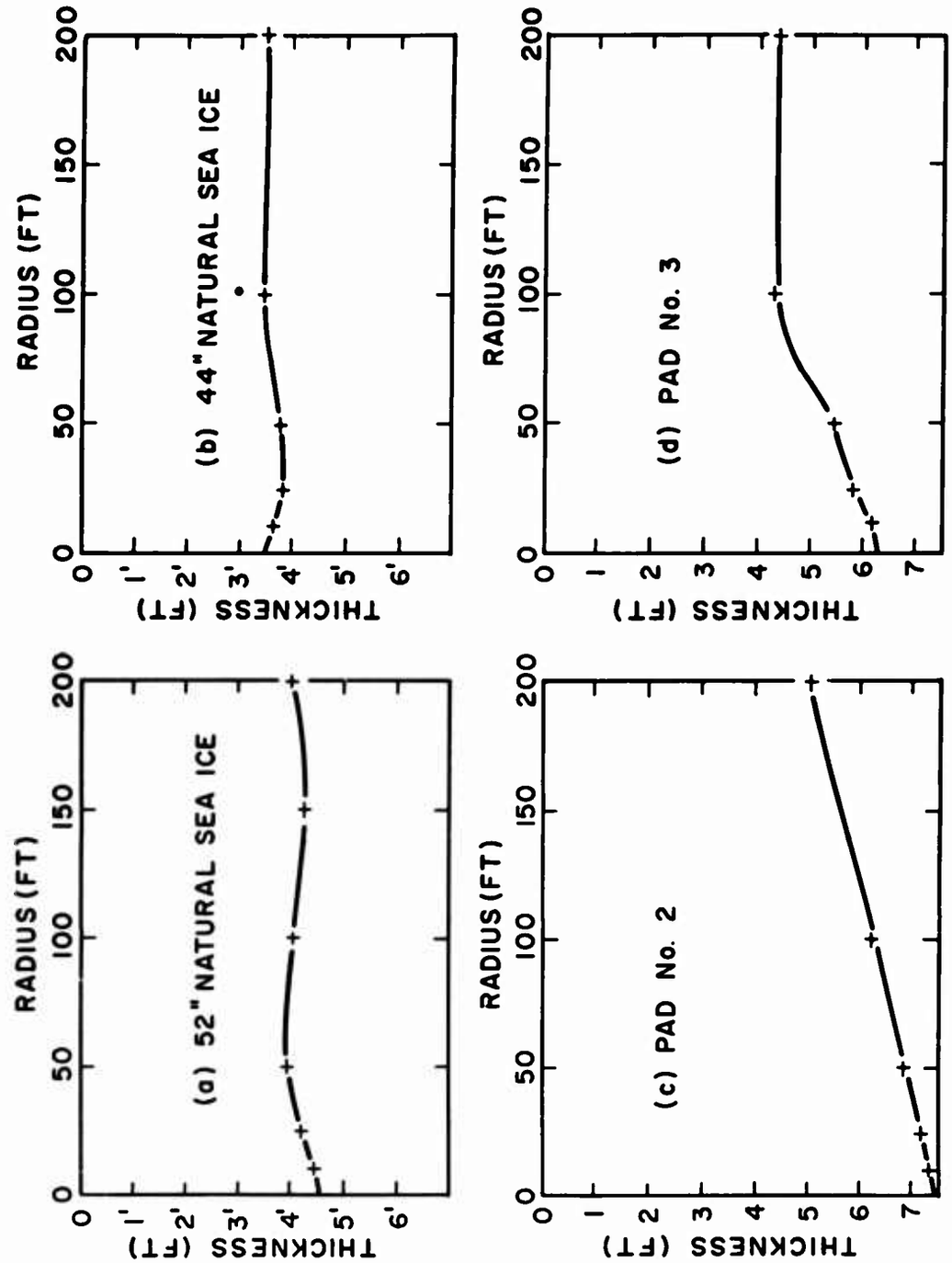

FIG. 13.2. Ice thickness profiles of the test areas studied

TABLE 13.1

Deflection vs. Time at Measuring Stakes on Test Area 1
(52" Natural Ice)

Time (Hours)	Load (lbs)	Deflection (feet) 12'	25'	50'	100'	150'	200'	350'
3	95,000	.065		.040				-.01
4	"	.070		.045	-.01	-.02	-.02	-.01
7	"	.070		.050	-.01	-.050	-.060	-.01
10	"	.080		.050	-.025			
23	"	.115		.060	-.005	-.020	-.030	-.01
25½	"	.115		.060	-.005			
27½	"	.115		.060	-.005	-.020	-.035	-.01
47	"	.135		.060	-.005	-.020	-.030	
52	143,000	.175		.075	-.005	-.020	-.404	-.01
53	"	.175		.070	-.010	-.030	-.040	-.01
54 1/4	"	.175		.070	-.010	-.030	-.040	-.01
69½	"	.220		.105	-.010	-.030	-.035	-.01
71 3/4	"	.220		.105	-.010	-.030	-.035	-.01
75 1/4	"	.225		.105	-.010	-.030	-.035	-.01
77½	"	.225		.105	-.010	-.030	-.035	-.01
79	"	.225		.105	-.010	-.030	-.035	-.01
99½	"	.270		.110	-.010	-.020	-.030	-.01
98½	"	.270		.110	-.010	-.030	-.040	-.01
101 3/4	"	.275		.110	-.010	-.030	-.035	-.01
119 1/4	"	.295	.020	.110	-.030	-.030	-.040	-.01
123½	"	.295	.020	.110	-.020	-.030	-.040	-.01
126	"	.300	.020	.105	-.025	-.035	-.045	-.01
144	"	.325	.035	.110	-.020	-.040	-.045	-.01
146½	"	.325	.035	.105	-.025	-.030	-.045	-.01
150½	"	.330	.035	.105	-.020	-.030	-.045	-.01
167	"	.375	.070	.110	-.020	-.035	-.045	-.01
170½	"	.375	.070	.110	-.030	-.035	-.040	-.02
174	"	.380	.070	.110	-.020	-.035	-.045	-.02
191	"	.420	.070	.110	-.020	-.060	-.045	-.02
194½	"	.420	.095	.110	-.025	-.060	-.050	-.02

TABLE 13.1

Deflection vs. Time at Measuring Stakes on Test Area 1
(52" Natural Ice) (Continued)

Time (Hours)	Load (lbs)	12'	25'	50'	100'	150'	200'	350'
197	184,000	.450	.095	.115				
198½	"	.450	.095	.115				
218	"	.570	.160	.125	-.030	-.060		-.01
224	198,000	.580	.160	.130				-.01
239	"	.625	.195	.140	-.035	-.055	-.065	-.02
242½	"	.630	.195	.145	-.035	-.060	-.070	-.02
246½	"	.640	.200	.140	-.035	-.060	-.065	-.02
266½	"	.695	.230	.150	-.035			-.02
270½	"	.695	.230	.145	-.035	-.065	-.060	-.02
287	"	.720	.245	.145	-.035	-.065	-.070	-.02
288½	235,000	.760	.275	.150	-.040	-.060	-.070	-.02
289½	"	.760	.275	.150	-.040	-.060	-.070	-.02
290½	"	.765	.275	.150	-.040	-.060	-.070	-.02
294½	"	.790	.310	.165	-.040	-.060	-.070	-.02
313	"	.895	.350	.185	-.040	-.060	-.065	-.02
318½	"	.905	.350	.185	-.040	-.060	-.070	-.02
335	"	.945	.360	.180	-.040	-.060	-.070	-.02
338½	"	.950	.360	.190	-.040	-.060	-.070	-.02
342½	"	.950	.365	.190	-.040	-.060	-.070	-.02
358½	"	.980	.380	.190	-.040	-.060	-.065	-.02
362½	"	.995	.380	.190	-.040	-.060	-.065	-.02
367	"	.995	.380	.190	-.040	-.060	-.070	-.02
383	"	1.030	.400	.190	-.040	-.060	-.070	-.02
389½	"	1.035	.405	.195	-.040	-.065	-.070	-.02

TABLE 13.2

Deflection vs. Time for Natural Ice 44" Thick

Time (Hours)	Load (lbs)	Deflection (feet) 12'	25'	50'	100'	200'	Ref.
.75	81,000	.100	.080	.030	.005	0	0
1.25	"	.130	.095	.045	.005	0	0
2.0	"	.125	.100	.045	.010	-.005	0
5.0	"	.140	.110	.055	.005	0	0
19.75	"	.185	.130	.055	0	0	0
22.0	"	.190	.130	.055	0	0	0
26.25	"	.195	.135	.055	0	0	0
41.5	"	.235	.170	.070	0	0	0
45.8	162,000	.420	.290	.130	-.010	-.010	0
46.75	"	.440	.305	.135	-.020	-.015	0
47.75	"	.470	.320	.135	-.025	-.030	0
48.75	"	.490	.325	.130	-.030	-.030	0
49.75	"	.505	.330	.135	-.025	-.030	0
51.75	"	.525	.348	.140	-.030	-.020	0
66	"	.635	.405	.130	-.040	-.025	0
69.25	"	.645	.410	.130	-.040	-.025	0
71,25	"	.650	.400	.130	-.055	-.030	-.01
73.25	"	.655	.405	.125	-.055	-.025	-.01
74.25	"	.655	.410	.125	-.050	-.030	-.02
89.25	"	.700	.420	.110	-.030	-.020	-.03
90.25	"	.725	.435	.115	-.020	0	0
92.25	241,000	.995	.610	.175	-.020	-.005	0
93.5	"	1.025	.620	.175	-.025	-.005	0
94.5	"	1.035	.620	.170	-.035	-.010	0
98	"	1.050	.620	.160	-.025	-.010	0
113.5	"	1.125	.625	.140	-.020	0	0
117.25	"	1.135	.635	.140	-.020	-.005	0
122.25	"	1.145	.625	.110	-.050	-.020	0
137.75	"	1.190	.640	.100	-.030	-.015	0
141.25	241,000	1.200	.640	.100	-.035	-.015	0
145.25	"	1.215	.645	.100	-.030	-.015	0
161.75	"	1.265	.680	.105	-.050	-.030	0
169.25	"	1.280	.690	.110	-.050	-.020	0
168.25	"	1.290	.700	.105	-.060	-.035	0
187.75	"	1.320	.705	.105	-.055	-.020	0
193.25	"	1.345	.715	.105	-.055	-.020	0

TABLE 13.3

Deflection vs. Time for Pad No. 2

Time (Hours)	Load (lbs)	Deflection (feet) 12'	25'	50'	100'	200'	Ref.
1	95,000	.020		.020	0	0	0
16	"	.030		.030	0	0	0
20							
24	"	.040		.030	0	0	0
41	"	.055		.040	0	0	0
45	"	.055		.040	0	0	0
48	"	.060		.040	0	0	0
66	"	.070	.010	.045	0	0	0
69	"	.070	.010	.045	0	0	0
72.5	"	.070	.010	.045	0	0	0
89	"	.080	.015	.045	-.030	-.030	0
92	"	.100	.015	.035	-.040	-.050	-.01
94	185,000	.115	.025	.035	-.040	-.050	-.01
95	"	.120	.035	.045	-.040	-.050	-.01
112	"	.195	.095	.075	-.040	-.050	-.01
120	"	.205	.100	.075	-.040	-.055	
140	"	.235	.125	.100	-.040	-.055	-.01
142	272,000	.280	.170	.120	-.035	-.055	-.01
146	"	.300	.190	.125	-.035	-.055	-.01
161	"	.350	.230	.150	-.040	-.060	-.01
164	"	.335	.230	.150	-.040	-.055	-.01
168	"	.365	.240	.150	-.040	-.055	-.01
185	"	.390	.255	.150	-.040	-.060	-.01
189	"	.395	.255	.150	-.040	-.055	-.01
193	"	.420	.270	.155	-.040	-.050	-.01
209	"	.455	.300	.170	-.040	-.055	-.01
213	"	.460	.300	.170	-.040	-.055	-.01
216	"	.470	.305	.175	-.040	-.055	-.01
235	272,000	.490	.315	.185	-.040	-.055	-.01
240	"	.500	.325	.190	-.040	-.055	-.01
257	"	.515	.335	.200	-.040	-.060	-.01

TABLE 13.4

Deflection vs. Time for Pad No. 3

Time (Hours)	Load (lbs)	Deflection (feet) 12'	25'	50'	100'	200'	Ref.
1	83,000	.015	.0	0	0	0	0
17	"	.100	.045	.020	.005	0	0
21	"	.100	.045	.0	0	0	0
24.5	"	.100	.005	.0	0	0	0
42	"	.140	.060	.055	0	0	0
45	"	.140	.060	.055	0	0	0
46	178,000	.245	.135	.055	.055	0	0
47	"	.265	.155	.055	0	0	0
49	"	.270	.155	.055	0	0	0
69	"	.410	.250	.060	-.005	-.005	-.01
75	"	.415	.250	.060	0	0	0
90	"	.435	.255	.060	0	0	0
93	"	.440	.255	.060	-.005	0	0
97	"	.445	.260	.060	- 0	0	0
111	"	.495	.285	.060	-.005	0	0
114	"	.495	.290	.060	-.005	0	0
118	"	.505	.290	.060	-.010	0	0
134	"	.925	.305	.060	-.010	-.005	-.01
138	"	.525	.345	.060	-.010	-.005	-.01
142	"	.555	.325	.065	-.015	0	-.01
161	"	.600	.355	.080	-.015	0	0

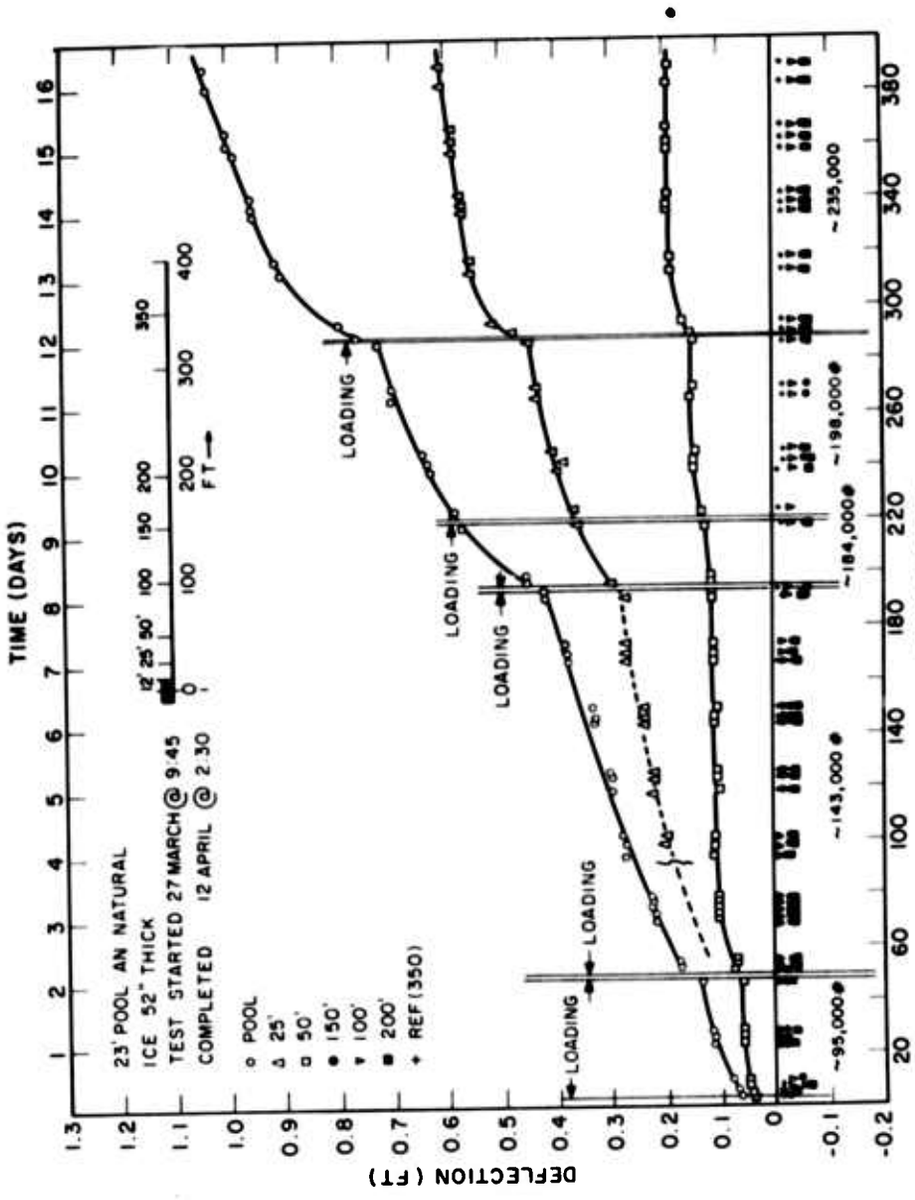

FIG 13.3. Deflection of 52-inch thick natural sea ice loaded with 23-ft diameter pool

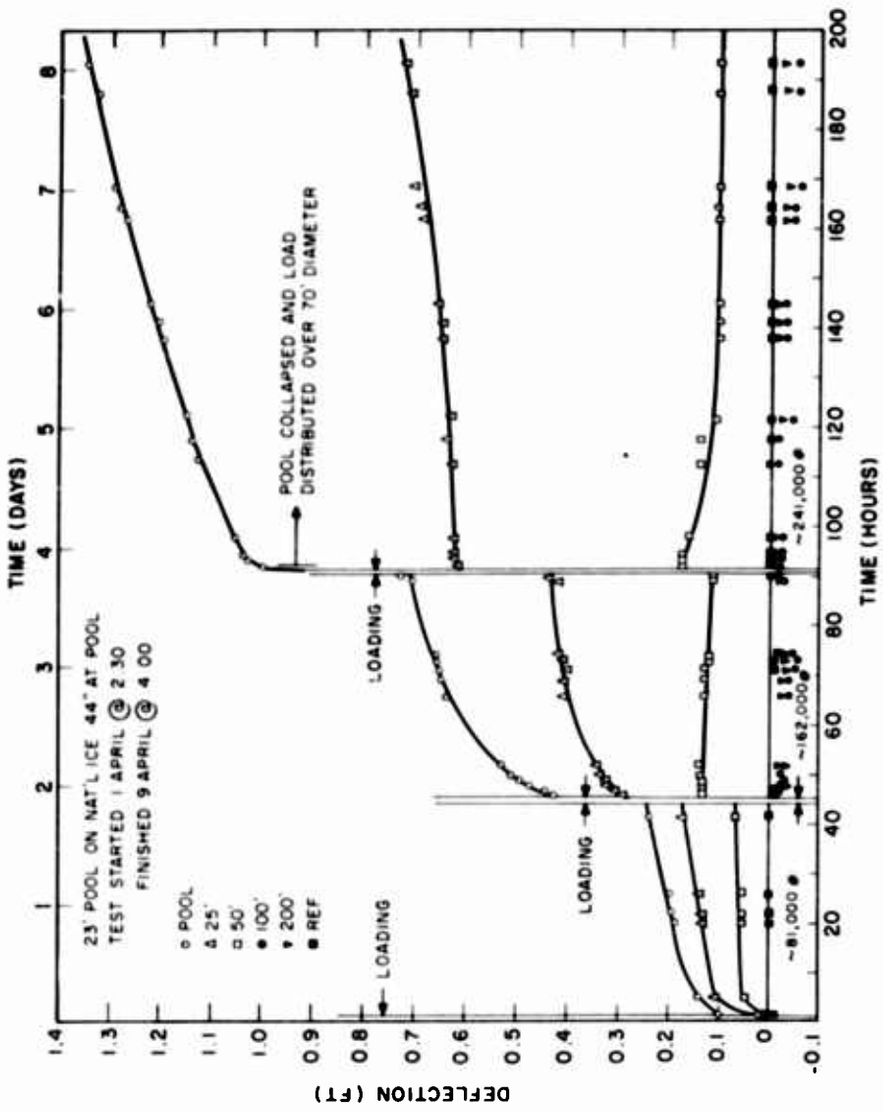

FIG. 13.4. Deflection of 44-inch thick natural sea ice loaded with 23-ft diameter pool

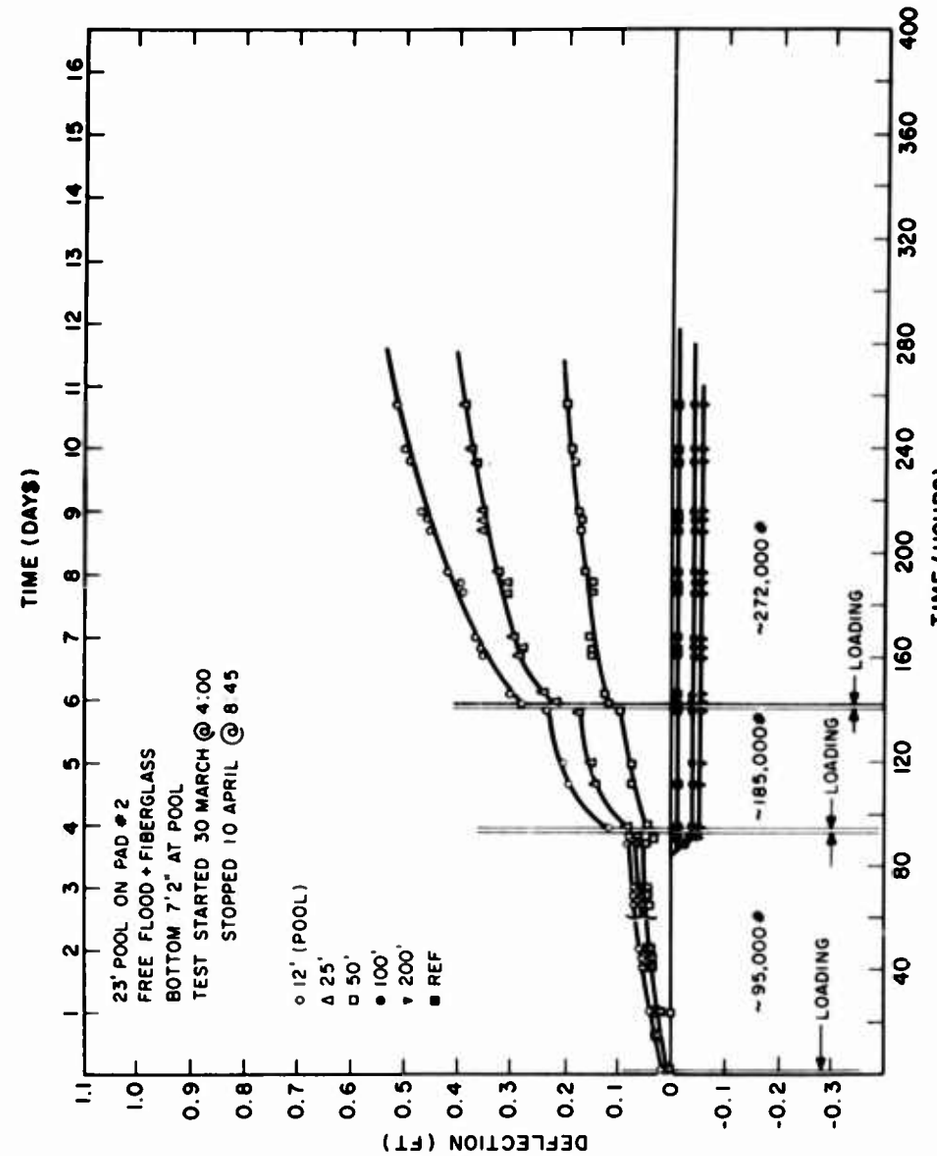

FIG. 13.5. Deflection of Pad No. 2 loaded with 23-ft diameter pool

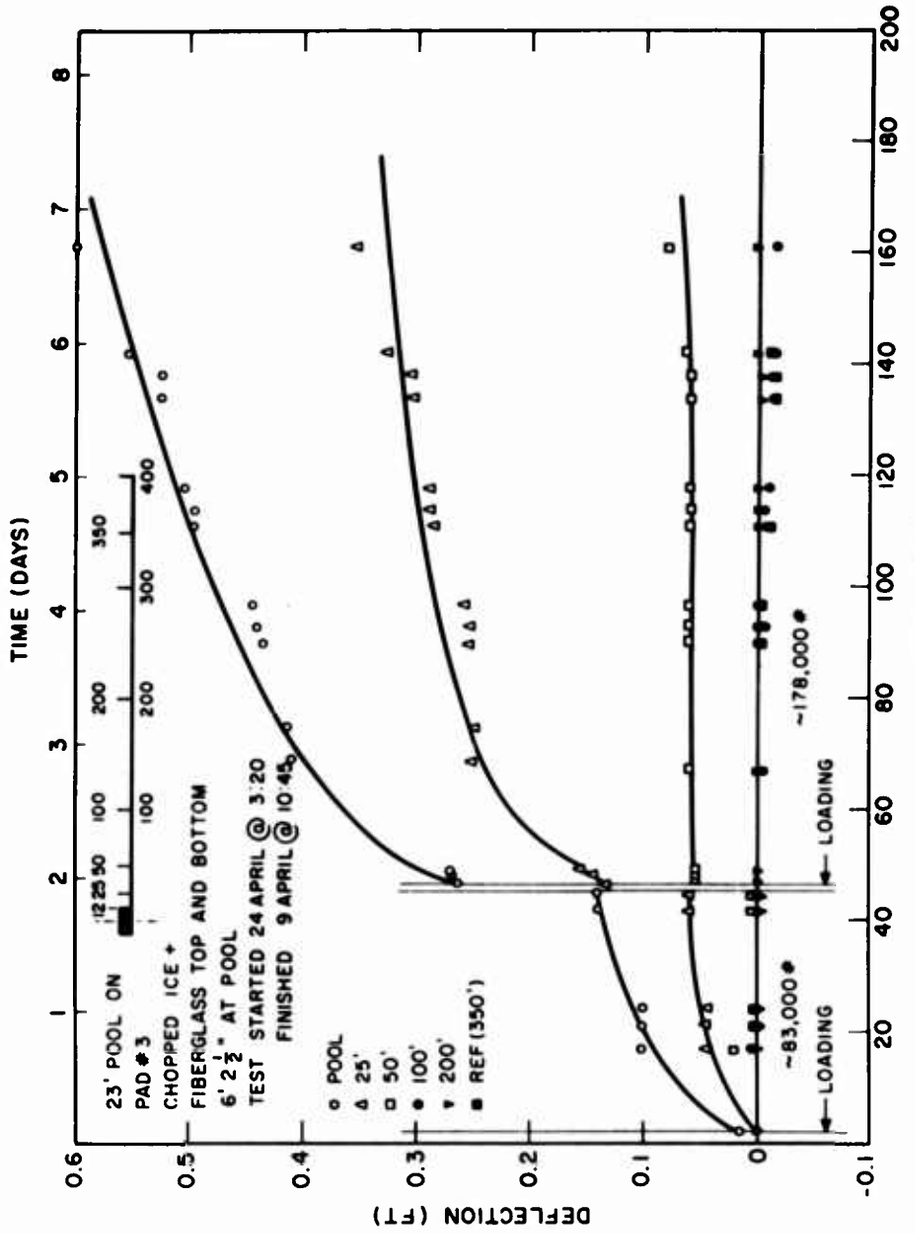

FIG. 13.6. Deflection of Pad No. 3 loaded with 23-ft diameter pool

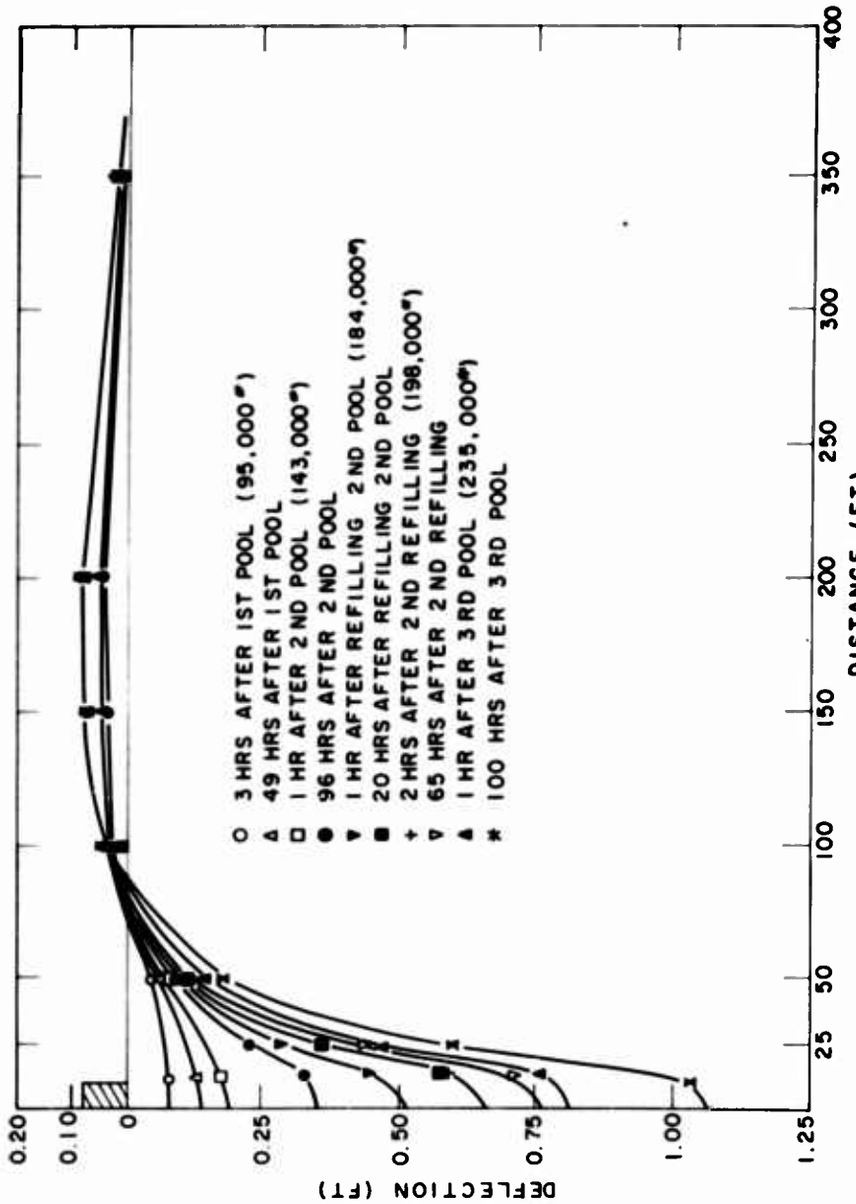

FIG. 13.7. Deflection profile of 52-inch thick natural sea ice loaded with 23-ft diameter pool

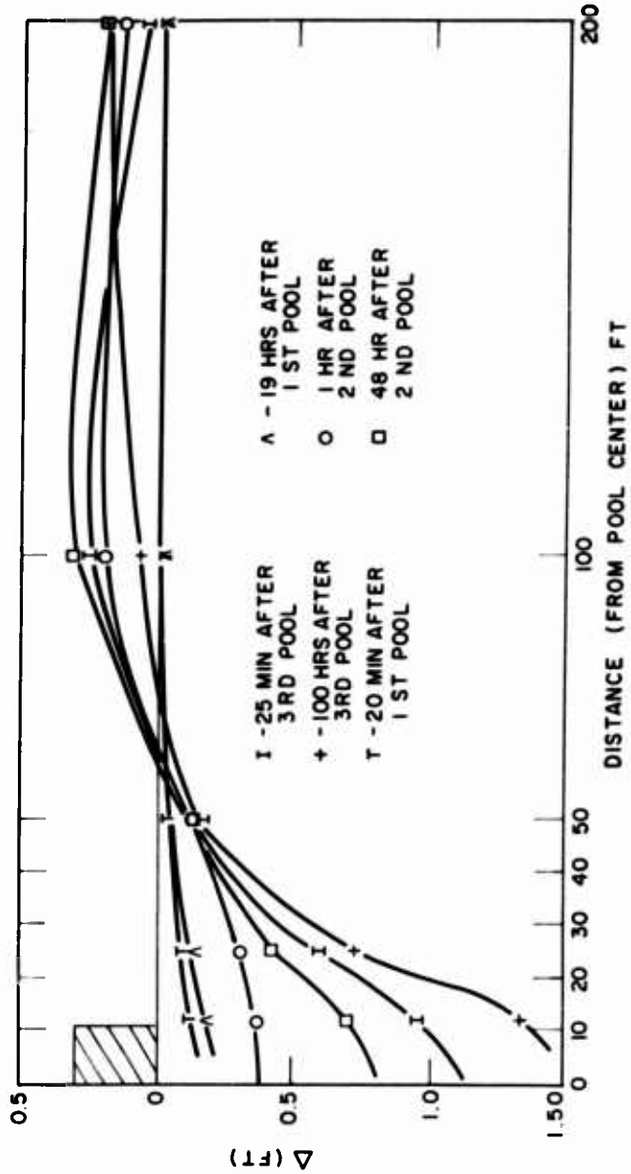

FIG. 13.8. Deflection profile of 44-inch thick natural sea ice loaded with 23-ft diameter pool

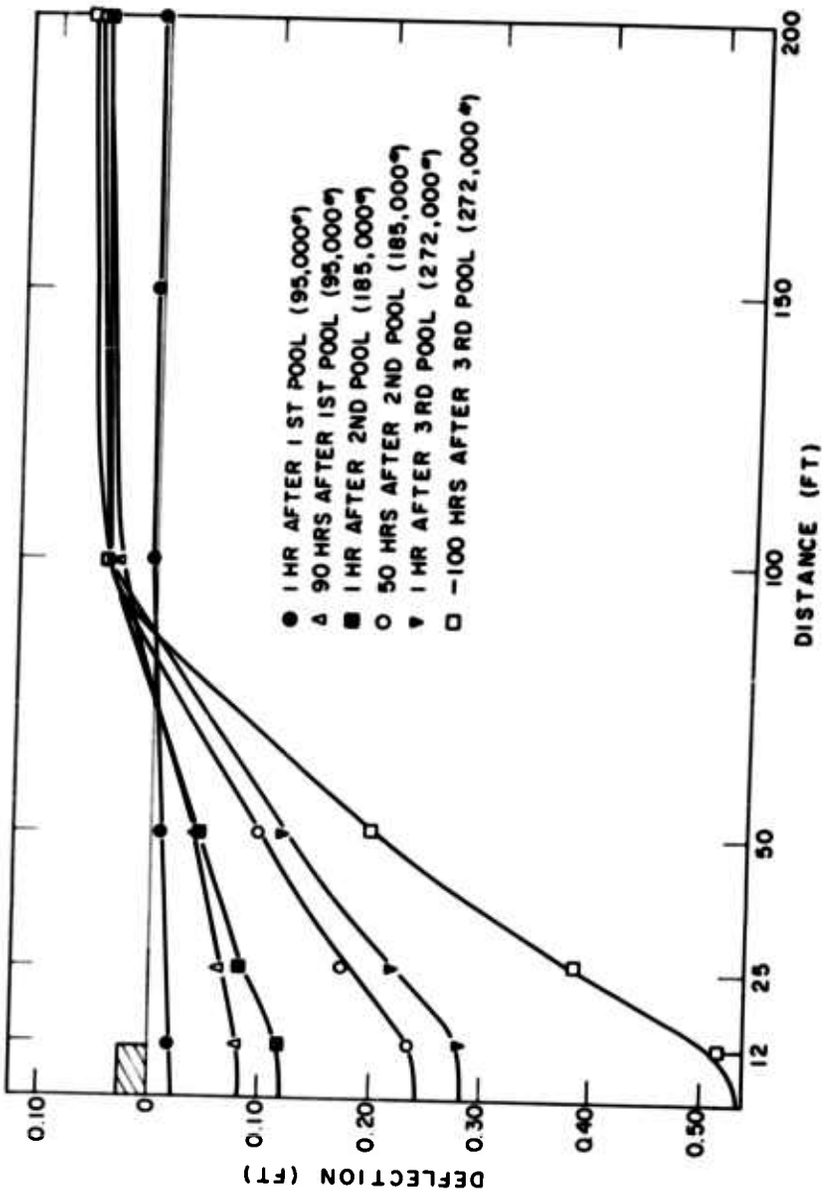

FIG. 13.9, Deflection profile of Pad No. 2 loaded with 23-ft diameter pool

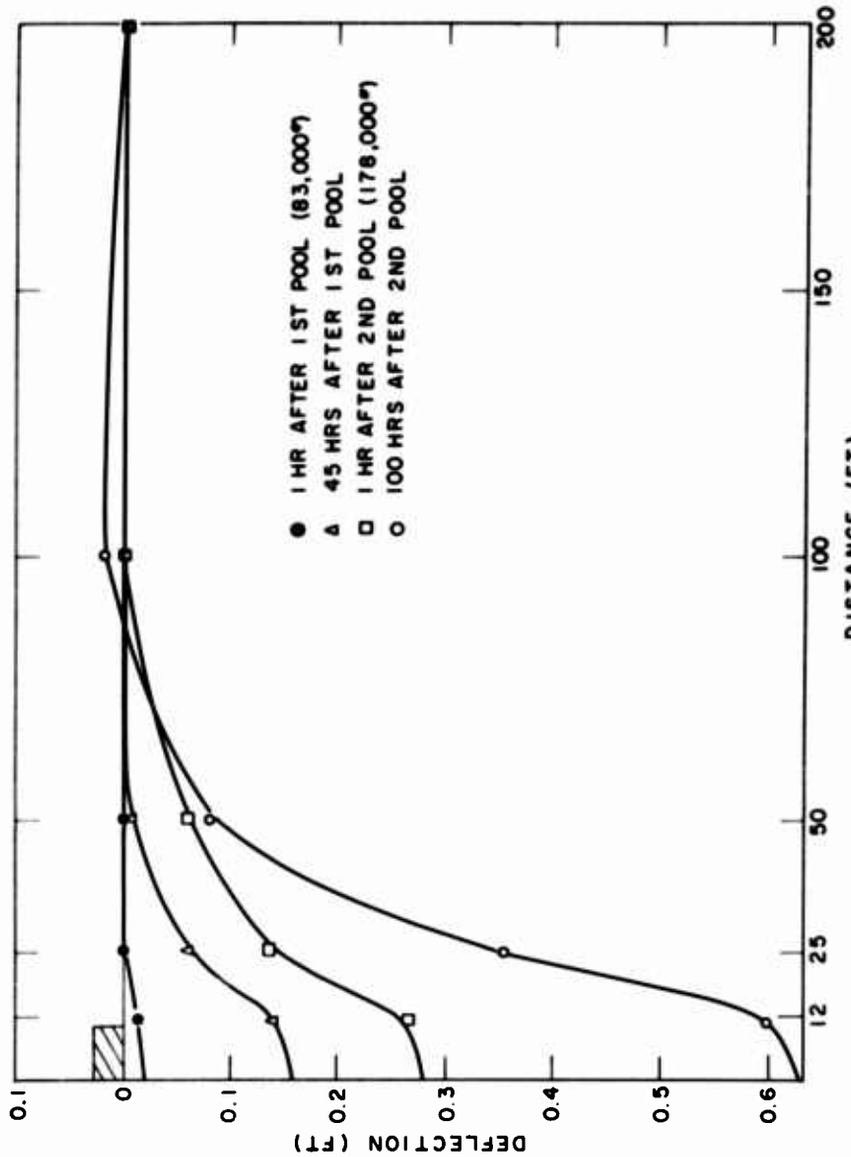

FIG. 13.10. Deflection profile of Pad No. 3 loaded with 23-ft diameter pool.

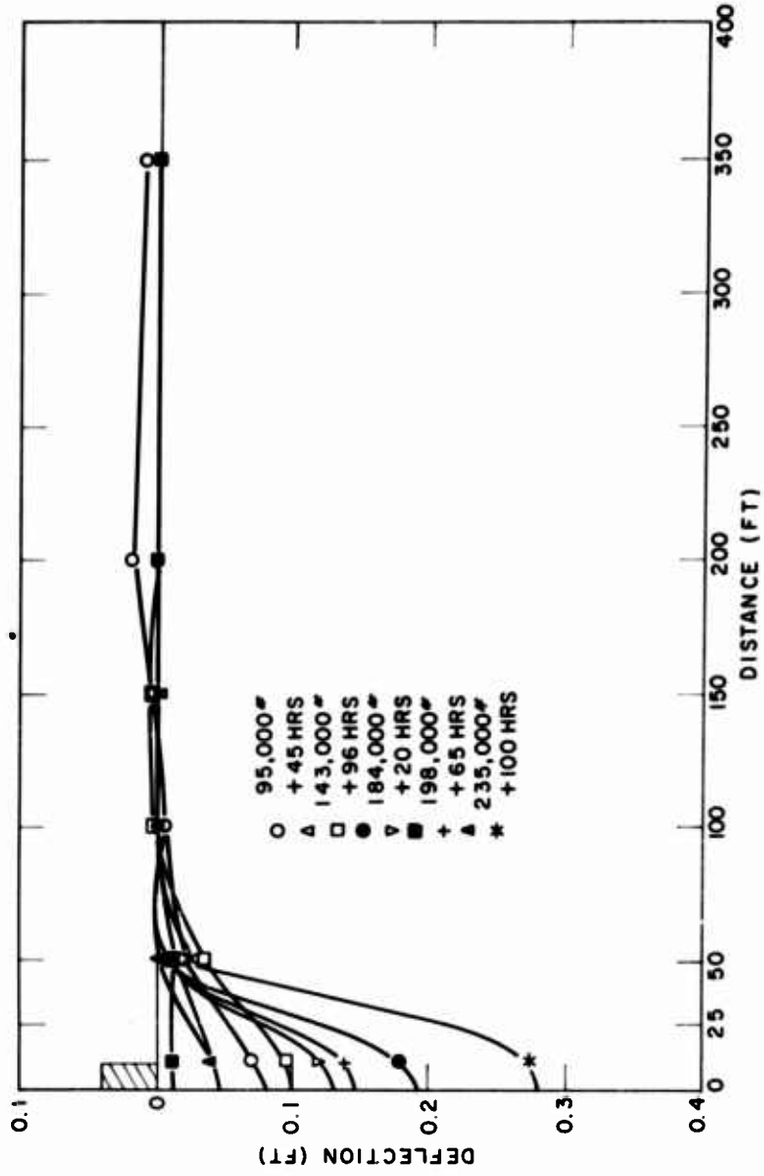

FIG. 13.11. Differential deflection of 52-inch thick natural sea ice loaded with 23-ft diameter pool

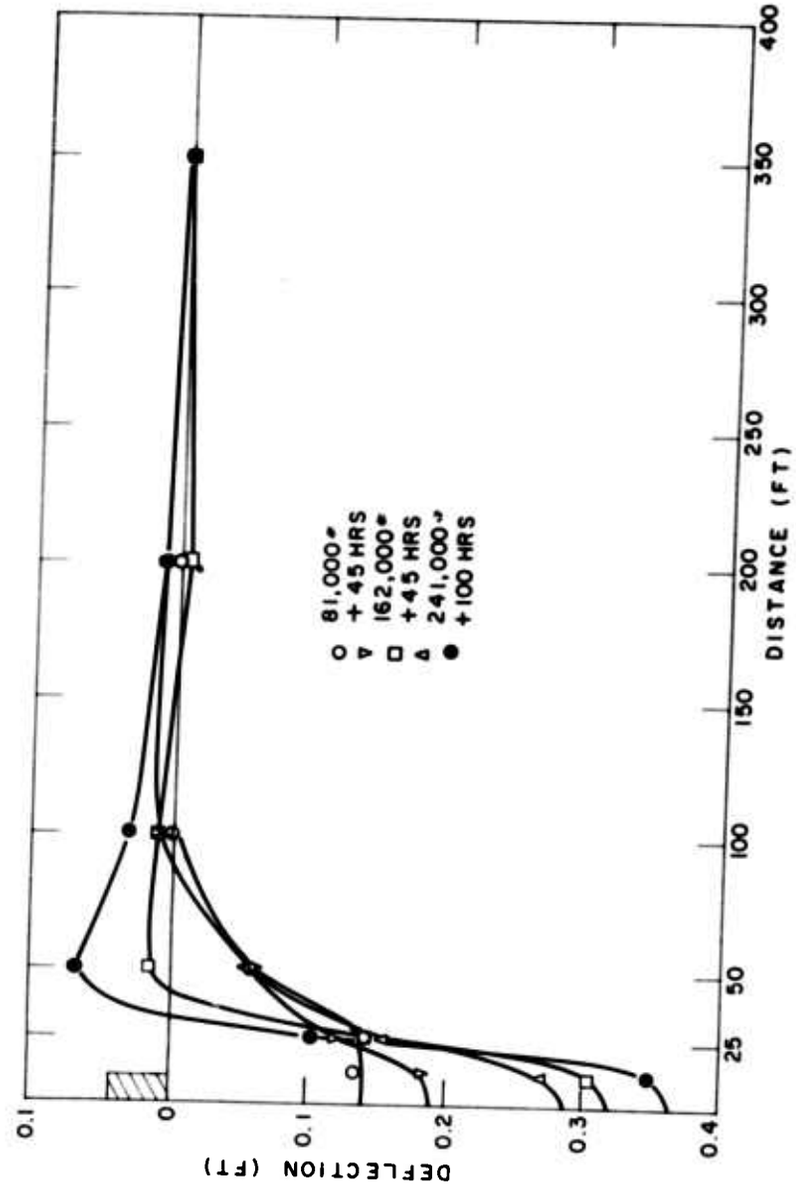

FIG. 13.12. Differential deflection of 44-inch thick natural sea ice loaded with 23-ft diameter pool

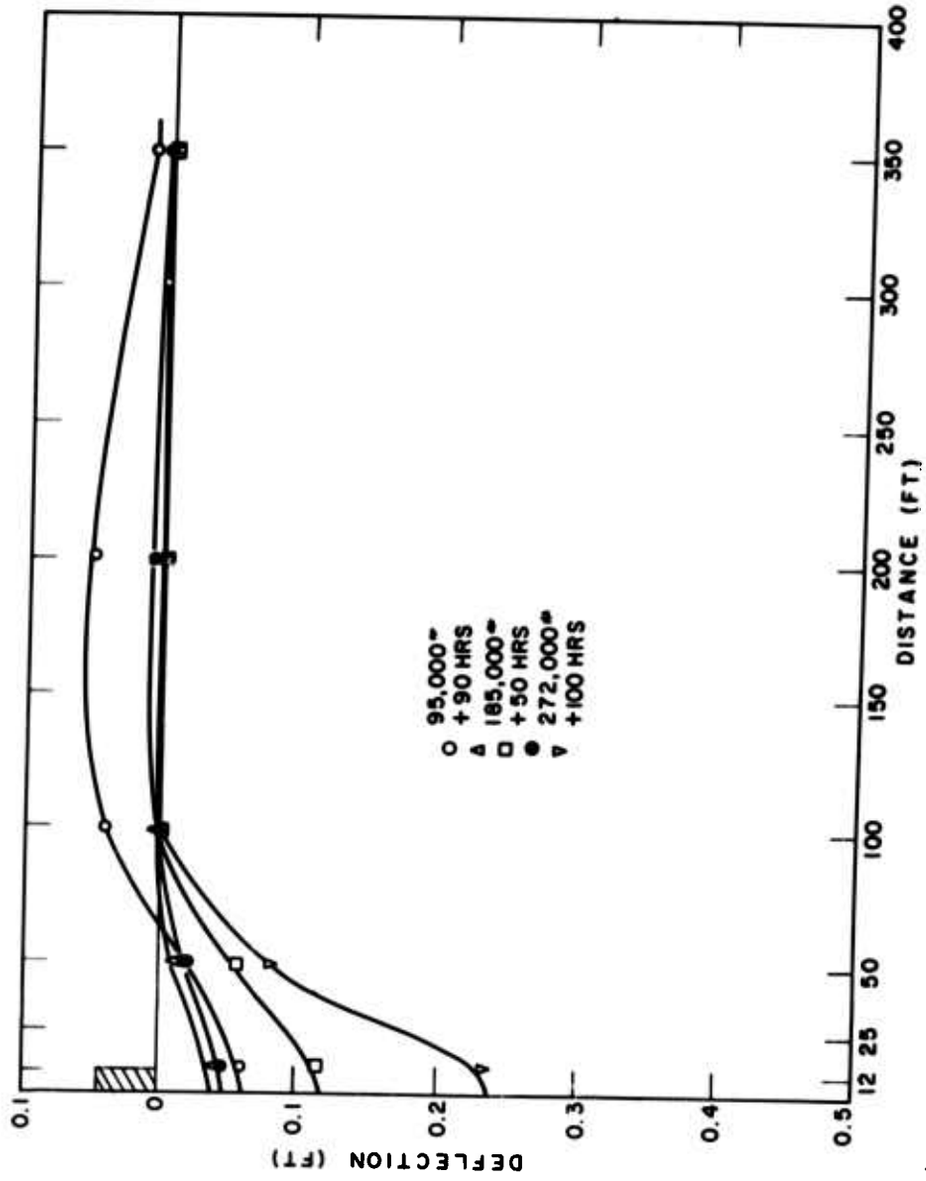

FIG. 13.13. Differential deflection of Pad No. 2

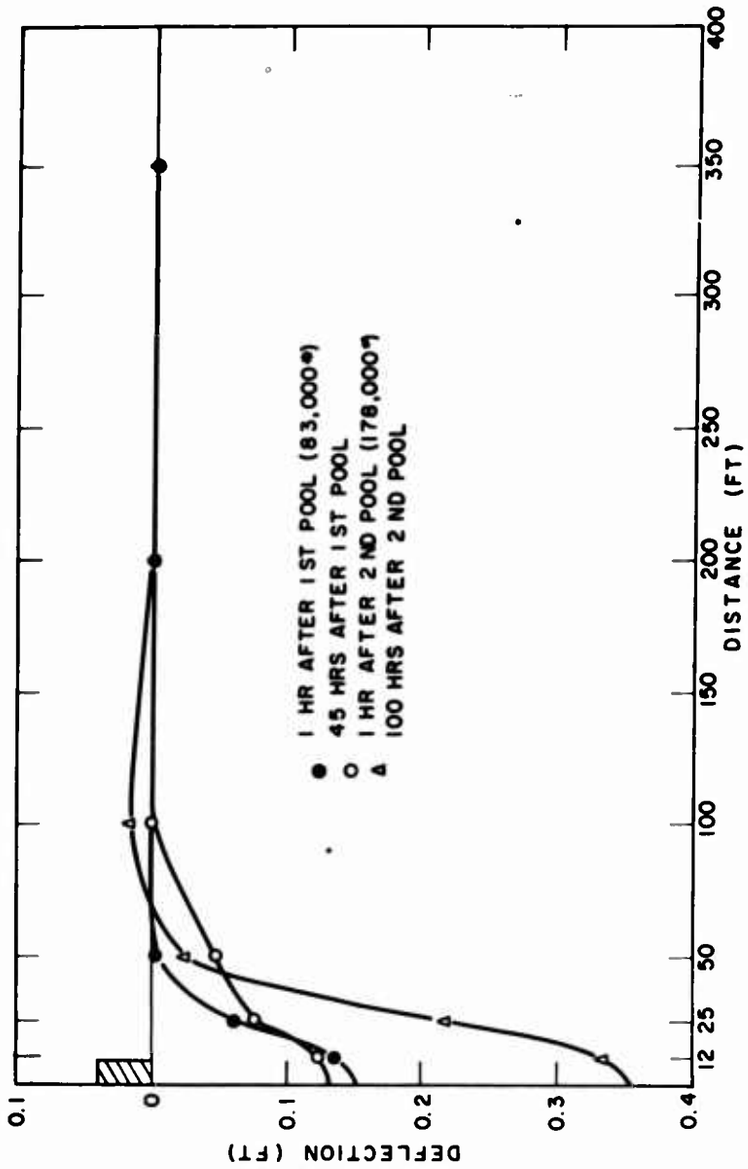

FIG. 13.14. Differential deflection of Pad No. 3

13.5 Discussion of Results

All of the tests show a considerable amount of time-dependent creep deformation. Depending on the ice and load, primary creep was completed within 10 to 30 hr after loading. For the natural-ice test area 52 inches thick, primary creep at the pool was completed within 10 hr for the first 95,000-lb load; when the load was increased to 143,000 lb, this initial creep stage was completed within 5 hr after filling. Primary creep occurs for 30 hr after the third loading; the fourth loading seems to have been too small to initiate any creep of its own; after the final load application (235,000 lb total), creep was again started with the primary creep stage being completed within 30 hr. Secondary creep continued up to the completion of the testing, 100 hr after the final pool was filled.

The 44-inch thick natural-ice test area shows the same type of curve as the 52-inch natural ice; elastic deformation followed by primary and secondary creep. However, the ice cracked within the 200 ft radius measuring area, as shown in Figure 13.15.

The third test area, Parking Pad No. 2, showed the least deflection for the greatest load of any of the test areas. However, Pad No. 2 was almost 3 ft thicker than the 52-inch natural ice, and 4 ft thicker than the 44-inch natural-ice areas. It appears that this area was just beginning secondary creep at the conclusion of the 100 hr elapsed time from the final filling (Figure 13.5). Primary creep only has occurred in the intervals between the first load (95,000 lb) and the second load (185,000 lb). Between the second and third loading, only the elastic deformation during loading and primary creep have occurred.

Pad No. 3 had deflection curves similar to the other three testing sites. Primary creep occurred after the first loading was completed (83,000 lb), and secondary creep began 30 hr after the second pool (178,000 lb) was filled. The total deflection of this site was greater than that of Parking Pad No. 2, less than the deflection of the 44-inch natural ice for the same load, and slightly greater for a 25 percent larger load than the deflection of the 52 inch natural ice.

While the shape of the initial deflection dish is similar to that expected from elastic theory as discussed in Section 7, subsequent creep deflection does not look anything like the elastic deflection dish as shown in Figures 13.7 through 13.14. This is not unexpected in light of the apparent yield point for the time dependent part of the deflection found in Section 7.

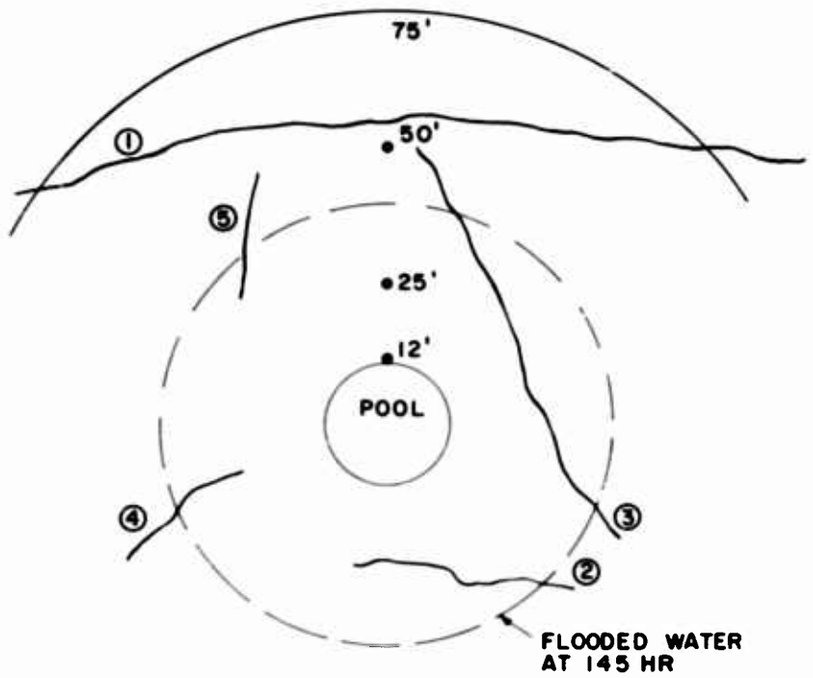

CRACK	APP TIME OF FORMATION	DISTANCE FROM POOL
①	BETWEEN 98 AND 113 HRS	55'
②	BETWEEN 122 AND 127 HRS	25'
③	BETWEEN 122 AND 137 HRS	25'
④	BETWEEN 122 AND 137 HRS	25'
⑤	BETWEEN 145 AND 162 HRS	35'

FIG. 13.15. Crack pattern forming around loaded area at 44-inch thick natural ice

The logarithm of the steady-state creep rate is plotted against log load in Figure 13.16. There are insufficient data for detailed analysis. Measurements can be represented by the relation,

$$\epsilon = \text{constant } (\sigma)^n$$

where n varies between 1.03 (viscous flow) and 0.32.

Analysis of the time-dependence and shape of the deflection curves will not be attempted until a stress analysis of the deformation of an ice sheet with variable temperature and consequently variable properties through it has been completed. This analysis is now in progress.

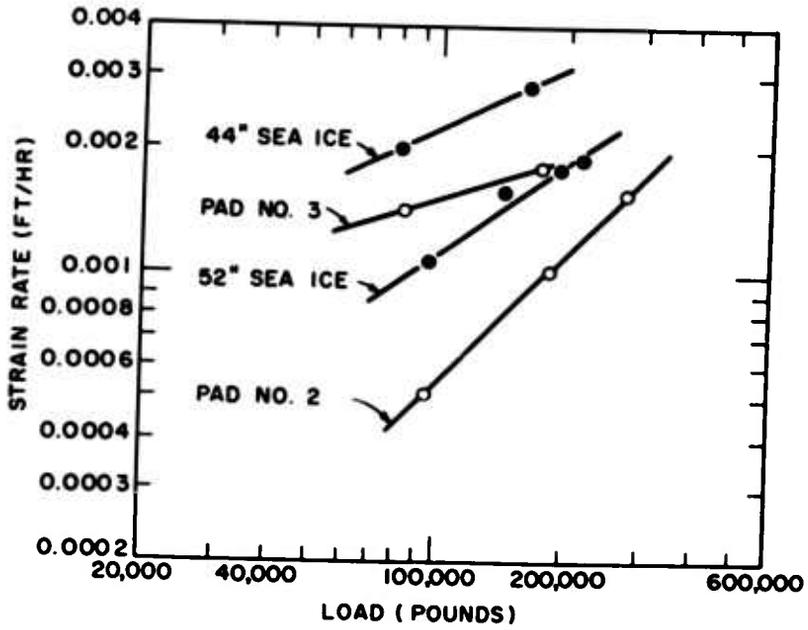

FIG. 13.16. Strain rate versus load for the steady-state part of the creep tests

14. ELASTIC PROPERTIES OF SEA ICE FROM DYNAMIC MEASUREMENTS (by D.L. Anderson)

14.1 Introduction

The general proposed scientific program is presented in Section 14.6. The actual field program followed the proposed one fairly closely with the addition of a small number of core resonance studies. The elastic properties of sea ice were determined by a variety of methods including: (a) body-wave travel time profiles, (b) high-frequency seismic profiles, (c) ice-core resonance, (d) surface-wave dispersion, (e) static and semi-static vehicle and aircraft load tests, and (f) ehicle, aircraft, and air-coupled surface waves. Since sea ice is a complicated substance, being heterogeneous, anisotropic, frequency dependent, and imperfectly elastic, a single type of test is not sufficient to fully evaluate the elastic properties. The above tests were designed to complement one another to give as complete a picture as possible of the elasticity of sea ice. Only the basic theory, field procedure, equipment desc. iption, and preliminary results are presented here. Final results, both experimental and theoretical, will be published in appropriate reports.

14.2 General Theory

Under the action of applied forces solid bodies exhibit deformation to some extent; that is, they change in shape and volume. These forces may be static or dynamic and, correspondingly, the deformation may be static, slowly varying, or a rapid vibration. Insofar as the body recovers its initial shape after removal of the forces and no heat energy is generated, we are in the realm of elasticity. In general, short-term and small deformations are controlled by the elasticity of the material. Long-term and large deformations are controlled by anelastic properties, such as plasticity, viscosity, and strength. Together these physical parameters of a solid are known as the rheological properties and they all must be known in detail in order to predict the bearing capacity of a given substance such as a floating ice sheet. This section will deal primarily with elasticity; other sections of this report give the time-dependent and strength properties of sea ice.

To measure elasticity in the field or laboratory, we must have: (a) some way to exert a force on the ice, that is, a source, (b) some way to measure the resulting deformation of the ice, and (c) some way to display the information in a useful form. The source may be an explosion, a hammer blow, or a heavy load such as a vehicle or aircraft. The resulting waves that spread out from an explosion or impact may be picked up by some sort of transducer; that is, a displacement, pressure, velocity, or acceleration pickup. The output must be amplified in some way and then displayed on an oscilloscope screen, or a film or paper record. Table 14.1 gives the methods of excitation, detection, and recording for the various tests.

14.2.1 SEISMIC THEORY

Elastic wave propagation has proved to be a powerful tool in the study of the mechanical properties of sea ice. The anisotropy, heterogeneity, and departure from perfect elasticity that plague conventional static mechanical tests can all be studied in detail by seismic techniques that have been developed for use both in the field and in the laboratory. Two types of elastic waves can be transmitted by an unbounded, isotropic, elastic media; dilational (P) and distortional (S) waves. The velocities of these two waves, along with the density, completely describe the elastic behavior of an extended (unbounded) elastic body. In an inhomogeneous, anisotropic, and imperfectly elastic-bonded solid body, these basic wave types are modified. Bounded media will transmit, in addition, guided waves that can be used to give corroborative information on elastic properties. The combined use of body-wave and guided-wave data permits a detailed description to be made of the elastic properties of a bounded body, such as sea ice, over a wide frequency range.

The same battery of elastic waves can be applied in the laboratory where the seismic, or ultra-seismic, method becomes a sensitive analytical tool for the determination of composition and structure.

The basic theory of elastic-wave propagation in floating ice sheets has been developed by Ewing and Crary, [1] Press and Ewing, [2] and Sato, [3] under the assumptions of isotropy, homogeneity, and unattenuated propagation. With slight modification these theories can be used to interpret most of the features observed on seismograms taken on sea ice. By taking into account the departure of sea ice from the ideal model assumed, virtually the entire seismogram is interpretable. Ewing and Crary took into account the presence of gravitational

TABLE 14.1

Elastic Measurements Summary

TYPE OF TEST	SOURCE	RECEIVER	DISPLAY	FREQUENCY RANGE
Seismic	Explosives; hammer blows	Geophones, Hydrophones	Galvanometer, Photographic	2-500 cps
Ultra-seismic	Caps; swinging weights	Acceleration and Velocity Transducers	Galvanometer, Direct Writing, Photographic	5-3000 cps
Dynamic	Vehicles and Aircraft	Deflectometers, Accelerometers, Bottom Pressure Recorders	Galvanometer, Direct Writing Photographic; Galvanometer, Direct Writing ink; Recording Potentiometer	0-20 cps
Static	Vehicles and Aircraft	Deflectometers	Recording Potentiometer	Static (0 cps)
Resonance	Loud Speaker Coil	Accelerometer	Galvanometer Direct Writing Photographic	500-10,000 cps

forces which make it possible to apply their results to the low-frequency waves generated by moving vehicles and taxiing aircraft.

When an elastic body has boundaries, such as a core or plate of sea ice, elastic-wave propagation is dispersive, that is, different frequencies travel at different velocities. The result is that pulse, such as may be generated by an explosion or a hammer blow, is spread out into a long train of waves. Each part of the wave train has its own frequency and travels at its own velocity. The farther the receiver is from the source, the longer and more spread out is the recorded signal. On the other hand, a moving vehicle or a taxiing aircraft picks out only those frequencies that have the same velocity as the load. In each case, the relation between frequency and velocity of a given portion of the wave train is controlled by the elastic properties; and, when we know this relation, we have a way of determining elastic properties from the long wave trains generated by explosives, hammer blows, or moving loads. These relations are given in succeeding paragraphs.

Studies on sea ice are complicated by the presence of anisotropy and leakage. Anisotropy is caused by the preferred C-axis horizontal orientation and results in the elastic-wave velocities being directionly dependent; that is, waves travelling horizontally do so at different velocities than those travelling vertically. Consequently, more measurements must be performed than would be necessary if the ice were isotropic. The presence of water causes some of the elastic energy in the ice to "leak out," making the elastic energy decay with time and distance. This requires the use of more sensitive instruments and also considerably complicates the theoretical analysis.

The general mathematical theory of elastic-wave propagation in floating ice sheets, including the effects of anisotropy and leakage, has been developed by Anderson[5].

The period equation expressing the relation between velocity and frequency of Rayleigh-type waves in a transversely isotropic floating plate is,

$$
\begin{aligned}
&\pi_1 \Omega_2 \operatorname{sh} \nu_1 H(\pi_1 \Gamma_2 \operatorname{sh} \nu_2 H \operatorname{ch} \nu_1 H - \pi_2 \Gamma_1 \operatorname{ch} \nu_2 H \operatorname{sh} \nu_1 H) \\
&+ \Lambda_2 \pi_2 \operatorname{sh} \nu_2 H(\pi_2 \Gamma_1 \operatorname{sh} \nu_1 H \operatorname{ch} \nu_2 H - \pi_1 \Gamma_2 \operatorname{sh} \nu_2 H \operatorname{ch} \nu_1 H) \\
&+ \pi_1 \Omega_1 \operatorname{ch} \nu_1 H(\pi_1 \Gamma_2 \operatorname{ch} \nu_2 H \operatorname{sh} \nu_1 H - \pi_2 \Gamma_1 \operatorname{sh} \nu_2 H \operatorname{ch} \nu_1 H) \\
&+ \Lambda_1 \pi_2 \operatorname{ch} \nu_2 H(\pi_2 \Gamma_1 \operatorname{sh} \nu_2 H \operatorname{ch} \nu_1 H - \pi_1 \Gamma_2 \operatorname{sh} \nu_1 H \operatorname{ch} \nu_2 H) = 0
\end{aligned}
\tag{14.1}
$$

where

$$\Gamma_1 = [-\gamma_1 v_1 C_{33} + C_{13} k] \qquad \pi_1 = [v_1 + k\gamma_1]$$

$$\Gamma_2 = [-v_2 \gamma_2 C_{33} + C_{13} k] \qquad \pi_2 = [v_2 + k\gamma_2]$$

$$\Lambda_1 = v^1 \Gamma_1 \operatorname{sh} v_1 H + \nearrow_2 \gamma_1 (k^2 - v_1^{1\,2}) \operatorname{ch} v_1 H$$

$$\Lambda_2 = v^1 \Gamma_1 \operatorname{ch} v_1 H + \nearrow_2 \gamma_1 (k^2 - v_1^{1\,2}) \operatorname{sh} v_1 H \qquad (14.2)$$

$$\Omega_1 = v^1 \Gamma_2 \operatorname{sh} v_2 H + \nearrow_2 \gamma_2 (k^2 - v_1^{1\,2}) \operatorname{ch} v_2 H$$

$$\Omega_2 = v^1 \Gamma_2 \operatorname{ch} v_2 H + \nearrow_2 \gamma_2 (k^2 - v_1^{1\,2}) \operatorname{sh} v_2 H$$

and

$$V_i^2 = \frac{1}{2C_{33}C_{44}} (-M_1 \pm M_3)$$

$$M_3 = M_1^2 - 4M_2 C_{33} C_{44}$$

$$M_1 = C_{33}(\rho_1 \omega^2 - C_{11} k^2) + C_{44}(\rho_1 \omega^2 - C_{44} k^2) + k^2 G^2 \qquad (14.3)$$

$$M_2 = (\rho_1 \omega^2 - C_{11} k^2)(\rho_1 \omega^2 - C_{44} k^2)$$

where

ρ_1, C_{ij}, = density and elastic constants of ice

$G = C_{13} + C_{14}$

$\nearrow_2$ = Lame's constant of water (14.4)

$2H$ = thickness of ice sheet

k, ω = wave number and frequency

This equation has an infinite number of real and complex roots and describes the free vibrations of a floating ice sheet. Evaluation of this equation is very tedious but it is being used to interpret the seismic data and to determine four of the five anisotropic elastic constants.

The long wavelength limit of the symmetric vibrations is the plate velocity and is given by,

$$\rho C_p^2 = \frac{C_{11}C_{33} - C_{13}^2}{C_{33}} \qquad (14.5)$$

To complete the description of free vibrations we need the period equation for Love type, or horizontally-polarized shear waves.

This period equation is. [5]

$$2kH \left(\frac{C_{11}-C_{12}}{2C_{44}}\right)^{1/2} \left(\frac{C^2}{\beta_2^2} - 1\right)^{1/2} = n\pi \qquad n = 0, 1, 2..... \qquad (14.6)$$

where

C = phase velocity

β_2 = horizontal SH velocity

This equation also has an infinity of solutions and can be used to evaluate the fifth of the anisotropic constants.

The advantage of these formulas is that they make it possible to completely describe the elastic properties of the ice from measurements made at the surface. To obtain an equivalent description of the ice using conventional or body wave measurements would require taking samples with various orientations from the ice, for example, cores 90°, 45°, and 0° to the ice surface. The above theory is being used to evaluate the elastic constants from the seismic and ultra-seismic data.

A similarly complicated theoretical analysis holds for elastic-wave propagation in anisotropic cylinders such as cores of sea ice. Again the waves are dispersive, and the velocities vary with the orientation of the ice cores. This theory, which will not be dealt with in detail here, will be used to analyze the results of the core resonance studies.

Figure 14.1 illustrates schematically the dispersion curves of the lowest modes of elastic-wave propagation in sea-ice plate. These curves can be used to predict the sequence of arrivals from either an explosion source in the air, ice, or water, or from a vehicle moving over the ice. The weight of the lines is an approximate indication of the amount of energy that will appear on the seismic record; these modes with phase velocities greater than the sound velocity in air will be slightly attenuated owing to radiation of energy into the air; similarly, those modes with phase velocities greater than the speed of sound in water will be highly attenuated owing to radiation into the water. The higher modes are attenuated because of radiation into the water but must be invoked to explain some of the arrivals at small distances, such as the early-arriving compressional wave. The routinely observed compressional plate waves, vertically polarized shear (SV) waves, flexural waves, and air-coupled flexural waves are all included in the above display.

Since it is the inhomogeneities, primarily the brine and air pockets, that control the properties of sea ice, it is possible to correlate the elastic properties with the strength and, ultimately, the bearing capacity of a sea-ice sheet. Using the results of a previous theoretical study [4] the author has been able to correlate elastic properties with brine content from field measurements and is presently undertaking a similar study in the laboratory where more control is possible. The present indications are that the brine has more than just a volume effect; it also reduces elastic-restoring forces by allowing interplatelet slippage.

The study of the anisotropy of sea ice is not only of theoretical interest but gives information as to the location of the neutral surface – a critical parameter in bearing capacity calculations. Sea ice has both macroscopic anisotropy, controlled by the thermal gradient, and microscopic anisotropy, controlled by the crystal orientation. The second effect takes place over distances of millimeters and the first over distances of meters; but, by combining flexural-wave and plate-wave data, even with wavelengths of the order of hundreds of meters, it is possible to obtain a measure of the directional properties. Even on cold sea ice, this anisotropy amounts to 15 percent for shear waves, the major part of which can be attributed to the crystal orientation. This is the reason why air-coupled flexural wave data in the past have underestimated the thickness of sea ice; anisotropy must be taken into account when an accurate interpretation of the air-coupled frequency is desired.

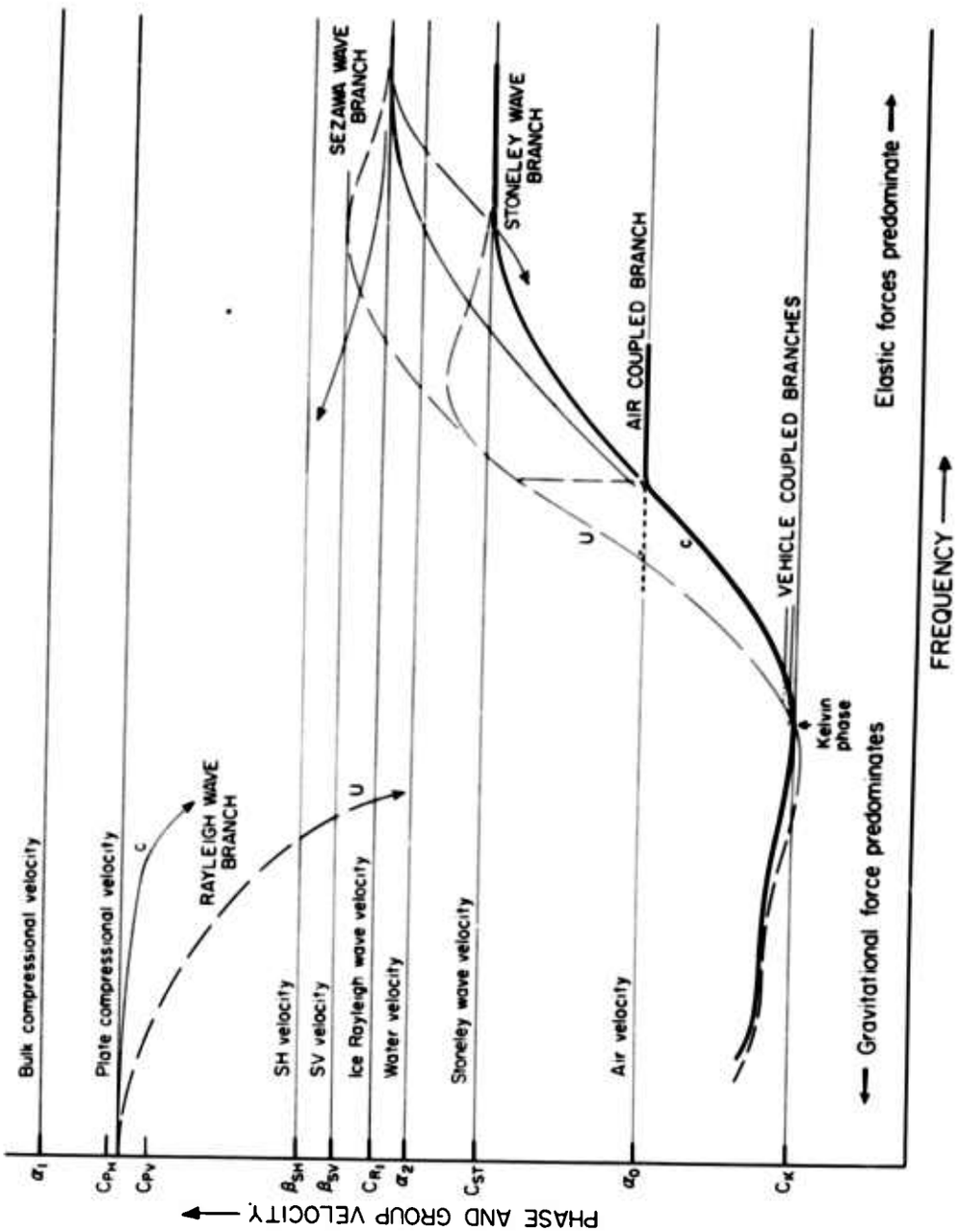

FIG. 14.1. Change in wave phase and velocity with frequency

14.2.2 PRELIMINARY THEORY OF MOVING VEHICLES AND TAXIING AIRCRAFT

Ewing and Crary[1] give the following expression for long flexural waves in a floating isotropic ice sheet overlying incompressible water:

$$c^2 = \frac{g/k + D k^3}{\coth k H + \rho/\rho_1 \, kh}$$

c = phase velocity, k = wave number, h = thickness of ice, H = depth of water, D = flexural rigidity, ρ / ρ_1 = ice to water density ratio, and g = gravitational acceleration.

For very long wavelengths, this becomes:

$$c^2 = (g/k + Dk^3) \tanh k H$$

which is similar to the well-known equation giving the velocity of water waves when gravity and capillarity are both taken into account:

$$c_o = (g/k + T'k) \tanh k H$$

The effect of the ice sheet is to increase the surface forces and to change the dispersion from that observed on a free body of water. Long waves see the ice only as a film on the surface. Gravity controls the long wavelengths, giving normal dispersion, while the flexural rigidity of the ice controls the short wavelengths, giving "anomalous" dispersion. This dual behavior gives rise to a phase velocity minimum as shown in Figure 14.1 and is one of the few places in nature where such an effect is observed. The existence of this minimum, in turn, introduces a powerful new method for determining the static deflection and, consequently, the static elastic properties of a sea-ice sheet. A load placed on a floating ice sheet will cause the ice to deflect in a dish-shaped pattern, the mathematical description of which is the kei function. The displacement under the load and the "wavelength" of the deflection pattern, for a perfectly elastic plate, are controlled by the elastic properties. Until recently the field technique has been to "shoot elevation" in the region of the load with a surveyor's level. This has been unsatisfactory because of the small deflections involved, the limited number and accuracy of the observations,

the necessity for locating the level outside of the deflection region (strictly, an impossibility), and the plastic sagging of the ice that is taking phase simultaneously with the measurements. Indeed this method is well suited for measuring the large plastic deformations associated with parked aircraft. The presence of plastic sagging makes a truly static measure of ice elasticity impossible. The existence of a minimum in the plate velocity curve, however, means that a load moving sufficiently slower than this minimum will drag its static, elastic deflection pattern along with it. Thus it is possible to effectively separate the elastic and plastic deflection by moving the load slowly past a deflectometer, and then parking over the deflectometer. A load moving faster than the minimum phase velocity will be preceded by a high-frequency "head" wave and followed by a lower frequency "rear" wave. This behavior can also be explained by the existence at a minimum phase velocity which requires two group (energy) velocities to be associated with each phase velocity. The frequencies of the "head" and "rear" waves are controlled by, among other factors, the elastic properties and their relative amplitudes by the slope of the dispersion curves and the damping in the ice-water system. The same deflectometer can be used to measure these waves and introduces still another way to determine the elasticity of the sea ice. Instrumentation has been improved so that in the field measurements it was possible to overlap the frequency ranges covered by the deflectometer and seismic techniques; this should increase our confidence in extrapolating seismic results to bearing capacity calculations. In fact the deflectometer proved very useful as a low-frequency strain seismometer, and was used to detect explosion-generated seismic waves. Figure 14.1 shows that the first arriving energy, the "plate" wave, arrives with infinite period, so a low-frequency instrument is vital in determining the onset of this arrival.

14.3 Equipment

Seismic equipment was supplied by the Navy Electronics Laboratory (NEL) and the Air Force Cambridge Research Laboratories, and consisted of a standard 24-channel Southwestern Industrial Electronics P-33 exploration seismograph recording in parallel on photographic paper and magnetic tape. Timing lines were placed on the record by tuning fork controlled timing motor every 0.010 sec. Power was supplied by 12-v aircraft batteries. The useful frequency range was from about 3-500 cps. The pickups were SIE and Hall-Sears geophones oriented vertically and horizontally on, in, and under the ice, Hall-Sears pressure-sensitive geophones suspended at various depths under the ice, and a microphone placed in the air. The explosive sources were blasting caps and C-3 compound; the shot break was

automatically placed on the records. A large axe was also used to more effectively excite shear (S) waves. A geophone or microphone placed close to the axe blow was used as the time break.

The ultra-seismic, or high-frequency seismic, equipment was assembled at the Naval Civil Engineering Laboratory (NCEL) and consisted of a variable speed direct-writing Consolidated Electrodynamic Company photographic recorder; Statham strain gage accelerometers; CEC vibration pickups; Endevco crystal accelerometers; and Endevco and CEC amplifiers. Two traces were used to record a 1-kcps timing signal. The effective frequency range for these tests was approximately 2-3000 cps. A microphone and a modified deflectometer were also used as pickups. Sources were electric blasting caps and impacts generated by swinging lead weights.

The ultra-seismic equipment was also used for the core resonance studies. A loudspeaker was modified to resonate a core of sea ice either longitudinally or in flexure. The loudspeaker was driven by a variable frequency audio-oscillator. An Endevco accelerometer frozen on to the end of the core was used to determine core motion. The input, output, and timing trace were displayed side-by-side on the CEC oscillograph record.

Since the design of the deflectometer was novel, it will be described in detail. A deflectometer is a device for automatically recording the deflection of an sheet under a load. It should be able to record static and dynamic deflections, and this introduces some design complications. Fortunately the period of the waves set up in ice by moving vehicles and aircraft are about 10 sec or longer so that dc instrumentation with a fairly fast response time can be used. A somewhat higher frequency response is desirable in order to overlap the seismic spectrum, and this proved possible with the deflectometer to be described.

The harbor bottom is used as reference, the distance from the top of the ice sheet to the bottom of the water being the quantity measured. This choice of reference simplifies the mechanics and electronics considerably, especially for low-frequency flexural studies, but the total deflection measured includes the effect of tide. Tide effect can be removed easily from the dynamic results but cannot be effectively removed from the plastic deformation caused by long-time parking tests. The deflectometer therefore can be used for determination of dynamic and static elasticity but not for determination of the plasticity or creep of the ice except under ideal tidal conditions.

Figure 14.2 schematically illustrates the deflectometer design. A waterproofed strain gage load cell measures the tension on a spring, both elements being mounted in series between the top of the ice and the bottom of the water. Both tide and ice deflection change the tension in the spring. The load cell is part of a four-arm bridge and the unbalance of the bridge is recorded directly or amplified and recorded.

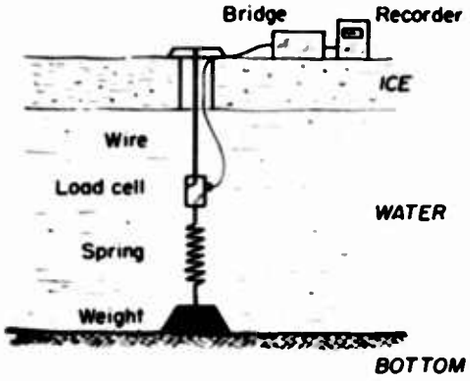

FIG. 14.2 Deflectometer

The deflectometer was primarily designed to detect and record the dynamic deflection pattern generated by moving loads, and the low-frequency explosion-generated seismic waves. These studies are based on the frequency spectrum of the wave pattern and do not require any knowledge of the instrumental amplitude response. Provisions were made, however, to mechanically calibrate the deflectometers so they could be used in static tests also, to extend and complement the dynamic loading tests on the one hand, and the optically-measured plastic creep measurements on the other. Instrumental drift, extreme tidal conditions, and system nonlinearities inhibits the accuracy of these measurements compared to the dynamic studies, but frequent recentering and calibration made it possible to obtain the desired results.

The deflectometers and associated equipment were built in the electronics laboratory of NCEL. The prototype model was assembled at NEL from parts supplied by the Arctic and Submarine Research Branch.

14.4 Field Procedures

In the seismic studies, pickups were laid out on the surface of the ice in groups 100 ft apart. Each group consisted of a high-frequency vertical seismometer, a low-frequency vertical seismometer, a longitudinal horizontal geophone, and a transverse horizontal geophone. Other traces were used for microphones, hydrophones, and geophones in and under the ice. The vertical instruments were sensitive to the flexural waves, reflected waves, one component of the SV motion,

and the bulging associated with the plate wave. The longitudinal horizontal instruments were sensitive to the plate (compressional) wave and the other component of the SV motion. The transverse geophones were sensitive to the SH and Love waves. Water arrivals, Stoneley waves, and leaking waves were recorded by the microphones.

Seismic energy was created by caps, C-3 compound, or axe blows at distances up to 5000 ft from the nearest group of pickups. The travel time of the various types of energy to each geophone group was plotted versus the distance, and the velocity was determined from the slope of the appropriate line on this time-distance plot. Dispersion of the surface, or guided waves, is determined from a period-velocity plot.

The procedure was similar for the ultra-seismic studies except that a greater variety of instruments were located at each station and fewer stations were used. Shot distances were also less. The ultra-seismic test is essentially a microscopic seismic investigation of the behavior of the ice in a small region. A given station consisted of horizontal and vertical CEC velocity pickups, H and V Endevco accelerometers, H and V Statham accelerometers, and a strain seismometer. Shot instants were picked up by microphone or directly from the cap break.

In the core-resonance studies a core of sea ice was driven by a modified loudspeaker. A small plastic arm was attached to the speaker diaphragm and was frozen to one end of the core. An Endevco accelerometer was frozen to the other end. The coil was driven by a variable frequency audio-oscillator. At the natural frequency of the core the response was a maximum. The core was first taken slowly through the frequency band about its expected resonance, and the frequency was read directly from the dial. It was then taken rapidly through this range using high-speed paper drive on the oscillograph. The resonance frequency was later read directly from the record.

Figure 14.3 is an example of a plot of relative amplitude versus frequency from a resonance test. Illustrated is the response for the fundamental and the first harmonic. Cores were driven longitudinally and in flexure. Tests were run on vertical cores and cores taken at different angles to the ice-sheet surface.

For the aircraft and vehicle tests, deflectometers were installed at several locations along the runway and in the parking areas. A bottom pressure recorder, supplied by NEL and the Naval Mine Countermeasures Station, was used to record bottom pressure changes due to landing and taxiing aircraft. Accelerometers were used to pick up the high-frequency vibrations of the ice sheet produced by landing aircraft.

The waterproofing of the load cells for the deflectometers proved to be inadequate and they were field modified to permit surface installation. This made calibration and adjustment much more difficult and also exposed the instruments to

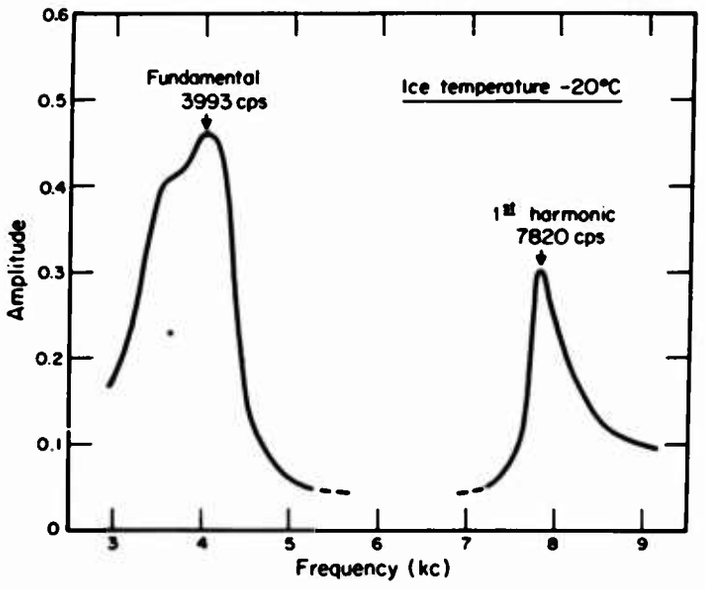

FIG. 14.3 Ice core longitudinal resonance; Sample No. 7

damage by the aircraft. In fact, during the course of the tests four deflectometers were destroyed by aircraft. It proved impossible to balance the load cells through more than 100 ft of cable with the CEC carrier amplifiers. Therefore the deflectometers at distant stations were battery-excited and balanced and recorded with the Varian Recording Potentiometer with a large loss of sensitivity and accuracy. The Varian was initially obtained to serve as a "slave" station at the touch-down end of the runway. The speed of the aircraft and vehicles across the deflectometers was determined from marks placed on the records by vehicle, aircraft, and hand-actuated switches. The deflectometers had to be constantly recentered because of tidal action and were calibrated before and after each test.

Vehicles and aircraft were run across the instruments at various speeds both below and above the critical velocity. Static deflection profiles were run by taxiing the load slowly across the instrument and then parking over the instrument. The natural ice sheet, Pad 1, and Pad 2 were instrumented.

14.5 Preliminary Results

All data is still in preliminary stages of reduction. A certain amount of essentially raw data will be presented here for each of the various studies.

Table 14.2 gives seismic velocities for compressional, plate, and shear waves as determined from time-distance plots. Each tabulated velocity is the average of several tests and represents an in situ average. The necessary supplementary information, such as temperature and salinity, needed for full evaluation of the results was not yet available at this writing. The seismic velocities will be correlated with the average brine content of the ice sheet. The average temperature in the ice sheet is about -10° C so the recorded velocities would be expected to be less than those taken on cores at air temperatures of -20° to -40°C.

Table 14.3 gives the results of a few of the resonance studies. The recorded velocities are minimums, not having been corrected for finite diameter of the sample.

Figure 14.4 shows trackings of deflectometer records for fire-truck runs at 5, 10, and 30 mph. Note the dish-shaped patterns carried along by the slowly moving load and the flexural wave train generated by the rapidly moving load. Clearly, 30 mph is greater than the critical velocity. The "static" elasticity of the ice can be determined by fitting a kei function to the "static" deflection pattern and by the frequency of the wave train for the rapidly moving load. The amplitudes of the waves gives a measure of the damping in the ice-water system.

Figure 14.5 clearly illustrates the difference between the "static" and dynamic deflection patterns for various aircraft. As predicted by theory a supercritical velocity load generates high-frequency waves which precede it and a low-frequency wave which follows it. The shape of the deflection pattern associated with the slowly moving C-130 is the same as would be measured about a stationary load if there were no plasticity.

Figure 14.6 shows the progress of the aircraft-generated flexural wave train between stations 500 ft apart on the natural ice sheet.

The following are examples of the deflections caused by various aircraft: KC-135, 1-inch deflection upon entering Pad No. 1 (147, 500 lb); B-47, 1-1/4-inch deflection within 3 minutes after entering Pad No. 1 (123,000 lb); B-47, 0.85-inch deflection, instantaneous, upon entering Pad No. 2; KC-135, 1.5-inch deflection, slowly taxiing across natural sheet; fire truck, static on natural ice sheet, 0.19-inch deflection; B-52, 0.71-inch deflection, instantaneous, upon entering Pad No. 1.

Interpretation of the deflection patterns in terms of elasticity must include the effects of landing-gear configuration and location of gear with respect to the instruments.

TABLE 14.2

Ultraseismic Results

Location	Thickness (in.)	α_1 (ft/sec)	C_p (ft/sec)	β_1 (ft/sec)	β_2 (ft/sec)	Air-Coupled Frequency (cps)
Natural Sheet*	53	10,050	9380	4850	5200	29.9
Natural Sheet	53	10,100	---	---	5170	30.0
Pad #1	--	10,000	---	4700	5100	---
Pad #2	--	9,100	---	---	4760	---

α_1 horizontal P velocity

C_p plate velocity

β_1 horizontal SV velocity

β_2 horizontal SH velocity

*Seismic result

TABLE 14.3

Resonance Results

Sample Number	Temp (° C)	Length (ft)	Natural Frequency (cps)	Compressional Velocity (ft/sec)	Orientation
1	-27	1.69	2950	10,000	Vertical
2	-27.5	1.54		10,000	Vertical
3	-20	1.17	4300	10,020	Vertical
4	-18	1.23	[illegible]00	9,890	Vertical
7	-20	1.16	[illegible]3	9,232	45°
Pad #1	-16.5	1.97	4300	8,480	Vertical

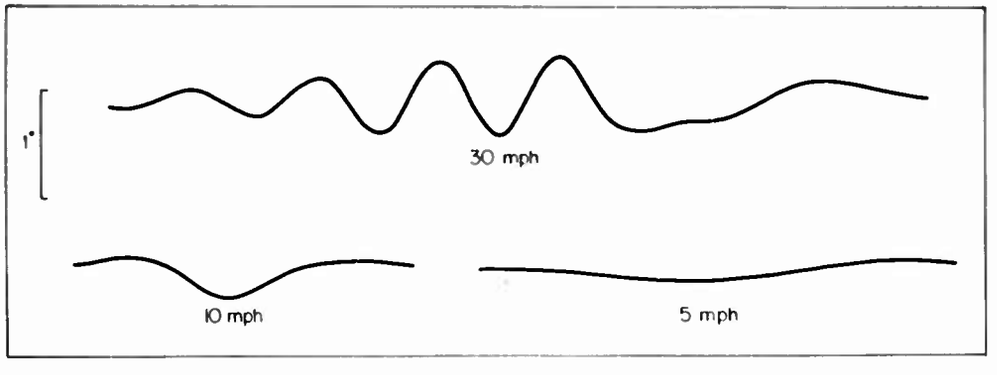

FIG. 14.4 Fire truck runs

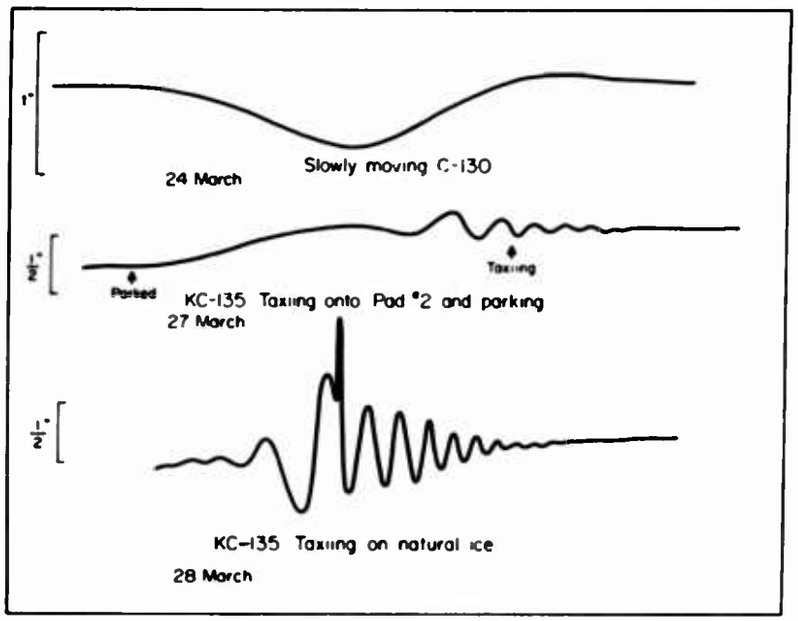

FIG. 14.5 "Static" and dynamic deflection profiles

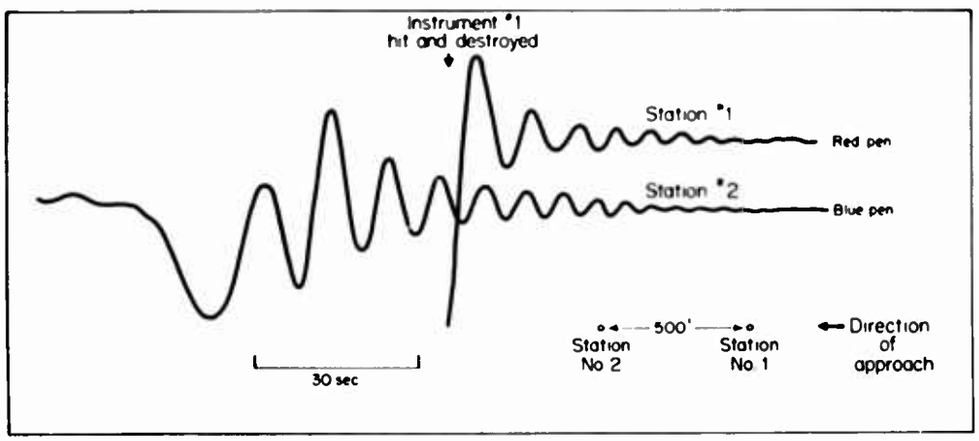

FIG. 14.6 C-130-generated flexural wave train

14.6 Appendix: Planned Program for Studying Visco-Elastic Properties of Sea Ice from Dynamic Measurements, North Star Bay, 1961

MAJOR OBJECTIVES – To determine the static and dynamic elastic and anelastic properties of sea ice up to at least 3000 cps by measuring velocity, frequency, and damping of explosive and vehicle generated visco-elastic waves, surface particle motion, and static deflection pattern. The measuring equipment will consist of deflectometers, velocity transducers, accelerometers, hydrophones, bottom pressure detectors, and the associated amplification and recording equipment.

INDIVIDUAL TESTS

A. Seismic

1. Test Procedure

a. Generate elastic waves (P, S, and Surface) by use of explosives and hammer blows. Determine elastic properties from (a) travel-time plots of P and S waves, (b) dispersion curves of real and complex surface waves including air-coupled and higher modes. Determine departure from elasticity by (a) dispersion of body waves, (b) attenuation of body waves, (c) tilt of surface particle motion ellipse.

2. Equipment

a. Standard seismic (SIE) exploration equipment supplied by AFCRL and NEL including H and V geophones, hydrophones, and cables. Frequency range 2-500 cps; spacing of detectors 20 ft, spread length 220 ft; source distance 0-10,000 ft.

B. Ultra-Seismic

1. Test Procedure

a. Essentially identical to above but in a broader, and in particular, a higher frequency range; also, the more versatile recording equipment will permit simultaneous display of information from deflectometers, seismometers, and accelerometers, not possible with standard seismic equipment.

2. Equipment (NCEL)

a. CEC Direct Writing 5-124, 18-Channel Oscillograph, 6 CEC 1-112 Linear-Integrating Amplifiers, 4 ENDEVCO 2242 accelerometers with cathode followers, 3 CEC 4-102A vibration pickups (see control center schematic for equipment set up).

C. Aircraft landing, taxiing, and parking tests; vehicle taxiing tests

1. Test Procedure

a. Using the instrumental setup as illustrated on map 2 and the runway schematic, aircraft will land, taxi, and park over the deflectometers and associated equipment in the various test areas. Aircraft will attempt to touch down at the designated point, maintain a constant speed (c.80 mph) in the designated zone, and come to rest at the end of the runway; and, if feasible, turn and taxi through the constant-speed zone at 20 mph and return at 40 mph (all speeds approximate). Aircraft will then park over center deflectometer on runway for approximately 15 minutes. It will then park in each of the two test areas for times to be designated. It will then take off in routine fashion.

b. Elastic properties of the ice sheet will be determined from velocity, frequency, and amplitude of aircraft generated flexural waves and resonance velocity. Anelastic properties will be determined from shape of resonance curve, damping of flexural waves, static deflection pattern, and sag.

c. Preceding the aircraft landing tests and with the same instrumental setup, two heavy fast vehicles will be used to test the ice in the various test areas. These vehicles (20-ton fire trucks) will make approximately ten runs past the instruments at speeds between 3 and 60 mph.

d. Following the vehicle runs a helicopter will "bounce" the ice at each of three designated points.

2. Equipment (NCEL)

See control center schematics and runway map.

D. Harmonic (Lazon) Oscillator

1. Test Procedure

a. The NCEL Lazon oscillator will be used to vibrate the ice in the frequency range 1 to 60 cps to determine mechanical complex impedance and to accurately determine phase velocity of P and S waves in this frequency range.

2. Equipment

a. The Lazon oscillator will be used in place of the explosive source in both the seismic and ultra-seismic tests and the equipment arrangement will be identical to that previously given for these tests.

REFERENCES

1. Ewing, M. and A. P. Crary, "Propagation of Elastic Waves in Ice, 2," Physics, 5, 181-184 (1934).
2. Press, F. and M. Ewing, "Propagation of Elastic Waves in Floating Ice Sheet," Trans. A. G. U., 32, 673-678 (1951).
3. Sato, Y., "Study of Surface Waves, 2. Velocity of Surface Waves Propagated upon Elastic Plates," Bull. Earthquake Res. Inst., Tokyo Univ., 29, 223-261 (1951).
4. Anderson, D. L., "Preliminary Results and Review of Sea Ice Elasticity and Related Studies," Trans. Eng. Inst. of Canada, 2, 116-122 (1958).
5. Anderson, D. L., "Elastic Wave Propagation in Layered Anisotropic Media (in press), 1961.

15. ELASTIC PROPERTIES OF SEA ICE AT ULTRASONIC FREQUENCIES (by M.P. Langleben)

15.1 Introduction

Extensive investigations of the elastic moduli of fresh-water ice are reviewed by Dorsey[1] and by SIPRE.[5] Values of Young's modulus for fresh-water ice have been reported in the range 3×10^{10} to 11×10^{10} dyne cm^{-2}. With few exceptions these values have been obtained by static methods such as the deflection or extension of a beam under loading. The large scatter of results may be attributed to the visco-elastic nature of ice. The results tend to become more reliable if dynamic methods of testing are used.

Data on the elastic moduli of sea ice are scanty. Seismic techniques have been used by Oliver et al[3] to obtain an average value of Young's modulus for pack ice. Pounder and Stalinski[4] used an acoustic method, but their measurements were limited to ice at -20°C and to a salinity range of about 4 $^{o}/_{oo}$ to 8 $^{o}/_{oo}$.

Included in the scientific program for Project ICE WAY was an investigation of the elastic properties of sea ice. An acoustic method was used and the results reported here cover a wide range of ice salinities (4 to 24 $^{o}/_{oo}$) and temperatures (-3° to -26°C).

15.2 Experimental Techniques

The elastic moduli of a solid substance can be determined from the velocity of propagation of compressional and shear waves in the solid. If the waves are of ultrasonic frequency, samples of modest size can effectively be considered as infinite media.

According to elastic theory, the velocities are given by:

$$C_B = \left[\frac{E}{\rho} \frac{(1 - \sigma)}{(1 + \sigma)(1 - 2\sigma)} \right]^{1/2} \qquad (15.1)$$

and

$$C_S = \left[\frac{E}{\rho} \frac{1}{2(1 + \sigma)} \right]^{1/2} \qquad (15.2)$$

where: C_B is the velocity of compressional waves in an extended solid, sometimes called the bulk velocity, C_S is the velocity of shear waves, ρ is the density of the material, E is Young's modulus, and σ is Poisson's ratio.

A pulsed ultrasonic system was used to obtain the velocities by determining transit times through samples of measured length. Barium titanate ceramic transducers, in suitable housings, are coupled to each end of the ice sample being tested through a microfilm of oil. The transmitting transducer is shock-excited at a repetition rate of 50 times/sec by a short high-voltage pulse, emitting in turn short bursts of ultrasound at its resonant frequency of approximately 500 kcps. The signal is detected by the second transducer and, after suitable amplification, is applied to the vertical deflection plates of a cathode-ray tube. The oscilloscope is triggered from a time-delay generator in synchronization with the pulse applied to the transmitter. The time delay of the pulse applied to trigger the oscilloscope is continuously variable and the amount can be read off of a calibrated dial. When the transmitting transducer and the horizontal sweep are triggered simultaneously, corresponding to zero time delay in the horizontal sweep, the received signal is displayed at some distance to the right of the origin of the sweep. (Visual measurement of the transit time through the ice sample, as obtained from the face of the scope, lacks the accuracy required.) As the time delay applied to the scope trigger is increased, and the horizontal sweep consequently initiated after the transmitting transducer is excited, the received signal moves from right to left on the scope face. The time delay is increased until the leading edge of the received signal coincides with the start of the horizontal sweep. This time delay corresponds to the transit time through the sample after a zero connection is applied by placing the two transducers into contact with each other.

An accuracy in time measurement of better than 0.5 percent is possible with well-calibrated equipment, provided that the leading edge of the wave packet of received signal is sharp. The velocities are, however, more inaccurate because of the rather crude method of measuring the length of the samples. A pair of outside calipers and a millimeter scale were used, and it is estimated that the possible error in length is about 1 percent, and that, therefore, the possible error in velocity is 1.5 percent.

The procedure used in testing is as follows. A vertical core of ice was extracted with a 3-inch SIPRE corer. This was sectioned in lengths of approximately 15 cm, each piece being identified according to its depth below the upper surface of the ice sheet for later correlation with salinity profiles. The sample from the bottom of the core was tested first, since a large temperature differential existed between it and the environment. The next from the bottom followed, and so on. In addition the temperature of each sample was measured immediately after testing by drilling a hole into its interior and inserting a thermometer.

The density and salinity of the samples tested were not determined. Arrangements had been made with the Scientific Leader of Project ICE WAY for NCEL to do these measurements on our samples, but the plans did not materialize. Instead, densities and salinities required in the analysis of our data are obtained from profiles provided by NCEL. The tacit assumption is, therefore, made that there is little horizontal variation in these properties through the ice sheet.

15.3 Results and Discussion

All observations reported here were made during the period 13-23 March. Tests were performed both on samples extracted from the natural ice sheet adjacent to the ice runway and from the free-flooded parking pad. The raw data are too cumbersome to reproduce here in tabular form. They were analyzed with regard to the following variables.

a. The bulk or compressional velocity as determined by the method described in the previous section.

b. The temperature of each sample, a direct measurement made immediately after sonic testing.

c. The brine content (fraction by volume). This was obtained indirectly. A table by Assur[6] permits one to relate the brine content to the temperature of the sample, assuming a salinity of 1 $^{o}/_{oo}$. The brine volume corresponding to 1 $^{o}/_{oo}$ salinity is then combined with the salinity of the sample and gives the brine content of the sample. Appropriate salinities were selected from Figure 15.1 by comparing the original depth of each sample below the ice surface with the salinity profiles shown in the figure. These profiles are plotted from observations made by NCEL on 16 and 19 March. Each profile is the average of two adjacent cores.

Figure 15.2 plots bulk velocity against negative temperature. Crosses and dots are used to differentiate between samples of natural sea ice and free-flooded ice, respectively. A numeral adjacent to the plotted point indicates that several samples yielded the same result.

Now to a first approximation, the salinity (Figure 15.1) of the natural sea ice can be considered as constant at about 6 $^{o}/_{oo}$ and that of the flooded ice at about 21 $^{o}/_{oo}$. In that case, in spite of the large scatter of points in Figure 15.2, it appears that for natural sea ice there is little, if any, variation of velocity with temperature at temperatures below about -8°C. (Gold,[2] in laboratory experiments on multigrain fresh-water ice finds that, over the range 0° to -40°C, there is a very slight linear increase in bulk velocity with decreasing temperature by an amount 0.0023×10^{5} cm sec^{-1} deg^{-1}.) Bulk velocities are lower, on the other hand, in the free-flooded ice than in the natural sea ice at equivalent temperatues, indicating that the significant variable may perhaps be the brine content. Further evidence for this is provided in Figure 15.2 where, for the natural sea ice at temperatures warmer than -8°C, and so with increasing brine content, the bulk velocity also decreases.

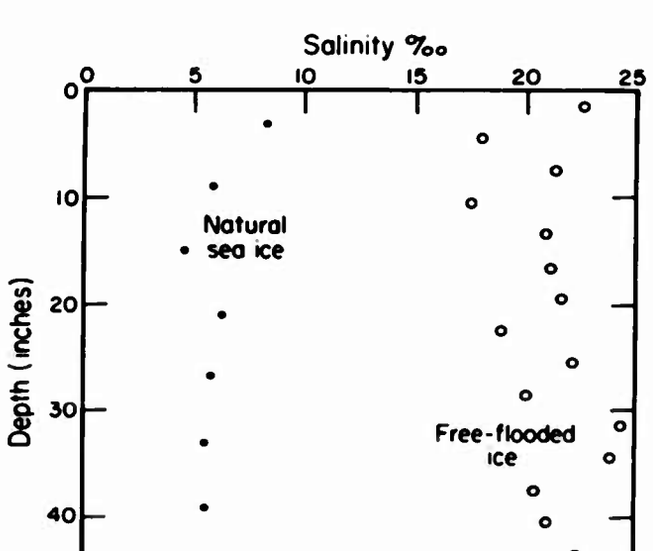

FIG. 15.1 Salinity vs depth for natural and free-flooded ice

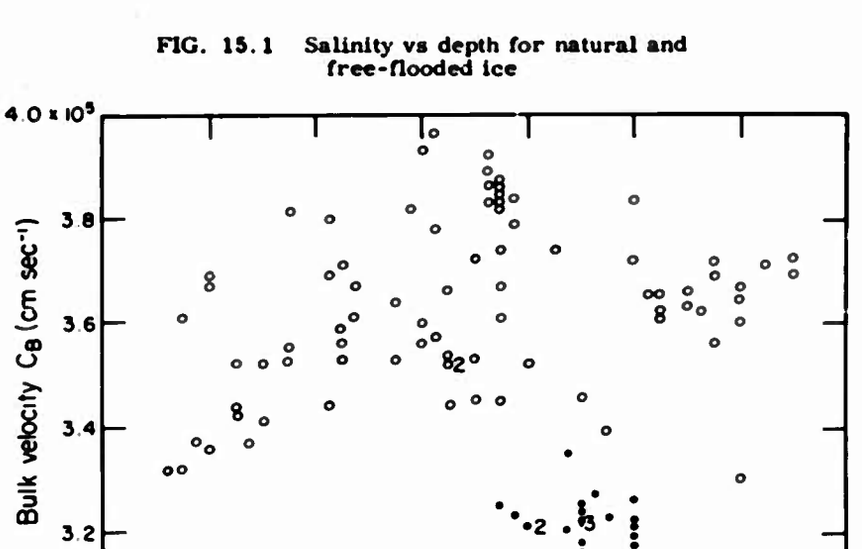

FIG. 15.2 Bulk velocity vs temperature for natural (circles) and free-flooded (solid points) ice

With this justification, the data have been rearranged to show bulk velocity as a function of brine content in Figure 15.3 Although the scatter is great, the decrease of velocity with increasing brine content is readily apparent. It was mentioned earlier that the estimated possible error in velocity is 1.5 percent. The scatter must, therefore, be attributed to other sources of error. Temperature measurements were at best accurate to 1°. The resulting possible error in brine content could be about 3.5 percent at -20°C, 9 percent at -10°C, and 21 percent at -5°C. The hydrometer used to determine salinity, in particular of the natural sea ice, can be read to about 2 percent. Finally, the use of isolated salinite profiles in the analysis is not desirable. Horizontal variations in salinity of the order of 10 percent are quite common over short distances in a sheet of uniform sea ice. Having examined these sources of possible error, it is rather surprising to find such good correlation between bulk velocity and brine content, as is evident in Figure 15.3. A least-squares fit of the data yields the relation:

$$C_B = (3.85 - 8.0\nu) \times 10^5 \text{ cm sec}^{-1} \qquad (15.3)$$

where ν is the brine content as a fraction of the total volume and C_B is the bulk or compressional velocity. For zero brine content, or fresh-water ice, the bulk velocity is, therefore, 3.85×10^5 cm sec^{-1}. This value is in excellent agreement with Gold[2] who finds a velocity of 3.86×10^5 cm sec^{-1} at 0°C and 3.88×10^5 cm sec^{-1} at -20°C.

For a substance of given density, Young's modulus is not uniquely defined through the compressional velocity, since Poisson's ratio is also involved. If the shear velocity can be measured, then both Young's modulus and Poisson's ratio can be determined. A set of transducers which were thought suitable for generation of shear waves were brought on the expedition without previous testing in the laboratory. They proved unsatisfactory and the shear velocity could not be measured. However, subsequent work on sea ice at Isachsen in May 1961 showed little difference in Poisson's ratio between ice of salinity 1 $^{o}/_{oo}$ and 5 $^{o}/_{oo}$. The value obtained was 0.293 ± 0.01. With this value of Poisson's ratio, and using the density profiles provided by NCEL, values of Young's modulus were computed from the bulk velocities. The data were arranged in increasing order of brine content and then separated into intervals of 0.01 in brine content. Values of Young's modulus and of brine content in each interval were averaged, and the averages are shown in Figure 15.4 as Young's modulus against brine content. The number of values

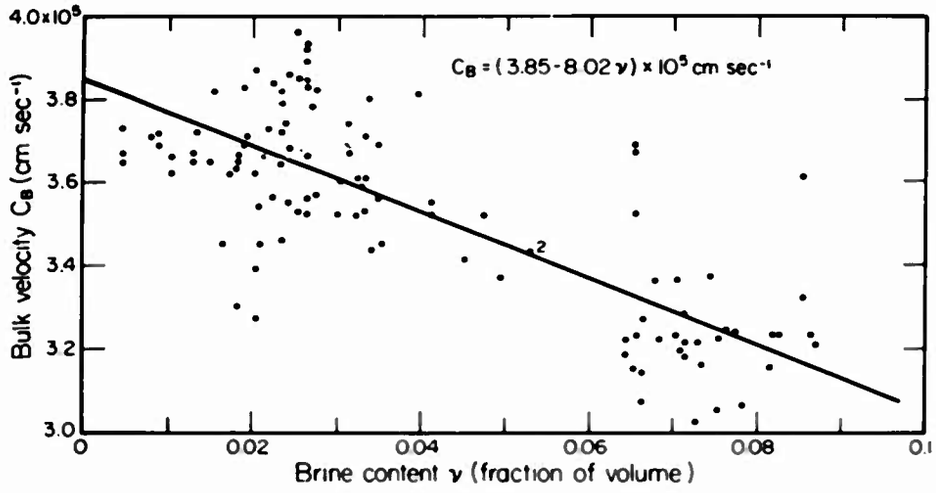

FIG. 15.3 Bulk velocity plotted vs brine content

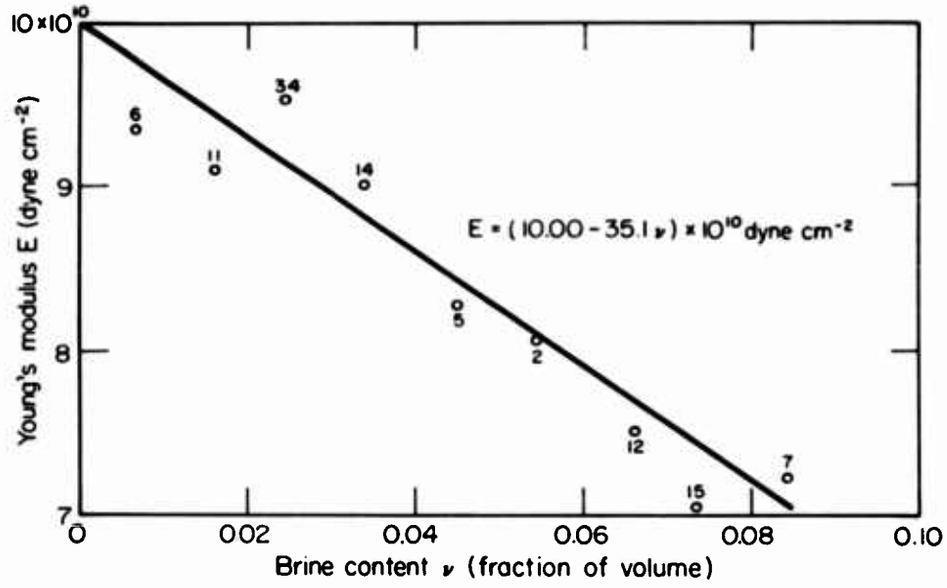

FIG. 15.4 Young's modulus plotted vs brine content

averaged in each interval is indicated beside the points. Again, it appears that a straight-line fit is justified. A least-squares analysis results in:

$$E = (10.00 - 35.1\nu) \times 10^{10} \text{ dyne cm}^{-2} \qquad (15.4)$$

where E is Young's modulus and ν is the brine content by volume.

Recent measurements on fresh-water ice at Isachsen yielded a value for Young's modulus of slightly over 10×10^{10} dyne cm^{-2}, whereas Gold[2] states that $E = 9.94 \times 10^{10}$ dyne cm^{-2} at -5°C. It appears that the value of Young's modulus obtained when the empirical relation above is extrapolated to zero brine content is quite reasonable.

15.4 Conclusions

The field investigations reported here on the elastic properties of natural sea ice and free-flooded ice resulted in an empirical relationship between E (Young's modulus) and ν (brine content), which is of the form:

$$E = (10.00 - 35.1\nu) \times 10^{10} \text{ dyne cm}^{-2} \qquad (15.5)$$

Using this relation it is possible to infer the profile of Young's modulus existing in an ice sheet, providing both temperature and salinity profiles are available.

Consider a simplified model for a sheet of natural sea ice which is roughly typical of conditions in North Star Bay in March. Assume a uniform salinity of 6 $^{o}/_{oo}$ and a linear temperature gradient starting at -20°C, near the top of the ice sheet. The temperature at the base is about -2°C. Then Young's modulus will be found to decrease linearly with depth from a value of 9.3×10^{10} dyne cm^{-2} at the top to 5×10^{-10} dyne cm^{-2} at the bottom, for an average value of 7.1×10^{10} dyne cm^{-2}.

The parking pad of free-flooded ice consisted of roughly 4 ft of free-flooded ice overlying an equal thickness of natural sea ice. Let the temperature gradient again be linear with the same temperature limits as above, and assume uniform salinities of 21 $^{o}/_{oo}$ for the free-flooded ice and 6 $^{o}/_{oo}$ for the natural sea ice. Young's modulus will decrease linearly with depth from 7.5 to 6.2×10^{10} dyne cm^{-2} in the free-flooded ice, will suffer a discontinuity at the interface with the

natural sea ice, and then once more decrease linearly with depth from 9.0 to 5 x 10^{10} dyne cm^{-2}. The overall average value of Young's modulus will be 6.9 x 10^{10} dyne cm^{-2}.

ACKNOWLEDGMENTS

I am indebted to Mr. Alex Becker for collecting most of the raw data. The research was jointly sponsored by the Defense Research Board of Canada under Contract GC. 69-000105 and by the Arctic Institute of North America.

REFERENCES

1. Dorsey, N. E., Properties of Ordinary Water-Substance, Reinhold Publishing Corp., New York (1940).
2. Gold, L. W. Can. J. Phys., 36, 1265 (1958).
3. Oliver, J., A. P. Crary, and R. Cottell, Trans. Am. Geophys. Union, 35, 282 (1954).
4. Pounder, E. R. and P. Stalinski, IUGG paper, Helsinki (in press).
5. SIPRE Report No. 4, Snow, Ice and Permafrost Research Establishment, U. S. Army Corps of Engineers, Wilmette, Illinois (1951).
6. Assur, A., "Phase Relations for Standard Sea Ice" in "Composition of Sea-Ice and Its Tensile Strength" Publication 598, Arctic Sea Ice, pp. 106-138, National Academy of Sciences, National Research Council (1958).

16. ICE DETERIORATION (by J.E. Dykins, NCEL)

16.1 Introduction

Deterioration of an ice sheet occurs internally as well as at the surface. What might be interpreted as internal deterioration of a property often may be only a temporary shift during permutation of the ice to a more stable material. Consequently experience coupled with careful observation and precise interpretation of data are needed to determine the internal deterioration of an ice mass. In this section, decline of the relative tensile strength within the ice was used as a measure of internal deterioration and ablation, and surface erosion was used as a measure of surface deterioration.

16.2 Methods Used

Relative tensile strengths for the ice were obtained from small specimens cored from the ice. The technique used to obtain these specimens and the method of test are described in Section 4 of this report.

Surface deterioration was determined by visual observation and limited measurement of surface erosion. During the period most conducive to deterioration (April and May), observation was maintained on all test areas as well as on the natural ice. Actual measurement of surface erosion, however, was only conducted in Parking Apron No. 1. In mid-April the deflection stakes set in this apron at the beginning of construction were scribed at the ice surface, and the surface recedence at each stake was observed periodically until mid-May.

16.3 Discussion of Findings

From the standpoint of strength, internal deterioration began in early April and was still in progress at the end of the test season in late May. The beginning of this deterioration is well defined on the trend graphs (Section 9) which show curves of physical properties for the full thickness of each ice type (Figures 9.3, 9.7, 9.11, and 9.15). A profile of the air temperature (Figure 9.1) indicates that at about the same time the strength began to decline there was a sharp rise in ambient temperature.

In general there was little erosion of the ice surface during the observation period. This was attributed in part to new snowfall during this period. Occasionally, however, high winds blew the snow cover off or contaminated it with sand and dirt from the surrounding land mass. The most erosion occurred in those areas contaminated with the highest concentration of dirt and sand. On Apron No. 1, where actual recedence of the ice surface was measured, it was found that the total loss was less than one inch between 15 April and 13 May.

APPENDIX A — Project Organization
(by D.W. Klick)

1. The Terrestrial Sciences Laboratory (TSL) was responsible for overall implementation of all phases of the project to include aircraft test operations and logistical matters.

2. The Naval Civil Engineering Laboratory (NCEL), as joint participant, was responsible for construction of the parking pads, erection of the load tanks, and certain portions of the research program. They closely coordinated their plans and field operations with TSL to insure attainment of mutual project objectives.

3. Captain Donald W. Klick (TSL) was the Project Officer and had the responsibility for insuring complete implementation and coordination of all phases of the project. He had direct responsibility for the aircraft test operations, for photo documentation, and for public information functions.

4. Mr. Robert H. Hinchcliffe (TSL) was responsible to the Project Officer for all matters relating to logistics to include movement of project material between point of origin and Thule AB, housing and messing of project personnel, and direct material and personnel support from Thule AB and other military units. He was also the Assistant Project Officer.

5. Dr. W. D. Kingery (Arctic Institute of North America [AINA]), as the Principal Investigator for the project, was responsible for all scientific aspects of the program and for the conduct of all research activities. He was also responsible for the subsequent documentation of project accomplishments. In addition he was the Group Leader in charge of the static loading tests.

6. Mr. David M. French (AINA), as Field Leader, was directly responsible to Dr. Kingery for implementation of the research program and assumed Dr. Kingery's role in the field during his absence. He was also Group Leader in charge of simultaneous studies of properties of ice.

7. Mr. Justin E. Dykins (NCEL), as senior member of the NCEL field group, was responsible for overall implementation of NCEL plans and programs. He also had ultimate charge of construction for the project and acted as advisor in those matters to the Project Officer.

8. Mr. Clark R. Hoffman (NCEL), as Field Leader, was in direct charge of the construction tasks in the field. He was directly responsible to Mr. Dykins and assumed his position in the field during Mr. Dykins' absence. He was also Group Leader in charge of tests of constructed ice.

9. Mr. Don L. Anderson (AINA) was the Group Leader in charge of the dynamic loading tests.

10. Mr. James H. Brown (Naval Electronic Laboratory) was the Group Leader in charge of seismic and in-place tongue and beam tests of the natural ice.

11. Dr. M. P. Langleben (McGill University) was the Group Leader in charge of the airdrop seismic tests.

12. Lieutenant Colonel Bernard A. Zohn (Base Civil Engineer of Thule AB) had been designated Project Officer for Thule AB and was responsible for providing support requested of Thule AB organizations.

13. See attached chart.

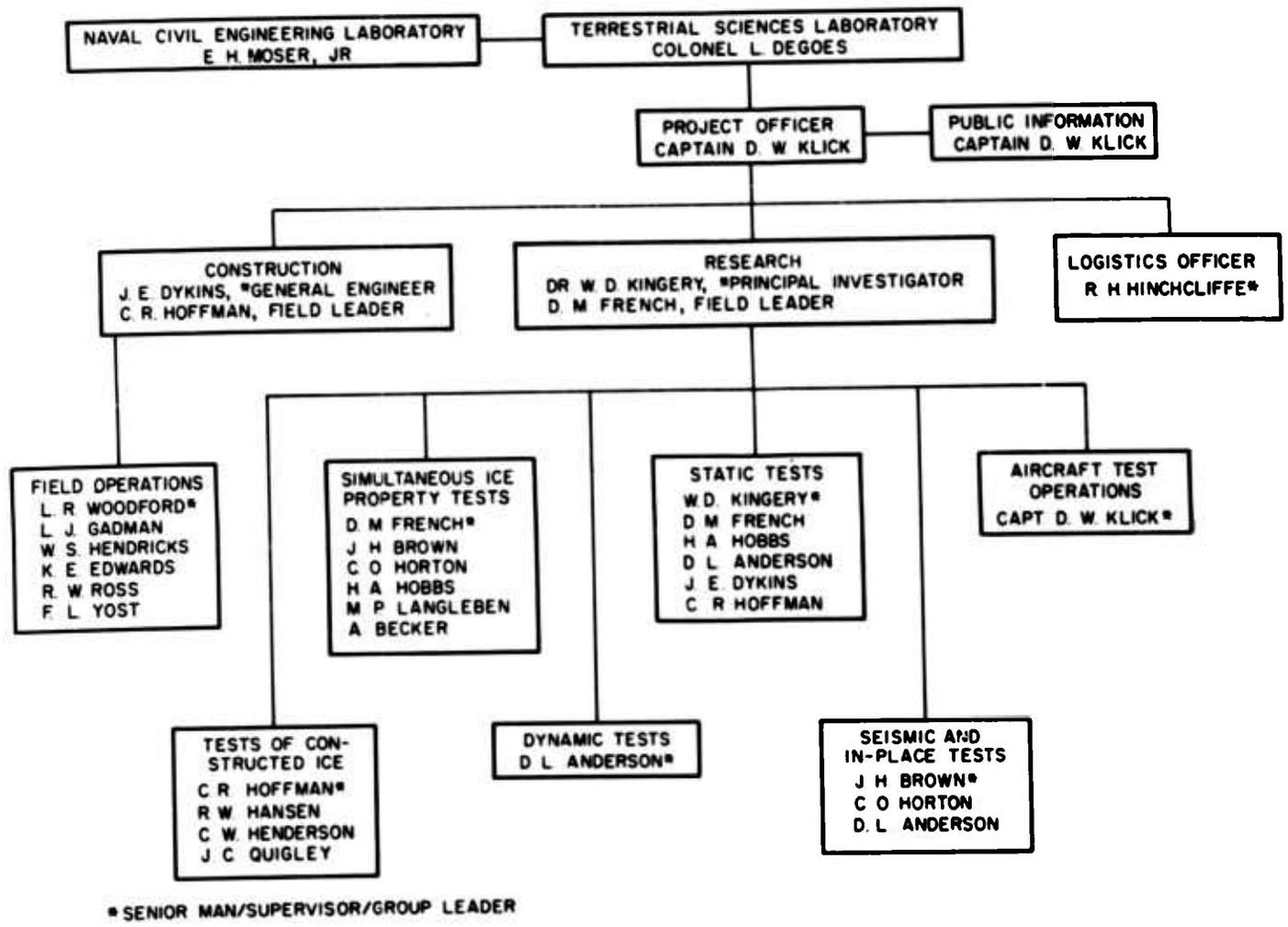

FIG. A.1 Chart showing project organization

APPENDIX B – List of Participants

Arctic Institute of North America (Contract Nos. AF19(604)-3073 and -7403):

Anderson, D. L. (-7403)
French, D. M. (-3073)
Hobbs, H. A., Jr. (-3073)
Kingery, W. D. (-3073)

Geophysics Research Directorate Photo Laboratory (AFCRL):

Hudson, R. A., Airman First Class, USAF
Marchesini, B., Master Sergeant, USAF

McGill University, Montreal, Canada (Contract No. AF19(604)-8378):

Becker, A.
Langleben, M. P.

Naval Civil Engineering Laboratory:

Dykins, J. E.
Edwards, K. E.
Gadman, L. J.
Hansen, R. W.
Hoffman, C. R.
Henderson, C. W.
Hendricks, W. S.
Quigley, J. C.
Ross, R. W.
Woodford, I. R.
Yost, F. L.

Navy Electronics Laboratory:

Brown, J. H.
Horton, C. O.

Terrestrial Sciences Laboratory (AFCRL):

Brady, M. T., Airman First Class, USAF
Hinchcliffe, R. R.
Klick, D. W., Captain, USAF

Aircraft Crews:

C-130 (#55024), 3245th Operations Group
Hanscom Field, Massachusetts

Capt G. M. Khoury (AC)
Capt G. E. Apple (P)
1/Lt R. E. McDevitt (CP)
1/Lt R. M. Naddeo (N)
2/Lt J. P. Rioux, Jr. (N)
SSgt B. G. Taylor (C/M)
A/1c E. E. White (C/M)
A/2c G. A. Boisvert (C/M)
A/2c R. L. Mahaffey (C/M)

B-47 (#532280), Flight and Engineering Test Group, Wright Air Development Division, Wright-Patterson AFB, Ohio

Capt J. A. Guthrie (AC)
Major S. J. Anthony (CP)
Major N. W. McCulley (N)
SSgt W. F. Handshy (C/M)
SSgt E. L. Suggs (C/M)

Aircraft Crews:

KC-135 (#553119A), Rome Air Development Center, Griffiss AFB, New York

Major H. L. Patrick (AC)
Capt J. H. Mykicz (CP)
Capt W. J. Ubinger (N)
2/Lt S. E. Danzer (N)
MSgt C. C. Dodge (C/M)
SSgt D. J. Bradley (C/M)

F-102, 332nd Fighter Interceptor Squadron, Thule AB, Greenland

L/Col W. R. Yarbrough (P)

B-52 (#520013), 4925th Test Group (A), AF Special Weapons Center, Kirtland AFB, New Mexico

Major R. G. Brinck (AC)
L/Col C. A. Pinney (P)
Major O. L. Clark (CP)
Capt R. M. Clausen (N)
Capt T. J. Gamm (N)
Capt L. G. Russ (N)
SSgt J. A. Fourneik (C/M)
A/1c L. F. Pieck (C/M)
A/1c E. L. Reid (C/M)
A/1c L. Richwine (C/M)

Legend:		
	AC	Aircraft Commander
	P	Pilot
	CP	Copilot
	N	Navigator
	C/M	Crewman

APPENDIX C – Pilot Reaction
(by D. W. Klick)

Excerpts from a letter from Captain James A. Pate who piloted the C-47:

> "The ice was extremely smooth, conditions were excellent, and braking action was good. From a pilot's standpoint, there was absolutely no problem and the ice runway had a better surface than the regular Thule runway."

Excerpts from a letter from Major R. G. Brinck who piloted the B-52:

> "The runway was smoother than the Thule runway and this was probably so because the asphalt runway was full of ice patches. Also, the turning of the aircraft was much easier on the ice runway than on the asphalt runway and we made tight turns on both. Making the sharp turns on the asphalt runway was very rough and we felt the aircraft skid and slide like we were on a washboard road. This again was probably due to the ice patches.
>
> "I feel we made smooth touchdowns on the ice runway and I was very surprised at the excellent braking action and generally good handling of the aircraft while maneuvering on the runway and parking pads. This again felt much better than the effect we received on the main Thule runway; for want of a better explanation, it felt as though we were in an automobile with slick tires on glare ice at Thule. In other words, it felt as though the aircraft were always going to slide sideways and the rear end break loose while taxiing and maneuvering on the main runway. And, as you recall, we were equipped with snow-and-ice tires.
>
> "I believe the runway markings were satisfactory, although the stripes were difficult to see when viewed from the side of the runway. They were very sharp only when viewed in line or from directly above. Also, the use of trucks or similar equipment on the approach end of the runway, as you provided, is a must to aid in depth perception."

Letters from LtCol Yarbrough (F-102), Major Patrick (KC-135), Capt Khoury (C-130) and Major Anthony and Capt Guthrie (B-47) follow.

"F102 Pilots Opinion – Project Ice Way"

1. The runway had been prepared and ready for use. On inspection it was found that the layer of the usual loose ice-crystal covering had been blown free of the runway. This presented a covering of solid ice, therefore, I requested the blower to replace the finely granulated ice crystals on the runway. This was accomplished.

2. From a maintenance standpoint it was not desirable to use the drag chute to touch down except in an actual emergency. With the maximum gross weight at touch down, weather conditions and with moderate braking action the Pilots Handbook stated the landing roll as 8400 ft. The final approach and touch down speeds were flown as prescribed in the handbook. Actual touch down was 300 ft from the marked approach end of the runway. Normal pilot technique on landing roll and braking action was accomplished. The aircraft was brought to a complete stop at approximately 8700 ft. Takeoff with afterburner was accomplished in accordance with the Handbook. In all cases the figures quoted were accurate. For these reasons I believe the figures in the Pilots Handbook to be accurate and adequate.

3. The smoothness of the runway was entirely satisfactory for the repeated use by high performance aircraft without endangering the aircraft or inducing materiel failure.

4. Aircraft operations were entirely normal and no difficulty was experienced at anytime.

5. Recommendations:

a. Wider marking be used on the approach end of the runway and along each shoulder. The centerline stripe was adequate.

b. The runway distance markers were all the same color which made it confusing and hard to keep in mind the actual distance remaining. I suggest something on this order, at each 100 ft interval, red, orange, yellow, green, black, green, yellow, orange, and red. These colors would be for a 10,000 ft runway.

c. The extension of the runway centerline at the approach end of the runway needs to be improved to assist the pilot in correct approach alignment due to the sameness of the terrain. I suggest a modified "V" with barrels painted a color to give maximum contrast.

6. The addition of a portable TACAN station and approach-lighting system. I believe that the ice runway will provide the Air Force with an all-weather operation capability for arctic remote areas.

/s/ Walter R. Yarbrough

WALTER R. YARBROUGH
Lt Col, USAF
Commander
332nd Fighter Interceptor Squadron

SUPPLEMENTAL PILOT'S REPORT ON PROJECT ARCTIC TERRAIN

31 May 61

1. All landings on the ice runway were conducted using standard aircraft operating procedures as outlined in the Dash One (-1 Handbook). The runway was very smooth and the braking action on all landings was considered fair to good. There was no skidding or sliding upon landing. The first takeoff followed standard operating procedures and was normal from the pilot's point of view but I (the pilot) was informed by the project people that the procedure of running the aircraft engines up to 100 percent power before brake release caused considerable vibration for the whole length of the runway. This situation was not noticed in the cockpit. All other takeoffs were made using the running takeoff techniques as outlined in the KC-135 Dash One. These takeoffs were all normal, acceleration was good, and no undue vibration was noticed. The runway markings on the strip were considered very good and were visible from at least five miles away.

2. In my opinion, landing on ice such as this strip would be a good way to recover aircraft in case of emergencies in the locality of the Arctic. I also believe that, with the normal wind which blows on the ice and leaving a very smooth crust of snow, an aircraft could land; and, if fuel was ferried in, the aircraft could be refueled and a takeoff made without any prior preparation as far as the runway is concerned.

3. Recommend that if these ice strips are intended for this use and aircraft do land in emergency conditions and are intended to be flown off the ice again, that their fuel load be kept to a bare minimum which would give them a takeoff roll of not over 2800 to 3000 feet. The landing rolls during this test were approximately 5000 feet, but they could have been reduced to around 3000 feet by applying full brakes, and I feel confident that there would have been no skidding or sliding of the aircraft.

/s/ Harold L. Patrick

HAROLD L. PATRICK
Major, USAF
Acft Commander, KC-135

HEADQUARTERS
3245TH OPERATIONS GROUP
3245TH AIR BASE WING
UNITED STATES AIR FORCE
LAURENCE G. HANSCOM FIELD, BEDFORD, MASSACHUSETTS

REPLY TO
ATTN OF: CWOOM 30 March 1961

SUBJECT: Ice Landings (Project Ice Way)

TO: Arctic Terrain Research
(Ice Way Project Officer)
Terrestrial Sciences Laboratory

1. The condition of the ice runway located at North Star Bay, Thule, Greenland is considered entirely satisfactory by the undersigned who participated in the C-130 test phase during 24 and 25 March 1961. The panels marking the approach ends of the runway as well as the cones denoting each 1000 feet of runway were easily visible from the air. The centerline and borders of the runway, which were marked with yellow dye, were easily recognizable from the air even though blowing snow had covered a portion of the dye marker.

2. Because of the prop reversing capability of the C-130, brakes were not applied at high speeds during the landing roll. However, at speeds of 30 knots and below, brakes were applied and the braking action was considered good.

/s/ George M. Khoury

GEORGE M. KHOURY, Captain, USAF
Aircraft Commander
Multi-Engine Branch

P. O. Box 2452, Area C,
Wright-Patterson AFB, O.

5 April 1961

Dear Don:

Following are our comments on operating and landing the B-47 on the ice runway at Thule in March 1961.

The runway was well marked and all the markers were easily discernible. The panels at the end of the runway on each side were especially helpful in marking the end of the runway. The little markers on the side of the runway marking each thousand feet were not much assistance as too much mental arithmetic was involved figuring just how far down the runway you were. The fire truck at the mid-point and the ambulance at the quarter point of the runway were much more helpful in determining position on the runway than the small thousand foot markers.

The chevrons marking the overrun were visible straight down over the runway, but were not easily seen coming in on final approach at a short angle. In this regard, the oil barrels helped in lining up and marking the unusable portion of the ice.

Both pilots felt that the oil barrels, plus the large panels and the vehicles, were a great aid to depth perception during flare-out and landing.

The runway surface itself was rather rough as compared to a concrete runway. However, overall, it was not bad and on two of the landings where the brake chute was used, and little braking was required, no undue roughness was noted. On the one landing where the brake chute was not used, the braking required to stop the aircraft actuated the anti-skid and caused the aircraft to lurch and porpoise. This produced a very rough ride until the speed diminished.

As far as the surface condition was concerned, both pilots felt it was not as slippery as the main runway at Thule and no problem was encountered stopping or steering the aircraft.

Sincerely,

/s/ Joseph A. Guthrie, Jr.
Joseph A. Guthrie, Jr.
Captain, USAF

/s/ Sheldon J. Anthony, Jr.
Shelton J. Anthony, Jr.
Major, USAF

APPENDIX D — Summary of Data on Temperature, Salinity, Density, and Ring Tensile Strength for Natural and Constructed Ice (by J.E. Dykins)

Field data for temperature, salinity, density, and strength for each parking apron and the undisturbed natural ice discussed in Section 9 are summarized in this appendix. The basic data were averaged into 1-ft stratum for each test area and then reduced to a mean monthly value. These values are shown graphically by depth for each test area in Figures D-1 through D-12. The number of specimens used to determine the monthly average for each stratum is shown in parentheses. For the relative tensile strength values, the mean test temperature is also shown. Included on the face of these graphs are the monthly means for the total ice-type thickness.

Single sampling values for strength and temperature by depth are shown at approximately bi-weekly intervals on Figures D-1, D-3, D-4, D-6, D-7, D-9, D-10, and D-12. The sampling dates for this data are given on the curves.

The tables on Figures D-1 through D-12 give the maximum and minimum values of the data for each stratum by month.

To examine the relation of the change in density with the change in salinity, a check was made using Assur's table, "Phase Relations for Standard Sea-Ice".* This comparison of calculated versus measured density was made for the top stratum of constructed ice of Parking Apron No. 1 (Figure D-5). For the April-May period, the theoretical weight of the brine lost through migration was calculated by using the difference in the measured salinity values for the two months (7.1 ppt) and the average temperature for May (-7.8°C). The theoretical brine weight was converted to density (0.46 g/cc), then added to the measured density for May (0.853 g/cc) giving 0.899 g/cc as the calculated April density. Comparing this value with the measured April density of 0.903 g/cc, it can be seen that they agree within about 0.5 percent.

*National Academy of Sciences – National Research Council. Publication 598, Arctic Sea-Ice, "Composition of Sea-Ice and Its Tensile Strength," by A. Assur, 1958, pp 106-138.

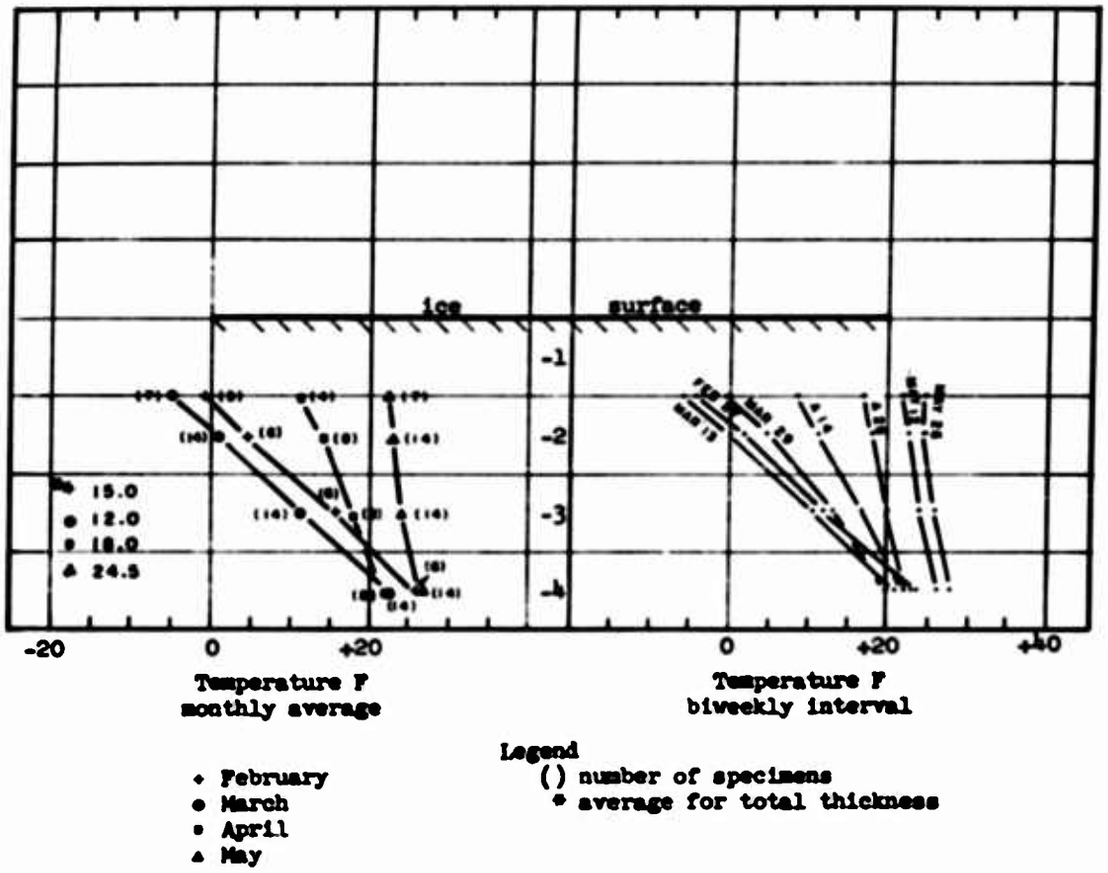

Range of Data by Stratum									
Month	Range	+4	+3	+2	+1	-1	-2	-3	-4
Feb	max					1.0	11.0	22.0	30.5
	min					-4.0	-4.0	7.0	17.0
Mar	max					-0.5	9.0	18.0	29.5
	min					-7.0	-7.0	4.0	16.5
Apr	max					17.0	19.0	21.0	25.5
	min					7.0	7.0	13.0	17.0
May	max					24.5	25.0	27.0	29.0
	min					21.0	21.0	22.0	24.0

FIG. D. 1 In situ temperature by 1-ft stratum for the undisturbed natural ice

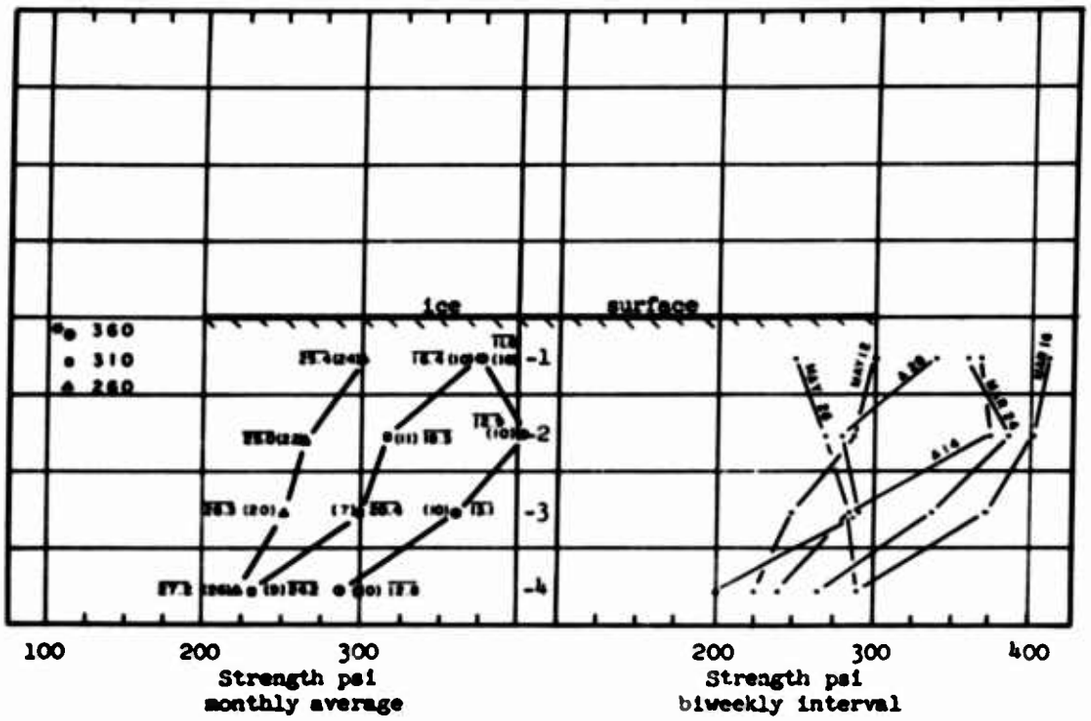

Legend

- March
- April
- May

() number of specimens
average for total thickness
- average temperature of specimens F

Range of Data by Stratum									
Month	Range	+4	+3	+2	+1	-1	-2	-3	-4
Mar	max					525	525	424	373
	min					237	309	296	195
Apr	max					453	457	378	343
	min					300	258	224	123
May	max					394	326	313	356
	min					228	186	178	93

FIG. D. 3 Relative tensile strength by 1-ft stratum for the undisturbed natural ice

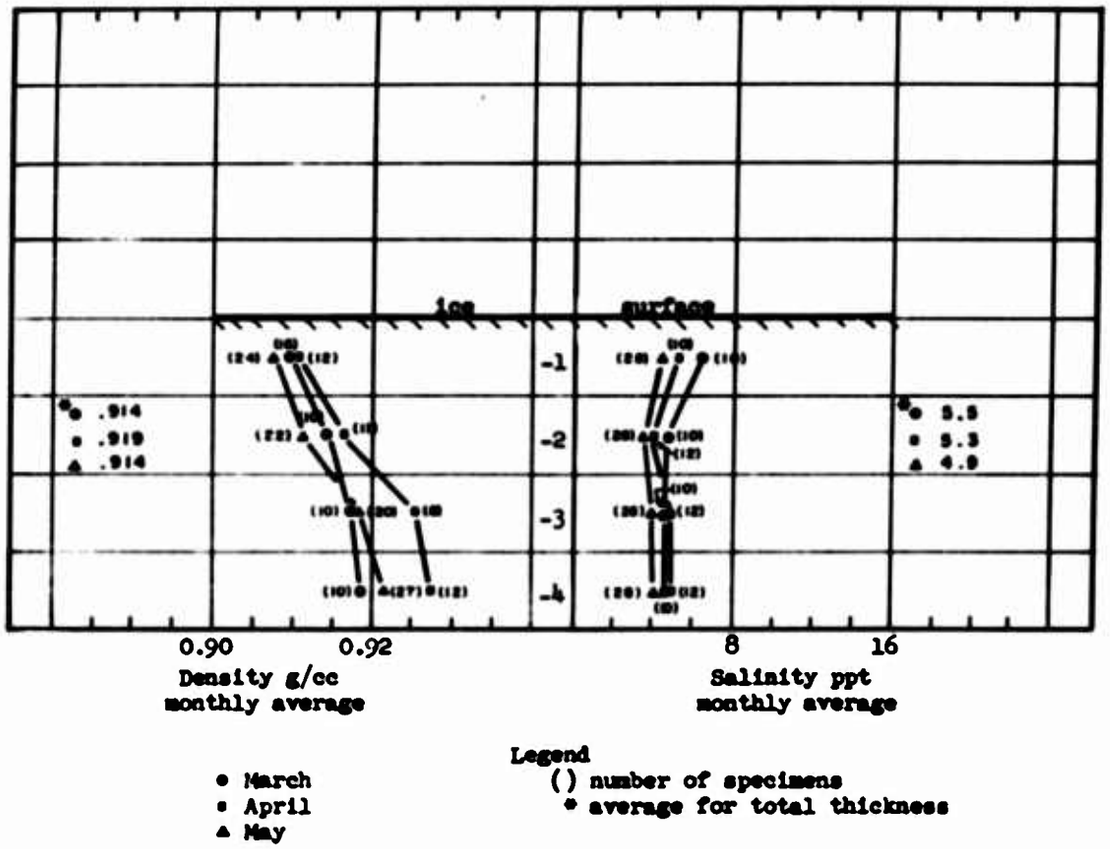

		Range of Data by Stratum							
	Month	Range	+4	+3	+2	+1	-1	-2	-3	-4
Density	Mar	max					.922	.921	.920	.926
		min					.900	.909	.914	.912
	Apr	max					.918	.926	.936	.936
		min					.893	.901	.906	.913
	May	max					.925	.924	.931	.928
		min					.885	.895	.893	.893
Salinity	Mar	max					8.6	7.3	6.0	6.2
		min					4.7	3.9	4.7	4.6
	Apr	max					8.3	6.3	6.8	6.4
		min					3.6	4.5	4.3	5.0
	May	max					7.8	5.6	6.4	7.1
		min					3.2	3.8	3.8	3.9

FIG. D. 2 Salinity and density by 1-ft stratum for the undisturbed natural ice

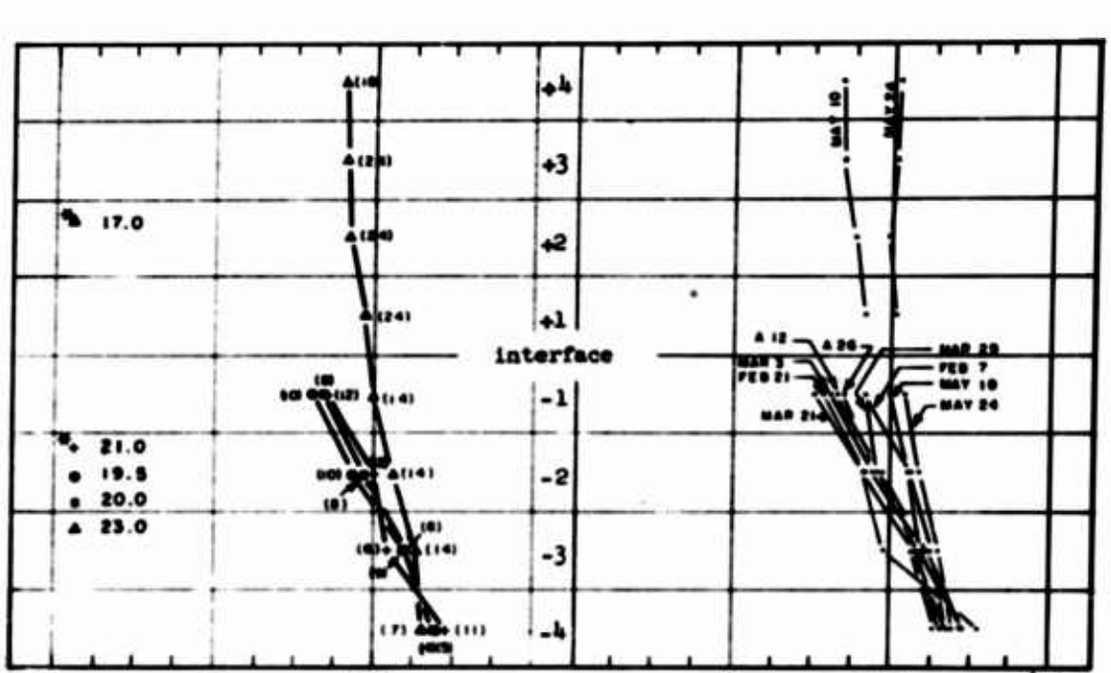

Legend

- February
- March
- April
- May

() number of specimens

* average for total thickness

Month	Range	Range of Data by Stratum +4	+3	+2	+1	-1	-2	-3	-4
Feb	max					21.5	24.0	24.0	31.0
	min					-5.0	14.0	19.0	28.8
Mar	max					19.0	24.0	29.0	29.0
	min					7.0	13.0	19.5	26.5
Apr	max					15.5	21.5	27.0	27.0
	min					11.0	15.5	20.5	25.5
May	max	20.5	20.5	20.5	20.5	22.5	24.5	27.5	27.5
	min	10.5	11.5	14.0	15.0	15.0	18.0	21.5	25.5

FIG. D. 4 In situ temperature by 1-ft stratum for the total ice thickness in the free-flooded parking apron (Parking Apron No. 1)

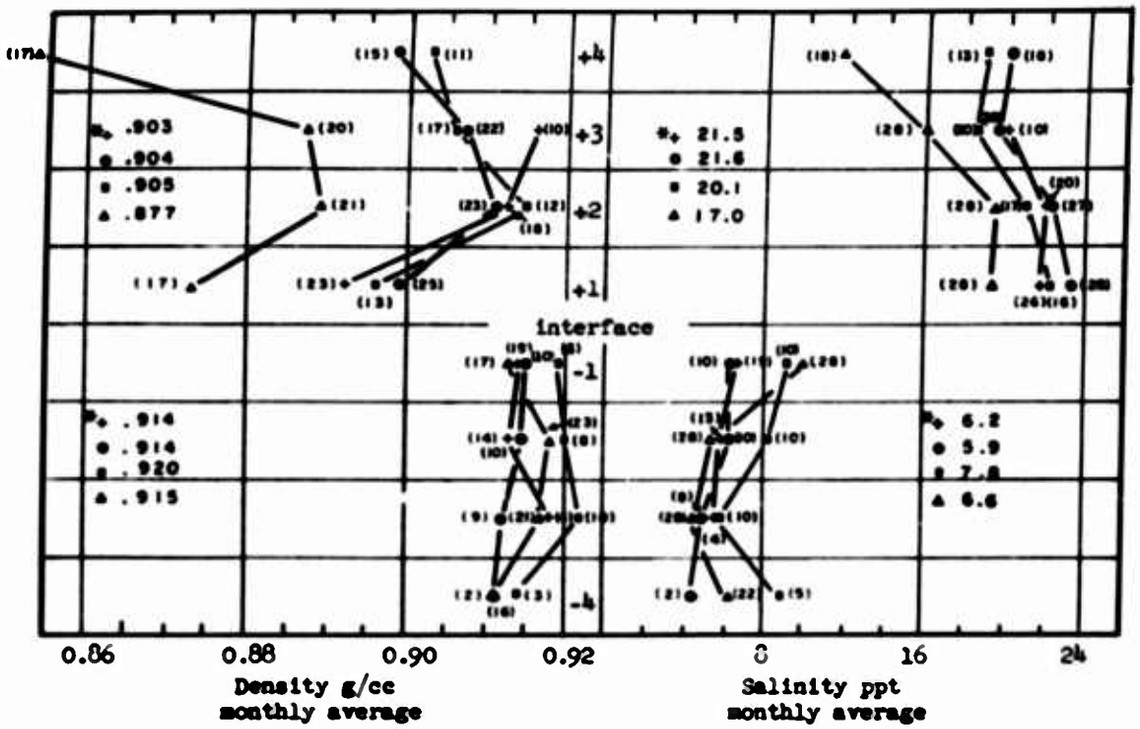

Legend

- ◆ February
- ● March
- ▪ April
- ▲ May

() number of specimens

* average for total thickness

		Range of Data by Stratum							
	Month	Range	+4	+3	+2	+1	-1	-2	-3	-4
Density	Feb	max		.925	.923	.929	.929	.922	.916	
		min		.910	.826	.857	.890	.903	.913	
	Mar	max	.921	.925	.928	.923	.921	.924	.918	.917
		min	.870	.881	.874	.877	.906	.907	.907	.905
	Apr	max	.915	.922	.924	.915	.928	.931	.936	.922
		min	.882	.875	.905	.857	.905	.901	.914	.907
	May	max	.911	.914	.920	.910	.927	.926	.929	.920
		min	.801	.806	.832	.833	.812	.903	.903	.889
Salinity	Feb	max		23.2	26.4	26.4	16.9	7.7	6.2	
		min		17.6	15.8	15.5	4.2	4.6	5.1	
	Mar	max	28.0	24.6	27.8	29.6	8.5	8.5	6.5	4.6
		min	12.3	9.2	17.8	8.9	3.5	5.0	4.4	4.6
	Apr	max	21.8	21.8	26.3	28.3	17.5	10.8	6.4	16.0
		min	15.3	14.3	18.1	13.9	6.0	5.0	4.6	5.6
	May	max	15.8	20.8	23.0	27.7	21.6	8.1	5.9	13.7
		min	6.8	6.9	13.8	8.7	4.7	3.7	2.9	4.0

FIG. D. 5 Salinity and density by 1-ft stratum for the total ice thickness in the free-flooded parking apron (Parking Apron No. 1)

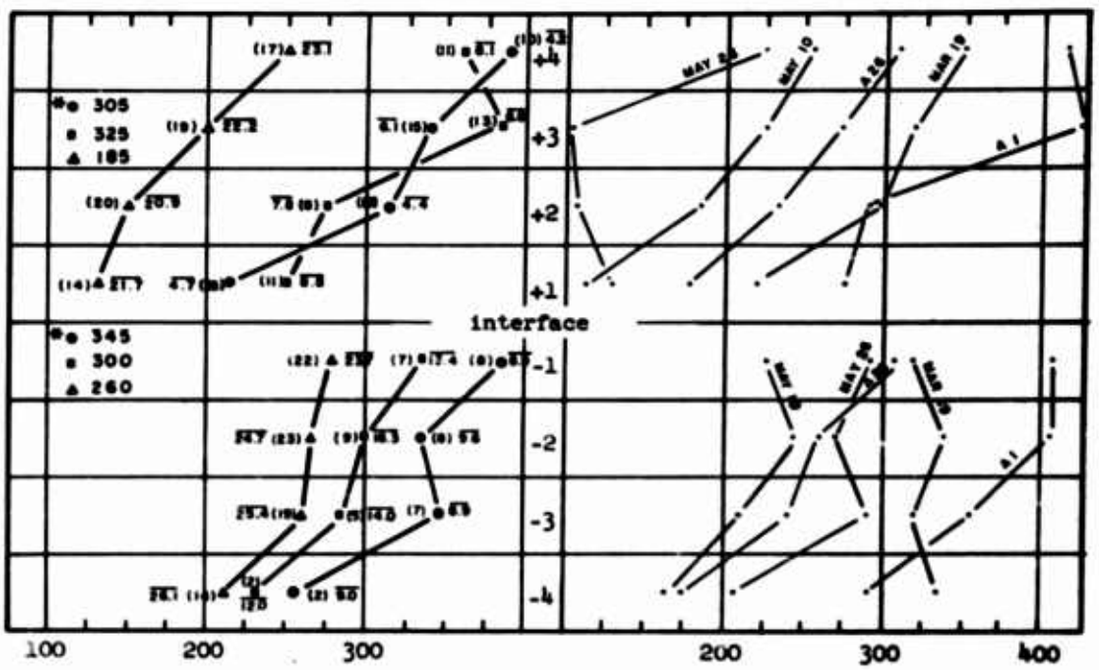

Legend

- ● March
- • April
- ▲ May

() number of specimens
* average for total thickness
- average temperature of specimens F

Range of Data by Stratum									
Month	Range	+4	+3	+2	+1	-1	-2	-3	-4
Mar	max	472	426	424	322	457	441	390	270
	min	339	254	101	135	278	228	296	237
Apr	max	424	472	339	356	441	449	373	288
	min	288	228	216	113	224	224	220	174
May	max	339	288	220	169	378	462	318	288
	min	190	105	88	93	93	190	186	148

FIG. D. 6 Relative tensile strength by 1-ft stratum for the total ice thickness in the free-flooded parking apron (Parking Apron No. 1)

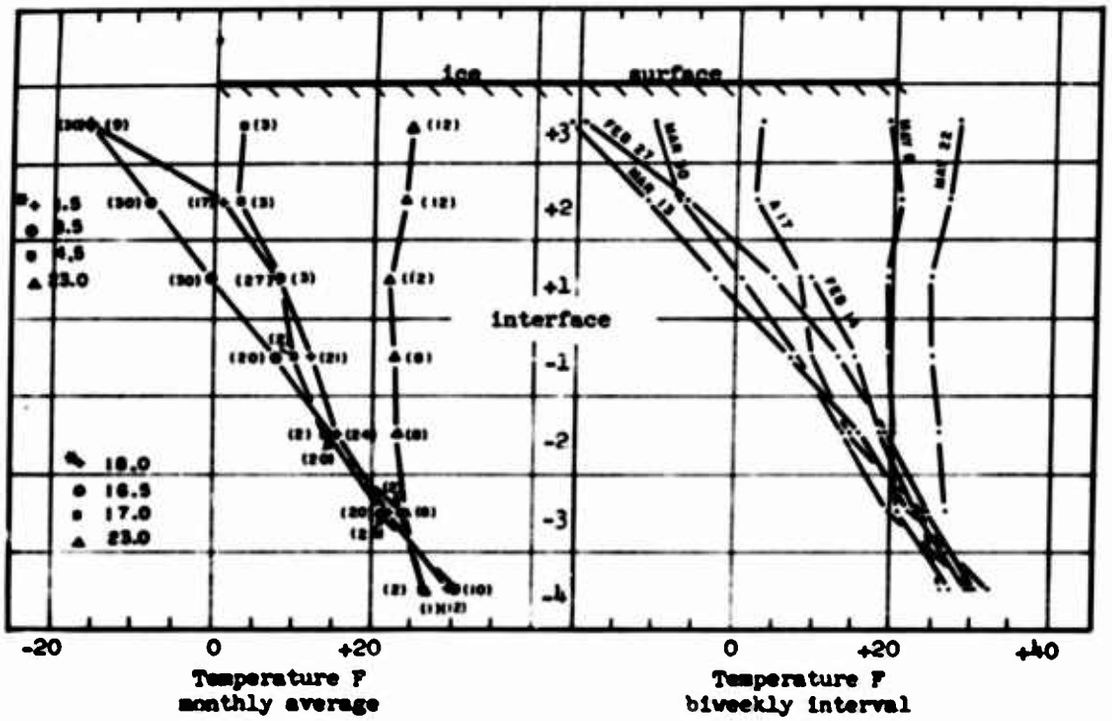

Legend
() number of specimens
* average for total thickness

* February
● March
• April
▲ May

Range of Data by Stratum									
Month	Range	+4	+3	+2	+1	-1	-2	-3	-4
Feb	max			14.0	14.0	18.0	22.0	28.8	30.5
	min			-14.0	-7.5	-3.0	-3.0	11.0	28.0
Mar	max			-1.0	8.0	16.0	21.0	26.5	32.0
	min			-18.0	-9.5	1.0	8.0	14.0	27.0
Apr	max			4.5	11.0	11.0	20.0	26.0	26.0
	min			0.0	4.5	8.5	8.5	20.0	26.0
May	max			30.5	25.0	26.0	26.5	26.5	26.5
	min			18.0	17.5	18.5	19.5	19.5	25.3

FIG. D. 7 In situ temperature by 1-ft stratum for the total ice thickness in the reinforced, free-flooded parking apron (Parking Apron No. 2)

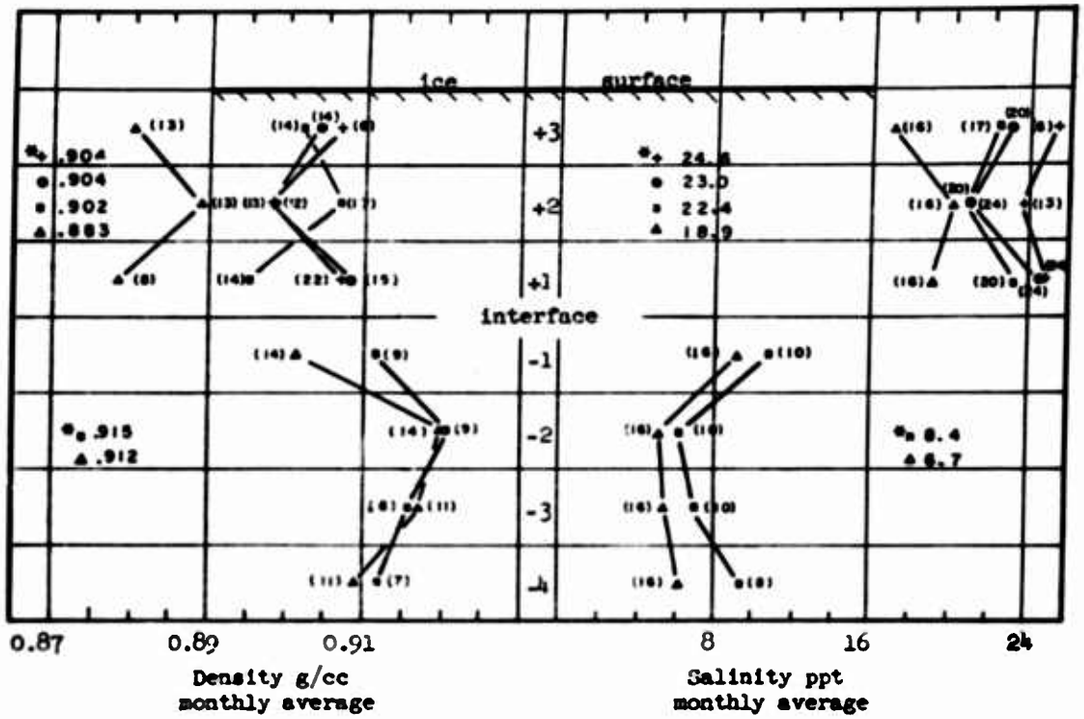

Legend

- February
- March
- April
- May

() number of specimens

* average for total thickness

		Range of Data by Stratum							
	Month	Range	+4	+3	+2	+1	-1	-2	-3	-4
Density	Feb	max		.916	.914	.936				
		min		.893	.886	.880				
	Mar	max		.919	.918	.924				
		min		.886	.880	.889				
	Apr	max		.924	.924	.914	.921	.925	.925	.922
		min		.867	.874	.867	.896	.915	.886	.886
	May	max		.913	.920	.909	.932	.925	.924	.921
		min		.821	.864	.820	.857	.912	.907	.875
Salinity	Feb	max		27.3	26.8	29.2				
		min		23.1	20.2	19.1				
	Mar	max		29.5	31.3	32.9				
		min		18.7	14.0	18.0				
	Apr	max		26.1	25.0	27.8	23.6	8.3	13.9	14.3
		min		18.4	15.2	17.8	4.7	3.9	4.4	4.3
	May	max		20.4	25.1	24.7	19.9	6.3	10.2	13.9
		min		11.7	15.0	10.8	5.0	4.4	4.2	4.3

FIG. D. 8 Salinity and density by 1-ft stratum for the total ice thickness in the reinforced, free-flooded parking apron (Parking Apron No. 2)

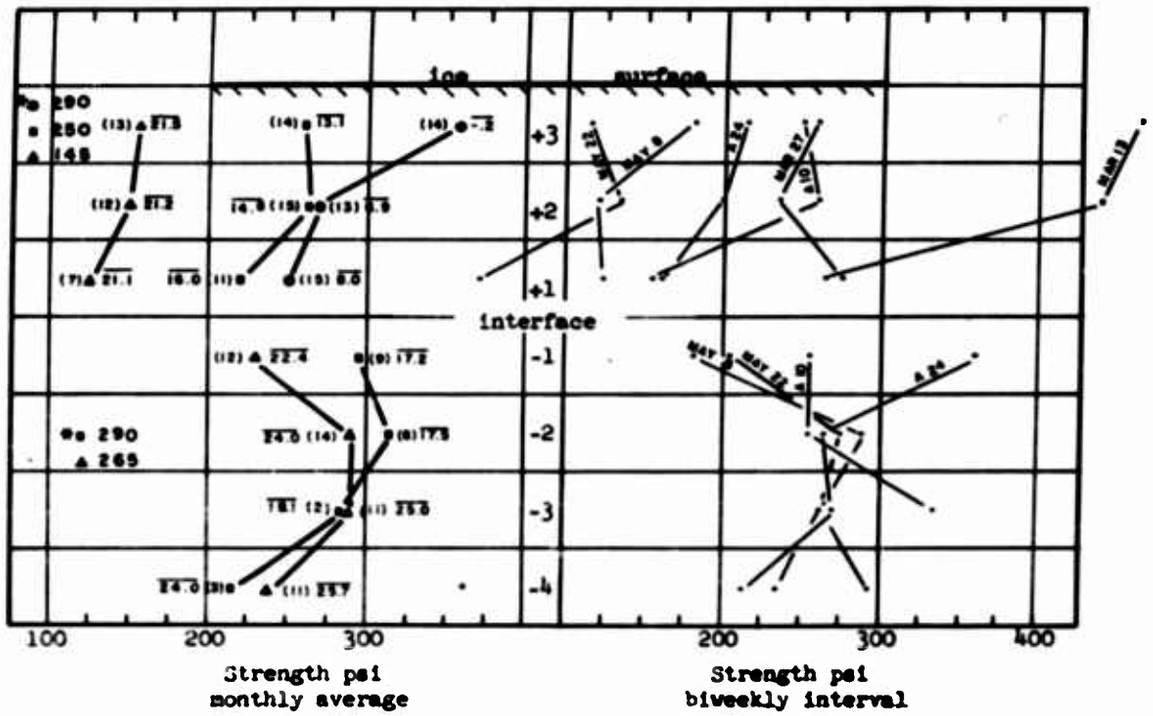

Legend

- March
- April
- May

( ) number of specimens
* average for total thickness
- average temperature of specimens F

Range of Data by Stratum									
Month	Range	+4	+3	+2	+1	-1	-2	-3	-4
Mar	max		517	457	390				
	min		186	117	84				
Apr	max		326	390	348	468	491	318	436
	min		211	152	105	216	220	232	117
May	max		224	250	211	330	426	432	364
	min		101	46	46	88	224	220	93

FIG. D. 9 Relative tensile strength by 1-ft stratum for the total ice thickness in the reinforced, free-flooded parking apron (Parking Apron No. 2)

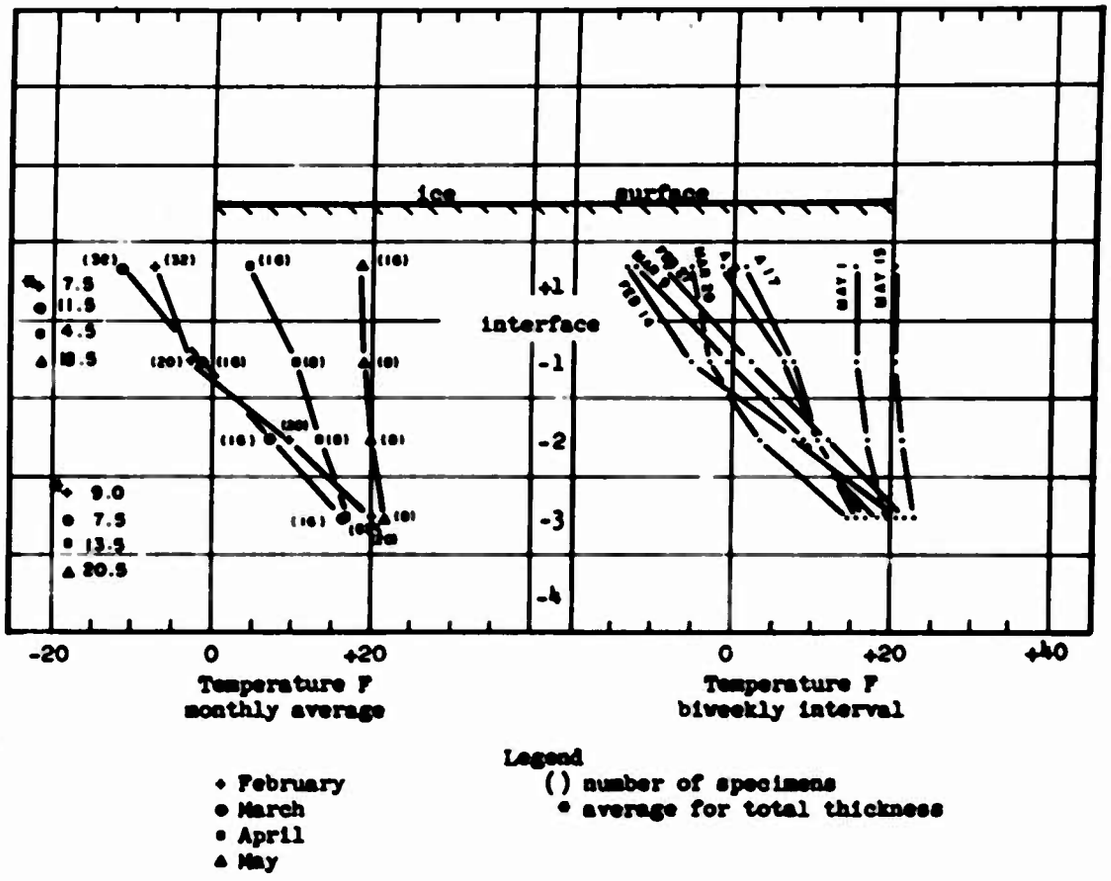

Month	Range	Range of Data by Stratum +4	+3	+2	+1	-1	-2	-3	-4
Feb	max					8.5	9.0	17.5	27.0
	min					-28.5	-16.0	-1.5	10.0
Mar	max					-1.5	4.5	14.0	24.5
	min					-25.0	-8.0	-4.0	10.0
Apr	max					15.0	17.0	19.5	23.0
	min					-8.0	4.5	9.0	13.0
May	max					25.0	25.0	25.5	27.5
	min					12.5	15.0	16.0	17.5

FIG. D. 10 In situ temperature by 1-ft stratum for the total ice thickness in the reinforced, ice-aggregate, parking apron (Parking Apron No. 3)

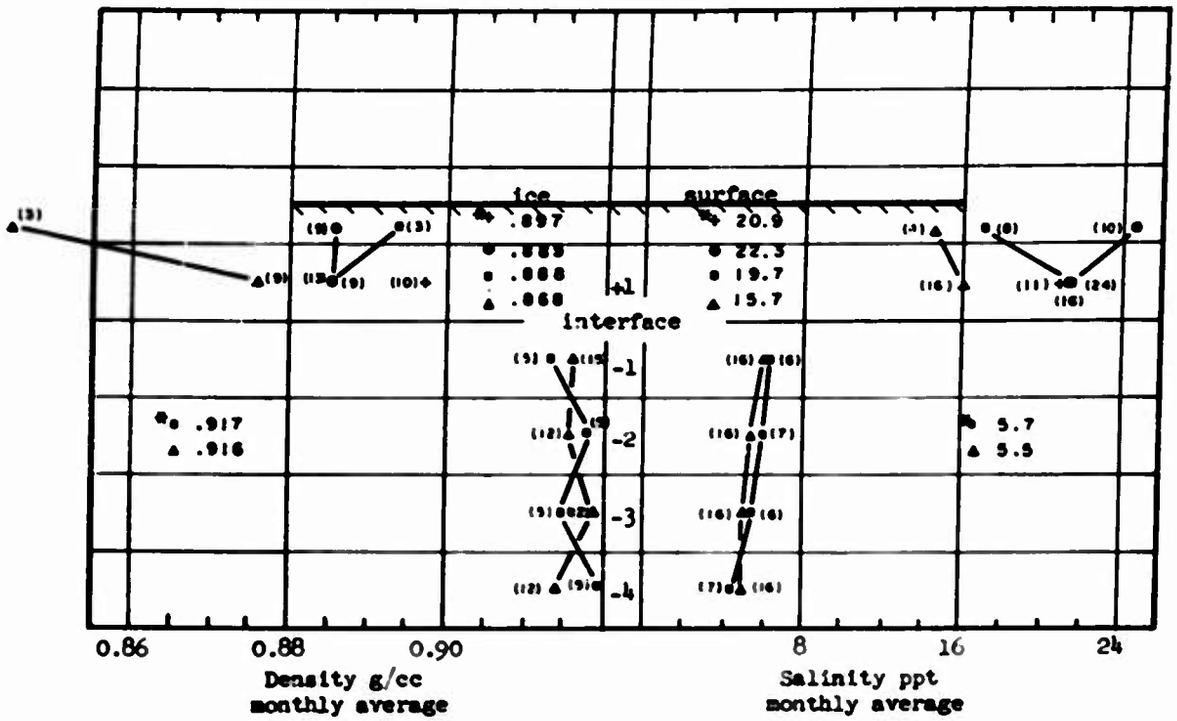

Legend

- ♦ February
- ● March
- ▪ April
- ▲ May

() number of specimens

* average for total thickness

		Range of Data by Stratum							
	Month	Range	+4	+3	+2	+1	-1	-2	-3	-4
Density	Feb	max				.920				
		min				.850				
	Mar	max			.925	.909				
		min			.860	.849				
	Apr	max			.907	.919	.923	.920	.918	.926
		min			.865	.862	.903	.911	.913	.916
	May	max			.863	.896	.925	.925	.928	.927
		min			.813	.837	.904	.901	.899	.906
Salinity	Feb	max				28.7				
		min				10.9				
	Mar	max			29.2	37.5				
		min			14.9	10.7				
	Apr	max			25.0	30.0	8.2	6.7	6.7	5.8
		min			11.1	10.6	4.8	5.4	5.1	4.0
	May	max			19.0	23.5	8.3	6.6	6.4	6.7
		min			10.7	9.0	4.7	4.4	3.8	4.2

FIG. D. 11 Salinity and density by 1-ft stratum for the total ice thickness in the reinforced, ice-aggregate parking apron (Parking Apron No. 3)

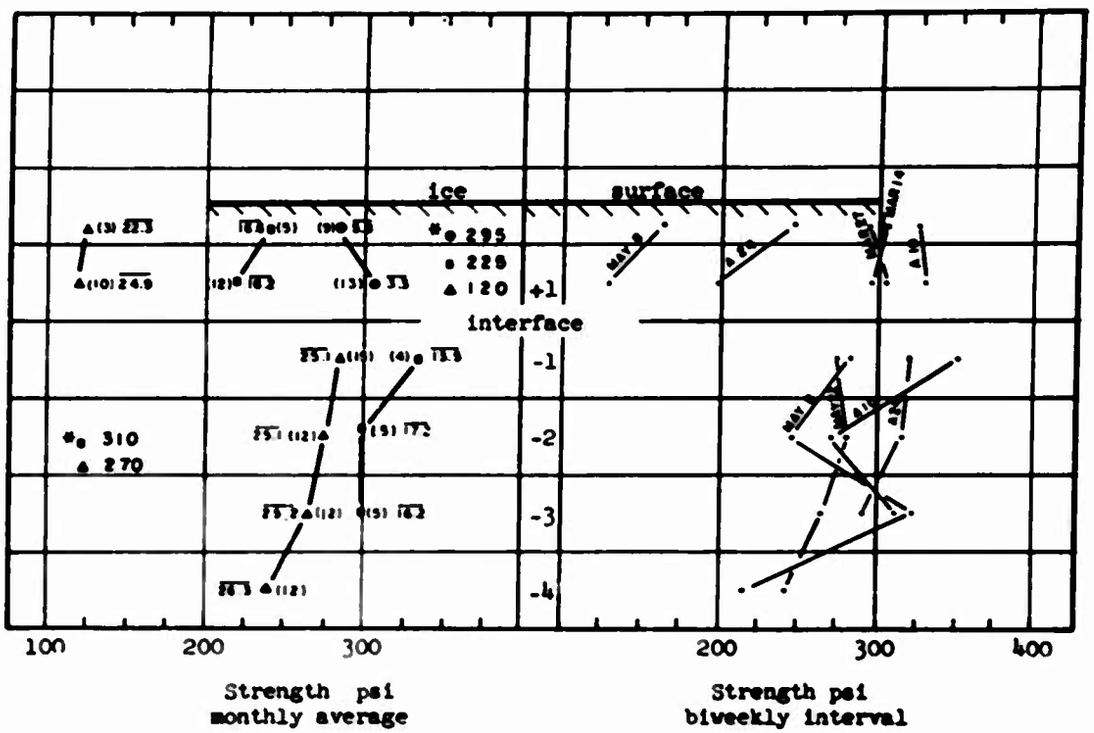

Range of Data by Stratum									
Month	Range	+4	+3	+2	+1	-1	-2	-3	-4
Mar	max			339	441				
	min			211	152				
Apr	max			326	288	415	330	378	
	min			203	135	283	224	246	
May	max			165	174	322	313	369	305
	min			93	58	232	216	105	199

FIG. D. 12 Relative tensile strength by 1-ft stratum for the total ice thickness in the reinforced, ice-aggregate parking apron (Parking Apron No. 3)

MONTHLY WEATHER SUMMARY

Thule AB, Greenland		Times are local	Month NOV, 1960

DAY	TEMP (°F) MAX	MIN	AVG	PRECIP (") WATER EQUIV	SNOW FALL	SNW DEP at 1230Z	AVG WIND DIRCTN TRUE	AVG WIND SPEED (MPH)	FASTEST MILE SPEED (MPH)	DIRCTN TRUE	AVG SLP (mb) 02, 08, 14 & 20	AVG TT (°F) 08 & 20	AVG $T_d T_d$ (°F) 08 & 20
1	16	0	9.0	.01	.1	T	15	135	30	150	1004.0	16	10
2	20	9	14.6	.04	.4	0	14	113	31	113	13.1	13	5
3	22	10	19.0	.02	.2	0	25	135	30	135	99.4	20	12
4	21	10	19.7	T	T	0	10	135	27	135	95.1	20	12
5	16	0	13.1	.03	.3	0	6	090	13	110	995.7	12	3
6	16	7	12.3	.04	.4	9	9	100	21	190	99.1	13	6
7	12	6	7.7	T	T	9	7	135	15	150	92.0	7	-1
8	11	-12	-.6	.03	.3	9	12	270	23	293	99.9	-1	-9
9	-4	-13	-6.0	0	0	9	10	113	15	113	94.4	-11	-23
10	5	-6	-.5	T	T	9	7	090	13	113	1004.1	-2	-11
11	9	3	6.1	.10	1.0	10	[illegible]	293	14	315	10.0	9	3
12	11	-4	3.0	.14	1.4	12	6	135	12	040	12.5	4	-2
13	5	-12	-4.6	0	0	13	6	270	14	113	11.6	-10	-19
14	16	-6	5.0	0	0	13	7	090	17	090	04.1	5	-4
15	20	7	13.7	T	T	13	8	113	15	330	04.0	15	9
16	14	4	9.0	.13	1.3	13	6	270	17	293	05.9	10	4
17	14	5	9.7	.07	.7	15	23	113	45	090	12.0	17	7
18	15	3	9.1	0	0	15	10	135	30	135	10.0	8	2
19	17	7	12.1	T	T	15	20	135	44	090	08.5	11	3
20	21	8	14.7	0	0	15	22	135	30	113	04.3	15	10
21	24	0	11.9	.07	.7	16	20	[illegible]	25	135	11.2	6	0
22	9	1	4.9	.17	1.7	16	6	270	12	240	17.5	5	-1
23	1	-16	-7.3	T	T	19	6	135	13	150	20.7	-4	-13
24	16	-1	6.4	.03	.3	20	5	135	17	150	14.0	11	-5
25	19	-4	7.4	T	T	20	10	090	13	090	14.2	9	4
26	12	-3	4.5	T	T	20	6	113	7	113	16.4	8	4
27	12	2	6.4	.01	.1	20	4	090	8	113	16.1	9	4
28	11	-13	-.0	T	T	20	6	090	13	090	13.5	-4.5	-13
29	-6	-17	-11.5	0	0	20	5	090	10	150	07.0	-11.7	-21
30	-.1	-19	-14.0	0	0	20	7	090	13	090	04.0	-14.2	-24.5
31													
Sum	372	-20	182.4	.92	9.2	441	330	4081	527	4806	7267	144	-51
AVG	12.4	-0.6	6.1				11	144			1004.1	4.7	-1.7

Temperature Data				MAX Wind Data		Precipitation Data	
Average monthly	6.1			Knots	41	Total for month	.92
Highest	24	on	21 Nov. 60				
Lowest	-19	on	30 Nov. 60	MPH	53	Greatest in 24 Hours	.10
				DIRCTN	98		
Max 32 or below	30			Date	24th 1960	Snowfall, sleet and hail	
				Time	0734	Total for month	9.2
Min 32 or below	30						
Min 0 or below	14					Greatest in 24 hours	1.0
Min -20 or below	0						
Min -30 or below	0					Greatest Depth on Ground	20

MONTHLY WEATHER SUMMARY

Thule AB, Greenland | Times are local | Month DEC. 1980

DAY	TEMP (°F) MAX	MIN	AVG	PRECIP (") WATER EQUIV	SNOW FALL	SNW DEP at 1130Z	AVG WIND DRCTN TRUE	AVG WIND SPEED (MPH)	FASTEST MILE SPEED (MPH)	FASTEST MILE DRCTN TRUE	AVG SLP (m/o) 02, 08 14 & 20	AVG TT (°F) 0642Z	AVG T_dT_d (°F) 0642Z
1	1	-20	-9.5	T	T	20	*	153	13	090	1006.6	-10.0	-21.5
2	1	-20	-9.0	T	T	20	6	113	11	090	998.3	-12.6	-25.0
3	-4	-17	-10.2	T	T	20	7	113	10	150	97.0	-12.0	-20.0
4	-3	-19	-11.1	0	0	20	7	113	13	090	97.9	-16.0	-19.0
5	2	-16	-8.0	.01	.1	20	6	113	12	113	1000.7	-9.0	-16.5
6	-6	-20	-14.1	T	T	20	10	113	15	090	06.2	-14.0	-24.3
7	-8	-23	-16.2	T	T	20	*	113	16	090	11.0	-6.5	-16.5
8	-12	-25	-19.6	T	T	20	6	113	12	090	13.1	-19.5	-30.5
9	-17	-25	-21.1	0	0	20	9	090	13	113	10.4	-20.5	-35.0
10	-2	-26	-16.1	0	0	20	9	090	17	090	999.1	-14.5	-26.5
11	0	-10	-9	0	0	20	7	090	13	090	96.9	-11.0	-25.0
12	9	-10	-1.1	T	T	20	12	135	23	150	99.7	-1.5	-9.0
13	0	-16	-25	.02	.2	20	7	113	13	090	97.4	-3.5	-10.0
14	0	-12	-6.9	.02	.2	20	6	113	12	090	95.9	0.0	-7.0
15	0	-17	-8.5	.01	.1	20	*	135	16	150	90.4	-9.0	-16.5
16	-3	-21	-12.1	0	0	20	*	090	16	090	1010.6	-12.3	-21.5
17	-13	-22	-17.5	0	0	20	*	090	12	090	29.5	-16.4	-3.1
18	-10	-22	16.0	0	0	20	5	090	15	090	22.9	-17.5	-3.2
19	16	-20	-1.7	.03	.3	20	10	090	20	090	994.0	2.2	-7.0
20	13	-6	6.7	.04	.4	21	9	090	32	113	1007.6	9.2	1.0
21	0	-6	2.0	0	0	21	6	090	13	090	15.6	3.6	3.0
22	0	-8	0	.01	.1	21	6	090	9	090	19.0	-4.4	-1.3
23	3	-22	-9.3	.01	.1	21	6	090	14	190	994.6	-14.7	-31.5
24	-2	-16	-9.1	0	0	21	6	090	12	190	91.0	-4.5	-24.5
25	-1	-17	-8.9	0	0	21	7	090	12	190	93.9	-13.5	-33.5
26	-1	-10	-5.0	T	T	21	*	090	10	135	1000.7	-2.5	-10.5
27	-9	-26	-16.6	0	0	21	5	090	12	090	10.7	-20.4	-37.0
28	-13	-23	-17.9	0	0	21	7	090	14	090	16.6	-20.3	-32.5
29	-13	-22	-17.0	0	0	21	5	090	15	090	04.3	-16.4	-36.0
30	2	-16	-6.9	0	0	21	6	090	16	090	09.7	-5.1	-16.0
31	-6	-16	-11.9	0	0	21	6	113	13	113	16.7	-12.5	-22.0
Sum	-56	-561	-316.0	.15	1.5	552	224	3173	400	3411	16582	316.5	804.7
AVG	-1.8	-17.0	-10.1	.02	.2	20.5	7	102	14.9	*110	1046.9	-10.2	-72.5

Temperature Data

Average monthly -10.1

Highest +16 on 19 DEC 1980

Lowest -26 on 10 and 27 DEC, 80

Max 32 or below +16

Min 32 or below 0

Min 0 or below -26

Min -20 or below -26

Min -30 or below -

MAX Wind Data

Route	20
MPH	32
DRCTN	90
Date	20
Time	0104

Precipitation Data

Total for month .15

Greatest in 24 Hours .02

Snowfall, sleet and hail 1.5

Total for month 1.5

Greatest in 24 hours .2

Greatest Depth on Ground 21

MONTHLY WEATHER SUMMARY

Thule AB, Greenland | Times are local | Month: FEB. 1961

DAY	TEMP (°F) MAX	MIN	AVG	PRECIP (") WATER EQUIV	SNOW FALL	SNW DEP at 1130Z	AVG WIND DRCTN TRUE	AVG WIND SPEED (MPH)	FASTEST MILE SPEED (MPH)	FASTEST MILE DRCTN TRUE	AVG SLP (m/o) 02, 08 14 & 20	AVG TT (°F) 08 & 20	AVG TT (°F) 08 & 20
1	-13	-22	-17.7	0	0	T	110	9	15	090	1016.5	-19.5	-20.5
2	-13	-24	-18.3	0	0	T	100	6	13	150	17.7	-19.6	-20.5
3	-7	-23	-15.1	0	0	T	100	8	23	150	12.4	-18.2	-20.5
4	+4	-10	-2.9	T	T	T	120	22	50	135	07.9	+0.9	-5.0
5	-2	-24	-12.7	T	T	T	160	15	27	160	04.4	-14.9	-25.5
6	-22	-31	-26.4	0	0	T	100	7	13	090	04.9	-25.0	-39.5
7	-26	-33	-29.7	0	0	T	100	0	16	090	00.4	-30.2	-45.5
8	-24	-31	-27.5	0	0	T	090	7	14	113	12.1	-26.2	-44.0
9	-20	-30	-25.0	0	0	T	100	9	14	113	00.9	-27.5	-45.5
10	-9	-24	-16.3	T	T	T	100	10	23	150	01.5	-17.0	-32.5
11	-12	-31	-21.6	T	T	T	100	9	16	090	07.6	-25.2	-40.5
12	-25	-32	-29.7	0	0	T	100	10	16	090	07.1	-27.5	-47.5
13	-22	-36	-30.0	0	0	T	100	9	24	135	999.7	-33.5	-54.5
14	-21	-27	-24.3	0	0	T	120	10	21	135	1003.5	-22.0	-36.0
15	-20	-36	-27.9	T	T	T	150	7	14	150	00.6	-27.0	-41.0
16	-33	-37	-34.7	0	0	T	100	7	16	080	03.0	-35.0	-44.0
17	-27	-36	-31.6	0	0	T	090	10	16	090	13.7	-33.7	-41.5
18	-27	-35	-31.1	0	0	T	100	6	13	113	02.1	-31.9	-44.5
19	-15	-29	-21.6	T	T	T	130	16	33	150	999.2	-20.4	-33.5
20	-16	-30	-22.4	T	T	T	150	20	30	150	1004.4	-23.3	-34.0
21	-23	-29	-26.6	0	0	T	090	6	21	160	07.5	-27.5	-44.5
22	-26	-39	-32.4	0	0	T	100	9	15	150	03.0	-33.2	-44.5
23	-35	-40	-36.1	0	0	T	100	9	13	113	04.2	-35.5	(-42.0)
24	-20	-36	-29.5	T	T	T	120	14	39	135	13.0	-29.3	-40.5
25	-31	-36	-34.1	T	T	T	100	7	17	113	13.2	-35.9	-44.0
26	-30	-37	-33.6	T	T	T	100	6	12	113	07.7	-32.5	-40.0
27	-32	-36	-33.9	T	T	T	100	7	12	090	00.2	-35.1	-44.0
28	-34	-39	-36.6	0	0	T	090	7	13	090	04.6	-36.3	-42.5
29													
30													
31													
Sum	579	970	726.2	T	T	T	3290	272	556	3672	4126	-736.6	-1090.0
AVG	-20.7	-31.5	-26.0	T	T	T	114	12	23	124	1007.9	-24.2	-39.2

Temperature Data

Average monthly -26.0

Highest +6 on 4th FEB. 61

Lowest -40 on 23rd FEB. 61

Max 32 or below 28

Min 32 or below 28

Min 0 or below 28

Min -20 or below 27

Min -30 or below 19

MAX Wind Data

Route	50	
MPH	50	
DRCTN	90	
Date	4th	
Time	0602	

Precipitation Data

Total for month T

Greatest in 24 Hours T

Snowfall, sleet and hail

Total for month T

Greatest in 24 hours T

Greatest Depth on Ground T

MONTHLY WEATHER SUMMARY

Thule AB, Greenland | Times are local | Month JAN. 1968

DAY	TEMP (°F) MAX	MIN	AVG	PRECIP (") WATER EQUIV	SNOW FALL	SNW DEP at 1130Z	AVG WIND DRCTN TRUE	AVG WIND SPEED (MPH)	FASTEST MILE SPEED (MPH)	FASTEST MILE DRCTN TRUE	AVG SLP (m/o) 02, 08 14 & 20	AVG TT (°F) 04420	AVG T_dT_d (°F) 04420
1	-17	-24	-17.6	0	0	21	100	7	13	090	1013.3	-16.0	-37.0
2	-13	-22	-17.4	0	0	21	100	6	13	113	16.9	-17.4	-31.5
3	-10	-17	-13.5	.02	.2	21	100	5	10	113	23.9	-12.9	-24.0
4	-12	-21	-17.7	T	T	21	100	6	10	090	22.2	-16.3	-27.0
5	-17	-31	-23.5	0	0	21	113	7	12	113	22.4	-25.4	-44.0
6	-19	-30	-24.5	0	0	21	090	6	12	113	19.9	-26.0	-52.0
7	-14	-30	-21.0	0	0	21	100	6	12	113	16.1	-23.0	-43.0
8	-11	-19	-14.9	.07	.7	21	100	3	9	090	16.0	-15.7	-28.5
9	-17	-31	-24.1	.04	.5	22	090	4	9	090	16.9	-23.5	-37.0
10	-20	-30	-33.3	T	T	23	100	7	14	113	12.1	-23.3	-43.0
11	-21	-29	-24.9	T	T	23	100	6	12	113	997.9	-25.9	(-42.5)
12	-32	-36	-34.1	0	0	23	110	6	13	113	1002.7	-34.1	-47.0
13	-27	-35	-31.1	T	T	23	100	5	13	090	07.7	-26.7	-43.0
14	-27	-36	-32.5	.01	1	23	110	6	15	113	11.9	-31.2	-46.5
15	-21	-32	-26.6	0	0	23	113	6	17	113	06.2	-26.9	-51.0
16	-15	-35	-25.0	0	0	19	090	6	16	135	982.9	-31.3	-47.0
17	-9	-32	-20.7	T	T	17	100	17	73	150	93.9	-16.3	-44.0
18	-20	-26	-24.2	0	0	9	100	7	14	113	96.2	-26.3	-46.5
19	-15	-31	-22.9	0	0	9	100	3	25	150	1004.9	-22.6	-34.5
20	-13	-32	-24.2	0	0	9	135	11	32	090	990.4	-16.0	-26.5
21	-15	-29	-21.6	T	T	9	135	13	27	140	1000.9	-22.0	-37.0
22	-15	-29	-21.9	T	T	9	113	17	27	150	04.3	-22.0	-37.5
23	-24	-30	-26.9	0	0	9	135	9	16	090	24.6	-27.0	-42.0
24	-14	-25	-18.6	0	0	9	100	6	14	090	11.2	-19.2	-33.5
25	-10	-15	-12.2	0	0	9	100	7	15	090	10.5	-11.3	-22.5
26	-12	-19	-13.9	0	0	9	090	6	15	113	994.2	-14.7	-25.0
27	-12	-16	-14.0	0	0	9	100	7	15	113	98.3	-15.9	-25.0
28	-13	-19	-15.7	0	0	9	100	7	15	090	1002.1	-17.0	-31.0
29	-5	-20	-17.3	T	T	9	101	5	15	113	11.9	-17.3	-23.5
30	-14	-22	-19.0	0	0	9	100	7	13	090	04.4	-19.5	-30.0
31	-15	-24	-19.5	0	0	7	113	9	15	113	07.9	-22.4	-35.0
Sum	537	850	691.9	.14	1.4	600	3237	220	522	3473	3424.2	694.3	1139.5
AVG	16.4	-27.4	-21.5	.005	.05	15.4	104	7	17	112	1009.2	-22.5	-36.8

Temperature Data

Average monthly		-21.5
Highest	-5	29th
Lowest	-39	11th
Max 32 or below	31	
Min 32 or below	31	
Min 0 or below	31	
Min -20 or below	25	
Min -30 or below	15	

MAX Wind Data

Knots	49
MPH	73
DRCTN	NW
Date	17th
Time	0852

Precipitation Data

Total for month	.14
Greatest in 24 Hours	.07
Rainfall, sleet and hail	
Total for month	1.4
Greatest in 24 hours	.7
Greatest Depth on Ground	23

MONTHLY WEATHER SUMMARY

Thule AB, Greenland | Times are local | Month MARCH 1968

DAY	TEMP (°F) MAX	MIN	AVG	PRECIP (") WATER EQUIV	SNOW FALL	SNW DEP at 1130Z	AVG WIND DRCTN TRUE	AVG WIND SPEED (MPH)	FASTEST MILE SPEED (MPH)	FASTEST MILE DRCTN TRUE	AVG SLP (m/o) 02, 08 14 & 20	AVG TT (°F) 02 & 20	AVG T_dT_d (°F) 02 & 20
1	-21	-36	-29.5	0	0	T	100	7	13	090	990.2	-35.9	(-42)
2	-24	-35	-29.6	0	0	T	100	6	12	090	99.4	-30.0	-45
3	-24	-30	-27.2	.07	.7	T	100	4	9	090	1004.7	-26.9	-39.5
4	-27	-34	-30.3	T	T	T	100	7	10	090	16.3	-31.9	-46
5	-21	-39	-29.9	0	0	T	100	7	20	150	19.7	-31.1	-42.5
6	-29	-36	-32.7	0	0	T	100	6	12	090	16.0	-35.1	(-41)
7	-25	-37	-32.0	0	0	T	090	6	12	090	13.4	-33.2	-43
8	-20	-34	-27.3	0	0	T	090	9	29	150	06.2	-27.9	-38
9	-24	-38	-32.0	0	0	T	100	7	12	113	15.8	-35.5	-44
10	-26	-36	-32.0	T	T	T	100	6	12	113	15.3	-31.0	-40.5
11	-25	-36	-31.7	T	T	T	090	7	15	090	22.9	-22.0	-43.0
12	-26	-42	-33.9	0	0	T	090	6	14	090	19.2	-36.0	-46
13	-31	-40	-35.9	0	0	T	100	7	14	113	20.2	-36.7	(-45)
14	-29	-44	-36.1	0	0	T	100	7	14	090	16.6	-37.0	-46.5
15	-30	-40	-35.0	0	0	T	100	5	13	090	15.5	-36.7	(-44)
16	-26	-40	-33.2	0	0	T	090	6	15	090	16.5	-35.7	-46.5
17	-20	-31	- 5.7	0	0	T	070	15	42	080	09.9	-10.3	-20.0
18	-24	-23	+ 0.7	0	0	T	110	30	49	110	01.4	-12.1	-20.0
19	- 6	-21	-13.3	T	T	T	130	9	27	140	11.0	-16.9	-23.5
20	+ 2	-20	- 6.9	0	0	T	090	5	12	090	03.0	- 9.4	-17.5
21	6	- 6	0	.03	.3	T	100	14	42	150	00.1	- 4.0	-11.0
22	- 6	-20	-13.1	T	T	T	110	5	15	090	11.7	-13.0	-23
23	- 5	-21	-13.9	0	0	T	100	7	22	090	15.5	-15.3	-25.5
24	-12	-26	-16.7	0	0	T	100	6	14	113	21.2	-21.0	-32.5
25	-14	-27	-20.5	0	0	T	100	6	13	090	27.0	-22.6	-34.5
26	-10	-30	-24.0	0	0	T	100	5	14	113	29.0	-24.3	-40.5
27	-11	-29	-19.7	0	0	T	090	6	13	090	29.4	-22.7	-35.0
28	-15	-27	-21.1	0	0	T	130	5	12	113	27.6	-23.6	-36.0
29	-15	-29	-21.5	T	T	T	100	4	9	090	24.3	-26.1	-42.0
30	-13	-24	-19.5	T	T	T	110	6	10	090	31.7	-21.0	-34.5
31	-13	-25	-19.1	0	0	T	100	5	14	090	32.4	-22.7	-41.0
Sum	+00	959	724.9	.10	1.0	217	2975	232	514	3245	97647	793.7	1131.0
AVG	-15.7	-30.9	-23.4	.003	.03	7	096	7	17	105	1031.5	-25.6	-36.5
							8			134			

Temperature Data

Average monthly -23.4

Highest +24 on 19th

Lowest -44 on 18th

Max 32 or below 31

Min 32 or below 31

Min 0 or below 31

Min -20 or below 30

Min -30 or below 18

MAX Wind Data

Knots	50	
MPH	69	
DRCTN	130	
Date	19th	
Time	0921	

Precipitation Data

Total for month .10

Greatest in 24 Hours .07

Snowfall, sleet and hail

Total for month .3

Greatest in 24 hours .2

Greatest Depth on Ground 7

MONTHLY WEATHER SUMMARY

Thule AB, Greenland | Times are local | Month APRIL 1961

DAY	TEMP (°F) MAX	MIN	AVG	PRECIP (") WATER EQUIV	SNOW FALL	SNW DEP at 1130Z	AVG WIND DRCTN TRUE	AVG WIND SPEED (MPH)	FASTEST MILE SPEED (MPH)	FASTEST MILE DRCTN TRUE	AVG SLP (m/o) 07, 00 13 & 20	AVG TT (°F) 07 & 20	AVG $T_d T_d$ (°F) 07 & 20
1	- 9	-23	-16.2	0	0	7	100	5	13	113	1029.1	-19.0	-34.0
2	+ 3	-15	- 6.0	.02	.2	7	190	5	9	270	19.1	- 5.3	-13.5
3	+ 3	- 3	- 0.7	.03	.3	7	230	7	13	330	12.3	- 0.7	- 6.0
4	- 2	-27	-14.4	.04	.4	9	090	5	12	090	14.6	-19.2	-31.3
5	-11	-30	-20.6	T	T	9	140	6	16	140	27.2	-25.4	-36.9
6	-19	-30	-28.2	0	0	9	090	7	13	090	33.9	-26.5	-41.0
7	- 9	-30	-19.9	0	0	9	090	5	12	090	24.3	-21.1	-35.9
8	+ 3	-13	- 4.8	.01	.1	8	130	5	10	270	17.3	- 4.9	-18.0
9	0	-19	- 9.4	.02	.2	8	120	8	22	120	25.5	- 8.1	-17.8
10	- 9	-19	-13.7	0	0	8	100	6	12	113	33.5	-15.9	-29.5
11	+ 2	-15	- 6.2	0	0	8	090	6	13	113	27.4	- 9.7	-17.9
12	+ 4	-10	-11.4	0	0	8	090	5	14	090	15.0	- 6.2	-15.5
13	+ 3	-16	- 6.9	0	0	8	130	6	15	090	24.0	- 6.1	-16.0
14	+ 9	-15	- 2.6	0	0	8	100	6	12	100	31.6	- 7.9	-13.5
15	+10	-10	+ 0.1	.01	.1	8	120	5	14	113	29.0	- 1.7	- 9.0
16	+ 3	-15	- 6.9	T	T	9	113	6	14	090	29.9	- 6.0	-17.5
17	+ 6	-14	- 4.1	0	0	9	130	5	10	090	32.3	- 0.7	- 6.0
18	+15	- 7	+14.1	T	0	9	120	5	12	113	33.9	- 0.5	- 6.5
19	+17	- 5	+ 6.6	0	0	9	090	5	12	090	33.6	+ 6.0	+ 3.0
20	+20	+ 2	+11.2	0	0	9	100	6	14	090	27.7	+ 9.6	+ 0.5
21	+22	- 5	+ 9.0	0	0	9	090	5	13	090	16.5	+ 6.7	- 3.0
22	+17	- 5	+ 5.0	0	0	9	100	6	10	090	21.0	+ 2.9	- 7.0
23	+16	- 7	+ 6.4	0	0	9	110	5	10	113	15.1	+ 6.9	- 6.0
24	+22	0	+11.3	0	0	9	110	5	10	090	14.3	+13.7	+ 5.5
25	+10	+ 1	+ 9.5	0	0	9	110	5	12	090	19.6	+ 9.5	- 1.5
26	+22	- 1	10.3	0	0	9	090	4	7	090	19.7	+12.3	+ 2.0
27	+27	+ 3	+16.9	0	0	9	110	4	9	090	21.1	+16.6	+ 6.0
28	+23	+ 3	+13.0	0	0	9	130	5	10	090	21.7	+17.0	+ 6.5
29	+26	+ 9	+18.5	0	0	9	200	5	12	090	17.5	+20.1	+13.5
30	+20	+14	+17.0	.05	.5	9	120	5	9	135	13.7	+17.0	+13.5
31													
Sum	288	-313	-32.3	.10	1.0	284	3553	163	396	3511	0000	-52.3	-319.1
AVG	+9.9	-10.4	-01.1	.006	.4	9	119	5	13	117	1029.2	- 1.7	-10.6
							101			101			

Temperature Data

Average monthly -01.1

Highest +26 on 29th

Lowest -30 on 5, 6th and 7th

Max 32 or below 30

Min 32 or below 30

Min 0 or below 23

Min -20 or below 5

Min -30 or below 3

MAX Wind Data

Route	19
MPH	22
DRCTN	9
Date	9th
Time	1447

Precipitation Data

Total for month .10

Greatest in 24 Hours .05

Snowfall, sleet and hail 1.0

Total for month 1.0

Greatest in 24 hours .5

Greatest Depth on Ground 9

MONTHLY WEATHER SUMMARY

Thule AB, Greenland — Times are local — Month: MAY 1961

DAY	TEMP (°F) MAX	MIN	AVG	PRECIP (") WATER EQUIV	SNOW FALL	SNW DPTH at 1130Z	AVG WIND DRCTN TRUE	AVG WIND SPEED (MPH)	FASTEST MILE SPEED (MPH)	FASTEST MILE DRCTN TRUE	AVG SLP (m/o) 02, 08 14 & 20	AVG TT (°F) 08 & 20	AVG T_d T_d (°F) 08 & 20
1	23	10	16.2	.06	.9	9	210	6	12	260	1019.7	19.5	14.5
2	16	- 2	6.9	.02	.2	9	150	6	16	150	11.5	9.4	3.0
3	14	- 7	3.0	T	T	10	090	5	12	135	14.5	5.6	- 4.5
4	11	- 9	1.2	T	T	10	120	5	15	150	17.3	1.4	- 9.5
5	11	- 9	1.7	0	0	9	110	7	13	090	19.0	1.3	- 7.0
6	10	- 9	4.4	0	0	9	090	6	12	090	19.2	3.4	- 3.5
7	17	- 4	6.6	0	0	9	110	5	12	090	15.2	7.0	- 4.0
8	19	- 2	8.3	T	T	9	030	5	10	080	15.0	10.5	- 2.0
9	24	1	12.3	.02	.2	9	120	6	9	090	19.3	13.4	7.0
10	20	4	12.1	.01	.1	9	110	5	9	090	21.2	11.2	5.5
11	21	2	11.0	0	0	9	100	5	10	090	22.2	11.7	6.0
12	20	2	11.9	0	0	9	120	6	12	090	06.6	14.9	6.5
13	25	10	17.6	T	T	9	140	5	9	110	07.2	19.5	9.0
14	29	10	19.4	.01	.1	9	110	10	29	135	07.9	23.2	13.5
15	25	14	20.6	.01	.1	9	100	9	23	150	10.9	20.7	14.0
16	23	16	19.1	T	T	9	150	14	23	240	17.0	20.5	13.0
17	26	14	19.7	.02	.2	9	150	9	20	150	15.9	20.5	14.5
18	32	16	23.9	.13	3.0	11	220	9	15	240	06.9	25.0	16.0
19	24	14	19.0	.02	.6	11	250	5	10	270	13.2	20.9	15.0
20	24	5	15.7	.03	.6	12	040	5	9	090	19.2	19.3	14.0
21	20	6	14.1	.01	.1	12	160	9	20	150	17.3	16.6	9.5
22	23	11	20.2	T	T	12	140	9	25	140	21.5	20.9	13.0
23	21	17	16.9	.02	.3	12	150	15	27	135	23.2	19.4	13.5
24	20	12	20.0	.02	.2	12	040	9	24	150	22.9	19.7	14.0
25	23	9	20.1	T	T	11	110	6	23	150	15.5	17.0	7.0
26	20	17	20.4	T	T	10	160	13	31	150	11.9	19.1	11.5
27	27	14	21.4	0	0	9	190	10	24	135	999.3	21.4	10.5
28	25	20	22.5	.01	.1	9	170	22	32	135	1009.0	22.0	15.0
29	25	19	21.0	0	0	9	210	9	25	150	10.7	22.6	12.0
30	29	19	23.5	T	T	9	140	7	17	240	06.4	22.9	17.5
31	27	19	23.0	T	T	9	270	6	12	270	19.0	24.1	15.5
Sum	731	269	6016	.39	6.5	301	4700	283	569	6732	1507	606.6	2570
AVG	23.6	8.7	19.5	.122	.21	9	150	9	17	157	1019.0	19.3	8.3
							32			305			

Temperature Data

Average monthly 19.5

Highest 33 on 29th

Lowest -9 on 4, 5, 6th

Max 32 or below 30

Min 32 or below 31

Min 0 or below 7

Min -20 or below 0

Min -30 or below 0

MAX Wind Data

Knots	34	
MPH	39	
DRCTN	05	
Date	14	
Time	1720	

Precipitation Data

Total for month .39

Greatest in 24 Hours .13

Rainfall, sleet and hail

Total for month 6.5

Greatest in 24 hours 3.0

Greatest Depth on Ground 12

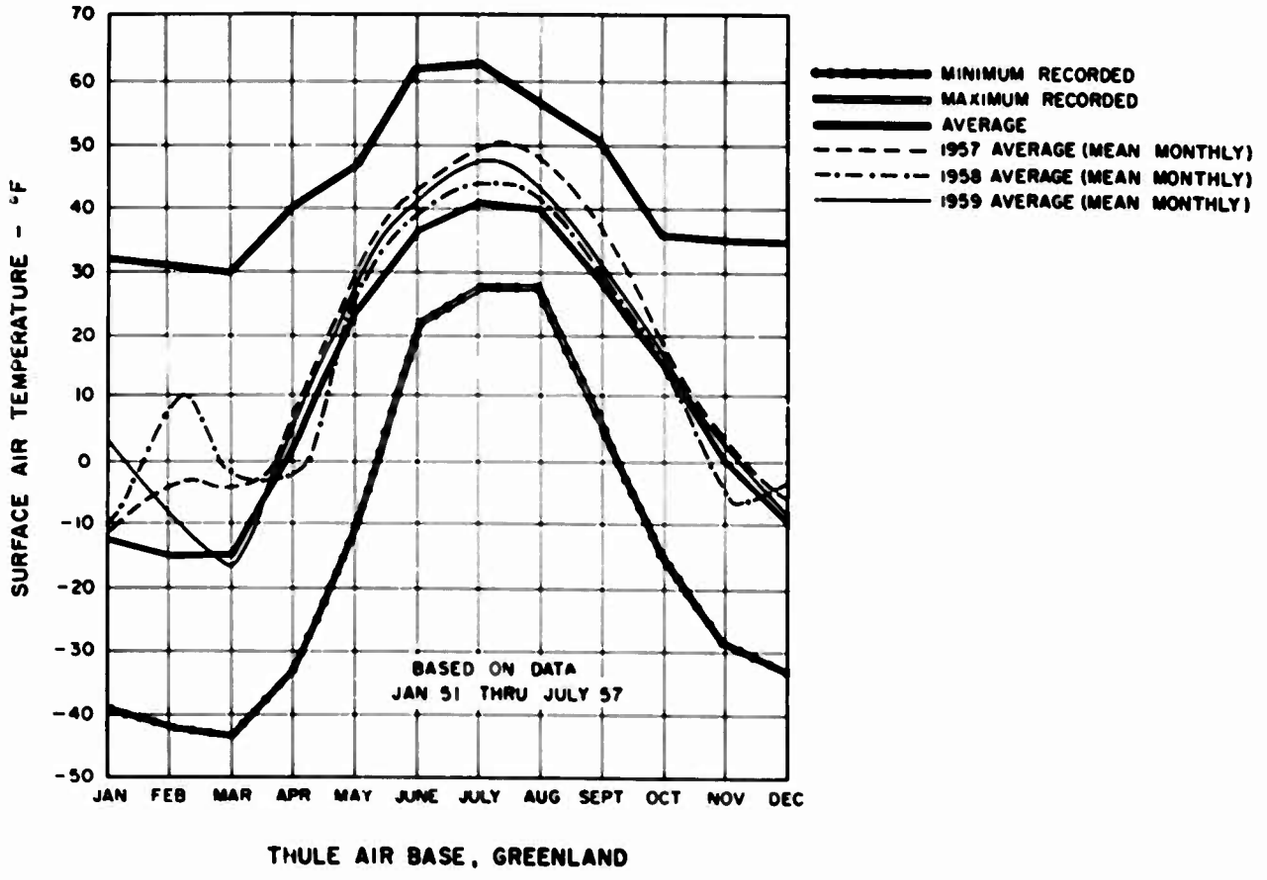

REPRODUCED BY TERRESTRIAL SCIENCES LABORATORY FROM DATA OF 5TH WEATHER GROUP, AIR WEATHER SERVICE, THULE AIR BASE, GREENLAND

FIG. E. 1. Surface air temperatures, Thule AB, Greenland

APPENDIX F – Logistics
(by R. H. Hinchcliffe)

1. Summary of Shipping Information

a. To Thule Air Base, Greenland

(1) Via MATS aircraft from:

Agency	No. Pcs.	Wt. (lb)	Cubic Feet
Naval Civil Engineering Laboratory*	143	86,457	6,870.5
Navy Electronics Laboratory	34	3,276	198.0
L. G. Hanscom Field (Terrestrial Sciences Lab & Contractors)	26	1,776	90.0
Commercial Suppliers	24	5,219	304.8
(2) Via RCAF aircraft from:			
McGill University, Montreal, Canada	6	350	25.0
Total shipments to Greenland	233	97,078	7,488.3

b. Retrograde from Thule Air Base, Greenland

(1) Via MATS aircraft to:			
Naval Civil Engineering Laboratory**	113	71,567	6,892.31
Navy Electronics Laboratory	29	2,596	172.1
L. G. Hanscom Field (Terrestrial Sciences Lab & Contractors)	19	2,000	75.5
California Institute of Technology	1	20	2.0
(2) Via RCAF aircraft to:			
McGill University, Montreal, Canada	6	300	25.0
Total retrograde from Greenland	168	76,483	7,166.9

2. General Logistics Information

a. Numerous items of heavy equipment, etc., were obtained on a loan basis from units in the Thule area. These items included two motorized road graders, a D-4 caterpillar tractor with dozer blade, a 1/2-ton pick-up truck, an 8-passenger carryall from the Corps of Engineers, and a large wannigan from the U. S. Army Polar Research and Development Center.

---

* A traxcavator (weight 22,450; cube 766.4) was the only item shipped from NCEL that did not reach the project site. This item was held up at Dover AFB because the hydraulic lifters were in such a position that the item could not be successfully loaded aboard MATS aircraft. By the time the difficulty was resolved the vehicle was no longer required at the project site and was returned to NCEL.

** Items in this listing include three weasels and two large sled-mounted pumps that had been stored at Thule for use on Project ICE WAY. These items had previously been used at Ward Hunt Island, Ellesmere Island, N.W.T., Canada.

b. A large portion of Hangar No. 1 (Roads & Grounds Section, Base Civil Engineering Squadron) was made available as a storage and staging area.

c. On 10 March a Thule Base Operation C-47 aircraft flight was made to the Alert weather station on Ellesmere Island to pick up two containers of McGill University equipment which had been left there by error by RCAF Service Flight No. 5 on 6 March.

d. Logistic support for Project ICE WAY was furnished at Thule by personnel and equipment from Base Civil Engineering Squadron and Base Transportation Squadron of the 4863rd Air Base Group, 1628th MATS Support Squadron and GRD Thule Operating Location Section.

APPENDIX G – Aircraft Operations
(by D. W. Klick)

F-102 (22 March):

Landed to shoreward; taxied through constant-speed zone (CSZ) at 20 knots; turned around, taxied through CSZ at 3-5 knots; turned around, taxied through CSZ at less than 3 knots; parked for 1/2 hour on natural ice in overrun zone; turned around, taxied through SCZ at 15 knots; turned around, taxied through CSZ at 10 knots; turned around, and took off using afterburner.

Landing weight - 29,500 lb Takeoff weight 28,000 lb

C-130 (24 March):

Landed to shoreward; taxied through CSZ, stopping momentarily at each hash mark 50 ft along centerline; parked for 1 3/4 hours on natural ice in overrun zone (2 snow plows parked alongside for 20 minutes); and took off.

Landing weight - 96,400 lb Takeoff weight - 90,000 lb

Weight through hash marks - Beginning 96,000 lb
Ending 93,000 lb

Weight during parking - Beginning 93,000 lb
Ending 90,000 lb
With snow plows 175,000 lb (42,000 lb per plow)

C-130 (25 March):

Landed to shoreward; parked on natural ice on runway 1000 ft east of midpoint for 1 hour; taxied to Pad No. 1 and parked for 20 minutes; taxied to Pad No. 2 and parked for 20 minutes; taxied onto runway, and took off. Returned immediately and landed to shoreward; taxied through CSZ at 20 knots; turned around, taxied through CSZ at 30 knots; turned around, taxied through CSZ at 40 knots; turned around, and took off. Returned immediately and made three touch-and-go landings to seaward at west end of runway, rolling through the CSZ on the ice each time.

Landing weight - 97,000 lb Parking weight - Beginning 96,400 lb
(natural ice) Ending 95,400 lb

Parking weight - Pad No. 1 95,000 lb
Pad No. 2 94,500 lb Takeoff weight - 92,400 lb

Weight during taxi runs - 89,000 lb Weight during touch-and-goes-88,400 lb

B-47 (26 March):

Landed to shoreward; parked on natural ice on runway for 45 minutes; taxied to Pad No. 1 and parked for 20 minutes; taxied to Pad No. 2 and parked for 20 minutes; taxied onto runway, and took off.

Landing weight - 123,000 lb Weight end of parking period on runway - 119,250 lb

Weight entering Pad No. 1 - 118,800 lb Weight entering Pad No. 2 - 117,500 lb
leaving Pad No. 1 - 117,800 lb leaving Pad No. 2 - 116,500 lb

Takeoff weight - 116,500 lb

B-47 (27 March):

Landed to shoreward, taxied to Pad No. 1 and parked for 20 minutes; taxied onto runway, and took off. Returned immediately after the KC-135 had landed and taken off for the first time, landed to shoreward; taxied to Pad No. 2 and parked for 5 minutes; taxied onto runway, and took off.

1st landing weight - 123,500 lb
takeoff weight - 122,000 lb

Weight entering Pad No. 1 - 123,000 lb
leaving Pad No. 1 - 122,000 lb

2nd landing weight - 103,000 lb
takeoff weight - 102,000 lb

Weight entering Pad No. 2 - 102,000 lb
leaving Pad No. 2 - 102,000 lb

KC-135 (27 March):

Landed to shoreward; taxied to Pad No. 1 and parked for 20 minutes; taxied onto runway, and took off. Returned immediately after the B-47 had landed and taken off for the second time, landed to shoreward; taxied to Pad No. 2 and parked for 5 minutes; taxied onto runway, and took off.

1st landing weight - 148,000 lb
takeoff weight - 146,000 lb

Weight entering Pad No. 1 - 147,500 lb
leaving Pad No. 1 - 146,000 lb

2nd landing weight - 131,000 lb
takeoff weight - 130,000 lb

Weight entering Pad No. 2 - 130,000 lb
leaving Pad No. 2 - 130,000 lb

KC-135 (28 March):

Landed to shoreward; parked on natural ice on runway for 40 minutes; taxied to Pad No. 1 and parked for 5 minutes; taxied onto runway, and took off. Returned immediately and landed to shoreward; taxied to Pad No. 1 and parked for 5 minutes; taxied onto runway, and took off.

1st landing weight - 158,000 lb
takeoff weight - 155,500 lb

2nd landing weight - 154,000 lb
takeoff weight - 153,000 lb

B-52 (31 March):

Landed to shoreward; taxied to Pad No. 1 and parked for 12 minutes; taxied onto runway, and took off. Returned three hours later after refueling and made two touch-and-go landings — one to seaward, touching down at east end of strip; and one to shoreward, touching down at west end of strip — rolling on the ice both times for about 3500 ft; then landed to shoreward; taxied to Pad No. 1 and parked for 15 minutes; taxied onto runway, and took off.

1st landing weight - 201,000 lb
takeoff weight - 196,000 lb

1st touch-and-go weight - 214,000 lb
2nd touch-and-go weight - 208,000 lb

2nd landing weight - 200,000 lb
takeoff weight - 194,000 lb

AIR FORCE SURVEYS IN GEOPHYSICS

No. 1. (Classified Title), *W. K. Widger, Jr.,, Mar 1952. (SECRET/RESTRICTED DATA Report)*

No. 2. Methods of Weather Presentation for Air Defense Operations *(U), W. K. Widger, Jr., Jun 1952. (CONFIDENTIAL Report)*

No. 3. Some Aspects of Thermal Radiation From the Atomic Bomb *(U), R. M. Chapman, Jun 1952. (SECRET Report)*

No. 4. Final Report on Project 8-52M-1 Tropopause *(U), S. Coroniti, Jul 1952. (SECRET Report)*

No. 5. Infrared as a Means of Identification *(U), N. Oliver and J. W. Chamberlain, Jul 1952. (SECRET Report)*

No. 6. Heights of Atomic Bomb Results Relative to Basic Thermal Effects Produced on the Ground *(U), R. M. Chapman and G. W. Wares, Jul 1952. (SECRET/RESTRICTED DATA Report)*

No. 7. Peak Over-Pressure at Ground Zero From High Altitude Bursts *(U), N. A. Haskell, Jul 1952. (SECRET Report)*

No. 8. Preliminary Data From Parachute Pressure Gauges, Operation Snapper. Project 1.1 Shots No. 5 and 8 *(U), N. A. Haskell, Jul 1952. (SECRET/RESTRICTED DATA Report)*

No. 9. Determination of the Horizontal *(U), R. M. Chapman and M. H. Seavey, Sep 1952. (SECRET Report)*

No. 10. Soil Stabilization Report, *C. Molineux, Sep 1952.*

No. 11. Geodesy and Gravimetry, Preliminary Report *(U), R. J. Ford, Sep 1952. (SECRET Report)*

No. 12. The Application of Weather Modification Techniques to Problems of Special Interest to the Strategic Air Command *(U), C. E. Anderson, Sep 1952. (SECRET Report)*

No. 13. Efficiency of Precipitation as a Scavenger *(U), C. E. Anderson, Aug 1952. (SECRET/RESTRICTED DATA Report)*

No. 14. Forecasting Diffusion in the Lower Layers of the Atmosphere *(U), B. Davidson, Sep 1952. (CONFIDENTIAL Report)*

No. 15. Forecasting the Mountain Wave, *C. F. Jenkins, Sep 1952.*

No. 16. A Preliminary Estimate of the Effect of Fog and Rain on the Peak Shock Pressure From an Atomic Bomb *(U), H. P. Gauvin and J. H. Healy, Sep 1952. (SECRET/RESTRICTED DATA Report)*

No. 17. Operation Tumbler-Snapper Project 1.1A. Thermal Radiation Measurements With a Vacuum Capacitor Microphone *(U), M. O'Day, J. L. Bohn, F. H. Nadig and R. J. Cowie, Jr., Sep 1952. (CONFIDENTIAL/RESTRICTED DATA Report)*

No. 18. Operation Snapper Project 1.1. The Measurement of Free Air Atomic Blast Pressures *(U), J. O. Vann and N. A. Haskell, Sep 1952. (SECRET/RESTRICTED DATA Report)*

No. 19. The Construction and Application of Contingency Tables in Weather Forecasting, *E. W. Wahl, R. M. White and H. A. Salmela, Nov 1952.*

No. 20. Peak Overpressure in Air Due to a Deep Underwater Explosion *(U), N. A. Haskell, Nov 1952. (SECRET Report)*

No. 21. Slant Visibility, *R. Penndorf, B. Goldberg and D. Lufkin, Dec 1952.*

No. 22. Geodesy and Gravimetry *(U), R. J. Ford, Dec 1952. (SECRET Report)*

No. 23. Weather Effects on Radar, *D. Atlas et al, Dec 1952.*

No. 24. A Survey of Available Information on Winds Above 30,000 Ft., *C. F. Jenkins, Dec 1952.*

No. 25. A Survey of Available Information on the Wind Fields Between the Surface and the Lower Stratosphere, *W. K. Widger, Jr., Dec 1952.*

No. 26. (Classified Title), *A. L. Aden and L. Katz, Dec 1952. (SECRET Report)*

No. 27. (Classified Title), *N. A. Haskell, Dec 1952 (SECRET Report)*

No. 28. A-Bomb Thermal Radiation Damage Envelopes for Aircraft *(U), R. H. Chapman, G. W. Wares and M. H. Seavey, Dec 1952, (SECRET/RESTRICTED DATA Report)*

No. 29. A Note on High Level Turbulence Encountered by a Glider, *J. Kuettner, Dec 1952.*

AIR FORCE SURVEYS IN GEOPHYSICS (Continued)

No. 30. Results of Controlled-Altitude Balloon Flights at 50,000 to 70,000 Feet During September 1952, *edited by T. O. Haig and R. A. Craig, Feb 1953.*

No. 31. Conference: Weather Effects on Nuclear Detonations *(U), edited by B. Grossman, Feb 1953. (SECRET/RESTRICTED DATA Report)*

No. 32. Operation IVY Project 6.11. Free Air Atomic Blast Pressure and Thermal Measurements *(U), N. A. Haskell and P. R. Gast, Mar 1953. (SECRET/RESTRICTED DATA Report)*

No. 33. Variability of Subjective Cloud Observations - I, *A. M. Gallagan, Mar 1953.*

No. 34. Feasibility of Detecting Atmospheric Inversions by Electromagnetic Probing, *A. L. Aden, Mar 1953.*

No. 35. Flight Aspects of the Mountain Wave, *C. F. Jenkins and J. Kuettner, Apr 1953.*

No. 36. Report on Particle Precipitation Measurements Performed During the Buster Tests at Nevada *(U), A. J. Parzaile, Apr 1953. (SECRET/RESTRICTED DATA Report)*

No. 37. Critical Envelope Study for the XB-63, B-52A, and F-89 *(U), N. A. Haskell, R. M. Chapman and M. H. Seavey, Apr 1953. (SECRET Report)*

No. 38. Notes on the Prediction of Overpressures From Very Large Thermo-Nuclear Bombs *(U), N. A. Haskell, Apr 1953. (SECRET Report)*

No. 39. Atmospheric Attenuation of Infrared Oxygen Afterglow Emission *(U), N. J. Oliver and J. W. Chamberlain, Apr 1953. (SECRET Report)*

No. 40. (Classified Title), *R. E. Hanson, May 1953, (SECRET Report)*

No. 41. The Silent Area Forecasting Problem *(U), W. K. Widger, Jr., May 1953. (SECRET Report)*

No. 42. An Analysis of the Contrail Problem *(U), R. A. Craig, Jun 1953. (CONFIDENTIAL Report)*

No. 43. Sodium in the Upper Atmosphere, *L. E. Miller, Jun 1953.*

No. 44. Silver Iodide Diffusion Experiments Conducted at Camp Wellfleet, Mass., During July-August 1952, *P. Goldberg et al, Jun 1953.*

No. 45. The Vertical Distribution of Water Vapor in the Stratosphere and the Upper Atmosphere, *L. E. Miller, Sep 1953.*

No. 46. Operation IVY Project 6.11. (Final Report). Free Air Atomic Blast Pressure and Thermal Measurements *(U), N. A. Haskell, J. O. Vann and P. R. Gast, Sep 1953 (SECRET/RESTRICTED DATA Report)*

No. 47. Critical Envelope Study for the B61-A *(U), N. A. Haskell, R. M. Chapman and M. H. Seavey, Sep 1953. (SECRET Report)*

No. 48. Operation Upshot-Knothole Project 1.3. Free Air Atomic Blast Pressure Measurements. Revised Report *(U), N. A. Haskell and R. M. Brubaker, Nov 1953. (SECRET/RESTRICTED DATA Report)*

No. 49. Maximum Humidity in Engineering Design, *N. Sissenwine, Oct 1953.*

No. 50. Probable Ice Island Locations in the Arctic Basin, January 1954, *A. P. Crary and I. Browne, May 1954.*

No. 51. Investigation of TRAC for Active Air Defense Purposes *(U), G. W. Wares, R. Penndorf, V. G. Plank and B. H. Grossman, Dec 1953. (SECRET/RESTRICTED DATA Report)*

No. 52. Radio Noise Emissions During Thermonuclear Reactions *(U), T. J. Keneshea, Jun 1954. (CONFIDENTIAL Report)*

No. 53. A Method of Correcting Tabulated Rawinsonde Wind Speeds for Curvature of the Earth, *R. Leviton, Jun 1954.*

No. 54. A Proposed Radar Storm Warning Service For Army Combat Operations, *M. G. H. Ligda, Aug 1954.*

No. 55. A Comparison of Altitude Corrections for Blast Overpressure *(U), N. A. Haskell, Sep 1954. (SECRET Report)*

No. 56. Attenuating Effects of Atmospheric Liquid Water on Peak Overpressures from Blast Waves *(U), H. P. Gauvin, J. H. Healy and M. A. Bennett, Oct 1954. (SECRET Report)*

AIR FORCE SURVEYS IN GEOPHYSICS (Continued)

No. 57. Windspeed Profile, Windshear, and Gusts for Design of Guidance Systems for Vertical Rising Air Vehicles, *N. Sissenwine, Nov 1954.*

No. 58. The Suppression of Aircraft Exhaust Trails, *C. E. Anderson, Nov 1954.*

No. 59. Preliminary Report on the Attenuation of Thermal Radiation From Atomic or Thermonuclear Weapons *(U), R. M. Chapman and M. H. Seavey, Nov 1954. (SECRET/RESTRICTED DATA Report)*

No. 60. Height Errors in a Rawin System, *R. Leviton, Dec 1954.*

No. 61. Meteorological Aspects of Constant Level Balloon Operations *(U), W. K. Widger, Jr. et al, Dec 1954. (SECRET Report)*

No. 62. Variations in Geometric Height of 30 to 60 Thousand Foot Pressure-Altitudes *(U), N. Sissenwine, A. E. Cole and W. Baginsky, Dec 1954. (CONFIDENTIAL Report)*

No. 63. Review of Time and Space Wind Fluctuations Applicable to Conventional Ballistic Determinations, *W. Baginsky, N. Sissenwine, B. Davidson and H. Letton, Dec 1954.*

No. 64. Cloudiness Above 20,000 Feet for Certain Stellar Navigation Problems *(U), A. E. Cole, Jan 1955. (SECRET Report)*

No. 65. The Feasibility of the Identification of Hail and Severe Storms, *D. Atlas and R. Donaldson, Jan 1955.*

No. 66. Rate of Rainfall Frequencies Over Selected Air Routes and Destinations *(U), A. E. Cole and N. Sissenwine, Mar 1955. (SECRET Report)*

No. 67. Some Considerations on the Modeling of Cratering Phenomena in Earth *(U), N. A. Haskell, Apr 1955. (SECRET/RESTRICTED DATA Report)*

No. 68. The Preparation of Extended Forecasts of the Pressure Height Distribution in the Free Atmosphere Over North America by Use of Empirical Influence Functions, *R. M. White, May 1955.*

No. 69. Cold Weather Effect on B-62 Launching Personnel *(U), N. Sissenwine, Jun 1955. (SECRET Report)*

No. 70. Atmospheric Pressure Pulse Measurements, Operation Castle *(U), E. A. Flourand, Aug 1955. (SECRET/RESTRICTED DATA Report)*

No. 71. Refraction of Shock Waves in the Atmosphere *(U), N. A. Haskell, Aug 1955 (SECRET Report)*

No. 72. Wind Variability as a Function of Time at Muroc, California, *B. Singer, Sep 1955.*

No. 73. The Atmosphere, *N. C. Gerson, Sep 1955.*

No. 74. Areal Variation of Ceiling Height *(U), W. Baginsky and A. E. Cole, Oct 1955. (CONFIDENTIAL Report)*

No. 75. An Objective System for Preparing Operational Weather Forecasts, *I. A. Lund and E. W. Wahl, Nov 1955.*

No. 76. The Practical Aspects of Tropical Meteorology, *C. E. Palmer, C. W. Wise, L. J. Stempson and G. H. Duncan, Sep 1955.*

No. 77. Remote Determination of Soil Trafficability by Aerial Penetrometer, *C. Molineux, Oct 1955.*

No. 78. Effects of the Primary Cosmic Radiation on Matter, *H. O. Curtis, Jan 1956.*

No. 79. Tropospheric Variations of Refractive Index at Microwave Frequencies, *C. F. Campen and A. E. Cole, Oct 1955.*

No. 80. A Program to Test Skill in Terminal Forecasting, *I. I. Gringorten, I. A. Lund and M. A. Miller, Jun 1955.*

No. 81. Extreme Atmospheres and Ballistic Densities, *N. Sissenwine and A. E. Cole, Jul 1955.*

No. 82. Rotational Frequencies and Absorption Coefficients of Atmospheric Gases, *S. N. Ghosh and H. D. Edwards, Mar 1956.*

No. 83. Ionospheric Effects on Positioning of Vehicles at High Altitudes, *W. Pfister and T. J. Keneshea, Mar 1956.*

No. 84. Pre-Trough Winter Precipitation Forecasting, *P. W. Funke, Feb 1957.*

No. 85. Geomagnetic Field Extrapolation Techniques – An Evaluation of the Poisson Integral for a Plane *(U), J. F. McClay and P. Fougere, Feb 1957. (SECRET Report)*

No. 86. The ARDC Model Atmosphere, 1956, *R. A. Minzner and W. S. Ripley, Dec 1956.*

No. 87. An Estimate of the Maximum Range of Detectability of Seismic Signals, *N. A. Haskell, Mar 1957.*

No. 88. Some Concepts for Predicting Nuclear Crater Size *(U), F. A. Crowley, Feb 1957. (SECRET/ RESTRICTED DATA Report)*

No. 89. Upper Wind Representation and Flight Planning, *I. I. Gringorten, Mar 1957.*

No. 90. Reflection of Point Source Radiation From a Lambert Plane Onto a Plane Receiver, *A. W. Guess, Jul 1957.*

No. 91. The Variations of Atmospheric Transmissivity and Cloud Height at Newark, *T. O. Haig, and W. C. Morton, III, Jan 1958.*

No. 92. Collection of Aeromagnetic Information For Guidance and Navigation *(U), R. Hutchinson, B. Shuman, K. Brereton and J. McClay, Aug 1957. (SECRET Report)*

No. 93. The Accuracy of Wind Determination From the Track of a Falling Object, *V. Lally and R. Leviton, Mar 1958.*

No. 94. Estimating Soil Moisture and Tractionability Conditions for Strategic Planning *(U),* Part 1 - General method, *and* Part 2 - Applications and interpretations, *C. W. Thornthwaite, J. R. Mather, D. B. Carter and C. E. Molineux, Mar 1958 (Unclassified Report).* Part 3 - Average soil moisture and tractionability conditions in Poland *(U), D. B. Carter and C. E. Molineux, Aug 1958 (CONFIDENTIAL Report).* Part 4 - Average soil moisture and tractionability conditions in Yugoslavia *(U), D. B. Carter and C. E. Molineux, Mar 1959 (CONFIDENTIAL Report)*

No. 95. Wind Speeds at 50,000 to 100,000 Feet and a Related Balloon Platform Design Problem *(U), N. Dvoskin and N. Sissenwine, Jul 1957. (SECRET Report)*

No. 96. Development of Missile Design Wind Profiles for Patrick AFB, *N. Sissenwine, Mar 1958.*

No. 97. Cloud Base Detection by Airborne Radar, *R. J. Donaldson, Jr., Mar 1958.*

No. 98. Mean Free Air Gravity Anomalies, Geoid Contour Curves, and the Average Deflections of the Vertical *(U), W. A. Heiskanen, L. A. Uotila and O. W. Williams, Mar 1958. (CONFIDENTIAL Report)*

No. 99. Evaluation of AN/GMD-2 Wind Shear Data for Development of Missile Design Criteria, *N. Dvoskin and N. Sissenwine, Apr 1958.*

No.100. A Phenomenological Theory of the Scaling of Fireball Minimum Radiant Intensity with Yield and Altitude *(U), H. K. Sen, Apr 1958. (SECRET Report)*

No.101. Evaluation of Satellite Observing Network for Project "Space Track", *G. R. Miczaika and H. O. Curtis, Jun 1958.*

No.102. An Operational System to Measure, Compute, and Present Approach Visibility Information, *T. O. Haig and W. C. Morton, III, Jun 1958.*

No.103. Hazards of Lightning Discharge to Aircraft, *G. A. Faucher and H. O. Curtis, Aug 1958.*

No.104. Contrail Prediction and Prevention *(U), C. S. Downie, C. E. Anderson, S. J. Birstein and B. A. Silverman, Aug 1958. (SECRET Report)*

No.105. Methods of Artificial Fog Dispersal and Their Evaluation, *C. E. Junge, Sep 1958.*

No.106. Thermal Techniques for Dissipating Fog From Aircraft Runways, *C. S. Downie and R. B. Smith, Sep 1958.*

No.107. Accuracy of RDF Position Fixes in Tracking Constant-Level Balloons, *K. C. Giles and R. E. Peterson, edited by W. K. Widger, Jr., Oct 1958.*

No.108. The Effect of Wind Errors on SAGE-Guided Intercepts *(U), E. M. Darling, Jr. and C. D. Kern, Oct 1958 (CONFIDENTIAL Report)*

No.109. Behavior of Atmospheric Density Profiles, *N. Sissenwine, W. S. Ripley and A. E. Cole, Dec 1958.*

AIR FORCE SURVEYS IN GEOPHYSICS (Continued)

No.110. Magnetic Determination of Space Vehicle Attitude *(U), J. F. McClay and P. F. Fougere, Mar 1959. (SECRET Report)*

No.111. Final Report on Exhaust Trail Physics: Project 7630, Task 76308 *(U), M. H. McKenna, and H. O. Curtis, Jul 1959. (SECRET Report)*

No.112. Accuracy of Mean Monthly Geostrophic Wind Vectors as a Function of Station Network Density, *H. A. Salmela, Jun 1959.*

No.113. An Estimate of the Strength of the Acoustic Signal Generated by an ICBM Nose Cone Reentry *(U), N. A. Haskell, Aug 1959. (CONFIDENTIAL Report)*

No.114. The Role of Radiation in Shock Propagation with Applications to Altitude and Yield Scaling of Nuclear Fireballs *(U), H. K. Sen and A. W. Guess, Sep 1959. (SECRET/RESTRICTED DATA Report)*

No.115. ARDC Model Atmosphere, 1959, *R. A. Minzner, K. S. W. Champion and H. L. Pond, Aug 1959.*

No.116. Refinements in Utilization of Contour Charts for Climatically Specified Wind Profiles, *A. E. Cole, Oct 1959.*

No.117. Design Wind Profiles From Japanese Relay Sounding Data, *N. Sissenwine, M. T. Mulkern, and H. A. Salmela, Dec 1959.*

No.118. Military Applications of Supercooled Cloud and Fog Dissipation, *C. S. Downie, and B. A. Silverman, Dec 1959.*

No.119. Factor Analysis and Stepwise Regression Applied to the 24-Hour Prediction of 500-mb Winds, Temperatures, and Heights Over a Silent Area *(U), E. J. Aubert, I. A. Lund, A. Thomasell, Jr., and J. J. Pazniokas, Feb 1960. (CONFIDENTIAL Report)*

No.120. An Estimate of Precipitable Water Along High-Altitude Ray Paths, *Murray Gutnick, Mar 1960.*

No.121. Analyzing and Forecasting Meteorological Conditions in the Upper Troposphere and Lower Stratosphere, *R. M. Endlich and G. S. McLean, Apr 1960.*

No.122. Analysis and Prediction of the 500-mb Surface in a Silent Area, *(U), E. A. Aubert, May 1960. (CONFIDENTIAL Report).*

No.123. A Diffusion-Deposition Model for In-Flight Release of Fission Fragments, *M. L. Bared, D. A. Haugen, and J. J. Fuquay, Jun 1960.*

No.124. Research and Development in the Field of Geodetic Science, *C. E. Ewing, Aug 1960.*

No.125. Extreme Value Statistics -- A Method of Application, *I. I. Gringorten, Jun 1960.*

No.126. Notes on the Meteorology of the Tropical Pacific and Southeast Asia, *W. D. Mount, Jun 1960.*

No.127. Investigations of Ice-Free Sites for Aircraft Landings in East Greenland, 1959, *J.H. Hartshorn, G. E. Stoerts, A. N. Kover, and S. N. Davis, Sep 1961.*

No.128. Guide for Computation of Horizontal Geodetic Surveys, *H. R. Kahler and N. A. Roy, Dec 1960.*

No.129. An Investigation of a Perennially Frozen Lake, *D. F. Barnes, Dec 1960.*

No.130. Analytic Specification of Magnetic Fields, *P. F. Fougere, Dec 1960. (CONFIDENTIAL Report)*

No.131. An Investigation of Symbol Coding for Weather Data Transmission, *P. I. Hershberg, Dec 1960.*

No.132. Evaluation of an Arctic Ice-Free Land Site and Results of C-130 Aircraft Test Landings -- Polaris Promontory, No. Greenland, 1958-1959, *S. Needleman, D. Klick, C. E. Molineux, Mar 1961.*

No.133. Effectiveness of the SAGE System in Relation to Wind Forecast Capability *(U), E. M. Darling, Jr., and Capt. C. D. Kern, May 1961. (CONFIDENTIAL Report)*

AIR FORCE SURVEYS IN GEOPHYSICS (Continued)

No. 134 Area-Dosage Relationships and Time of Tracer Arrival in the Green Glow Program, *W. P. Elliott, R. J. Engelmann, P. W. Nickola, May 1961.*

No. 135 Evaluation of Arctic Ice-Free Land Sites - Kronprins Christian Land and Peary Land, North Greenland, 1960, *W. E. Davies and D. B. Krinsley, May 1961.*

No. 136 Missile Borne Radiometer Measurements of the Thermal Emission Characteristics of ICBM Plumes *(U), R. E. Hunter and L. P. Marcotte, Jul 1961. (SECRET Report)*

No. 137 Infrared Studies of ICBM Plumes Using Missile - Borne Spectrometers *(U), R. E. Hunter and L. P. Marcotte, Sep 1961. (SECRET Report).*

No. 138 Arctic Terrain Investigations Centrum Lake, N E Greenland, 1960, *S. M. Needleman (to be published).*

No. 139 Space and Planetary Environments, *S. I. Valley, Editor, Jan 1962*

No. 140 Proceedings of National Symposium on Winds for Aerospace Vehicle Design, *N. Sissenwine and H. G. Kasten, Co-Chairmen, Mar 1962.*

No. 141 Atlas of Monthly Mean Stratosphere Charts, 1955-1959, Vol. I, January to June, *H. S. Muench (to be published).*

No. 142 Infrared Atmospheric Transmissions: Some Papers on the Solar Spectrum from 3 to 15 Microns, *J. N. Howard and J. S. Garing, Dec 1961.*

UNCLASSIFIED

Geophysics Research Directorate
Air Force Cambridge Research Laboratories
L. G. Hanscom Field, Bedford, Mass.

SUMMARY REPORT-PROJECT ICE WAY, edited by W. D. Kingery. May 1962. 216 pp. incl. illus. tables. Air Force Surveys in Geophysics No. 145; AFCRL-62-498 Unclassified report

Project ICE WAY consisted of construction, operational evaluation, and scientific study of a sea-ice airfield on North Star Bay near Thule AB during January through May 1961. This report includes a technical discussion of site selection, engineering aspects of construction technical evaluation of operational experience, and scientific and engineering studies of sea-ice strength, mechanical properties, salinity, deformation, and deterioration characteristics. Separate sections describe elastic and time-dependent deformation during aircraft operations, influence of crack patterns on operational use, temperature, salinity, density, and ring tensile strengths of natural and constructed sea ice, stress-rupture data for sea ice, in-place strength

1. Runways—Sea Ice
2. Ice Formation
3. Greenland
4. Arctic Regions

I. Kingery, W.D.(ed)

UNCLASSIFIED

UNCLASSIFIED

Geophysics Research Directorate
Air Force Cambridge Research Laboratories
L. G. Hanscom Field, Bedford, Mass.

SUMMARY REPORT-PROJECT ICE WAY, edited by W. D. Kingery. May 1962. 216 pp. incl. illus. tables. Air Force Surveys in Geophysics No. 145; AFCRL-62-498 Unclassified report

Project ICE WAY consisted of construction, operational evaluation, and scientific study of a sea-ice airfield on North Star Bay near Thule AB during January through May 1961. This report includes a technical discussion of site selection, engineering aspects of construction technical evaluation of operational experience, and scientific and engineering studies of sea-ice strength, mechanical properties, salinity, deformation, and deterioration characteristics. Separate sections describe elastic and time-dependent deformation during aircraft operations, influence of crack patterns on operational use, temperature, salinity, density, and ring tensile strengths of natural and constructed sea ice, stress-rupture data for sea ice, in-place strength

1. Runways—Sea Ice
2. Ice Formation
3. Greenland
4. Arctic Regions

I. Kingery, W. D. (ed)

UNCLASSIFIED

UNCLASSIFIED

Geophysics Research Directorate
Air Force Cambridge Research Laboratories
L. G. Hanscom Field, Bedford, Mass.

SUMMARY REPORT-PROJECT ICE WAY, edited by W. D. Kingery. May 1962. 216 pp. incl. illus. tables. Air Force Surveys in Geophysics No. 145; AFCRL-62-498 Unclassified report

Project ICE WAY consisted of construction, operational evaluation, and scientific study of a sea-ice airfield on North Star Bay near Thule AB during January through May 1961. This report includes a technical discussion of site selection, engineering aspects of construction technical evaluation of operational experience, and scientific and engineering studies of sea-ice strength, mechanical properties, salinity, deformation, and deterioration characteristics. Separate sections describe elastic and time-dependent deformation during aircraft operations, influence of crack patterns on operational use, temperature, salinity, density, and ring tensile strengths of natural and constructed sea ice, stress-rupture data for sea ice, in-place strength

1. Runways—Sea Ice
2. Ice Formation
3. Greenland
4. Arctic Regions

I. Kingery, W. D. (ed)

UNCLASSIFIED

UNCLASSIFIED

Geophysics Research Directorate
Air Force Cambridge Research Laboratories
L. G. Hanscom Field, Bedford, Mass.

SUMMARY REPORT-PROJECT ICE WAY, edited by W. D. Kingery. May 1962. 216 pp. incl. illus. tables. Air Force Surveys in Geophysics No. 145; AFCRL-62-498 Unclassified report

Project ICE WAY consisted of construction, operational evaluation, and scientific study of a sea-ice airfield on North Star Bay near Thule AB during January through May 1961. This report includes a technical discussion of site selection, engineering aspects of construction technical evaluation of operational experience, and scientific and engineering studies of sea-ice strength, mechanical properties, salinity, deformation, and deterioration characteristics. Separate sections describe elastic and time-dependent deformation during aircraft operations, influence of crack patterns on operational use, temperature, salinity, density, and ring tensile strengths of natural and constructed sea ice, stress-rupture data for sea ice, in-place strength

1. Runways—Sea Ice
2. Ice Formation
3. Greenland
4. Arctic Regions

I. Kingery, W. D. (ed)

UNCLASSIFIED

Geophysics Research Directorate
Air Force Cambridge Research Laboratories
L. G. Hanscom Field, Bedford, Mass.

tests of sea ice, long-time deformation of ice sheets, elastic properties of sea ice from ultrasonic and dynamic measurements, and ice deterioration. Successful operational tests of aircraft of different sizes up to and including a B-52 jet bomber indicated that sea-ice platforms can carry heavier loads than has previously been recognized.

UNCLASSIFIED

UNCLASSIFIED

Geophysics Research Directorate
Air Force Cambridge Research Laboratories
L. G. Hanscom Field, Bedford, Mass.

tests of sea ice, long-time deformation of ice sheets, elastic properties of sea ice from ultrasonic and dynamic measurements, and ice deterioration. Successful operational tests of aircraft of different sizes up to and including a B-52 jet bomber indicated that sea-ice platforms can carry heavier loads than has previously been recognized.

UNCLASSIFIED

UNCLASSIFIED

Geophysics Research Directorate
Air Force Cambridge Research Laboratories
L. G. Hanscom Field, Bedford, Mass.

tests of sea ice, long-time deformation of ice sheets, elastic properties of sea ice from ultrasonic and dynamic measurements, and ice deterioration. Successful operational tests of aircraft of different sizes up to and including a B-52 jet bomber indicated that sea-ice platforms can carry heavier loads than has previously been recognized.

UNCLASSIFIED

UNCLASSIFIED

Geophysics Research Directorate
Air Force Cambridge Research Laboratories
L. G. Hanscom Field, Bedford, Mass.

tests of sea ice, long-time deformation of ice sheets, elastic properties of sea ice from ultrasonic and dynamic measurements, and ice deterioration. Successful operational tests of aircraft of different sizes up to and including a B-52 jet bomber indicated that sea-ice platforms can carry heavier loads than has previously been recognized.

UNCLASSIFIED

UNCLASSIFIED

UNCLASSIFIED

UNCLASSIFIED